TECHNICAL REPORT
69-31-CM

INVESTIGATIONS OF HEAT AND MASS (WATER VAPOR AND LIQUID) MOVEMENT THROUGH CLOTHING SYSTEMS

by
R. E. Larson, L. W. Rust, Jr.,
A.R. Kydd and G. A. Gauvin
Applied Science Division
Litton Systems, Inc.
Minneapolis, Minnesota

Contract No. DA-19-129-AMC-683 (N)

September 1968

Clothing & Organic Materials Laboratory
C&OM-56

269

DISCLAIMER NOTICE

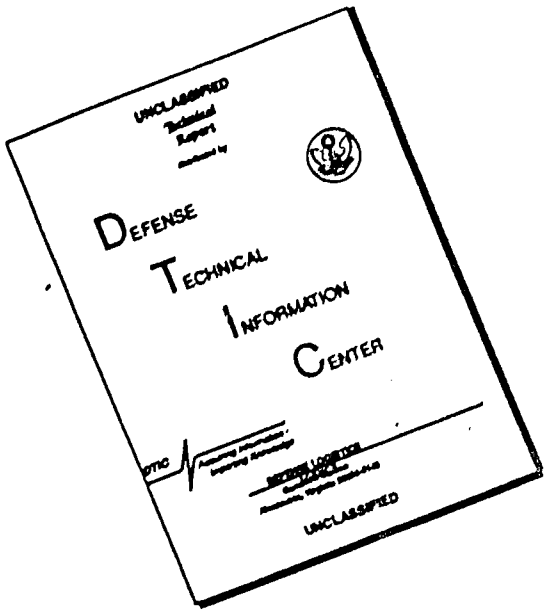

THIS DOCUMENT IS BEST QUALITY AVAILABLE. THE COPY FURNISHED TO DTIC CONTAINED A SIGNIFICANT NUMBER OF PAGES WHICH DO NOT REPRODUCE LEGIBLY.

AD_____

TECHNICAL REPORT

69-31- CM

INVESTIGATIONS OF HEAT AND MASS

(WATER VAPOR AND LIQUID)

MOVEMENT THROUGH CLOTHING SYSTEMS

by

R. E. Larson, L. W. Rust, Jr.,
A. R. Kydd and G. A. Gauvin

Applied Science Division
Litton Systems, Inc.
Minneapolis, Minnesota

Contract No. DA-19-129- AMC-683(N)

Project Reference:
1K012501A302

Series: C&OM-56

September 1968

Clothing & Organic Materials Division
U. S. Army Natick Laboratories
Natick, Massachusetts 01760

FOREWORD

This is the Final Report of research conducted by the Applied Science Division of Litton Systems, Inc., for the U. S. Army Natick Laboratories under Contract No. DA 19-129-AMC-683(N) for the period 25 June 1965 to 24 June 1966. The report includes the work presented in the two Progress Reports prepared previously and supersedes their contents. Project monitor for the U. S. Army Natick Laboratories was Mr. Leo A. Spano of the Advanced Projects Division.

CONTENTS

CONTENTS (Con't)

LIST OF ILLUSTRATIONS

LIST OF ILLUSTRATIONS (Con't)

LIST OF ILLUSTRATIONS (Con't)

LIST OF ILLUSTRATIONS (Con't)

LIST OF ILLUSTRATIONS (Con't)

LIST OF TABLES

NOMENCLATURE

Symbol	Definition and Dimensions
A	hot-wire calibration constant (V^2)
A_s	total skin surface area (ft^2)
B	hot-wire calibration constant $\left(V^2 (ft^2 \text{ sec/slug})^{1/2}\right)$
C	vapor concentration (lb/ft^3)
c	specific heat (Btu/lb °F)
c_p	specific heat at constant pressure (Btu/lb °F)
D	vapor diffusion coefficient (ft^2/hr)
E	energy flux (Btu/ft^2 hr); energy production rate due to exercise (Btu/ft^3 hr)
$\bar{E}_b$	hot-wire mean bridge voltage (V)
e_b'	hot-wire fluctuating rms bridge voltage (V)
h	enthalpy (Etu/lb °F)
K_o	overall mass transfer coefficient at the fabric outer surface (ft/hr)
K_l	overall mass transfer coefficient at the fabric inner surface (ft/hr)
K_s	overall mass transfer coefficient at the skin surface (ft/hr)
k_s	local mass transfer coefficient at the skin surface (ft/hr)
k	thermal conductivity (Btu/ft hr °F)
k_{s_o}	reference skin conductivity (Btu/ft hr °F)
L	thickness of fabric, air space, or skin-body system (ft)

L_1	skin layer thickness of the skin-body system (ft)
L_2	muscle layer thickness of the skin-body system (ft)
L_3	deep body core thickness of the skin-body system (ft)
M	dimensionless mass of absorbed water vapor; metabolism rate (Btu/ft^2 hr)
$\dot{m}$	mass flux (lb/ft^2 hr)
$m_{avai.}$	mass of liquid available for evaporation at the skin surface (lb/ft^2)
Q	basal metabolism (Btu/ft^3 hr)
Q'	total heat production rate (Btu/ft^3 hr)
$\Delta Q_{shi.}$	increase in metabolism due to shivering (Btu/ft^3 hr)
q	heat flux (Btu/ft^2 hr)
r	relative humidity (dimensionless)
S	sweat generation rate (lb/ft^2 hr)
S_o	reference sweat generation rate (lb/ft^2 hr)
T	temperature (°F)
ΔT_B	deviation of the instantaneous average body temperature from its reference value (°F)
t	time (hr)
$\overline{U}$	mean velocity (ft/hr), in hot-wire equations (ft/sec)
U_o	overall heat transfer coefficient at the fabric outer surface (Btu/ft^2 hr °F)
U_1	overall heat transfer coefficient at the fabric inner surface (Btu/ft^2 hr °F)
U_s	overall heat transfer coefficient at the skin surface (Btu/ft^2 hr °F)

u_s	local heat transfer coefficient at the skin surface (Btu/ft^2 hr °F)
u'	rms fluctuating velocity (ft/sec)
V	vaporization rate (Btu/ft^2 hr)
$\dot{V}_1$, $\dot{V}_2$	total volumetric flow rate through the fabric and airspace, respectively (ft^3/hr)
x	coordinate (ft)
α	geometric (volumetric) porosity of the fabric (dimensionless)
α_1, α_2	physiological conductivity constants (1/°F)
α_{m_1}, α_{m_2}, α_{m_3}	control coefficients for shivering (Btu/ft^3 hr °F); Btu/ft^3 hr °F^2; Btu/ft^3 hr °F)
α_s	first power proportional control coefficient for sweating (lb/ft^2 hr °F)
γ	physiological conductivity constant (hr/°F)
λ	heat of vaporization (Btu/lb)
λ_s	fourth power control coefficient for sweating (lb/ft^2 hr °F^4)
	dummy variable
ρ	density (lb/ft^3), in hot-wire equations (slugs/ft^3)
	$(\partial M/\partial C)_T$ (ft^3/lb), or turbulence parameter (1/V)
ω	$(\partial M/\partial T)_C$ (1/°F)

Subscripts

a	airspace
b	hot-wire bridge value
B	average body value

c	compressor
f	fabric
fi	fiber
f_o	outer fabric surface
f_1	inner fabric surface
for.	forced
i	initial
l	liquid
max	maximum
min	minimum
o	zero velocity value
or.	orifice
ref	reference
s	skin-body system; sweat
s_o	outer skin surface
v	vapor
∞	free stream

ABSTRACT

This report of research on the Investigations of Heat and Mass (Water Vapor and Liquid) Movement Through Clothing Systems summarizes the results of a theoretical and experimental research program.

Modifications and improvements were made on the mathematical model and governing equations previously described in an Annual Progress Report. The equations were converted into an explicit finite difference form and programmed for solution on the Honeywell 1800 digital computer.

Experimental studies included measurements of profiles of mean and fluctuating velocity, temperature, and water vapor concentration for various fabric spacings and ventilating flow rates. Transfer coefficient data obtained from these profiles were compared with total water and heat loss rates.

INVESTIGATIONS OF HEAT AND MASS (WATER VAPOR AND LIQUID) MOVEMENT THROUGH CLOTHING SYSTEMS

I. INTRODUCTION

The general objective of the present research study is to establish definitive relationships of those variables that control heat and mass (water vapor and/or liquid) flow through composite clothing systems under static and dynamic conditions. These data will ultimately be applied in the design and engineering of clothing systems for troops.

During the first year of the program, (1) a simplified mathematical model consisting of a heat and sweat generating skin surface overlaid by a fabric layer was developed. The heat and mass flow equations were solved using an explicit finite difference calculation procedure programmed for solution on a digital computer. Several calculations were performed to compare this model with existing solutions. Included were cases of the temperature responses of a nude male exercising and movement from a warm to a cold environment. Another calculation considered a clothed male in the act of exercising.

Experimental studies included the development of a wind tunnel and heat and sweat generating skin simulator model. Velocity and humidity profiles were measured using hot-wire and mass flux probes. Interferometric observations of flow over the simulator surface for wet and dry conditions were also performed.

During the second year, the major emphasis was directed toward the experimental portion of the program. Measurements of profiles of mean and fluctuating velocities, temperature, and water vapor concentration for various air gap spacings and combinations of external and ventilating

flows were carried out. For several of these test combinations, measurements of heat and water loss from the skin simulator were performed. Data were obtained for both dry and wet conditions of the simulator surface, which was maintained at 100°F. The probing data were compared with the skin simulator surface heat and water vapor losses and calculations of the heat and mass transfer coefficients required by the mathematical model were carried out.

During the past year, the theoretical development presented (1) was modified and improved to make it more applicable to the experiments carried out. It was decided that a better understanding of the complicated mechanisms involved was necessary before the bulk of the experimental measurements would be initiated. Included is a more detailed description of the heat and mass flow processes in the fabric and air space. In addition, several modifications were made in the skin model.

The mathematical model was programmed for a finite difference solution using the Honeywell 1800 digital computer. Large capacity computers of this type are essential for solution of the problem which involves calculation at many small discrete time increments. Several sample calculations were performed to determine the validity of the mathematical model and to check for programming errors. Only limited computer runs were carried out during the present phase of the investigations. However, the complete computer program is included, and a detailed parameter study can be made when desired.

II. THEORETICAL STUDIES

A. General Discussion

A combined theoretical and experimental program, intended to increase the understanding of the basic mechanisms which govern heat and mass transfer through composite clothing systems, was initiated by Litton's Applied Science Division in June 1963. These studies are documented in detail (1).

A preliminary mathematical model was established in this study, which described the heat and mass transfer processes through a skin-air gap-fabric system. Because of many extremely complex process which occur in such a system, it was found necessary to make several simplifying assumptions in mathematical development. It was anticipated that subsequent experimental/analytical studies would shed new light on the transport mechanisms involved.

During the past year, the mathematical model previously developed was re-evaluated and significant improvements were made. Improved analytical approximations of fabric property variation and physiological responses were obtained. These studies, combined with the experimental results, have provided a mathematical model which more accurately predicts the behavior of a fabric-skin system exposed to various environmental/physiological stresses.

Even though the present mathematical model is more complete and accurate than the preceding one, heavy reliance had to be placed on experimental determinations of the surface heat and mass transfer coefficients. The determination of these coefficients is discussed in Section III.

B. Mathematical Model for the Skin

The three main layers of skin structure, as well as the skin coordinate system, are presented in Figure 1. In the following model it will be assumed, as in Reference 2, that the internal heat generation caused by exercising or shivering is produced in the muscle layer, while the internal generations (basal) will be assumed to occur within the deep body core. A small element of thickness δx at any point within the body is shown in Figure 2. A general formulation of the heat transfer problem which includes heat transfer in three coordinate directions, becomes exceedingly difficult, if not impossible, and tends to mask some of the basic characteristics in which interest is presently centered. Thus, it will be assumed throughout

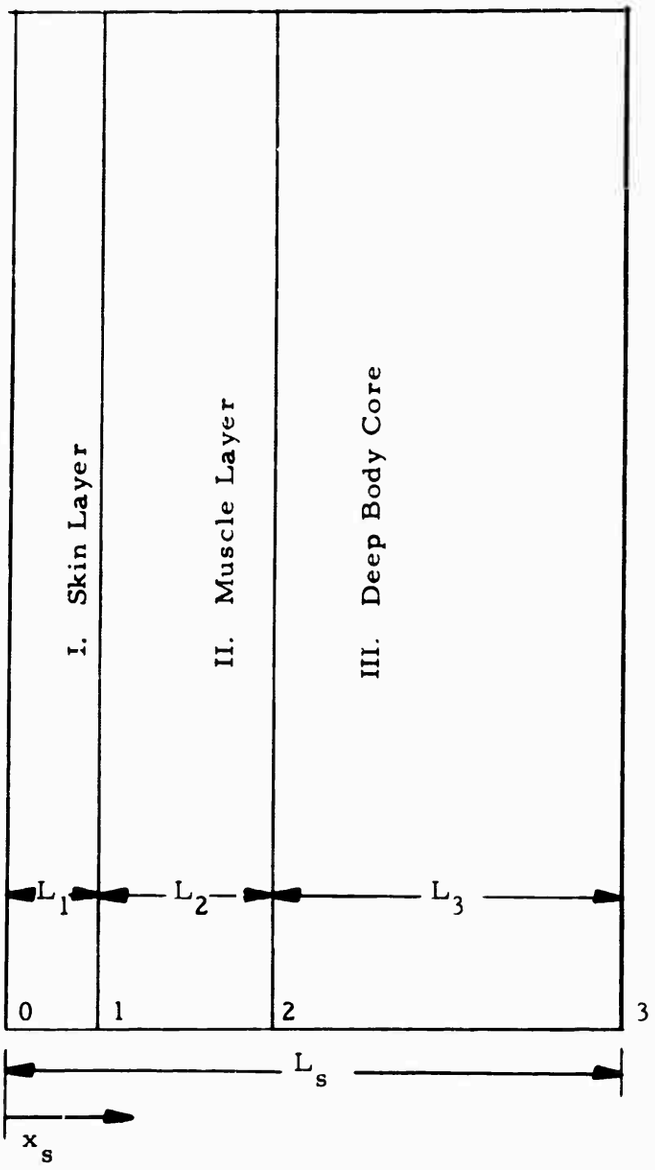

Figure 1. Idealized Skin Structure

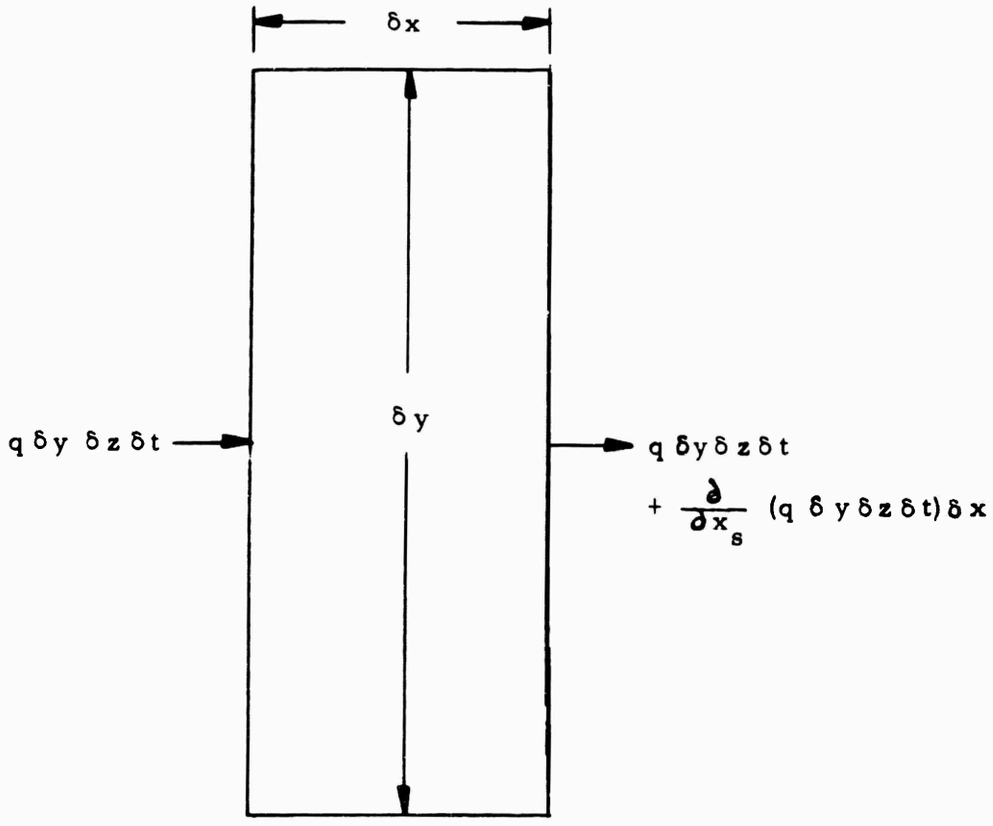

Figure 2. Control Volume within the Skin

the remainder of this report that all heat and mass transfer may be considered to be one dimensional (i.e., in a direction perpendicular to the skin and fabric surfaces).

If q represents the energy crossing the left surface of the slice (Figure 2) per unit area and unit time due to conduction, then $q\ \delta y\ \delta x\ \delta t$ represents the energy which will enter the slice in a time interval δt. When an internal heat generation exists, an additional energy input appears as $Q'\ \delta x\ \delta y\ \delta z\ \delta t$ where Q' is the local heat generation per unit volume and unit time. Denoting the total energy input by E_{in}, one may write

$$E_{in} = q\ \delta y\ \delta z\ \delta t + Q'\delta x\ \delta y \delta z\ \delta t; \tag{1}$$

for small δx, the energy outflow from the right face during the time interval δt, may be written as

$$E_{out} = q\ \delta y\ \delta z\ \delta t + \frac{\partial}{\partial x}\ (q\ \delta y\ \delta z\ \delta t)\ \delta x. \tag{2}$$

The energy contained within the thin slice at any time may be expressed as

$$E = (c\rho)_s\ (T_s - T_{ref})\ \delta x\ \delta y\ \delta z \tag{3}$$

Assuming that the product of skin specific heat and density is constant, the increase in energy (δE) within the slice in a time δt may be expressed as:

$$\delta E = \frac{\partial E}{\partial t}\ \delta t = (c\rho)_s\ \frac{\partial T_s}{\partial t}\ \delta x\ \delta y\ \delta z\ \delta t. \tag{4}$$

Conservation of energy requires that this increase in energy be equal to the difference between the energy input and the energy output ($\delta E = E_{in} - E_{out}$). Using Equations (1), (2), and (4), one obtains after rearranging

$$(c\rho)_s\ \frac{\partial T_s}{\partial t} = Q' - \frac{\partial q}{\partial x_s} \tag{5}$$

Assuming the Fourier conduction heat transfer law to be valid, one may express q as:

$$q = -k_s \left(\frac{\partial T_s}{\partial x_s} \right) \tag{6}$$

where k_s = conductivity of the skin (Btu/ft/sec °F), which, when substituted into Equation (5), yields

$$(c\rho)_s \frac{\partial T_s}{\partial t} = Q' + \frac{\partial}{\partial x_s} \left[k_s \left(\frac{\partial T_s}{\partial x_s} \right) \right]. \tag{7}$$

The skin conductivity cannot be considered constant, as has been pointed out by Crosbie, et al[2]. Utilizing steady state and transient experimental measurements by Hardy and DuBois[3], k_s can be expressed as:

$$k_s = k_{s_o} \left(1 + \alpha_1 \Delta T_B + \gamma \frac{dT_B}{dt} \right) \leq 1.511\, k_{s_o} \quad \text{for } \Delta T_B > 0$$

$$k_s = k_{s_o} \left(1 + \alpha_2 \Delta T_B + \gamma \frac{dT_B}{dt} \right) \geq 0.675\, k_{s_o} \quad \text{for } \Delta T_B \leq 0 \tag{8}$$

where $T_B = \frac{1}{L_s} \int_0^{L_s} T_s(\xi, t)\, d\xi$ = average body temperature (°F)

$$\Delta T_B = T_B - 96.35 \ (°F)$$

$$\alpha_1 = 0.4044 \ (1/°F)$$

$$\alpha_2 = 0.1811 \ (1/°F) \tag{9}$$

$$k_{s_o} = 7.9946 \times 10^{-5} \ (\text{Btu/ft sec } °F).$$

The values listed above for the various physiological constants differ from those as reported in Reference 2. These constants were determined as shown in Appendix A through exact solutions of the heat transfer equations within the body for steady-state conditions. The value of the constants as originally presented in the above references differ from the present values

because they were evaluated by using a finite difference solution for the governing heat transfer equations. The numerical value of γ, quoted by Crosbie, appears incorrect. A re-evaluation of γ, utilizing Crosbie's computer solutions is presented in Appendix A which shows:

$$\gamma = 615 \frac{\text{sec}}{^\circ F} .$$

From (Equation 8) for k_s and the definition of ΔT_B (Equation 9), one notes that the conductivity depends only on time. Thus, k_s may be taken outside the derivative with respect to x_s in Equation (7) and one obtains:

$$(c\rho)_s \frac{\partial T_s}{\partial t} = k_s \frac{\partial^2 T_s}{\partial x_s^2} + Q' . \qquad (10)$$

1. Internal Heat Generation

In the manner of Crosbie[2], it shall be postulated that the internal heat generation due to exercise or shivering is contained entirely within the muscle layer whereas the basal metabolism is generated within the deep body core. The former may be expressed mathematically as:

$$\text{For } L_1 \leq x_s \leq L_1 + L_2$$

$$Q' = E \qquad \text{for } \Delta T_B \geq 0 \qquad (11)$$

$$Q' = E + \Delta Q_{shi} \qquad \text{for } \Delta T_B \leq 0$$

where: E = the internal energy production due to exercise ($Btu/ft^3/sec$). It is shown in Appendix A that the internal heat production due to shivering can be adequately approximated by the following expressions:

$$\Delta Q_{shi.} = -\alpha_{m_1} \Delta T_B + \alpha_{m_2} \Delta T^2_B \qquad \text{for } -1.8^\circ F \leq \Delta T_B \leq 0$$

$$\Delta Q_{shi.} = 1.77219 \times 10^{-2} - \alpha_{m_3} (1.8 + \Delta T_B) \qquad \text{for } \Delta T_B < -1.8^\circ F \qquad (12)$$

where $\alpha_{m_1} = 5.3544 \times 10^{-3}$ (Btu/ft^3 sec °F)

$\alpha_{m_2} = 2.4949 \times 10^{-3}$ (Btu/ft^3 sec °F^2)

$\alpha_{m_3} = 1.4336 \times 10^{-2}$ (Btu/ft^3 sec °F)

The basal metabolism as given by Crosbie[2] equals 37 kcal/m^2/hr. It should be noted that this internal heat generation is given in terms of energy per unit skin area, whereas the present analysis requires the energy production per unit skin volume. Since we shall assume that the basal metabolism is evenly distributed throughout the deep body core, the value of Q may be written as:

For $L_1 + L_2 \leq x_s \leq L_s$

$$Q' = Q = \frac{37}{L_3} = \frac{37}{0.032} = 1.15625 \times 10^3 \text{ kcal/m}^3\text{hr} \qquad (13)$$

$$= 3.5949 \times 10^{-2} \text{ Btu/ft}^3 \text{ sec}$$

2. The Sweat Generation Rate

Utilizing the experimental data for sweat evaporation from Reference 2, it is possible to determine the sweat generation rate as a function of the average body temperature. The expression for the evaporation rate is:

$$V = V_o \qquad \text{for } \Delta T_B \leq 0$$

$$V = V_o + \delta_E (\alpha_v \Delta T_B + \lambda_v \Delta T^4_B) \qquad \text{for } \Delta T_B > 0. \qquad (14)$$

The term δ_E in the above equation allows for a greater vaporization rate due to increased activity. In view of the discussion in Crosbie's paper, V actually includes the effects of air motion on the skin surface, free stream vapor pressure, etc. Since the present analysis will include these effects

in the skin surface mass transfer coefficient, the above equation cannot be applied in our case. Thus, a determination of the sweat generation rate is presented in Appendix A which results in the following expressions:

$$S = S_o + \alpha_s \Delta T_B + \lambda_s \Delta T_B^4 \leq 60\, S_o \qquad \text{for } \Delta T_B > 0$$

$$S = S_o \qquad \text{for } \Delta T_B \leq 0 \tag{15}$$

where $S_o = 5.7285 \times 10^{-7}$ (lb/ft^2 sec)

$\alpha_s = 7.9457 \times 10^{-7}$ (lb/ft^2 sec °F)

$\lambda_s = 5.2514 \times 10^{-4}$ (lb/ft^2 sec °F^4).

3. The Initial and Boundary Conditions

As a general initial condition, it shall be assumed that:

$$\text{at } t = 0,\ T_s = T_{s_i}(x_s) = T_{s_i}. \tag{16}$$

The boundary condition at $x_s = L_s$ can be expressed as:

$$\frac{\partial T_s}{\partial x_s} = 0. \tag{17}$$

The boundary condition at $x_s = 0$ requires further examination. The energy entering the surface plane of the skin (from the interior of the skin) must equal the energy leaving the surface (into the air gap). The energy entering from the skin can be expressed as:

$$q_{in} = k_s \left(\frac{\partial T_s}{\partial x_s} \right)_{x_s = 0} \tag{18}$$

The energy leaving is comprised of the enthalpy of the water vapor plus the heat conducted and radiated from the skin surface. This may be expressed in linearized terms as:

$$q_{out} = m_s h_s + U_s (T_{s_o} - T_a) \qquad (19)$$

where m_s = mass of vapor evaporated (lb/ft^2 sec)

$h_s = c_{p_v} (T_{s_o} - T_{ref}) + \lambda$

= enthalpy of vapor (Btu/lb)

U_s = heat transfer coefficient at the skin outer surface (Btu/ft^2 sec ^oF)

T_{s_o} = temperature of the skin outer surface (^oF)

T_a = average air gap temperature (^oF)

As long as sufficient liquid is available at the skin surface, the mass transfer can be described by:

$$m_s = K_s (C_{s_o} - C_a) \qquad (20)$$

where K_s = the mass transfer coefficient (ft/sec)

C_{s_o} = the vapor concentration at the skin surface (lb/ft^3)

C_a = the average air gap concentration (lb/ft^3).

However, it must be remembered that the supply of water due to sweating is not unlimited and it is conceivable that conditions can arise where the mass transfer predicted by Equation (20) cannot occur because of lack of sufficient moisture. Thus, it is necessary to maintain a constant check on the amount of water available for evaporation at any time. With this is mind, the net rate of increase of liquid on the skin surface may be expressed by:

$$\frac{dm_{avai.}}{dt} = S - m_s$$

Integration of this relation yields :

$$m_{avai.}(t) = m_{avai.}(0) + \int_0^t (S - \dot{m}_s)\, dt. \qquad (21)$$

As long as $m_{avai.}(t) > 0$, $\dot{m}_s$ is given by Equation (20). However, if at any time $m_{avai.}$ becomes 0 (which can only occur if $S - \dot{m}_s \leq 0$), then $\dot{m}_s$ is given by:

$$\dot{m}_s = \text{min.} \left[S,\ K_s(C_{s_o} - C_a) \right] \text{ for } m_{avai.} = 0 \qquad (22)$$

Therefore, the following criteria must be used·

Let $m_{avai.}(t) = m_{avai.}(0) + \int_0^t \left[S(\xi) - \dot{m}_s(\xi) \right] d\xi$

Then, $\dot{m}_s$ is given by:

$$\begin{aligned} \dot{m}_s &= K_s(C_{s_o} - C_a) && \text{when } m_{avai.}(t) > 0 \\ \dot{m}_s &= \text{min.} \left[S,\ K_s(C_{s_o} - C_a) \right] && \text{when } m_{avai.}(t) = 0 . \end{aligned} \qquad (23)$$

The skin boundary condition on the outer surface can now be expressed as:

$$k_s \left(\frac{\partial T_s}{\partial x_s} \right)_{x_s = 0} = \dot{m}_s \left[c_{p_v}(T_{s_o} - T_{ref}) + \lambda \right] + U_s(T_{s_o} - T_a) \qquad (24)$$

where $\dot{m}_s = K_s(C_{s_o} - C_a)$ when $m_{avai.}(t) > 0$

$\dot{m}_s = \text{min.} \left[S,\ K_s(C_{s_o} - C_a) \right]$ when $m_{avai.}(t) = 0.$

4. Summary of Equations and Assumptions

The various assumptions utilized in the preceding sections of this chapter are summarized below:

1) The skin is assumed to be one dimensional.

2) The product of skin specific heat and density is constant.

3) The Fourier conduction heat transfer law is assumed to be valid.

4) The heat conductivity (k_s) depends only on time, not on the skin coordinate.

The equation describing the heat transfer (or temperature distribution) within the body layer can be expressed as:

$$(c\rho)_s \frac{\partial T_s}{\partial t} = k_s \frac{\partial^2 T_s}{\partial x_s^2} + Q'$$

For $0 \leq x_s < L_1$

$$Q' = 0$$

For $L_1 \leq x_s < L_1 + L_2$ (25)

$$Q' = E + \Delta Q_{shi.} \quad \text{for } \Delta T_E \leq 0$$

$$= E \quad \text{for } \Delta T_B > 0$$

For $L_1 + L_2 \leq x_s \leq L_s$

$$Q' = 3.5949 \times 10^{-2} \ (\text{Btu/ft}^3 \text{ sec}).$$

The skin conductivity may be expressed as:

$$k_s = k_{s_o}\left(1 + \alpha_1 \Delta T_B + \gamma \frac{dT_B}{dt}\right) \leq 1.511\, k_{s_o} \quad \text{for } \Delta T_B > 0 \tag{26}$$

$$= k_{s_o}\left(1 + \alpha_2 \Delta T_B + \gamma \frac{dT_B}{dt}\right) \geq 0.675\, k_{s_o} \quad \text{for } \Delta T_B \leq 0.$$

The average body temperature as well as ΔT_B are written as:

$$T_B = \frac{1}{L_s}\int_o^{L_s} T_s(\xi, t)\, d\xi \tag{27}$$

$$\Delta T_B = T_B - 96.35.$$

The sweat generation rate is expressed by:

$$S = S_o + \alpha_s \Delta T_B + \lambda_s \Delta T_B^4 \leq 60\, S_o \quad \text{for } \Delta T_B > 0 \tag{28}$$

$$S = S_o \quad \text{for } \Delta T_B \leq 0.$$

The initial condition for the skin layer is written as:

$$T_s = T_{s_i}(x_s, 0). \tag{29}$$

The boundary conditions at the skin outer surface is written as:

$$k_s\left(\frac{\partial T_s}{\partial x_s}\right)_{x_s = 0} = \dot{m}_s\left[c_{p_v}(T_{s_o} - T_{ref}) + \lambda\right] + U_s(T_{s_o} - T_a)$$

where $\dot{m}_s = K_s(C_{s_o} - C_a)$ when $m_{avai.}(t) > 0$ (30)

$$\dot{m}_s = \min\left[S, K_s(C_{s_o} - C_a)\right] \text{ when } m_{avai.}(t) = 0$$

$$m_{avai.} = m_{avai.}(0) + \int_o^t \left[S(\xi) - \dot{m}_s(\xi)\right] d\xi$$

and the boundary condition at the skin inner surface is expressed by:

$$\left(\frac{\partial T_s}{\partial x_s}\right)_{x_s = L_s} = 0. \tag{31}$$

C. The Mathematical Model for the Fabric

Several improvements to the mathematical model for the fabric will be presented in this section. The assumption that the total pressure gradient is nil, as utilized in Reference 1, will not be required in the present analysis. Indeed, such an assumption is unrealistic in the present case, since bulk flow of air caused by forced ventilation will now be included in the mathematical model. It is obvious that bulk flow through the fabric pores cannot occur unless a pressure differential between the fabric inner and outer surfaces exists. Thus, the existence of a pressure gradient through the cloth must be implicitly assumed when one assumes a forced ventilating flow through the pores of the fabrics.

The assumption made in Reference 1 that the heat content of the air is negligible compared with the heat content of the solid portions of the fabric appears reasonable from physical reasoning. However, the inclusion of the effects of the heat capacity of the air and vapor within the pores of the fabric does not complicate the analysis to any marked degree and therefore will be included in this chapter for the sake of completeness and more generality.

To facilitate a complete mathematical analysis of the heat and mass transfer processes through the fabric system, several simplifying assumptions shall now be made.

1) The diffusion of vapor or liquid water through the solid portions of the fabric is negligible in comparison to diffusion through the pores of the fabric.

2) A macroscopic (or overall) diffusion coefficient can be used for the entire fabric slab.

3) The diffusion of mass due to thermal effects is taken into account by a modification of the diffusion coefficient.

4) The porosity of the fabric is independent of time (i.e., the slab does not swell).

5) There is no capillary effect.

6) Quasi-equilibrium exists at all times, i.e., the solid portions of the slab reach equilibrium with their immediate surroundings instantaneously.

1. The Mass Balance Equation

Referring to Figure 3, the mass of water vapor entering the control volume in a time δt is given by:

$$m_{in} = \dot{m} d H \delta t \tag{32}$$

and the mass leaving the control volume by:

$$m_{out} = m_{in} + \frac{\partial}{\partial x_f}(\dot{m})\, d H \delta t \delta x_f \tag{33}$$

where $\dot{m}$ = mass flux through the surface of the control volume ($lb/ft^2/sec$)

d = depth of the control volume (ft)

H = height of the control volume (ft)

δx_f = thickness of the control volume (ft).

Designating the rate of absorption per unit area per unit time by $\dot{m}'$, the mass of water absorbed in a unit time and area is given by:

$$m_{ab.} = \dot{m}' d \delta x_f \delta t. \tag{34}$$

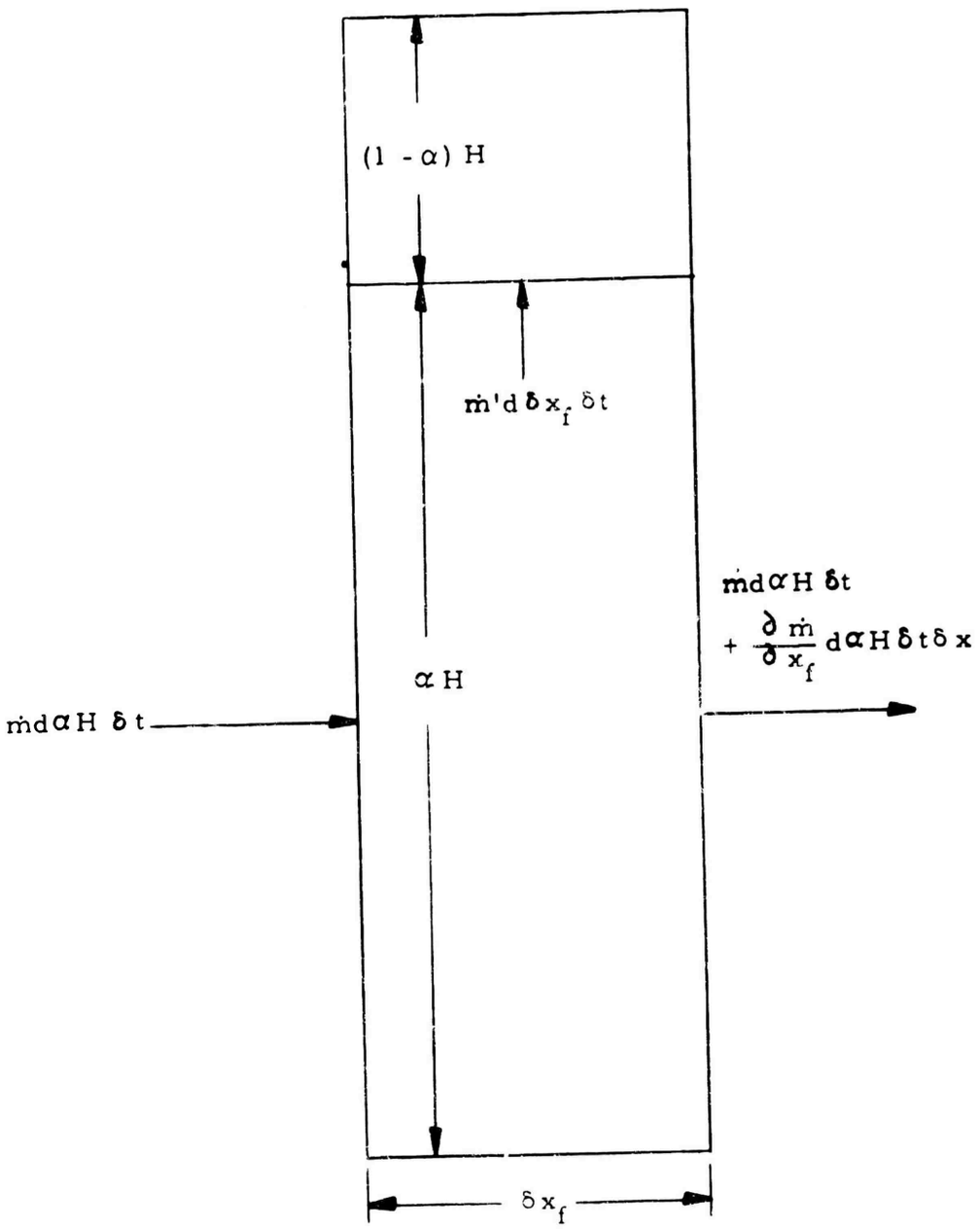

Figure 3. Control Volume within the Fabric

The mass of water vapor contained within the control volume at any time may be expressed as:

$$m = C_f \alpha H d\delta x_f \tag{35}$$

and the increase in vapor mass within the control volume in a time δt is given by:

$$\delta m = \frac{\partial C_f}{\partial t} \alpha H d\delta x_f \delta t \, . \tag{36}$$

The statement of conservation of vapor mass may be written as:

$$m_{in} - m_{out} - m_{ab.} = \delta m. \tag{37}$$

Substituting Equations (32) through (36) into Equation (37) yields:

$$\frac{\partial C_f}{\partial t} = - \frac{\partial \dot{m}}{\partial x_f} - \frac{\dot{m}'}{\alpha H} . \tag{38}$$

The mass flux through any plane due to diffusion can be expressed as:

$$\dot{m}_{dif.} = - D \frac{\partial C_f}{\partial x_f} \tag{39}$$

and the vapor mass flux due to bulk (or forced) convection flow as:

$$\dot{m}_{v_{for.}} = - \frac{\dot{V}_l C_f}{\alpha A_s} \tag{40}$$

where αA_s = total open area of the fabric (ft^2)

$\dot{V}_l$ = total volumetric flow rate through the fabric (ft^3/sec)

C_f = local vapor concentration in the fabric (lb/ft^3).

It should be noted at this point that $\dot{V}_1$ is positive when the bulk flow is in the negative x direction. One may now write $\dot{m}$ as:

$$\dot{m} = \dot{m}_{dif.} + \dot{m}_{v_{for.}}$$

or, utilizing Equations (39) and (40), one obtains:

$$\dot{m} = -\left[D \frac{\partial C_f}{\partial x_f} + \frac{\dot{V}_1 C_f}{\alpha A_s}\right] . \tag{41}$$

Let us now define the dimensionless absorbed mass of water vapor by:

$$M = \frac{m_\ell}{m_{fi.}} \tag{42}$$

where m_ℓ = mass of liquid in the fibre at a time (t)

m_{fi} = mass of the fibre.

But, the mass of fibre can be expressed as:

$$m_{fi.} = \rho_{fi.} (1 - \alpha) H d \delta x_f \tag{43}$$

and thus:

$$m_\ell = M \rho_{fi.} (1 - \alpha) H d \delta x_f. \tag{44}$$

In a time increment δt, m_ℓ increases by an amount:

$$\delta m_\ell = \frac{\partial m_\ell}{\partial t} \delta t = \frac{\partial M}{\partial t} \rho_{fi.} (1 - \alpha) H d \delta x_f \delta t \tag{45}$$

Equating this increase in liquid within the fibres to the increase due to rate of absorption given by $\dot{m}' d \delta x_f \delta t$, one finds:

$$\frac{\partial M}{\partial t} \rho_{fi.} (1 - \alpha) H d \delta x_f \delta t = \dot{m}' d \delta x_f \delta t \tag{46}$$

or:

$$\frac{\dot{m}'}{\alpha H} = \left(\frac{1 - \sigma}{\sigma}\right) \rho_{fi.} \frac{\partial M}{\partial t}. \qquad (47)$$

Substitution of Equations (41) and (47) into (38) yields the final governing equation for the mass diffusion process in the fabric:

$$\frac{\partial C_f}{\partial t} = \frac{\partial}{\partial x_f}\left[D \frac{\partial C_f}{\partial x_f} + \frac{\dot{V}_l C_f}{\sigma A_s}\right] - \left(\frac{1 - \alpha}{\alpha}\right) \rho_{fi.} \frac{\partial M}{\partial t}. \qquad (48)$$

2. The Energy Equation

The energy which enters and leaves the control volume shown in Figure 3 through the various surfaces will now be established. The energy entering due to diffusion through the left-hand face of the control volume can be written as:

$$E_{in_{dif.}} = \dot{m}_{dif.}\, d\alpha H \delta t \left[c_{p_v} (T_f - T_{ref}) + \lambda\right] \qquad (49)$$

and the energy leaving through the right-hand face by:

$$E_{out_{dif.}} = E_{in_{dif.}} + \frac{\partial}{\partial x_f} E_{in_{dif.}} \delta x_f; \qquad (50)$$

thus, the net energy inflow, due to diffusion only, can be expressed as:

$$\Delta E_{dif.} = E_{in_{dif.}} - E_{out_{dif.}}$$

$$= -\frac{\partial}{\partial x_f}\left[\dot{m}_{dif.} \left(c_{p_v} (T_f - T_{ref}) + \lambda\right)\right] d\alpha H \delta t\, \delta x_f. \qquad (51)$$

The energy entering the control volume through bulk (or forced) flow is:

$$E_{in_{for.}} = d\alpha H\delta t \left[c_{p_v} (T_f - T_{ref}) + \lambda\right] \dot{m}_{v_{for.}} \tag{52}$$

$$+ \dot{m}_{air_{for.}} \; d\alpha H\delta t \left[c_{p_{air}} (T_f - T_{ref})\right]$$

where $\dot{m}_{air_{for.}}$ represents the air mass flux $\left(= - \frac{\dot{V}_1 \rho air}{\alpha A_s}\right)$.

The energy leaving the control volume due to bulk flow can be expressed as:

$$E_{out_{for.}} = E_{in_{for.}} + \frac{\partial}{\partial x_f} E_{in_{for.}} \delta x_f. \tag{53}$$

Thus, the net inflow of energy due to the forced flow may be written as:

$$\Delta E_{for.} = E_{in_{for.}} - E_{out_{for.}} \tag{54}$$

$$= - \frac{\partial}{\partial x_f} \left\{ \dot{m}_{v_{for.}} \left[c_{p_v} (T_f - T_{ref}) + \lambda\right] + \dot{m}_{air_{for.}} c_{p_{air}} \cdot (T_f - T_{ref}) \right\} d\alpha H \delta t \delta x_f.$$

The energy entering by conduction processes may be expressed as:

$$E_{in_{cond.}} = -k_f \frac{\partial T_f}{\partial x_f} Hd\delta t \tag{55}$$

where k_f represents the local fabric conductivity (Btu/ft/sec/°F). The energy leaving the control volume, through use of Taylor's expansion theorem, may be written as:

$$E_{out_{cond}} = E_{in_{cond}} + \frac{\partial}{\partial x_f} E_{in_{cond}} \delta x_f \tag{56}$$

Thus, the net inflow may be expressed as:

$$\Delta E_{cond.} = \frac{\partial}{\partial x_f}\left(k_f \frac{\partial T_f}{\partial x_f}\right) H d \delta x_f \delta t. \qquad (57)$$

An expression which gives the instantaneous value of the thermal conductivity of the entire fabric is derived and presented in Appendix B. It will be noted that the thermal conductivity depends on several parameters and variables including the conductivity of the fibres, liquid, and air, the density of the fibres and liquid, the dimensionless absorbed water vapor mass, and the porosity of the fabric.

The total energy contained within the control volume at any instant may be expressed as:

$$E = (c_p\rho)_{air}(T_f - T_{ref})\alpha H \delta x_f d + C_f\left[c_{p_v}(T_f - T_{ref}) + \lambda\right]\alpha H \delta x_f d$$

$$+ \rho_{fi.}(1-\alpha) H d \delta x_f c_{fi.}(T_f - T_{ref}) + m_{fi.}\frac{m_\ell}{m_{fi.}} c_\ell (T_f - T_{ref})$$

or, with $m_{fi.} = \rho_{fi.}\delta x_f d(1-\alpha)H$ and $\frac{m_\ell}{m_{fi.}} = M$, this becomes:

$$E = \left\{\left[\alpha(c_p\rho)_{air} + \alpha c_{p_v} C_f + (1-\alpha)\rho_{fi.} c_{fi.} + (1-\alpha)\rho_{fi.} c_\ell M\right] \cdot (T_f - T_{ref}) + \alpha\lambda C_f\right\} H d \delta x_f . \qquad (58)$$

In a time increment δt, this energy increases by an amount:

$$\delta E = \frac{\partial E}{\partial t}\delta t \qquad (59)$$

$$= \frac{\partial}{\partial t}\left\{\left[\alpha(c_p\rho)_{air} + \alpha c_{p_v} C_f + (1-\alpha)\rho_{fi.}(c_{fi.} + c_\ell M)\right](T_f - T_{ref}) + \alpha\lambda C_f\right\} H d \delta x_f \delta t.$$

The statement of conservation of energy may be expressed mathematically as:

$$\delta E = \Delta E_{dif.} + \Delta E_{for.} + \Delta E_{cond.} \tag{60}$$

Substituting Equations (51), (54), (57), and (59) into Equation (60) yields:

$$\frac{\partial}{\partial t}\left\{\left[\alpha(c_{p_{air}}\rho_{air} + c_{p_v}C_f) + (1-\alpha)\rho_{fi.}\,(c_{fi.} + c_\ell M)\right](T_f - T_{ref}) + \alpha\lambda C_f\right\}$$

$$= -\frac{\partial}{\partial x_f}\left\{\dot{m}_{dif.}\left[c_{p_v}(T_f - T_{ref}) + \lambda\right]\right\}\alpha \tag{61}$$

$$-\frac{\partial}{\partial x_f}\left\{\dot{m}_{v_{for.}}\left[c_{p_v}(T_f - T_{ref}) + \lambda\right] + \dot{m}_{air_{for.}}\left[c_{p_{air}}(T_f - T_{ref})\right]\right\}\alpha$$

$$+\frac{\partial}{\partial x_f}\left[k_f\frac{\partial T_f}{\partial x_f}\right] .$$

Introducing relations (39), (40), and $\dot{m}_{air_{for.}} = -\dfrac{\dot{V}_l\,\rho_{air}}{\alpha A_s}$ into this equation yields:

$$\frac{\partial}{\partial t}\left\{\left[\alpha(c_{p_{air}}\rho_{air} + c_{p_v}C_f) + (1-\alpha)\rho_{fi.}\,(c_{fi.} + c_\ell M)\right](T_f - T_{ref})\right\}$$

$$+\alpha\lambda\left[\frac{\partial C_f}{\partial t} - \frac{\partial}{\partial x_f}\left(D\frac{\partial C_f}{\partial x_f}\right) - \frac{\partial}{\partial x_f}\left(\frac{\dot{V}_l C_f}{\alpha A_s}\right)\right] \tag{62}$$

$$= \alpha\frac{\partial}{\partial x_f}\left[c_{p_v}\left(D\,\frac{\partial C_f}{\partial x_f}\right)(T_f - T_{ref})\right] + \alpha\frac{\partial}{\partial x_f}\left[\frac{\dot{V}_l C_f}{\alpha A_s}\,c_{p_v}(T_f - T_{ref})\right]$$

$$+\alpha\frac{\partial}{\partial x_f}\left[c_{p_{air}}\,\frac{\dot{V}_l\,\rho_{air}}{\alpha A_s}\,(T_f - T_{ref})\right] + \frac{\partial}{\partial x_f}\left[k_f\frac{\partial T_f}{\partial x_f}\right].$$

In view of the vapor transport equation, the second group of terms on the left side of the above equation may be replaced by:

$$\sigma\lambda\left[\frac{\partial C_f}{\partial t} - \frac{\partial}{\partial x_f}\left(D\frac{\partial C_f}{\partial x_f}\right) - \frac{\partial}{\partial x_f}\left(\frac{\dot{V}_l C_f}{\alpha A_s}\right)\right] = -\sigma\lambda\left(\frac{1-\alpha}{\sigma}\right)\rho_{fi.}\frac{\partial M}{\partial t}$$

and, dividing the resulting expression by σ, one obtains:

$$\frac{\partial}{\partial t}\left\{\left[(c_p\rho)_{air} + c_{p_v}C_f\right] + \left(\frac{1-\alpha}{\alpha}\right)\rho_{fi.}\,(c_{fi.} + c_\ell M)\right\}\left\{T_f - T_{ref}\right\}$$

$$= \left(\frac{1-\alpha}{\alpha}\right)\lambda\rho_{fi.}\frac{\partial M}{\partial t} + \frac{\partial}{\partial x_f}\left[\left(D\frac{\partial C_f}{\partial x_f}\right)c_{p_v}(T_f - T_{ref}) + \frac{\dot{V}_l C_f}{\alpha A_s}c_{p_v}(T_f - T_{ref})\right]$$

$$+ \frac{\partial}{\partial x_f}\left[(c_p\rho)_{air}\frac{\dot{V}_l}{\alpha A_s}(T_f - T_{ref})\right] + \frac{\partial}{\partial x_f}\left[\frac{k_f}{\sigma}\frac{\partial T_f}{\partial x_f}\right]. \qquad (63)$$

The derivative on the left side of this relation can be expanded to:

$$\left[(c_p\rho)_{air} + c_{p_v}C_f + \frac{1-\alpha}{\sigma}\rho_{fi.}\,(c_{fi.} + c_\ell M)\right]\frac{\partial T_f}{\partial t}$$

$$+ (T_f - T_{ref})\left[c_{p_v}\frac{\partial C_f}{\partial t} + \left(\frac{1-\alpha}{\sigma}\right)\rho_{fi.}\,c_\ell\,\frac{\partial M}{\partial t}\right]$$

and, using the vapor transport equation, one obtains:

$$\text{L. S.} = \left[(c_p\rho)_{air} + c_{p_v}C_f + \frac{1-\alpha}{\alpha}\rho_{fi.}\,(c_{fi.} + c_\ell)\,M\right]\frac{\partial T_f}{\partial t}$$

$$+ (T_f - T_{ref})\left\{\left(\frac{1-\alpha}{\alpha}\right)\rho_{fi.}\,c_\ell\frac{\partial M}{\partial t} + c_{p_v}\left[\frac{\partial}{\partial x_f}\left(D\frac{\partial C_f}{\partial x_f}\right)\right.\right. \qquad (64)$$

$$\left.\left. + \frac{\partial}{\partial x_f}\left(\frac{\dot{V}_l C_f}{\alpha A_s}\right) - \left(\frac{1-\alpha}{\sigma}\right)\rho_{fi.}\frac{\partial M}{\partial t}\right]\right\}.$$

Substituting relation (64) into (63) yields:

$$\left[(c_p\rho)_{air} + c_{p_v} C_f + \left(\frac{1-\alpha}{\alpha}\right)\rho_{fi.}\,(c_{fi.} + c_\ell M)\right]\frac{\partial T_f}{\partial t}$$

$$= \lambda\left(\frac{1-\alpha}{\alpha}\right)\rho_{fi.}\,\frac{\partial M}{\partial t} + \frac{\partial}{\partial x_f}\left\{\left[D\,\frac{\partial C_f}{\partial x_f}\,c_{p_v} + \frac{\dot{V}_l\,c_{p_v}\,C_f}{\alpha A_s}\right](T_f - T_{ref})\right\}$$

$$+ \frac{\partial}{\partial x_f}\left[\frac{\dot{V}_l \rho_{air} c_{p_{air}}}{\alpha A_s}(T_f - T_{ref})\right] + \frac{\partial}{\partial x_f}\left(\frac{k_f}{\alpha}\frac{\partial T_f}{\partial x_f}\right) - (T_f - T_{ref})\frac{1-\alpha}{\alpha}\rho_{fi.}c_\ell\frac{\partial M}{\partial t} \tag{65}$$

$$- (T_f - T_{ref})c_{p_v}\frac{\partial}{\partial x_f}\left[D\,\frac{\partial C_f}{\partial x_f} + \frac{\dot{V}_l C_f}{\alpha A_s}\right] + (T_f - T_{ref})c_{p_v}\left(\frac{1-\alpha}{\alpha}\right)\rho_{fi.}\,\frac{\partial M}{\partial t}\ .$$

The second term on the right side may be expanded to give:

$$\text{second term on R.S.} = (T_f - T_{ref})c_{p_v}\frac{\partial}{\partial x_f}\left[D\,\frac{\partial C_f}{\partial x_f} + \frac{\dot{V}_l C_f}{\alpha A_s}\right]$$

$$+ c_{p_v}\left[D\,\frac{\partial C_f}{\partial x_f} + \frac{\dot{V}_l C_f}{\alpha A_s}\right]\frac{\partial T_f}{\partial x_f} \tag{66}$$

which, when substituted into Equation (65) yields:

$$\left[(c_p\rho)_{air} + c_{p_v} C_f + \left(\frac{1-\alpha}{\alpha}\right)\rho_{fi.}\,(c_{fi.} + c_\ell M)\right]\frac{\partial T_f}{\partial t}$$

$$= c_{p_v}\left[D\,\frac{\partial C_f}{\partial x_f} + \frac{\dot{V}_l C_f}{\alpha A_s}\right]\frac{\partial T_f}{\partial x_f} + (c_p\rho)_{air}\,\frac{\partial}{\partial x_f}\left[\frac{\dot{V}_l}{\alpha A_s}\right](T_f - T_{ref}) \tag{67}$$

$$+ \frac{\partial}{\partial x_f}\left[\frac{k_f}{\alpha}\frac{\partial T_f}{\partial x_f}\right] + \left(\frac{1-\alpha}{\alpha}\right)\rho_{fi.}\,\left[\lambda - (c_\ell - c_{p_v})(T_f - T_{ref})\right]\frac{\partial M}{\partial t}\ .$$

3. The Dimensionless Absorbed Water Vapor (M)

The absorbed water vapor can be shown to depend on the two variables C_f and T_f. Mathematically this is expressed as:

$$M = M(C_f, T_f)$$

where it is assumed M is always in equilibrium with the surrounding water vapor concentration and temperature. A very complete discussion of the validity of this assumption, together with experimental verification, is presented in a paper by King and Cassie.[4] Since M is now expressed as a function of two dependent variables the derivative of M with respect to any independent variable may be expanded in the following manner:

$$\frac{\partial M}{\partial(\ )} = \frac{\partial M}{\partial C_f}\frac{\partial C_f}{\partial(\ )} + \frac{\partial M}{\partial T_f}\frac{\partial T_f}{\partial(\ )} \quad .$$

If the following definitions are now made:

$$\sigma = \frac{\partial M}{\partial C_f}; \quad \omega = -\frac{\partial M}{\partial T_f} \tag{68}$$

one may rewrite the preceding expressions as:

$$\frac{\partial M}{\partial(\ )} = \sigma\frac{\partial C_f}{\partial(\ )} - \omega\frac{\partial T_f}{\partial(\ )} \quad . \tag{69}$$

Substituting this expansion of derivatives into the mass balance, Equation (48) gives:

$$\left[1 + \frac{1-\alpha}{\alpha}\rho_{fi.}\sigma\right]\frac{\partial C_f}{\partial t} - \left(\frac{1-\alpha}{\alpha}\right)\rho_{fi.}\,\omega\frac{\partial T_f}{\partial t} = \frac{\partial}{\partial x_f}\left[D\frac{\partial C_f}{\partial x_f} + \frac{\dot{V}_1 C_f}{\alpha A_s}\right] \tag{70}$$

and Equation (67) may also be rewritten as:

$$\left\{(c_p\rho)_{air} + c_{p_v} C_f + \left(\frac{1-\sigma}{\sigma}\right)\rho_{fi.} c_{fi.} + c_\ell M + \omega\left[\lambda - (c_\ell - c_{p_v})(T_f - T_{ref})\right]\right\} \frac{\partial T_f}{\partial t}$$

$$- \left(\frac{1-\sigma}{\sigma}\right)\rho_{fi.}\left[\lambda - (c_\ell - c_{p_v})(T_f - T_{ref})\right] \frac{\partial C_f}{\partial t} = c_{p_v}\left[D\frac{\partial C_f}{\partial x_f} + \frac{\dot{V}_l C_f}{\sigma A_s}\right]\frac{\partial T_f}{\partial x_f}$$

$$+ \frac{\partial}{\partial x_f}\left[(c_p\rho)_{air}\frac{\dot{V}_l}{\sigma A_s}(T_f - T_{ref})\right] + \frac{\partial}{\partial x_f}\left[\frac{k_f}{\sigma}\frac{\partial T_f}{\partial x_f}\right] \quad . \qquad (71)$$

The evaluation of sigma and omega is presented in Appendix B.

4. The Initial and Boundary Conditions

The initial condition for the fabric temperature distribution and vapor concentration distribution shall be written as:

$$\text{at } t = 0 \qquad T_f = T_{f_i}(x_f)$$

$$C_f = C_{f_i}(x_f) \quad .$$

The boundary condition for the fabric at the fabric outer surface ($x_f = 0$) is obtained by equating the vapor mass entering the surface plane from the interior of the fabric to the vapor mass leaving the surface plane into the external air environment. The energy boundary condition is similarly obtained by equating the energy conducted into the surface of the fabric from the interior to the energy leaving the surface of the fabric into the surrounding ambient air. These two physical facts may be expressed in mathematical terms by the relations:

$$\text{at } x_f = 0 \qquad \left(D \frac{\partial C_f}{\partial x_f}\right)_{x_f = 0} = K_o(C_{f_o} - C_\infty)$$

$$\left(k_f \frac{\partial T_f}{\partial x_f}\right)_{x_f = 0} = U_o(T_{f_o} - T_\infty) \quad . \tag{72}$$

In a similar manner, the boundary conditions for the fabric inner surface may be expressed as:

$$\text{at } x_f = L_f \qquad \left(D \frac{\partial C_f}{\partial x_f}\right)_{x_f = L_f} = - K_1(C_{f_1} - C_a)$$

$$\left(k_f \frac{\partial T_f}{\partial x_f}\right)_{x_f = L_f} = - U_1(T_{f_1} - T_a) \quad . \tag{73}$$

D. The Mathematical Model for the Air Gap

A schematic diagram of the air gap control volume is presented in Figure 4. The mass of water vapor and energy entering or leaving the control volume are designated by m and E, respectively. In the following derivations, it should be noted that m and E represent the mass and energy per unit time which enter the control volume from the entire skin surface and leave through the entire fabric surface (that is, not on a unit area basis).

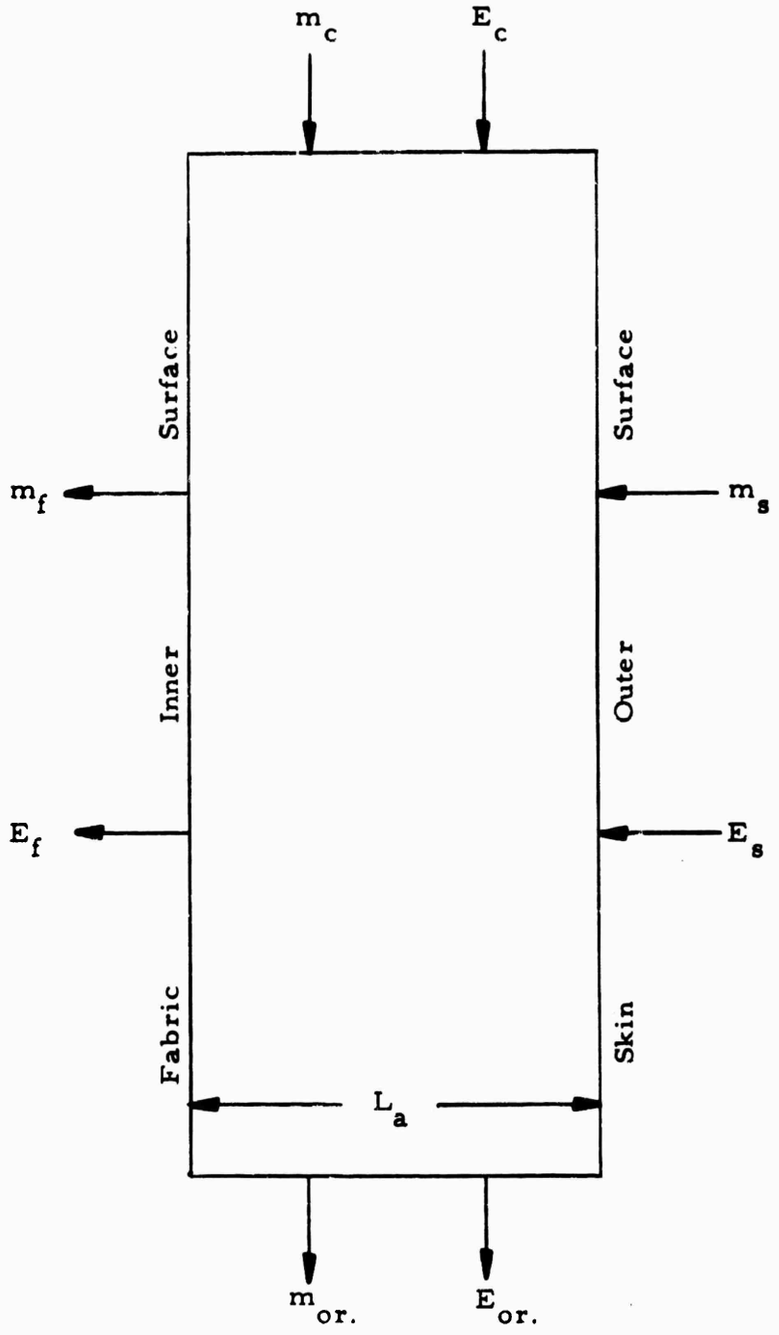

Figure 4. The Air Gap Control Volume

1. The Skin Surface

The mass of water vapor entering the control volume from the entire skin surface per unit time can be expressed as:

$$m_s = \dot{m}_s A_s \tag{74}$$

where:

m_s = entering water vapor mass from the skin (lb/sec)

A_s = total skin surface area (ft^2)

$\dot{m}_s$ = vapor transport from the skin surface ($lb/ft^2/sec$).

The enthalpy of this water vapor may be expressed as:

$$h_s = c_{p_v}(T_{s_o} - T_{ref}) + \lambda \ . \tag{75}$$

The energy entering from the skin surface is comprised of this enthalpy plus the heat transfer due to conduction in the air at the skin surface. The latter has been expressed as:

$$q_{cond.} = U_s(T_{s_o} - T_a) \tag{76}$$

Thus, the total energy entering per unit time from the skin surface may be expressed as:

$$E_s = m_s h_s + q_{cond.} A_s$$

or, using Equations (75) and (76):

$$E_s = \dot{m}_s A_s \left[c_{p_v}(T_{s_o} - T_{ref}) + \lambda \right] + U_s A_s (T_{s_o} - T_a) \ . \tag{77}$$

2. The Compressor

It will be assumed that forced ventilation is occurring and that a compressor supplies a volumetric flow rate described by:

$$\dot{V} = \dot{V}_1 + \dot{V}_2 \tag{78}$$

where:

$\dot{V}$ = total volumetric flow rate (ft^3/sec)

$\dot{V}_1$ = volumetric flow rate which passes through the pores of the fabric (ft^3/sec)

$\dot{V}_2$ = volumetric flow rate which passes through auxiliary vents or orifices (ft^3/sec).

The mass of water vapor entering from the compressor can be expressed as:

$$m_c = \dot{V}C_c = (\dot{V}_1 + \dot{V}_2)C_c \quad . \tag{79}$$

The energy entering from the compressor can be expressed as:

$$E_c = C_c \dot{V} h_{v_c} + \dot{V} h_{air_c} \rho_{air} \tag{80}$$

where:

h_{v_c} = $c_{p_v}(T_c - T_{ref}) + \lambda$ = enthalpy of water vapor at the the compressor (Btu/lb)

h_{air_c} = $c_{p_{air}}(T_c - T_{ref})$ = enthalpy of the air at the compressor (Btu/lb).

It will be assumed that the air density is constant throughout the air gap, fabric pores, compressor, and ambient air. With the definitions for enthalpy as given above, one may now rewrite Equation (80) as:

$$E_c = (\dot{V}_1 + \dot{V}_2)\left[(C_c c_{p_v} + c_{p_{air}} \rho_{air})(T_c - T_{ref}) + C_c \lambda\right] . \quad (81)$$

3. The Orifice

It shall be assumed that the air and water vapor leaving through the orifices is at the average air gap temperature (T_a) and the concentration (C_a). Thus, the water vapor leaving per unit time may be written as:

$$m_{or.} = C_a \dot{V}_2 . \quad (82)$$

The energy leaving can be written as:

$$E_{or.} = \dot{V}_2\left[(c_{p_v} C_a + c_p \rho_{air})(T_a - T_{ref}) + \lambda C_a\right] . \quad (83)$$

4. The Fabric Inner Surface

The water vapor leaves the control volume through the fabric inner surface by both diffusion and forced bulk flow. The total mass leaving by diffusion will be expressed as:

$$m_{f_{dif.}} = - K_1 A_s (C_{f_1} - C_a) \quad (84)$$

where:

K_1 = mass transfer coefficient at the fabric inner surface (ft/sec)

C_{f_1} = vapor concentration at the fabric inner surface (lb/ft^3).

The mass of vapor leaving due to forced flow is:

$$m_{f_{for.}} = \dot{V}_1 C_{f_1} \quad . \tag{85}$$

The energy leaving due to conduction and radiation at the fabric surface is expressed as:

$$E_{f_1} = - U_1 A_s (T_{f_1} - T_a) \tag{86}$$

where:

U_1 = heat transfer coefficient at the fabric inner surface (Btu/ft^2/sec/°F)

T_{f_1} = fabric inner surface temperature (°F).

The energy removed with the water vapor by diffusion can be expressed as:

$$\begin{aligned} E_{f_2} &= m_{f_{dif.}} \left[c_{p_v} (T_{f_1} - T_{ref}) + \lambda \right] \\ &= - K_1 A_s (C_{f_1} - C_a) \left[c_{p_v} (T_{f_1} - T_{ref}) + \lambda \right] \end{aligned} \tag{87}$$

where we have assumed the vapor to leave at a concentration C_{f_1} and the temperature (T_{f_1}).

The energy removed by the forced flow can be expressed as:

$$E_{f_3} = \dot{V}_1 \left[(c_{p_v} C_{f_1} + c_{p_{air}} \rho_{air})(T_{f_1} - T_{ref}) + \lambda C_{f_1} \right] \quad . \tag{88}$$

5. The Mass and Energy Balance Equations

The mass of water vapor contained within the air gap can be expressed as:

$$m = C_a A_s L_a \tag{89}$$

and the energy within the air gap by:

$$E = \left[(c_{p_v} C_a + c_{p_{air}} \rho_{air})(T_a - T_{ref}) + \lambda C_a \right] A_s L_a \, . \tag{90}$$

Conservation of mass and energy require that:

$$\begin{aligned} \frac{dm}{dt} &= m_s + m_c - m_{or.} - m_{f_{dif.}} - m_{f_{for.}} \\ \frac{dE}{dt} &= E_s + E_c - E_{or.} - E_{f_1} - E_{f_2} - E_{f_3} \, . \end{aligned} \tag{91}$$

Utilizing the relations previously given for the quantities appearing in Equation (91), one may now write the mass balance and energy equations as:

$$A_s L_a \frac{dC_a}{dt} = A_s \dot{m}_s + (\dot{V}_1 + \dot{V}_2) C_c - C_a \dot{V}_2 + K_1 A_s (C_{f_1} - C_a) - \dot{V}_1 C_{f_1} \, . \tag{92}$$

and

$$A_s L_a \frac{d}{dt}\left[(c_{p_v} C_a + c_{p_{air}} \rho_{air})(T_a - T_{ref}) + \boxed{\lambda C_a}\right]$$

$$= \dot{m}_s A_s c_{p_v} (T_{s_o} - T_{ref}) + \boxed{\dot{m}_s A_s \lambda} + U_s A_s (T_{s_o} - T_a) \qquad (93)$$

$$+ (\dot{V}_1 + \dot{V}_2)\left[(c_{p_v} C_c + C_{p_{air}} \rho_{air})(T_c - T_{ref}) + \boxed{\lambda C_c (\dot{V}_1 + \dot{V}_2)} + U_1 A_s (T_{f_1} - T_a)\right.$$

$$- \dot{V}_2 (c_{p_v} C_a + c_{p_{air}} \rho_{air})(T_a - T_{ref}) - \boxed{\dot{V}_2 \lambda C_a} + K_1 A_s (C_{f_1} - C_a) c_{p_v} (T_{f_1} - T_{ref})$$

$$\left. + \boxed{K_1 A_s (C_{f_1} - C_a)\lambda} - \dot{V}_1 (c_{p_v} C_{f_1} + c_{p_{air}} \rho_{air})(T_{f_1} - T_{ref}) - \boxed{\dot{V}_1 \lambda C_{f_1}}\right] .$$

In view of the mass transfer Equation (92), the terms in Equation (93) set off in squares cancel one another.

Expanding the derivative on the left side of Equation (93), one obtains:

$$\text{L.S.} = (c_{p_v} C_a + c_{p_{air}} \rho_{air}) \frac{dT_a}{dt} + c_{p_v} (T_a - T_{ref}) \frac{dC_a}{dt} . \qquad (94)$$

Substitution of Equation (92) into (94), and the resulting expression into Equation (93) yields, after considerable algebraic manipulations:

$$\left[c_{p_v} C_a + c_{p_{air}} \rho_{air} \right] \frac{dT_a}{dt}$$

$$= \frac{\dot{m}_s c_{p_v}}{L_a} (T_{s_o} - T_a) + \frac{K_1 c_{p_v}}{L_a} (C_{f_1} - C_a)(T_{f_1} - T_a)$$

$$+ \frac{U_s}{L_a} (T_{s_o} - T_a) + \frac{U_1}{L_a} (T_{f_1} - T_a) \qquad (95)$$

$$+ \frac{\dot{V}_1 c_{p_v}}{A_s L_a} \left[C_c (T_c - T_a) - C_{f_1} (T_{f_1} - T_a) \right] + \frac{\dot{V}_2 c_{p_v}}{A_s L_a} C_c (T_c - T_a)$$

$$+ \frac{\dot{V}_1}{A_s L_a} c_{p_{air}} \rho_{air} (T_c - T_{f_1}) + \frac{\dot{V}_2}{A_s L_a} c_{p_{air}} \rho_{air} (T_c - T_a) .$$

The vapor transport equation (92) may also be rewritten as:

$$\frac{dC_a}{dt} = \frac{\dot{m}_s}{L_a} + \frac{K_1}{L_a} (C_{f_1} - C_a) + \frac{\dot{V}_1}{A_s L_a} (C_c - C_{f_1}) + \frac{\dot{V}_2}{A_s L_a} (C_c - C_a) . \qquad (96)$$

E. The Simplified Governing Equations

It is apparent from the preceding section that a large number of complicated coupled differential equations must be solved to obtain a complete description of the heat and mass transfer processes through a fabric-air gap-skin system. For the sake of completeness, the derivation of the various governing equations has been made very complete in the preceding three sections. Examination of these equations indicates that various numerical methods of solution may be employed in their present form.

However, one may deduce from various order of magnitude analyses that certain terms in some of the governing equations are entirely negligible compared with the remaining terms. Thus, the inclusion of such terms (or exclusion) will not significantly affect the results of any computer study.

1. Simplifying Assumptions for the Skin

An examination of the governing equations for energy transport through the various layers of the skin structure does not reveal any terms which may be safety disregarded in a fairly complete analysis. Consequently, the equations for the skin portion of the complete structure, as presented in Section II-B, must still be retained and used in a numerical analysis.

2. Simplifying Assumptions for the Fabric

It is known that the diffusion coefficient for water vapor in air depends to a certain degree on the air temperature and very little upon the air pressure. To maintain a reasonably simple mathematical model for the vapor diffusion through the fabric, it shall be assumed that the diffusion coefficient remains constant with time. For these initial studies, attention will be directed only at situations where the volumetric flow rate through the orifices and the porous fabric remains constant with time and, accordingly, it will be assumed at this point that V_1 and V_2 are constant.

Examination of the energy equation for the fabric reveals that for most physically realistic systems the heat capacity ($c_p \rho$) of the air and water vapor are negligible compared with the heat capacity of the fibers and liquid water absorbed by the fibers. Also, the product of the specific heat of the liquid minus the specific heat of the vapor multiplied by the

difference between the fabric temperature and the reference temperature can be neglected in the energy equation in comparison with the heat of vaporization of water. Utilizing the above discussed assumptions and simplifications, the water vapor transport and energy transport equations through the fabric structure may be simplified to the following forms:

$$\left[1 + \left(\frac{1-\alpha}{\alpha}\right)\rho_{fi}\,\sigma\right]\frac{\partial C_f}{\partial t} - \left(\frac{1-\alpha}{\alpha}\right)\rho_{fi}\,\omega\,\frac{\partial T_f}{\partial t} = D\,\frac{\partial^2 C_f}{\partial x_f^2} + \frac{\dot{V}_l}{\alpha A_s}\,\frac{\partial C_f}{\partial x_f}$$

and

$$\left(\frac{1-\alpha}{\alpha}\right)\rho_{fi}\left[c_{f_i} + c_l M + \lambda\omega\right]\frac{\partial T_f}{\partial t} - \left(\frac{1-\alpha}{\alpha}\right)\rho_{fi}\,\lambda\sigma\,\frac{\partial C_f}{\partial t}$$

$$= \frac{\partial}{\partial x_f}\left[\frac{k_f}{\sigma}\,\frac{\partial T_f}{\partial x_f}\right] + \left(c_{p_v} C_f + c_{p_{air}}\rho_{air}\right)\frac{\dot{V}_l}{\alpha A_s}\,\frac{\partial T_f}{\partial x_f}\ .$$

The initial and boundary conditions for the fabric cannot be further simplified and are reproduced below from Section II-B.

$$\text{at } t = 0 \qquad T_f = T_{f_1}(x_f); \quad C_f = C_{f_1}(x_f)$$

$$\text{at } x_f = 0 \qquad \left(D\,\frac{\partial C_f}{\partial x_f}\right)_{x_f = 0} = K_o(C_{f_o} - C_\infty)$$

$$\left(k_f\,\frac{\partial T_f}{\partial x_f}\right)_{x_f = 0} = U_o(T_{f_o} - T_\infty)$$

$$\text{at } x_f = L_f \qquad \rho \left(D \frac{\partial C_f}{\partial x_f} \right)_{x_f = L_f} = - K_1 (C_{f_1} - C_a)$$

$$\left(k_f \frac{\partial T_f}{\partial x_f} \right)_{x_f = L_f} = - U_1 (T_{f_1} - T_a) .$$

3. Simplifying Assumptions for the Air Gap

The vapor transport equation through the air gap cannot be further simplified from that in the preceding section.. However, examination of the temperature distribution in the air gap (or energy equation) indicates that several terms may be neglected in comparison with others. In particular, all terms which represent the sensible energy carried into and out of the air gap by diffusion processes are very small in comparison with the conduction heat transfer rates as well as the bulk flow or forced ventilation transfer rates. Neglecting such terms, the energy transport equation through the air gap may be simplified to the following form:

$$(c_{p_v} C_a + c_{p_{air}} \rho_{air}) \frac{dT_a}{dt} = \frac{U_s}{L_a} (T_{s_o} - T_a) + \frac{U_1}{L_a} (T_{f_1} - T_a)$$

$$+ \frac{\dot{V}_1}{A_s L_a} c_{p_v} \left[C_c (T_c - T_a) - C_{f_1} (T_{f_1} - T_a) \right] + \frac{\dot{V}_1}{A_s L_a} c_{p_v} C_c (T_c - T_a)$$

$$+ \frac{\dot{V}_1}{A_s L_a} (c_p \rho)_{air} (T_c - T_{f_1}) + \frac{\dot{V}_2}{A_s L_a} (c_p \rho)_{air} (T_c - T_a) .$$

The solution of the complete set of differential equations is presented in Appendix C.

III. EXPERIMENTAL STUDIES

A. General

Before the experiments were initiated the parameters to be varied were isolated and the variation increments were selected. A tabulation of the parameters and test increments is presented in Table 1. It can be immediately realized that a systematic and complete study of all the tabulated parameters and increments would result in a research program beyond the scope of the present study. A reasonable number of test configurations were selected, which assisted by proper evaluation and interpretation resulted in an overall understanding of the effects of the many variations involved. To obtain the best results it is essential that very careful control of the test parameters be exercised, which requires considerable time for all variables to be stabilized. For instance, approximately eight profiles of total temperature or velocity require a complete working day of eight hours. Measurements of simulator heat and water vapor loss require even more time, as the attainment of steady-state conditions is essential.

All measurements were performed utilizing a standard 8.8-oz cotton sateen fabric which has a porosity of 12 cfm/ft^2 at 1/2 in. H_2O. This particular fabric was chosen because the largest amount of experimental data pertaining to fabric physical and thermal properties has been obtained for this particular type. Further, the theoretical studies presented in Reference 1 and Section II of this report utilized thermal and physical constants representative of this type of material. Future measurements are planned utilizing a fabric of higher porosity and one of considerably lower porosity.

Most measurements were performed with the skin simulator surface temperature maintained at 100°F. A selected number of tests were performed with the surface at dry equilibrium temperature (no heat or sweat generation). Mean and fluctuating velocities and total temperature

Table 1. Variation of Parameters and Test Items

Items to be Measured

Temperature profiles
Mean and fluctuating velocity profiles
Humidity profiles
Skin simulator heat loss
Skin simulator moisture loss

Parameters to be Varied	Range of Variation Increments
Skin simulator conditions	
Surface temperature	Wet bulb, dry recovery, 100°F
Moisture	Wet, dry
Fabric porosity	Low, medium, high
External airflow conditions	
Temperature	Low, room ambient, 100°F
Humidity	Dry, room ambient, saturated
Turbulence level	Laminar, turbulent, transitional
Velocity (ft/sec)	0, 5, 10, 15, 20, 25
Ventilating airflow conditions	
Temperature	Low, room ambient, 100°F
Humidity	Dry, room ambient, saturated
Turbulence level	Laminar, turbulent, transitional
Velocity (ft/sec)	0, 5, 10, 15, 20, 25
Probing stations (x/H)	0.25, 0.50, 0.75, 1.00
Fabric spacings (in.)	0.1, 0.2, 0.4, 0.6, 0.8, 1.0

profiles were measured for various combinations of external and internal ventilating flows and fabric spacings. The profiles were measured at a probing station located at the middle of the rear half of the skin simulator model. These experimental data, combined with empirical predictions of the boundary layer growth, allow the attainment of a fairly good understanding of the boundary layer characteristics over the skin simulator surface.

The large bulk of experiments was concerned with measurements of heat and mass transfer rates for various ventilating flow rates and fabric spacings. These data were obtained by measuring the water losses and electrical power dissipated by the simulator. Care was taken to insure that a proper accounting of all internal and edge heat losses were obtained.

Probings of total temperature, mean and fluctuating velocities, and water vapor concentration in the air gap were obtained during the heat and water loss measurements.

Although the experimental configuration is as simple as can be obtained, several factors exist which tend to complicate the heat and mass transfer flow processes. It should be emphasized that the mathematical model was developed for conditions of one-dimensional flow. That is, it is assumed that conditions are not changing in the streamwise or spanwise directions. For various external and internal ventilating flow velocities, it is possible to change both the magnitude and sign of the pressure gradient across the fabric. For instance, when the internal ventilating flow static pressure is lower than the external, a cross flow of air through the fabric into the air gap is achieved. When the external pressure is lower, the reverse is true. In either case, the boundary layer developments are influenced by distributed blowing or suction in the streamwise direction.

It has been well established in previous experimental studies that the amount of heat and mass lost from a surface exposed to an airflow is a function of the ventilating flow Reynolds number. Of equal importance is the degree of free stream turbulence existing in the core of potential flow between the two boundary layers. This turbulence intensity, in addition to the wetted length, determines whether the flow will remain laminar or transide to a turbulent boundary layer.

B. Experimental Equipment, Techniques and Procedure

1. Equipment

a. Hot-Wire Equipment

(1) Anemometers and Accessory Equipment.- Mean and fluctuating flow velocities were measured with a Disa Model 55A01 constant temperature anemometer, whose nominal frequency response extends to 50 kc/sec. A panel meter indicates wire voltages to an accuracy of $\pm$ 1 percent. Velocity fluctuation data in the form of rms values were read on the Disa panel meter and on a Ballatine Model 320 true root-mean-square electronic voltmeter. Traces of the fluctuating velocities were recorded from a Tektronix Model 535 oscilloscope using a Polaroid camera. The Disa anemometer and associated equipment are shown in Figure 5, and a schematic drawing of the circuits is presented in Figure 6.

(2) Hot-Wire Probes.- A photograph of the type of hot-wire probe utilized for these studies is shown in Figure 7. It was designed to allow probings both close to the skin simulator surface and the fabric inner surface. The sensing element is a 0.2-mil diameter platinum-plated tungsten wire soldered to two needle supports.

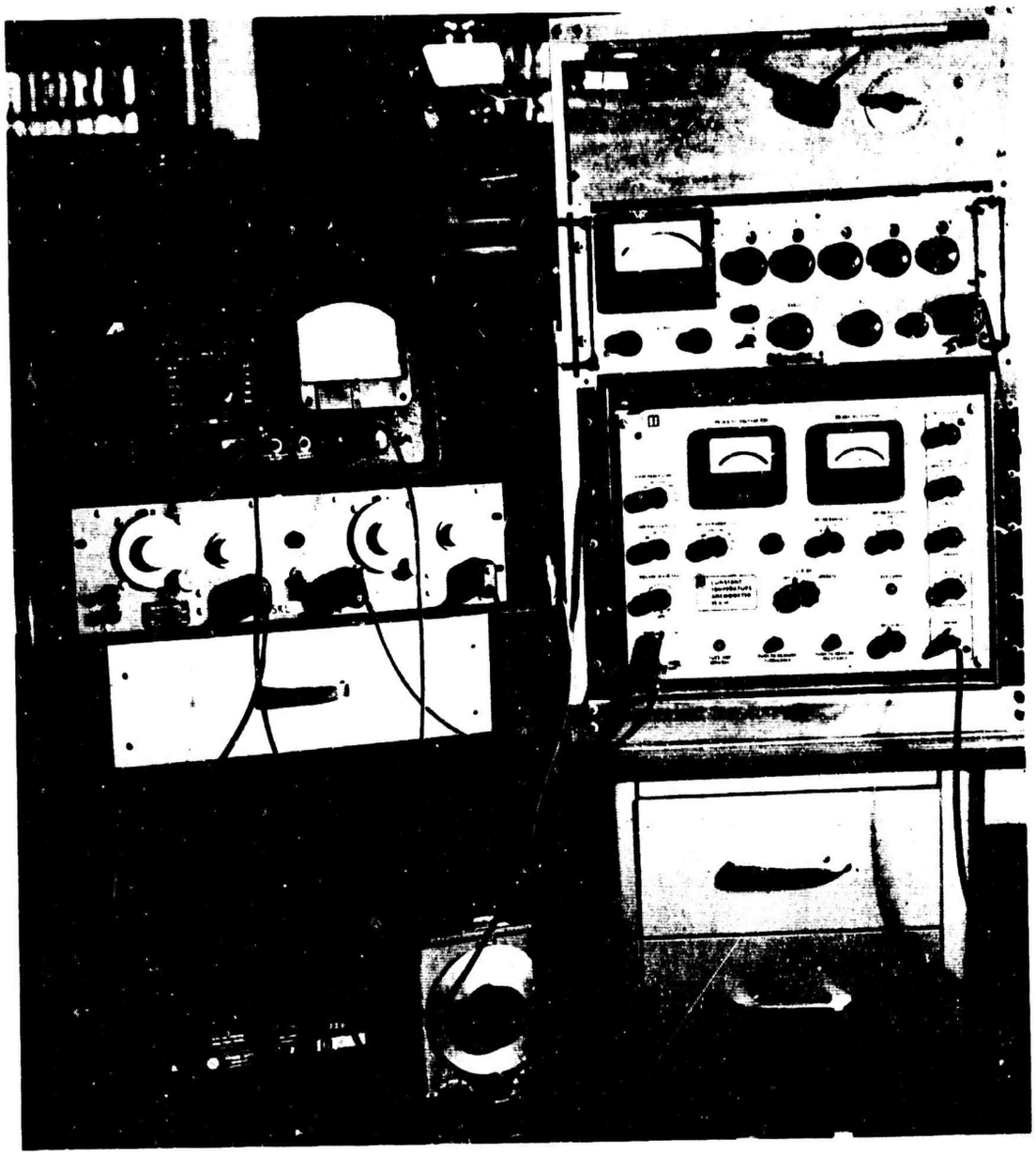

Figure 5. Hot-Wire Anemometer and Accessory Equipment

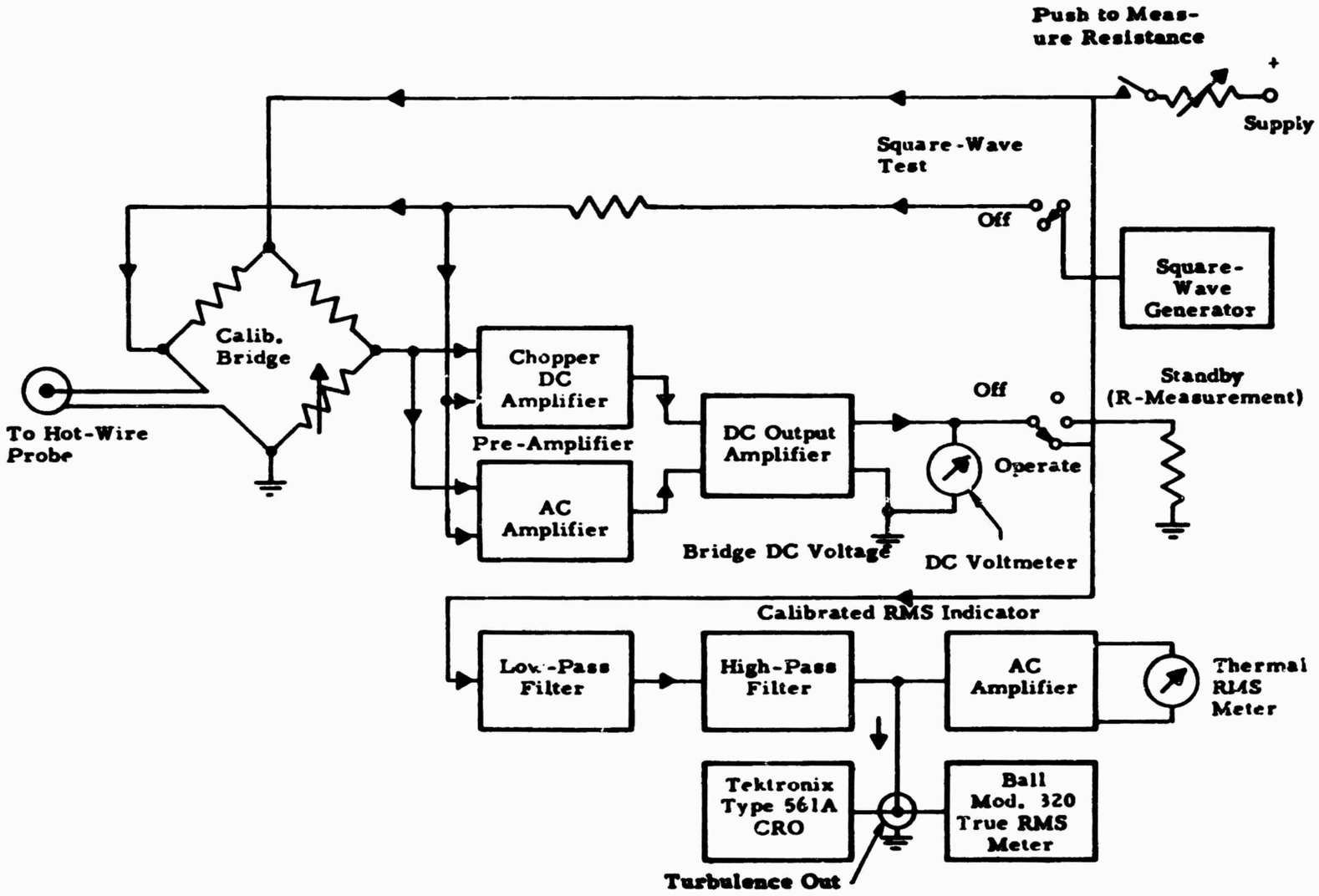

Figure 6. Block Diagram of DISA Constant-Temperature Anemometer and Accessory Equipment

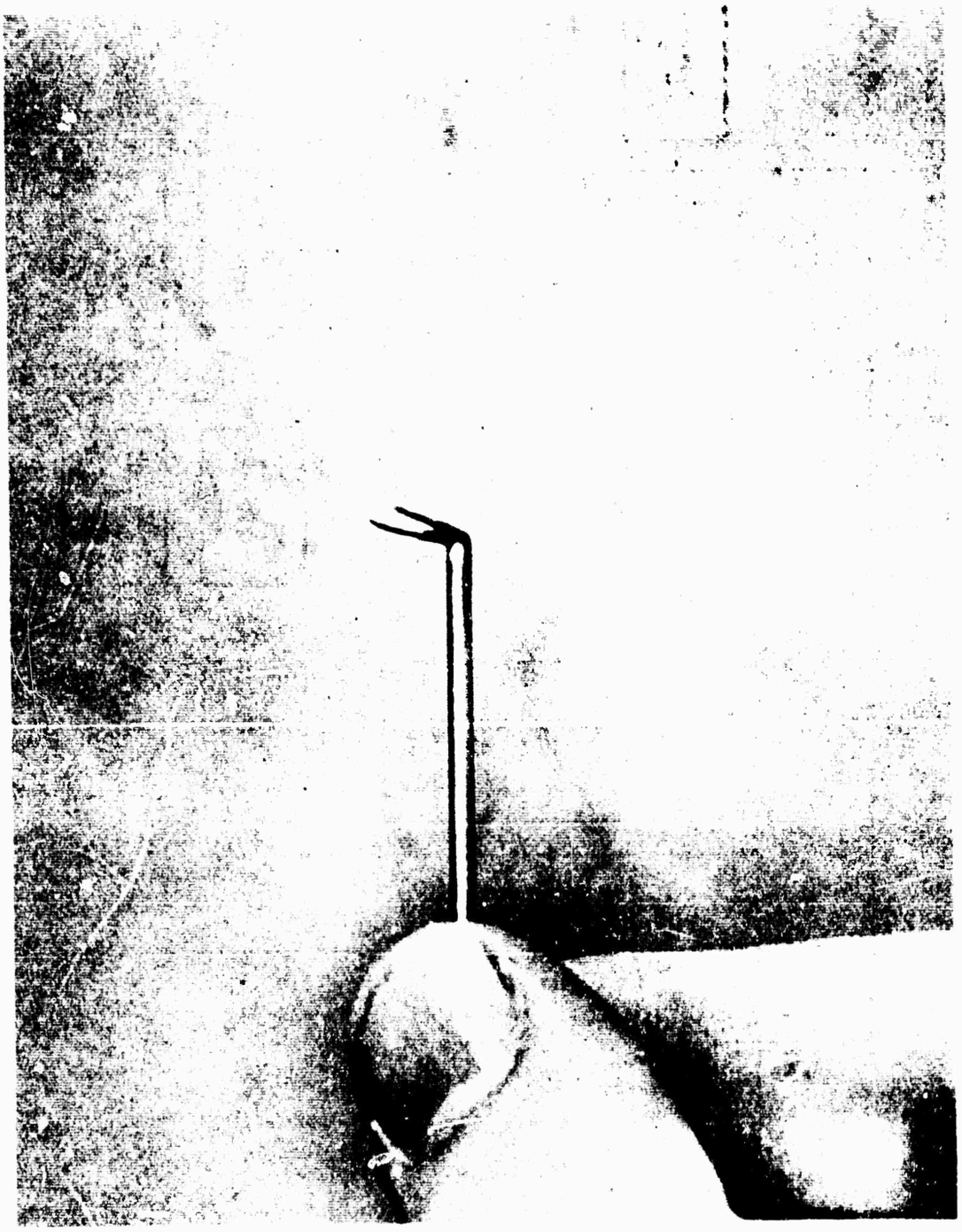

Figure 7. Hot-Wire Probe

b. Temperature Measuring Equipment

Skin surface and probe thermocouple output voltages were accurately measured with a Fluke Model 821A precision differential voltmeter which can measure voltages to ±0.01 percent plus 1V. The skin simulator temperature-regulating thermocouples were read on an automatic cycling, 24-point, Honeywell Brown stripchart recorder.

The sensing element of the temperature probe is made of 1-mil diameter copper-constantan thermocouple wire stretched across two supports formed of an insulating glass material to reduce conduction errors. A drawing of the thermocouple temperature probe is shown in Figure 8.

c. Pressure Measuring Equipment

Pressures were read on a precision Betz micromanometer. This instrument has a reading accuracy of ±0.0008 in. H_2O.

d. Water Vapor Measuring Equipment

Water vapor concentration profiles were measured utilizing a Litton Model SP-100-IR infrared hygrometer and miniature mass flux probe. The infrared hygrometer is sensitive to water vapor concentration with a calibration in terms of grams per cubic meter. This information, combined with a knowledge of the boundary layer temperature profile allows calculations of water vapor concentration in terms of partial pressure. A schematic diagram and photograph of the hygrometer are shown in Figure 9 and the mass flux probe is shown in Figure 10.

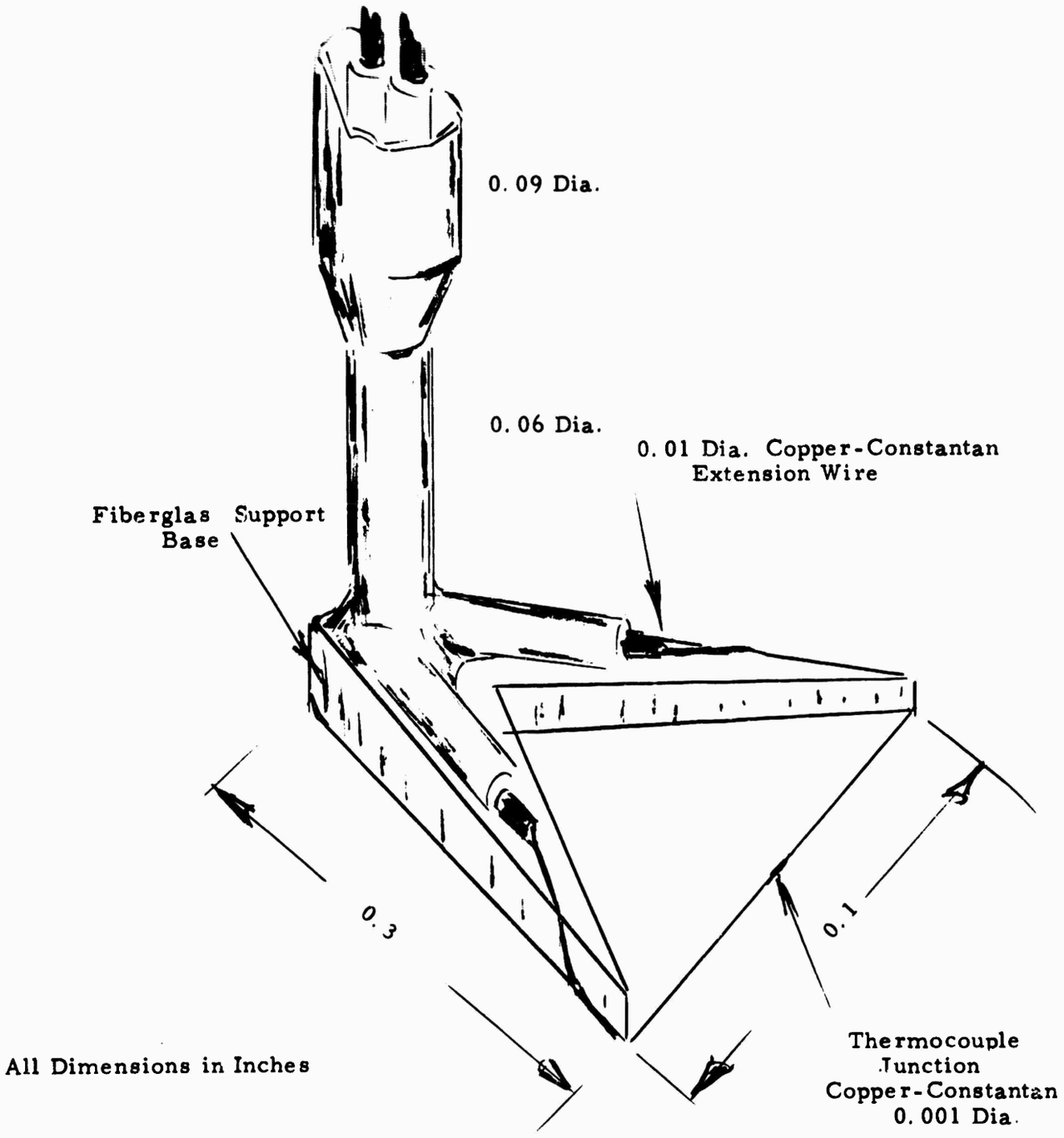

Figure 8. Thermocouple Probe

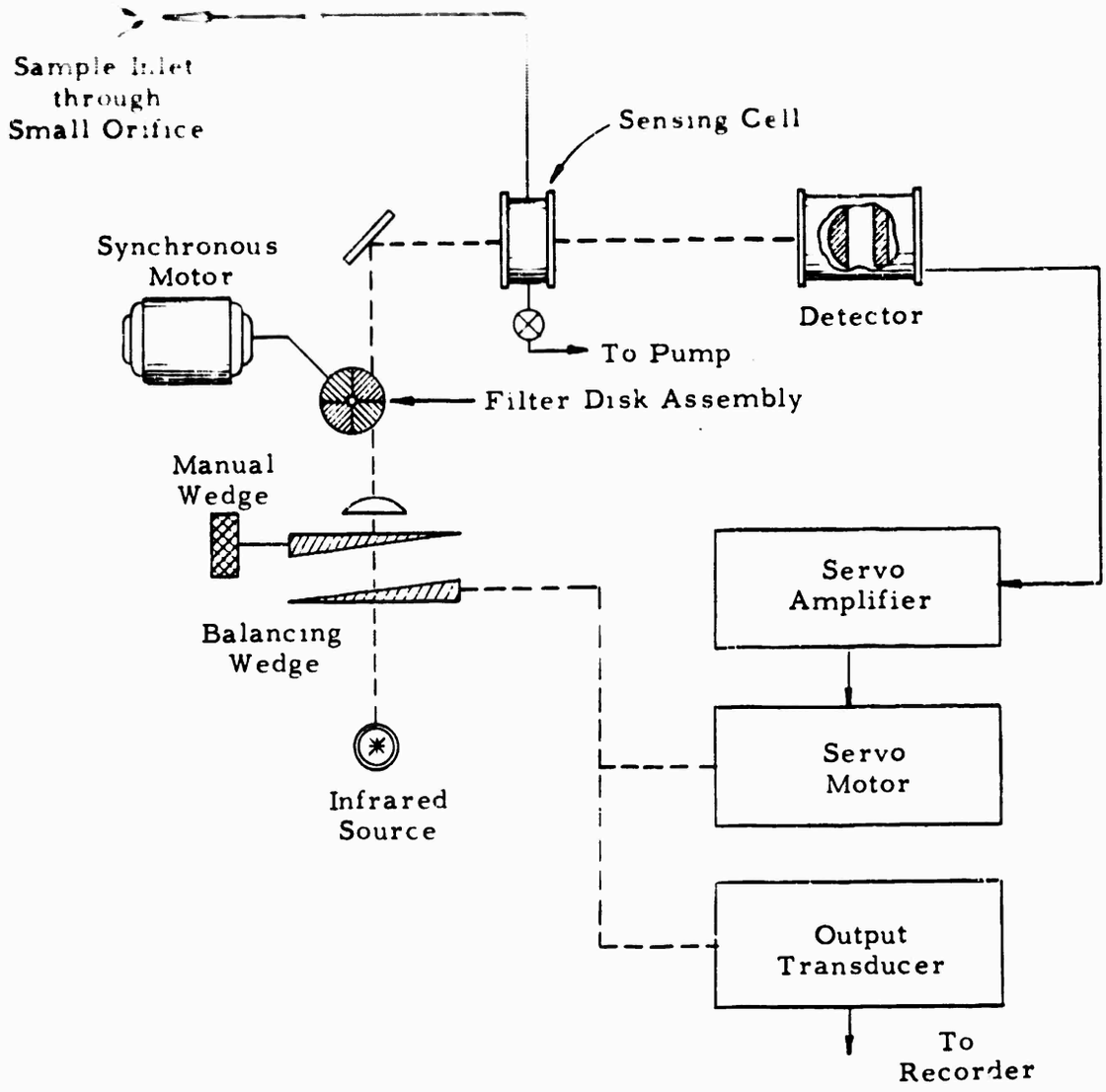

Figure 9. Schematic Diagram and Photograph of Infrared Hygrometer

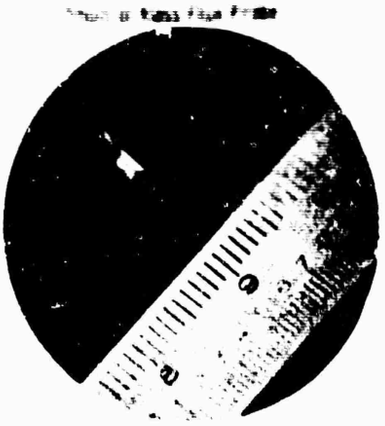

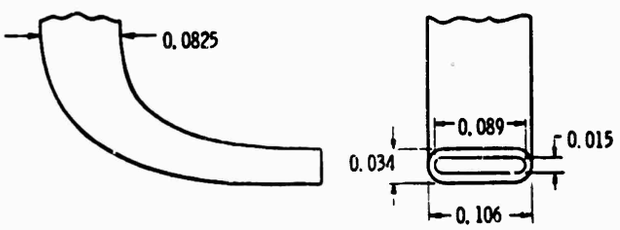

MASS FLUX PROBE DIMENSIONS

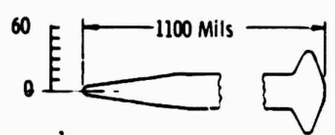

1 Mil = $\frac{1}{1000}$ inch 3.96 Mils = 1 mm

REPRESENTATIVE SIZE OF COMMON PIN

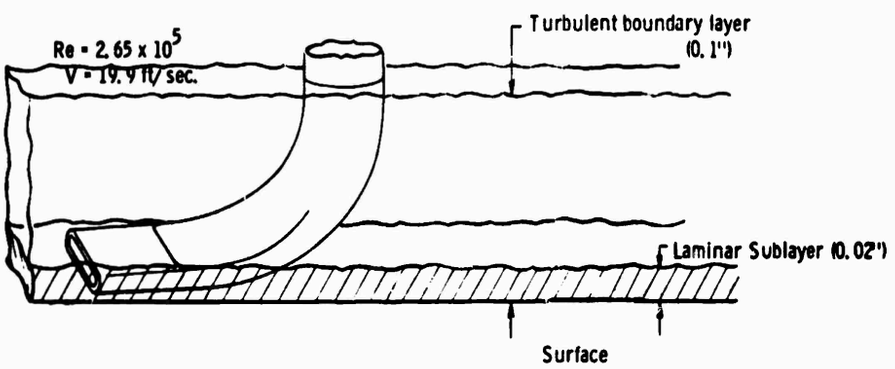

Figure 10. Mass Flux Probe

e. Probe Actuation Device

For improved accuracy and simplification of the probing measurements, a method was devised in which the hot-wire, temperature, and mass flux probes were actuated simultaneously. The probes were arranged in a spanwise orientation. All indications show that flow variations in this direction are very small and any errors introduced by this method are considerably less than those obtained by comparison of probing results for separate runs.

The probe support is made of stainless steel tubing of two different diameters to minimize probe disturbance effects, while allowing a fairly rigid insertion method. The grouping is positioned utilizing a precision vernier caliper actuating mechanism which allows a positioning accuracy of $\pm$ 0.001-inch. Figure 11 shows the probes attached to the actuation mechanism.

f. Skin Simulator Model

The previous measurements[1] were performed utilizing a fairly small skin simulator model. In addition, it had other limitations on water supply and temperature control.

To improve the validity of the results and to allow a better comparison with theory, the following improvements were made:

1) Longer model.- As the theory does not consider two-dimensional effects, created by changes in the streamwise direction, it was decided that a longer model was required. This helps to reduce leading edge effects caused by the discontinuity at the joining surfaces between the skin simulator front edge and the tunnel floor plate. The longer effective "wetted" length also creates a thicker boundary layer and allows probings at higher Reynolds numbers.

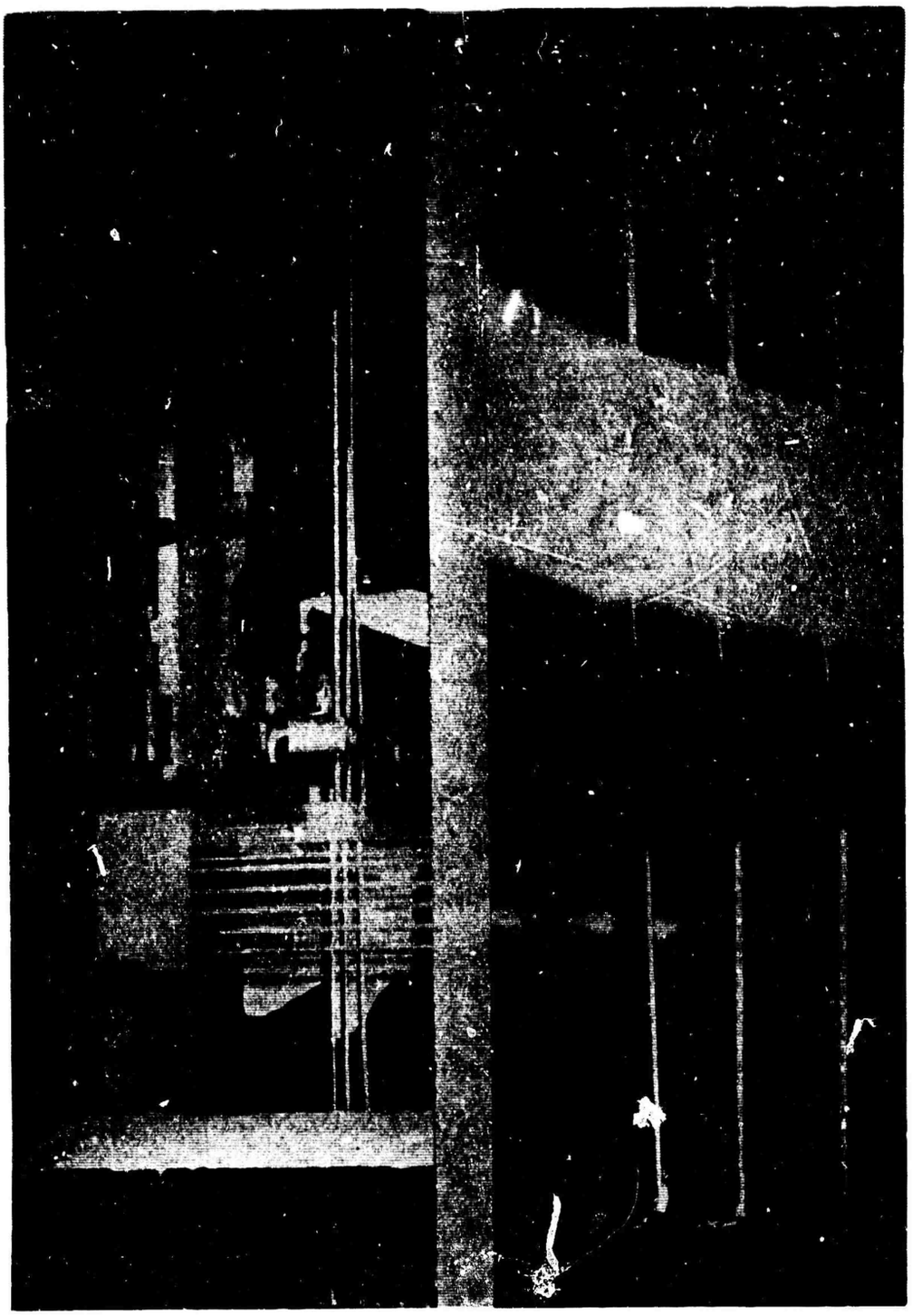

Figure 11. Probes Attached to Actuation Mechanism

2) Better control of heat release in the model. - To accurately determine the heat actually lost to the airstream, it is essential that edge and internal losses be carefully controlled. This is accomplished with an improved guard heater system. Because of the method of adding heat to the outer surfaces of the early skin simulator model, it was not possible to maintain a constant temperature at the higher Reynolds numbers. New methods of temperature measurement and control are incorporated in the new model.

3) Better control of water release in the model. - A new system to distribute and meter the water to the simulator was designed and fabricated. This allows better control of the water flow and results in easier adjustment of surface temperatures.

The simulator (see Figure 12) is housed in a Lucite test section having inner dimensions of 6 x 4 x 18 inches. The major component of the test model is the outer surface upon which the heat and mass transfer effects take place. It is formed of sintered bronze of 7-micron porosity and has a width of 6 inches and a length of 12 inches.

Immediately below the top plate is a sintered bronze plate which has larger pores (100 micron) and irrigation canals to distribute the water, insuring a uniform moisture supply to the top surface. Polyethylene insulating strips surround the porous layers. A solid copper plate is located below the porous section and is sealed to the polyethylene side insulators to confine the water supply within the sintered bronze. The water enters through a plastic feed pipe through the center of the copper plate. The main heater bed contains 35 feet of fine nichrome wire (0.025-inch diameter) imbedded in a thin epoxy layer on the underside of the solid copper heat distribution plate. The guard heater system consists of the main guard heater, which is applied to another copper plate, separated from the main heater bed by a triple layer of 1/8-inch thick polyethylene sheets. Peripheral guard heaters of nichrome wire ribbon are imbedded within the polyethylene strips surrounding the surface layers.

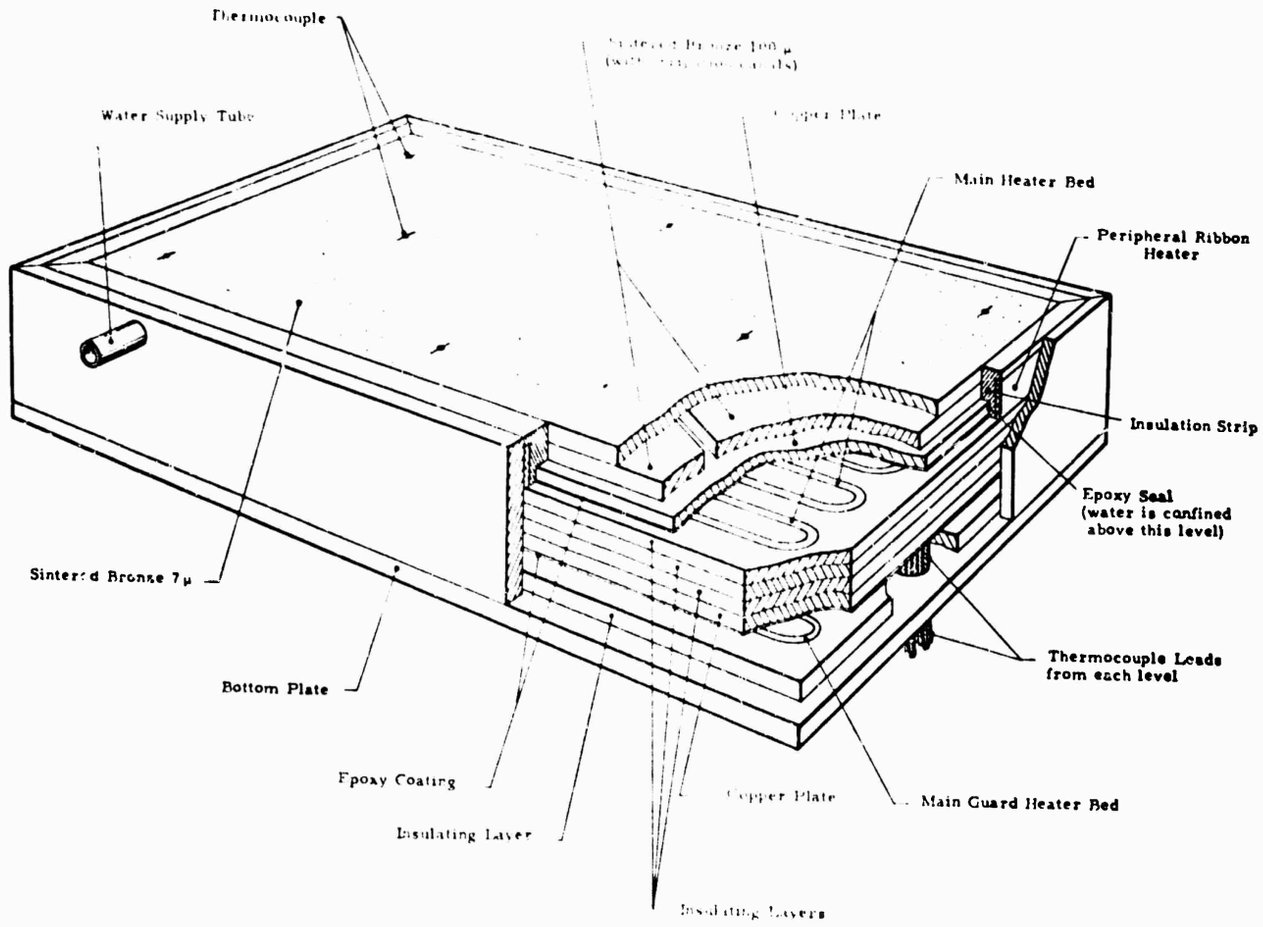

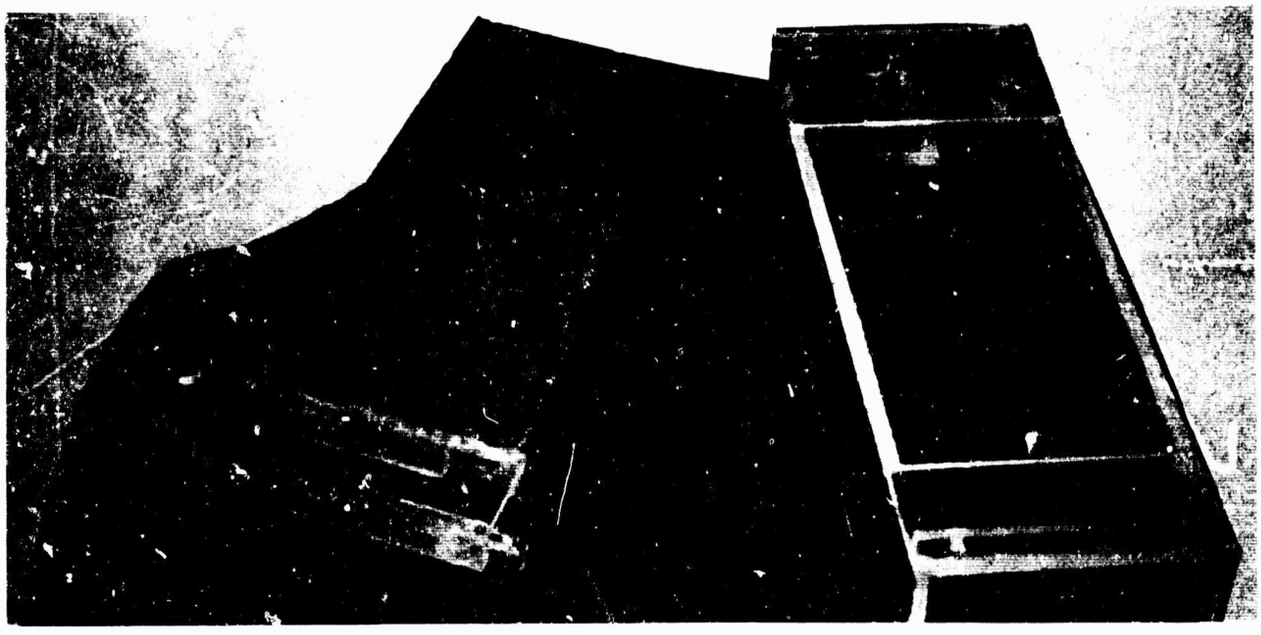

Figure 12. Skin Simulator Model

The guard heater temperature monitoring system consists of copper-constantan thermocouples mounted in pairs across the various insulating control layers. A pair is attached across each polyethylene side strip and the ribbon guard heaters are adjusted for zero difference in the output of these control pairs. Similar pairs are mounted across the middle sheet of the insulating layer between the main heater and the main guard heater beds. When all guard heaters are adjusted to yield zero heat flux through the insulation materials, as indicated by a null condition for each thermocouple control pair, all of the energy dissipated in the main heater bed must appear as heat flux through the skin surface. These thermocouples were connected to the 24-point Honeywell Brown strip chart recorder which had been calibrated for copper-constantan junctions.

Heating power adjustments were made with a variable Perkin d-c power supply with magnetic regulation. The main heater and main guard heaters operated in parallel from the output of this supply but each heater's relative current could be controlled with series-wired power resistors of the slide wire type (see Figure 13 for a schematic of the electrical system). Ribbon peripheral heaters were a-c powered by a Variac autotransformer.

The temperature of the skin was measured with a set of eight copper-constantan thermocouples surface-mounted on the top bronze plate. To insure that true surface temperatures are sensed, special installation procedures were utilized. Teflon-coated, copper-constantan thermocouple wire of 0.005-inch diameter was utilized to form the junctions.

The leads are brought to the surface through separate holes on 1/8-inch centers. At the surface they are bent horizontally and cemented into a shallow groove between the holes. In the center they are soldered together and to the bronze surface; the Teflon insulation is retained except in the immediate vicinity of the joint. These thermocouples are referenced to an ice bath and the output voltages read on the Fluke digital voltmeter.

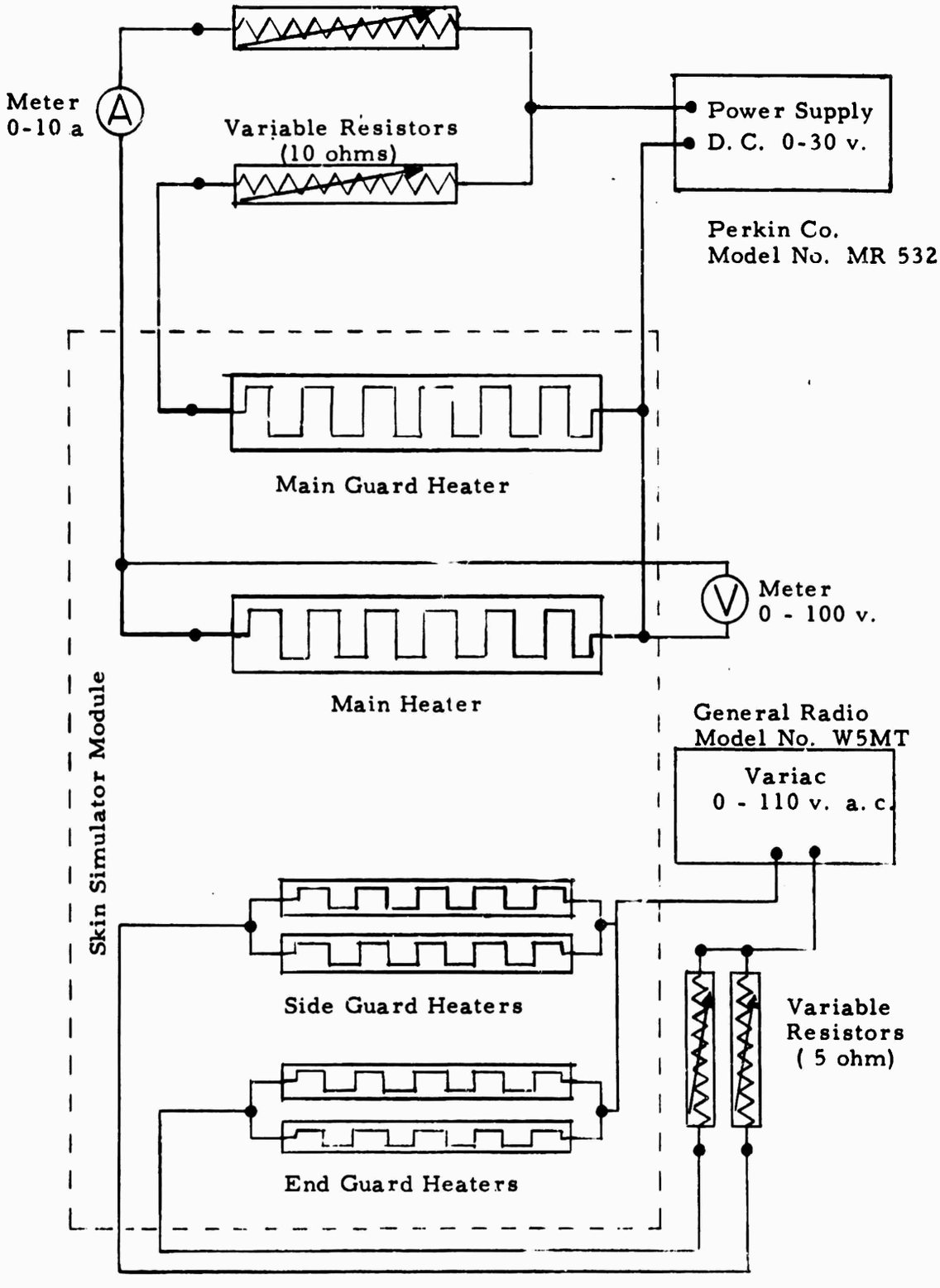

Figure 13. Schematic Diagram - Heater Circuits

The entire assembly is inserted into an open-top Lucite retaining box with a heavy insulation layer below the lower guard heater. The water feed pipe and all heater and thermocouples leads exit through the bottom of the box.

g. Test Chamber and Fabric Positioning Components

The improved skin simulator model is housed in a Lucite chamber which allows visual observation of the test components during the measurements.

The fabric test samples are mounted on a mounting frame which consists of two pieces of 1/32-inch thick aluminum plate. The fabric was stretched across the bottom plate and epoxy cement applied around the edges. The top plate was then positioned and the assembly was ready for use after the epoxy had cured.

Several types of positioning methods were utilized, depending upon the test configuration utilized. For the early tests the frame was inserted in slots machined into the test chamber side walls, allowing positioning increments of 0.1, 0.2, 0.4, 0.6, 0.8 and 1 inch. The fabric spacing is changed by removing one of the test chamber sidewalls. A second method allows more flexibility in positioning and reduces the danger to the probes when changes are made. This utilizes Silastic gaskets on each side of the mounting frame which hold the unit in the desired position. The test chamber and fabric mounting plate are shown in Figure 14.

For the final heat and mass transfer rates the test chamber configuration had the cover open and the upper channel blocked at both ends with sheet metal plates. This arrangement simulated a condition of no external flow with the fabric exposed to the outer environment. These plates fastened to the fabric holder frame and extended vertically out of slots in the tunnel roof. Lines were scribed horizontally across these plates

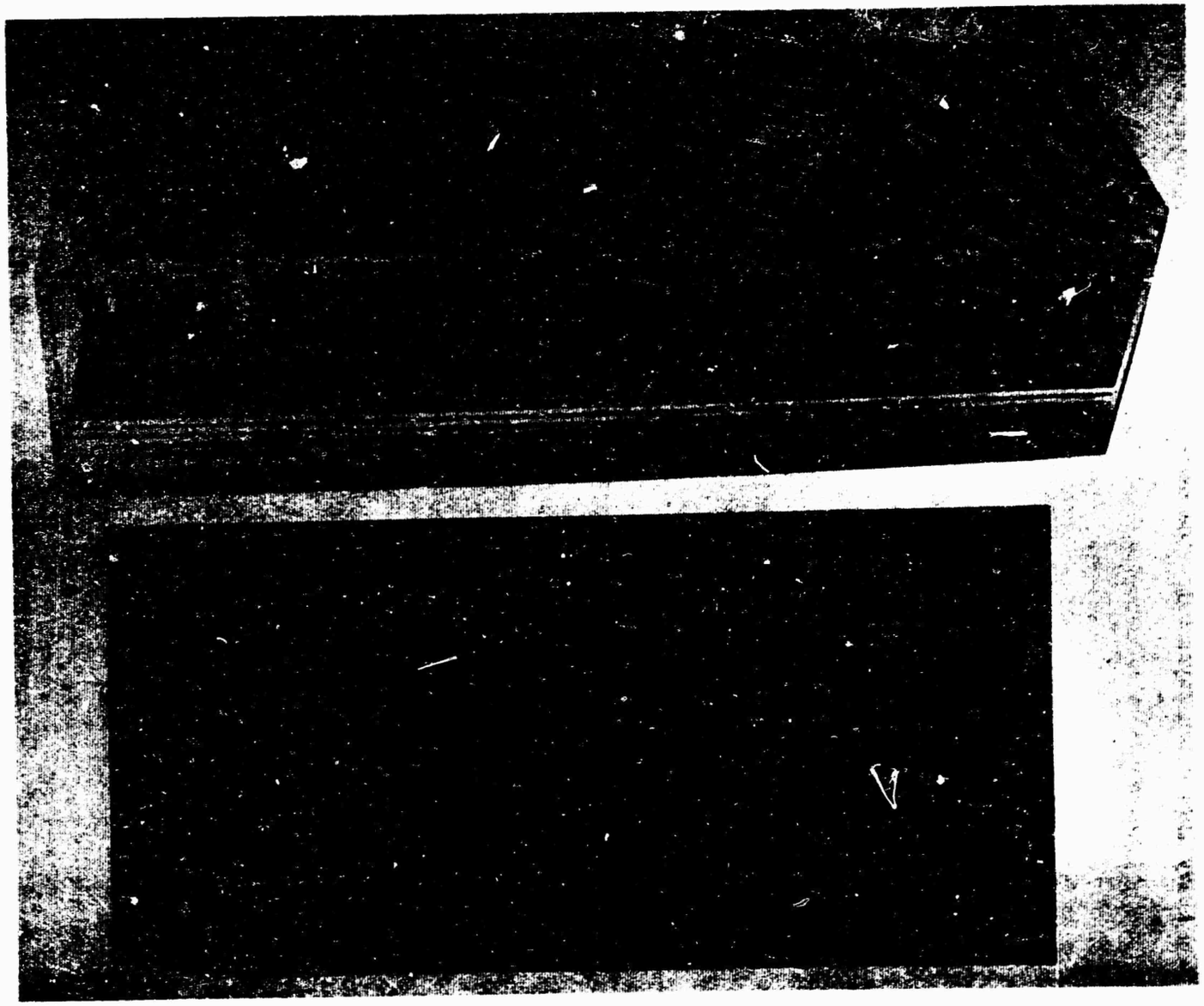

Figure 14. Fabric Test Chamber and Mounting Plate

corresponding to air gap dimensions of 0.1, 0.2, 0.4, 0.6, 0.8 and 1.0 inch. The desired gap dimension was easily selected by manipulating the fabric holder by means of these projecting sheets until the correct scribe lines coincided with a fixed reference line on the tunnel top.

h. Water Supply System

Water to simulate mass transfer effects created by perspiration is supplied by the system shown in Figure 15. This consists of supply tube (A) which drips into reservoir (B) and stand pipe (C) maintains the water level in the reservoir while container (D) catches the overflow. Water is transported to the skin through feed pipe (E) and tubing (F) acts as a height gauge to judge the level of the water table relative to the skin surface. Using a reservoir with a large surface area made it possible to adjust the drip rate to produce a minimal amount of over flow.

2. Reduction of Hot-Wire Mean and Fluctuating Velocity Data

a. Mean Data

The hot-wire probes (see Figure 7) were calibrated in the fabric test facility. This was accomplished by positioning the probe in the potential flow region in the channel (away from the walls) and obtaining corresponding values of velocity (from micromanometer pressure readings) and hot-wire bridge mean voltage. The velocity was varied from 0 to 30 ft/sec. Refer to Appendix E for a detailed discussion of the appropriate equations.

A plot of mean bridge voltage $\overline{E}_b$ versus mean velocity $\overline{U}$ for two probes is shown in Figure 16. As shown in the above appendix, the calibration procedure can be simplified if we take advantage of the following linear relationship:

$$\overline{E}_b^2 = A + B(\rho \overline{U})^{1/2} .$$

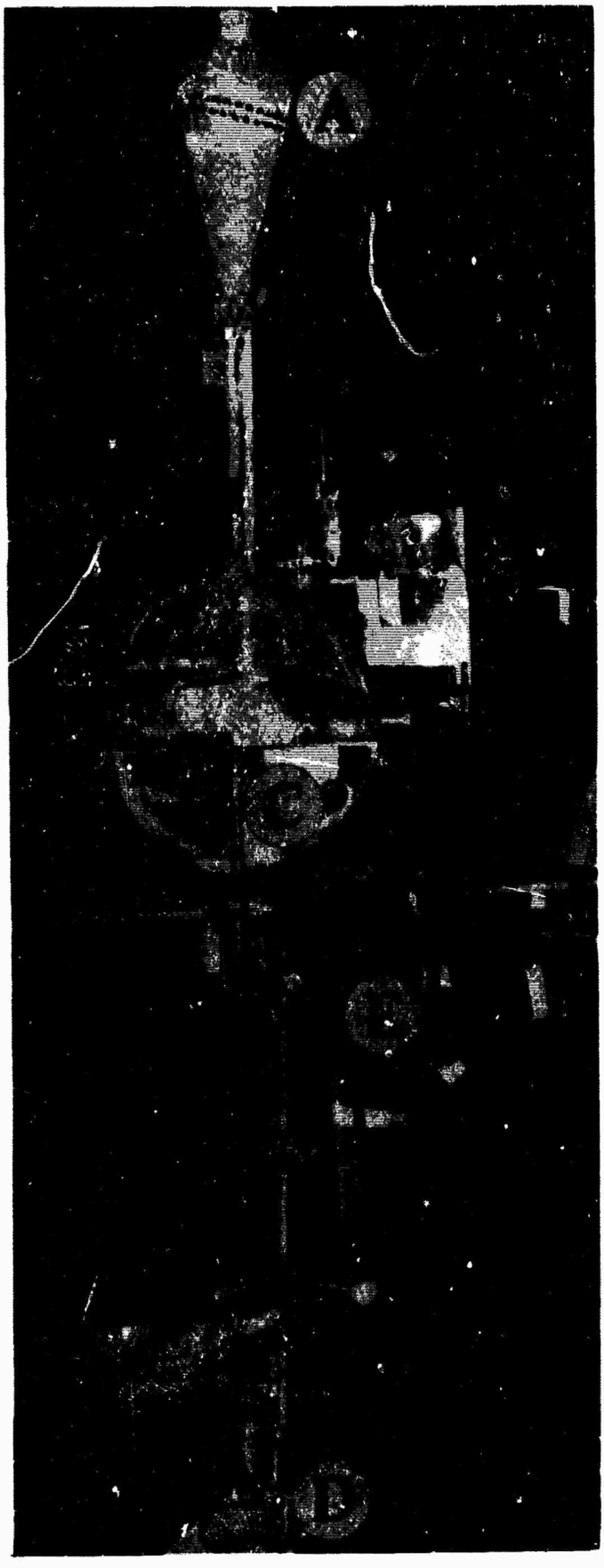

A Water Supply Tube

B Reservoir

C Stand Pipe

D Overflow Flask

E Feed Pipe

Figure 15. Skin Simulator Water Supply and Control System

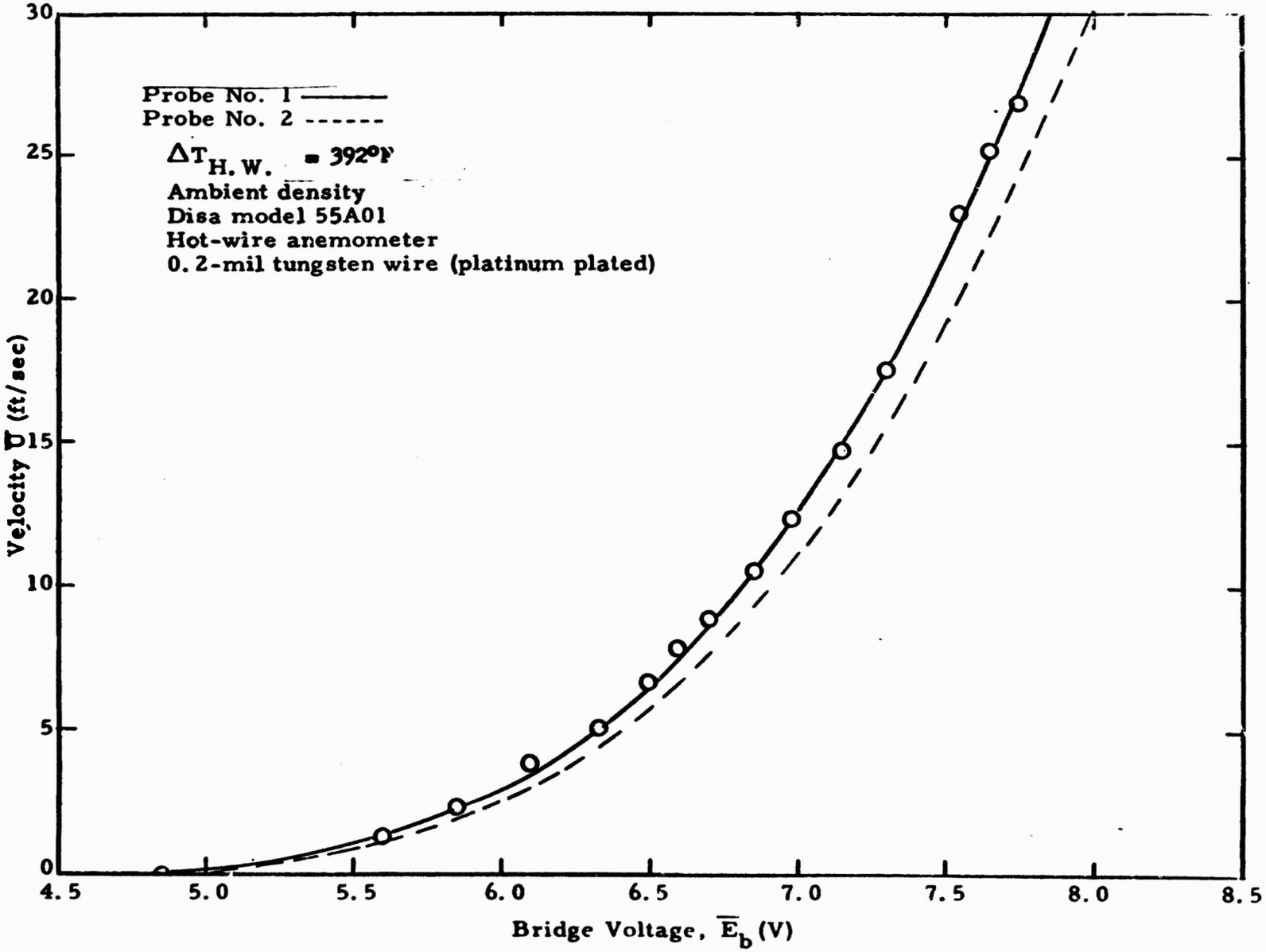
Probe No. 1 ———
Probe No. 2 ------
$\Delta T_{H.W.}$ = 392°F
Ambient density
Disa model 55A01
Hot-wire anemometer
0.2-mil tungsten wire (platinum plated)
Velocity $\overline{U}$ (ft/sec)
Bridge Voltage, $\overline{E}_b$ (V)
0
5
10
15
20
25
30
4.5
5.0
5.5
6.0
6.5
7.0
7.5
8.0
8.5

When the density ρ is constant, the above equation can be written in the form

$$\overline{E}_b^2 = A + B'(\overline{U})^{1/2} ,$$

where A is the ordinate intercept and B' is the slope of the line. This linear relationship for the two probes is shown in Figure 17.

b. Fluctuating Data

Turbulence intensities are obtained utilizing the following equation from Appendix E:

$$\frac{u'}{\overline{U}} = \frac{400\,\overline{E}_b}{(\overline{E}_b)^2 - (\overline{E}_{bo})^2}\, e_b' \text{ (percent)}$$

where:

u' = rms fluctuating velocity

e_b' = rms fluctuating bridge voltage

$\overline{E}_{bo}$ = mean bridge voltage at zero velocity.

The mean and fluctuating velocities are read on the Disa anemometer panel meters.

To simplify the calculations, the term

$$\frac{400\,\overline{E}_b}{(\overline{E}_b)^2 - (\overline{E}_{bo})^2} ,$$

designated as the turbulence parameter σ, is plotted as a function of $\overline{E}_b$ in Figure 18. The turbulence intensity $u'/\overline{U}$ can then be calculated for various values of e_b' and $\overline{E}_b$.

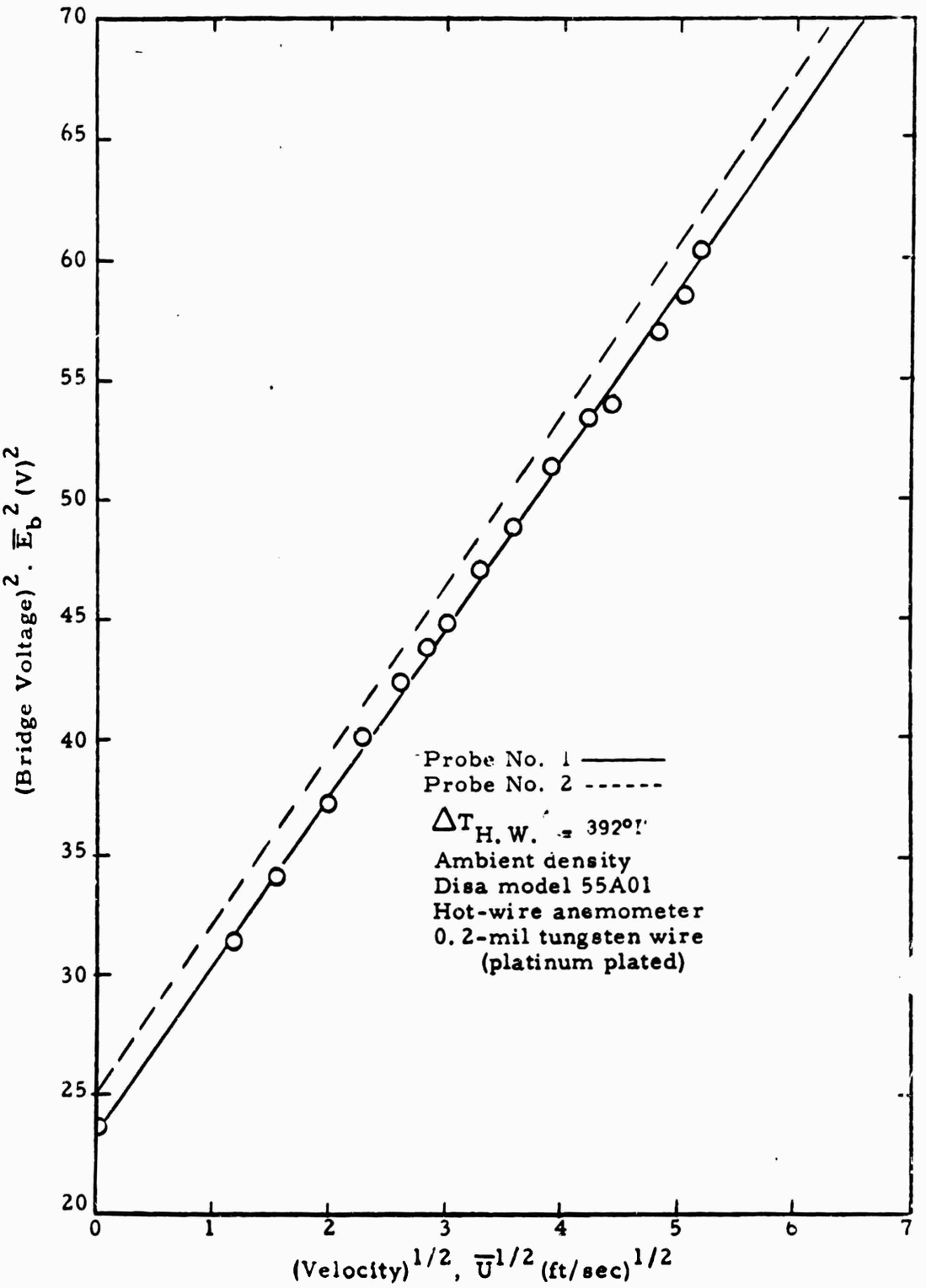

Figure 17. Linearized Hot-Wire Calibration Curves

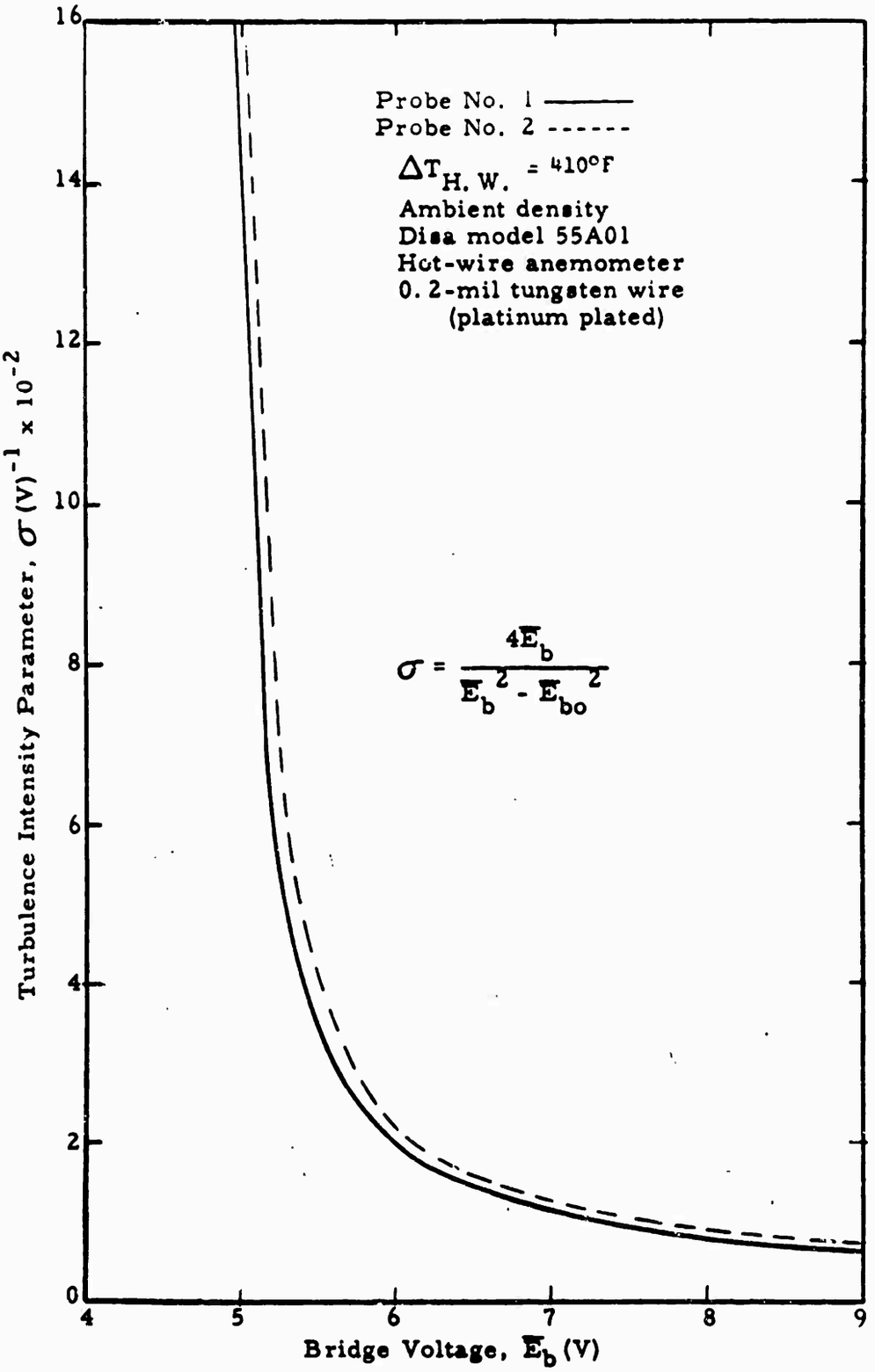

Figure 18. Turbulence Intensity Parameters

3. Procedure

The various parameters determining a particular test run condition generally interact with each other; i. e., a change in velocity requires a readjustment of heater power, which requires a readjustment of guard heaters, etc. It was found that a change in the air gap dimension required the least amount of rebalance in the control of the remaining parameters, thus it was chosen as the parameter to be varied first and most frequently.

With the air gap adjusted, the velocity was selected by a valve in the outlet from the plenum chamber of the blower. The velocity was determined either from pressure readings with the Betz micromanometer or from the bridge voltage of a calibrated hot-wire anemometer using the Disa equipment.

The main heater was adjusted to yield 100°F as measured by the surface thermocouple located at the probing station. The guard heaters were balanced to produce the same temperature on each member of the control thermocouple pairs mounted across the insulating layers between the main bed and the guard elements. The rate of heat loss was determined from the current flow and voltage drop across the main heater.

Moisture consumption rates were computed from the amount of water gone from the supply tube less the amount present in the overflow container, averaged over a period of several hours. It is important that the system be in steady-state equilibrium before recording heat and moisture loss. Operation in a steady or controlled ambient environment greatly facilitates the establishment of equilibrium conditions.

The skin simulator, for the wetted runs, was leveled utilizing the four support screw legs. The height of the water table was maintained just below the top of the porous skin surface by adjusting the height of the reservoir. The use of distilled water helped prevent accumulations of scale or scum which could clog the pores in the skin surface.

Temperature, velocity, and humidity profiles were recorded by traversing the air gap with the specially designed probe mechanism previously described. The micrometer drive head actuates, simultaneously, three probes arranged side by side with their sensing elements in the same horizontal plane. Thus, at each height position in air gap, temperature is obtained from the thermocouple velocity from the hot-wire, and humidity via the mass flux probe at exactly the same values of ambient and test chamber parameters.

Traverses for the wetted runs were always started at the underside of the fabric and proceeded downward to the skin surface. This procedure was necessary because capillary action would cause a bead of water to be drawn up around the probe tips when they contacted the skin surface. This bead of water would cling to the probes for some time after they were raised off the surface, during which time the thermocouple reading would approach "wet-bulb" values while humidity readings would tend to indicate saturation. During the dry skin runs, the mass flux sampling tube was used to yield a total pressure profile.

The infrared hygrometer was also used to monitor the ambient humidity. The hygrometer calibration was checked daily since the density in the sensing chamber was affected by the small sensing orifice in the probe as well as changing flow conditions in the test chamber. The sampling rate was adjusted to obtain isokinetic sampling, thus minimizing the disturbance of the flow field by the probe's presence.

C. Discussion of Results

1. Preliminary Measurements

a. Variation of External and Internal Ventilating Flows

It was decided that knowledge of the flow conditions in the air gap was necessary before other measurements would be carried out. This consisted of measurements of mean and fluctuating flow velocities in the air gap for various spacings and external and internal ventilating flow rates. The top cover was in place for these measurements. This information was necessary to determine the nature of the viscous boundary layers growing on the skin simulator and fabric surfaces.

These velocities were measured with the DISA hot-wire equipment. Surface static pressures were obtained with the Betz micromanometer. The skin simulator surface was allowed to remain at dry recovery conditions.

(1) Mean Velocity Data. - The mean velocity data were normalized by dividing the measured local velocities by the nominal ventilating flow velocities at the leading edge of the fabric. The vertical ordinate was divided by the nominal fabric spacing L_a. Figures 19 through 25 show velocity data for various constant nominal air gap spacings and outer ventilating flow rates with the internal ventilating flow as a parameter. At the low velocities a characteristic laminar profile is obtained, while at the higher velocities the flow tends to be turbulent.

Because of cross-flow rates through the fabric at various combinations of flow velocities, some of the measured mean velocities in the air gap are greater than the nominal values at the fabric leading edge. It can also be seen in some cases that the fabric bows up because of pressure differences, which accounts for some normalized vertical probing positions being greater than unity.

Air gap, L_a = 0.2 in.
Prob. stat., x = 8.4 in.
Run no. 25, 26, 27
8.8-oz cotton sateen

Amb. Air Cond.
D. B. T. = 76.5 °F
W. B. T. = 52 °F
B. P. = 29.38 in. Hga

Airflow Cond.
Nom. ext. flow vel. = ~0 ft/sec
Ext. flow stat. press. = in. Hga
Nom. vent. flow vel. = VAR ft/sec
Vent. flow stat. press. = in. Hga

Skin Sim. Sur. Cond.
Temp. = 75 °F
Dry

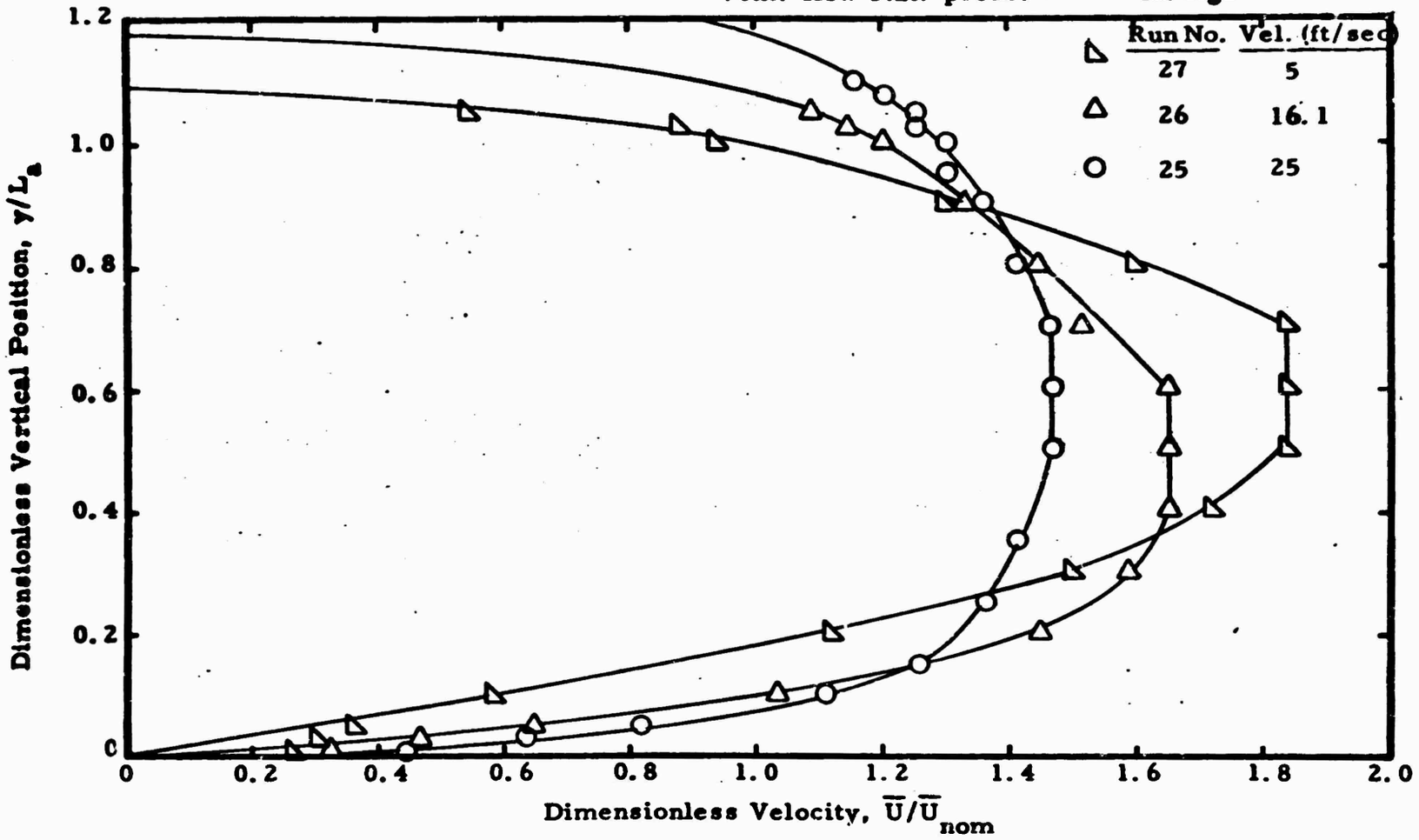

Figure 19. Mean Velocity Variation in Air Gap
(Nominal External Airflow Velocity = ~0 ft/sec, Air Gap = 0.2 in.)

Air gap, L_a = 0.4 in.
Prob. stat., x = 8.4 in.
Run no. 39, 40, 41, 42
8.8-oz cotton sateen

Amb. Air Cond.
D. B. T. = 76.1 °F
W. B. T. = 57.9 °F
B. P. = 28.94 in. Hga

Airflow Cond.
Nom. ext. flow vel. = MEG, ft/sec
Ext. flow stat. press. = — in. Hga
Nom. vent. flow vel. = VHR ft/sec
Vent. flow stat. press. = — in. Hga

Skin Sim. Sur. Cond.
Temp. = 76 °F
Dry

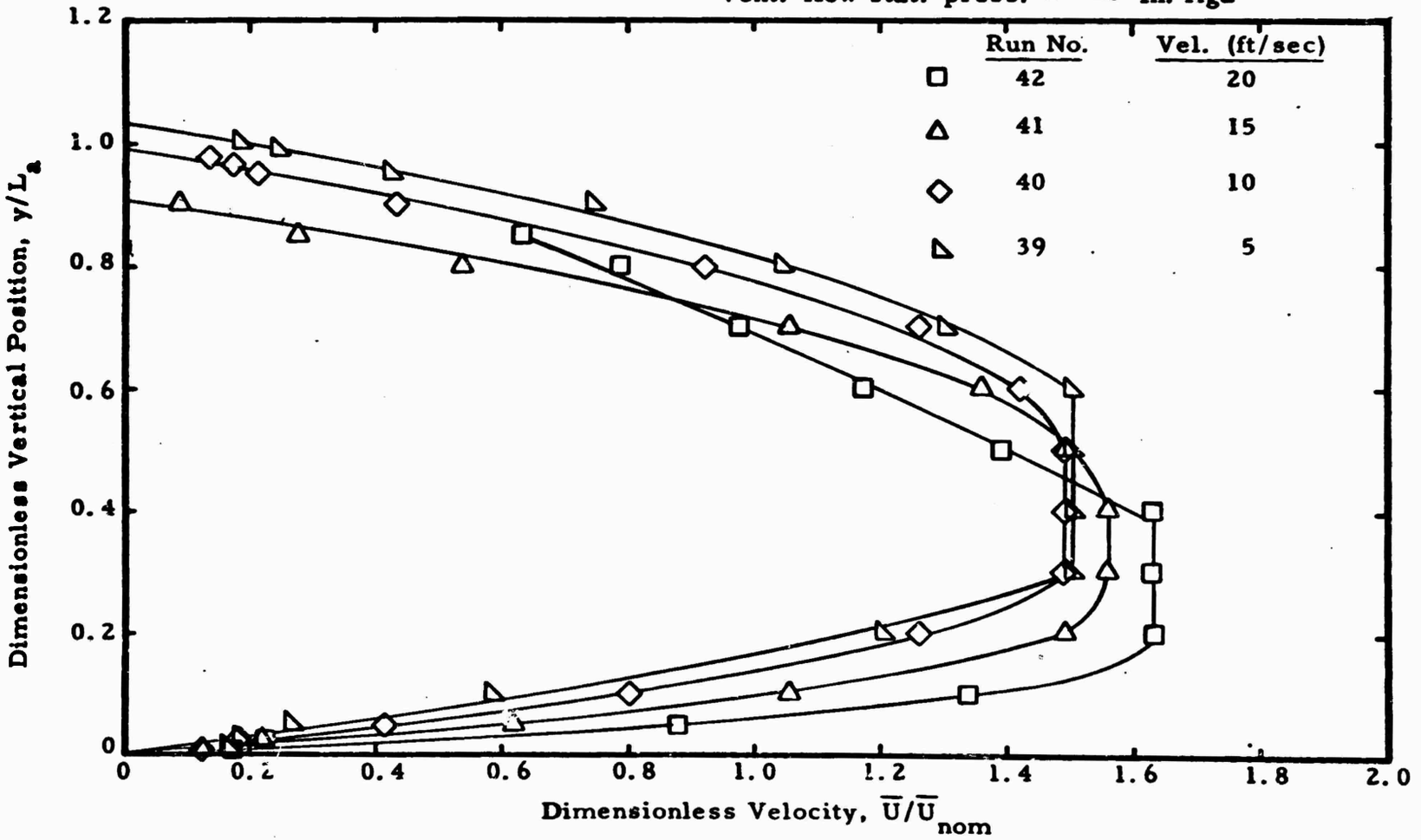

Figure 20. Mean Velocity Variation in Air Gap
(Nominal External Airflow Velocity = MEG ft/sec, Air Gap = 0.4 in.)

Air gap, L_a = 1.0 in.
Prob. stat., x = 6.4 in.
Run no. 17, 18
8.8-oz cotton sateen

Amb. Air Cond.
D. B. T. = 76 °F
W. B. T. = 53.5 °F
B. P. = 29.28 in. Hga

Airflow Cond.
Nom. ext. flow vel. = 0 ft/sec
Ext. flow stat. press. = — in. Hga
Nom. vent. flow vel. = VAR ft/sec
Vent. flow stat. press. = — in. Hga

Skin Sim. Sur. Cond.
Temp. = 76 °F
Dry

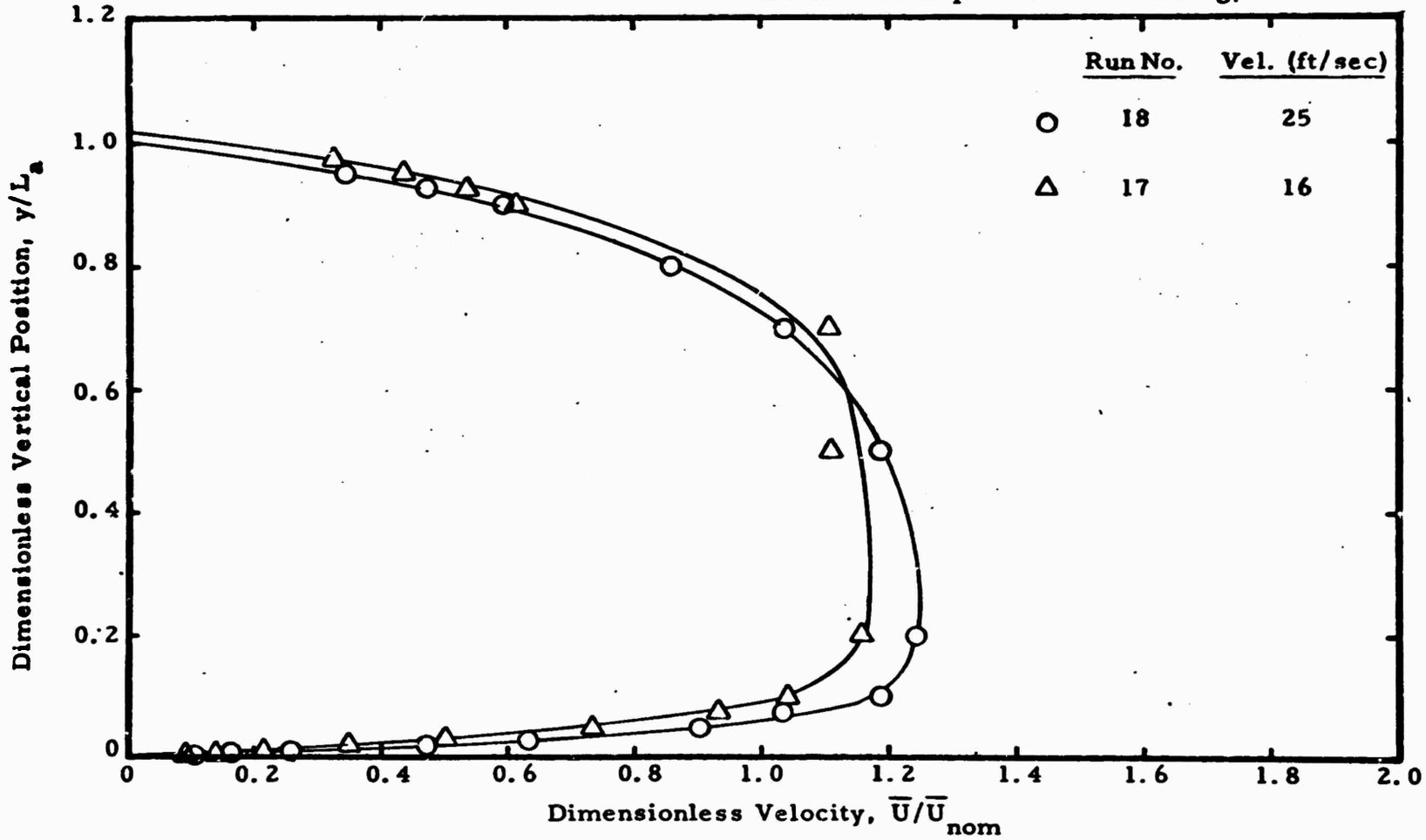

Figure 21. Mean Velocity Variation in Air Gap
(Nominal External Airflow Velocity = 0 ft/sec, Air Gap = 1.0 in.)

Air gap, L_a = 0.4 in.
Prob. stat., x = 8.4 in.
Run no. 39, 40, 41, 42
8.8-oz cotton sateen

Amb. Air Cond.
D. B. T. = 76.1 °F
W. B. T. = 51.9 °F
B. P. = 28.94 in. Hga

Airflow Cond.
Nom. ext. flow vel. = 146, ft/sec
Ext. flow stat. press. = — in. Hga
Nom. vent. flow vel. = ~~146~~ ft/sec
Vent. flow stat. press. = — in. Hga

Skin Sim. Sur. Cond.
Temp. = 76 °F
Dry

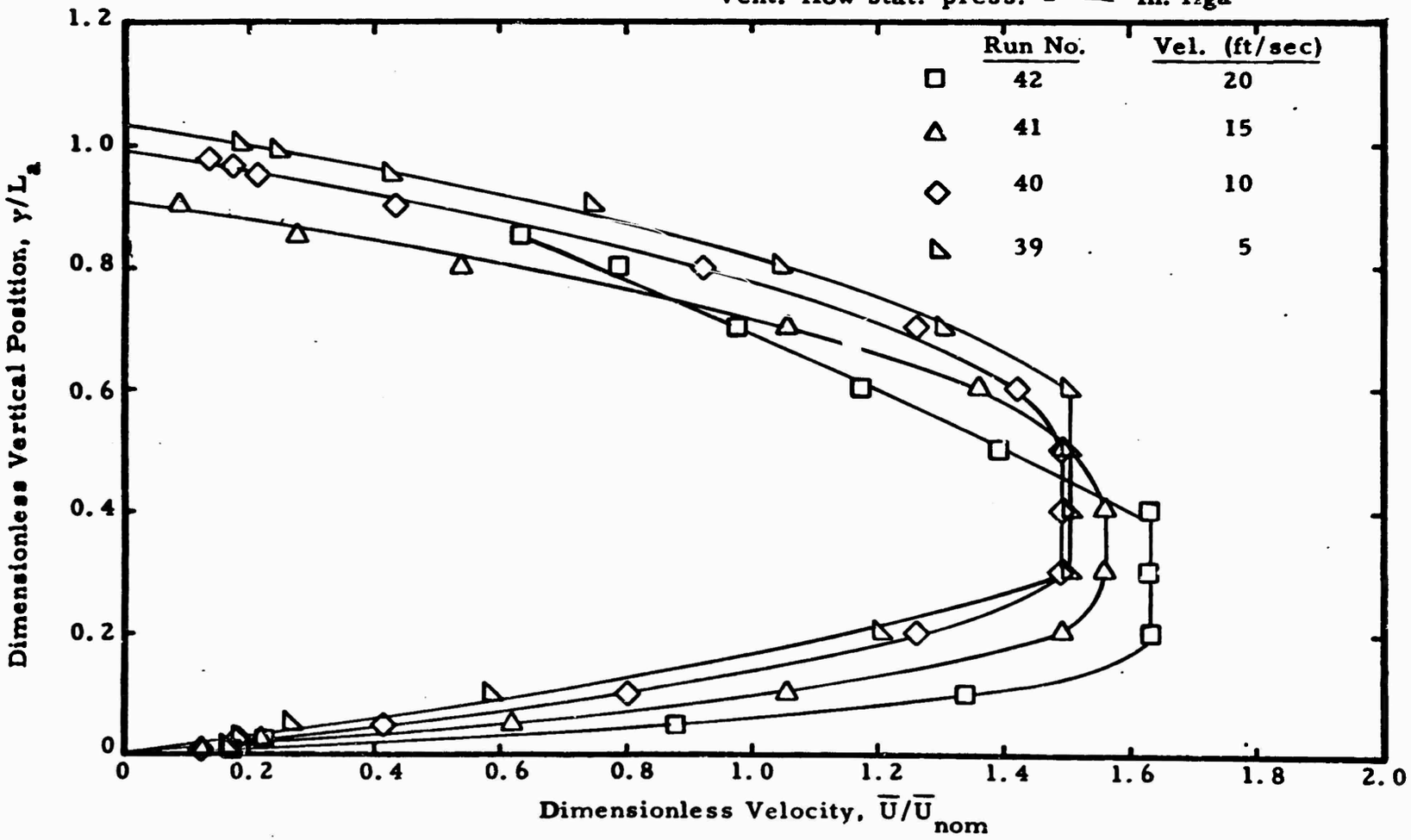

Figure 20. Mean Velocity Variation in Air Gap
(Nominal External Airflow Velocity = 146 ft/sec, Air Gap = 0.4 in.)

Air gap, L_a = 1.0 in.
Prob. stat., x = 6.4 in.
Run no. 17, 18
8.8-oz cotton sateen

Amb. Air Cond.
D. B. T. = 76 °F
W. B. T. = 53.5 °F
B. P. = 29.28 in. Hga

Airflow Cond.
Nom. ext. flow vel. = 0 ft/sec
Ext. flow stat. press. = — in. Hga
Nom. vent. flow vel. = VAR ft/sec
Vent. flow stat. press. = — in. Hga

Skin Sim. Sur. Cond.
Temp. = 76 °F
Dry

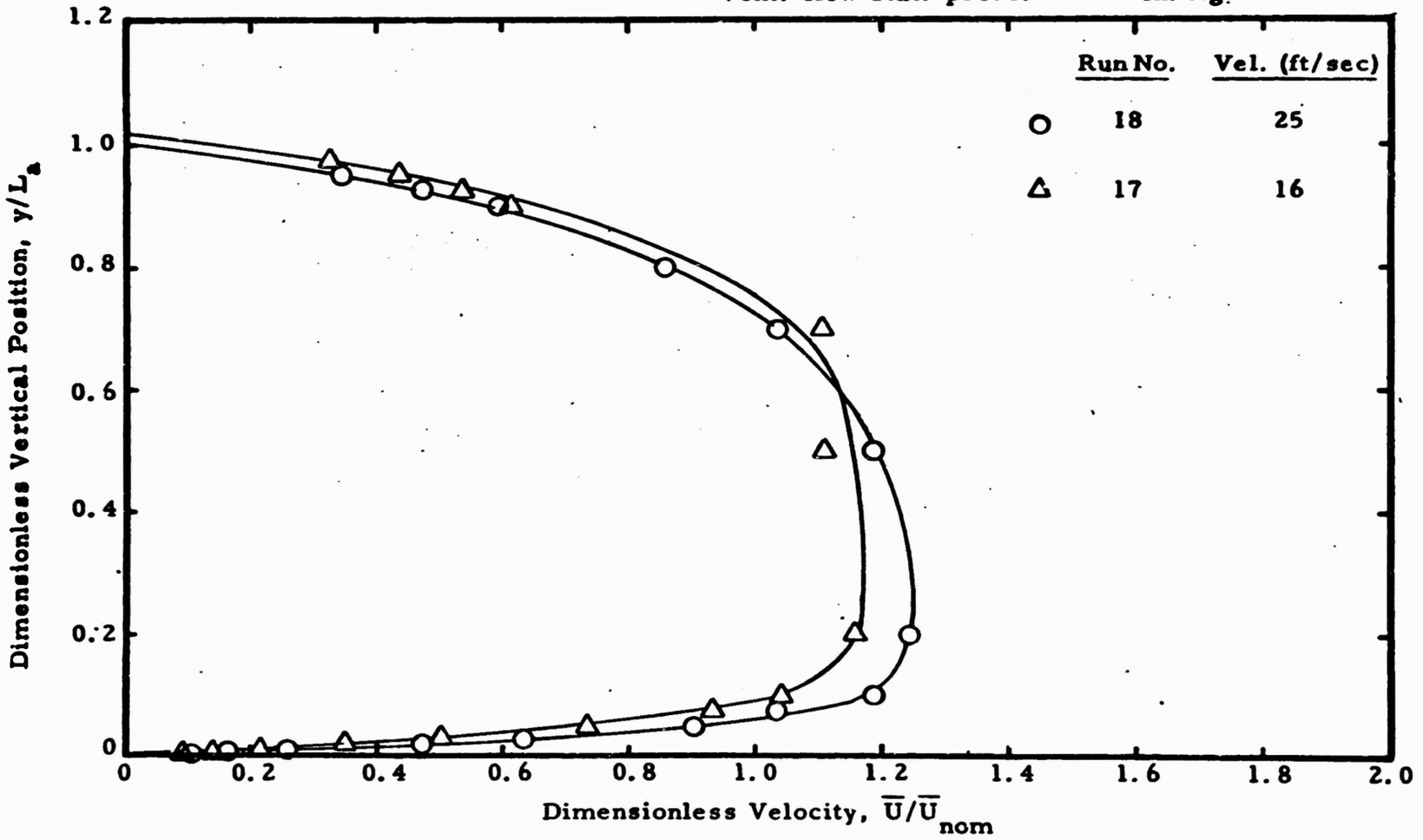

Figure 21. Mean Velocity Variation in Air Gap
(Nominal External Airflow Velocity = 0 ft/sec, Air Gap = 1.0 in.)

Air gap, L_a = 0.2 in.
Prob. stat., x = 8.4 in.
Run no. 29, 30
8.8-oz cotton sateen

Amb. Air Cond.
D. B. T. = 76.5 °F
W. B. T. = 52 °F
B. P. = 29.39 in. Hga

Airflow Cond.
Nom. ext. flow vel. = 5 ft/sec
Ext. flow stat. press. = — in. Hga
Nom. vent. flow vel. = NR ft/sec
Vent. flow stat. press. = — in. Hga

Skin Sim. Sur. Cond.
Temp. = 75 °F
Dry

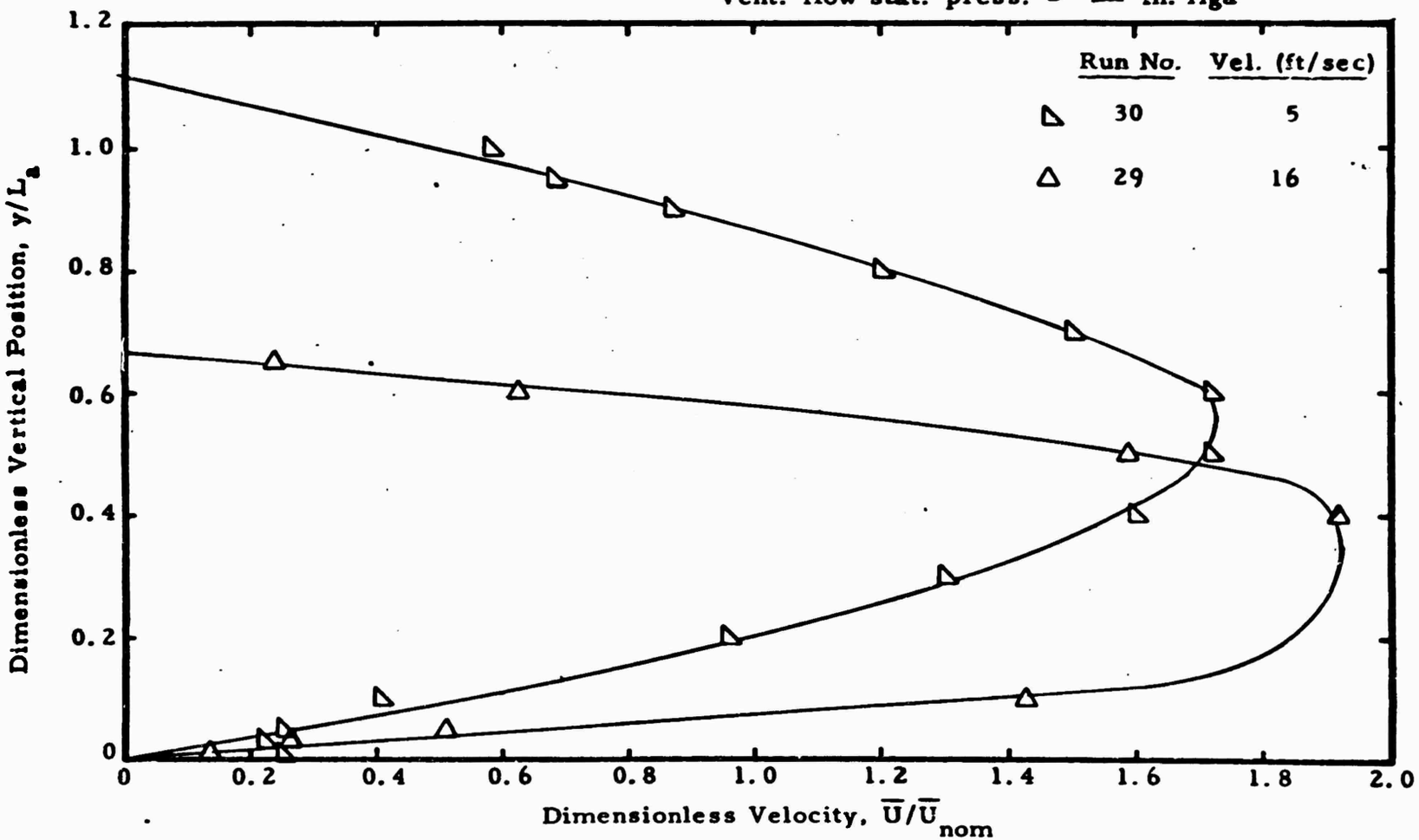

Figure 22. Mean Velocity Variation in Air Gap
(Nominal External Airflow Velocity = 5 ft/sec, Air Gap = 0.2 in.)

Air gap, L_a = 0.6 in.
Prob. stat., x = 8.4 in.
Run no. 48, 49, 50, 51, 52
8.8-oz cotton sateen

Amb. Air Cond.
D. B. T. = 76 °F
W. B. T. = 52 °F
B. P. = 29.10 in. Hga

Airflow Cond.
Nom. ext. flow vel. = 5 ft/sec
Ext. flow stat. press. = — in. Hga
Nom. vent. flow vel. = N/A ft/sec
Vent. flow stat. press. = — in. Hga

Skin Sim. Sur. Cond.
Temp. = 76 °F
Dry

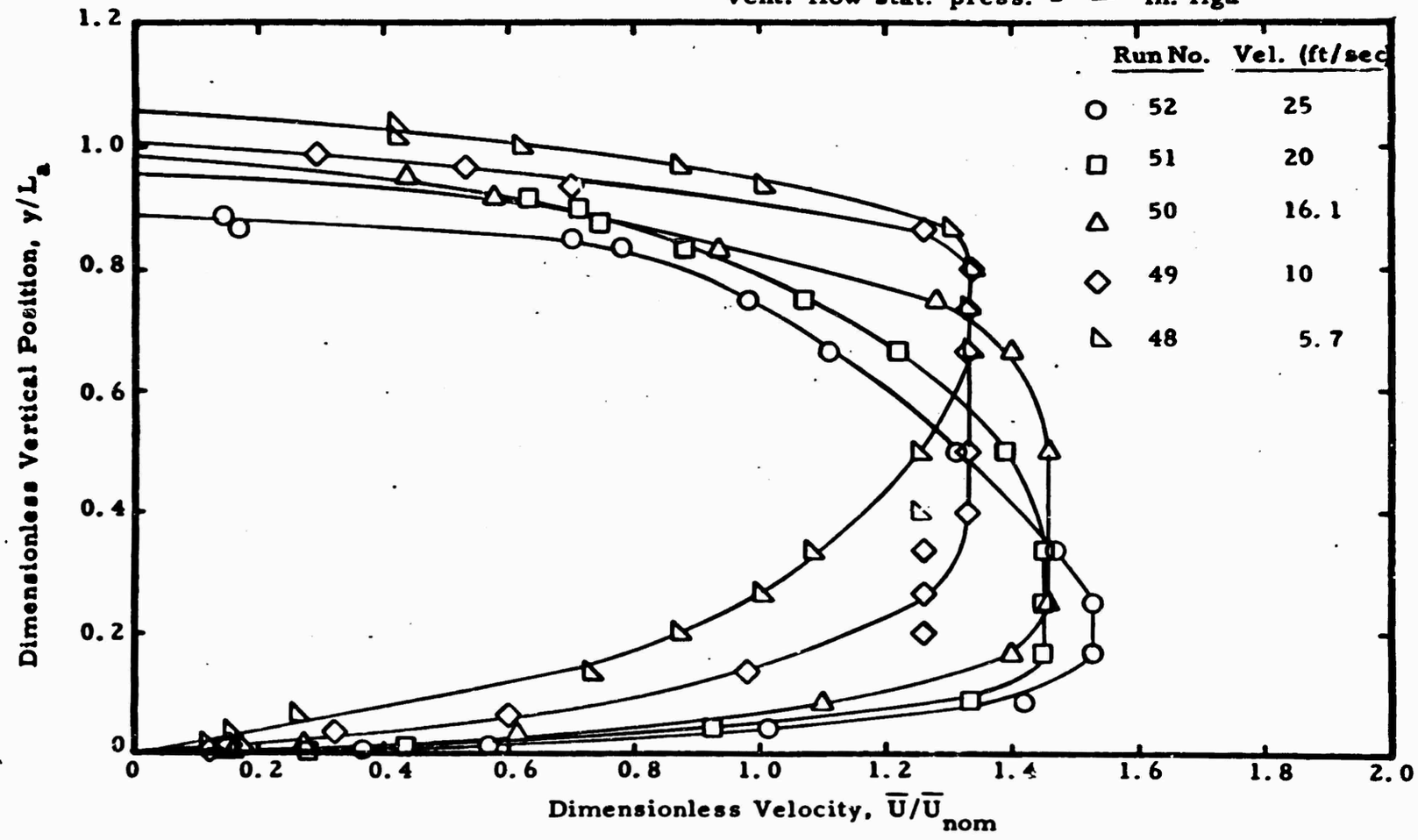

Figure 23 Mean Velocity Variation in Air Gap
(Nominal External Airflow Velocity = 5 ft/sec, Air Gap = 0.6 in.)

Air gap, L_a = 1.0 in.
Prob. stat., x = 8.4 in.
Run no. 15, 16
8.8-oz cotton sateen

Amb. Air Cond.
D. B. T. = 76 °F
W. B. T. = 53.5 °F
B. P. = 29.28 in. Hga

Airflow Cond.
Nom. ext. flow vel. = 5 ft/sec
Ext. flow stat. press. = — in. Hga
Nom. vent. flow vel. = VAR ft/sec
Vent. flow stat. press. = — in. Hga

Skin Sim. Sur. Cond.
Temp. = 76 °F
Dry

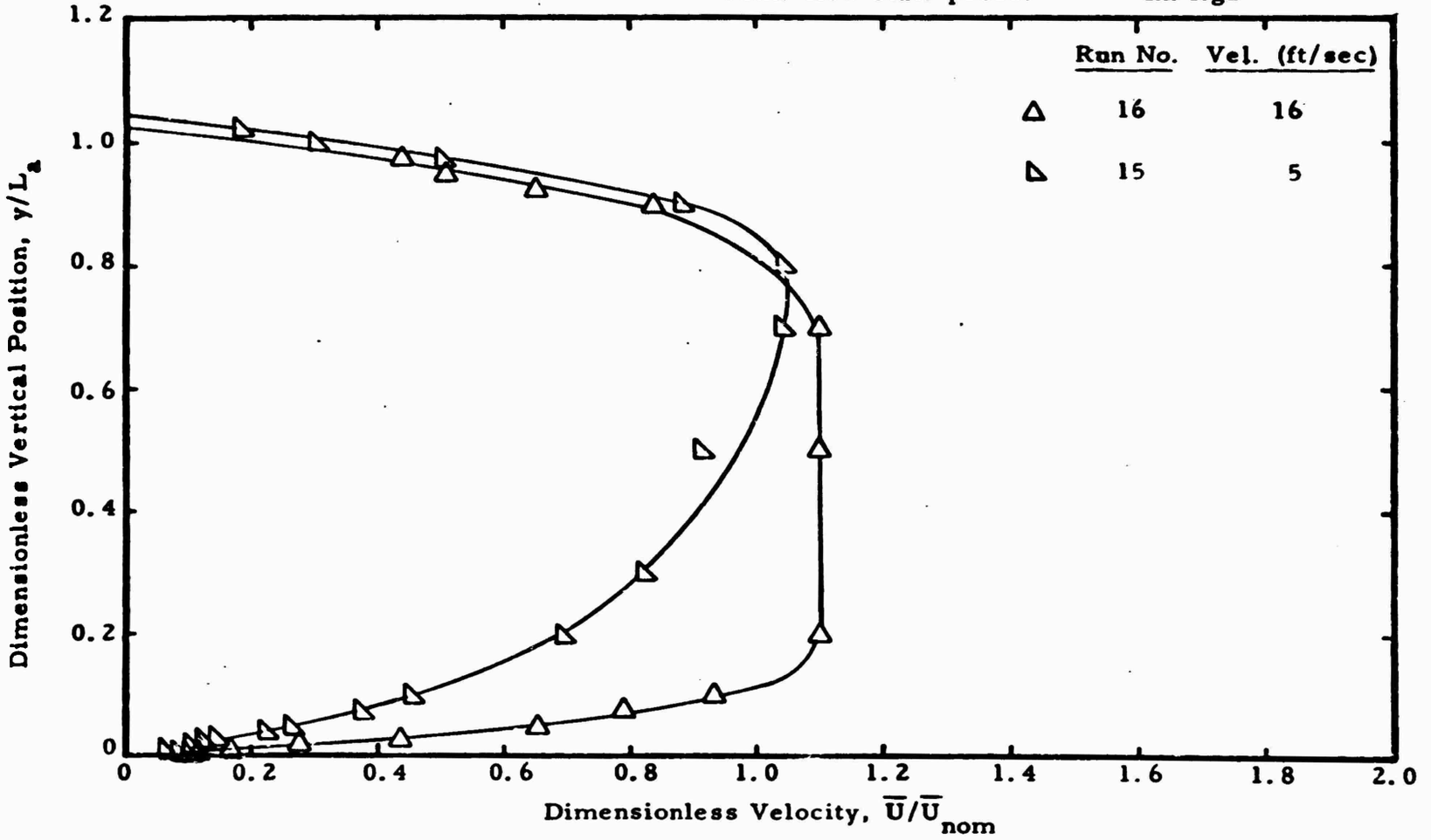

Figure 24. Mean Velocity Variation in Air Gap
(Nominal External Airflow Velocity = 5 ft/sec, Air Gap = 1.0 in.)

Air gap, L_a = 0.6 in.
Prob. stat., x = 8.4 in.
Run no. 56, 55, 54, 53
8.8-oz cotton sateen

Amb. Air Cond.
D. B. T. = 75 °F
W. B. T. = 51.5 °F
B. P. = 29.3 in. Hga

Airflow Cond.
Nom. ext. flow vel. = 10 ft/sec
Ext. flow stat. press. = — in. Hga
Nom. vent. flow vel. = VAR. ft/sec
Vent. flow stat. press. = — in. Hga

Skin Sim. Sur. Cond.
Temp. = 74 °F
Dry

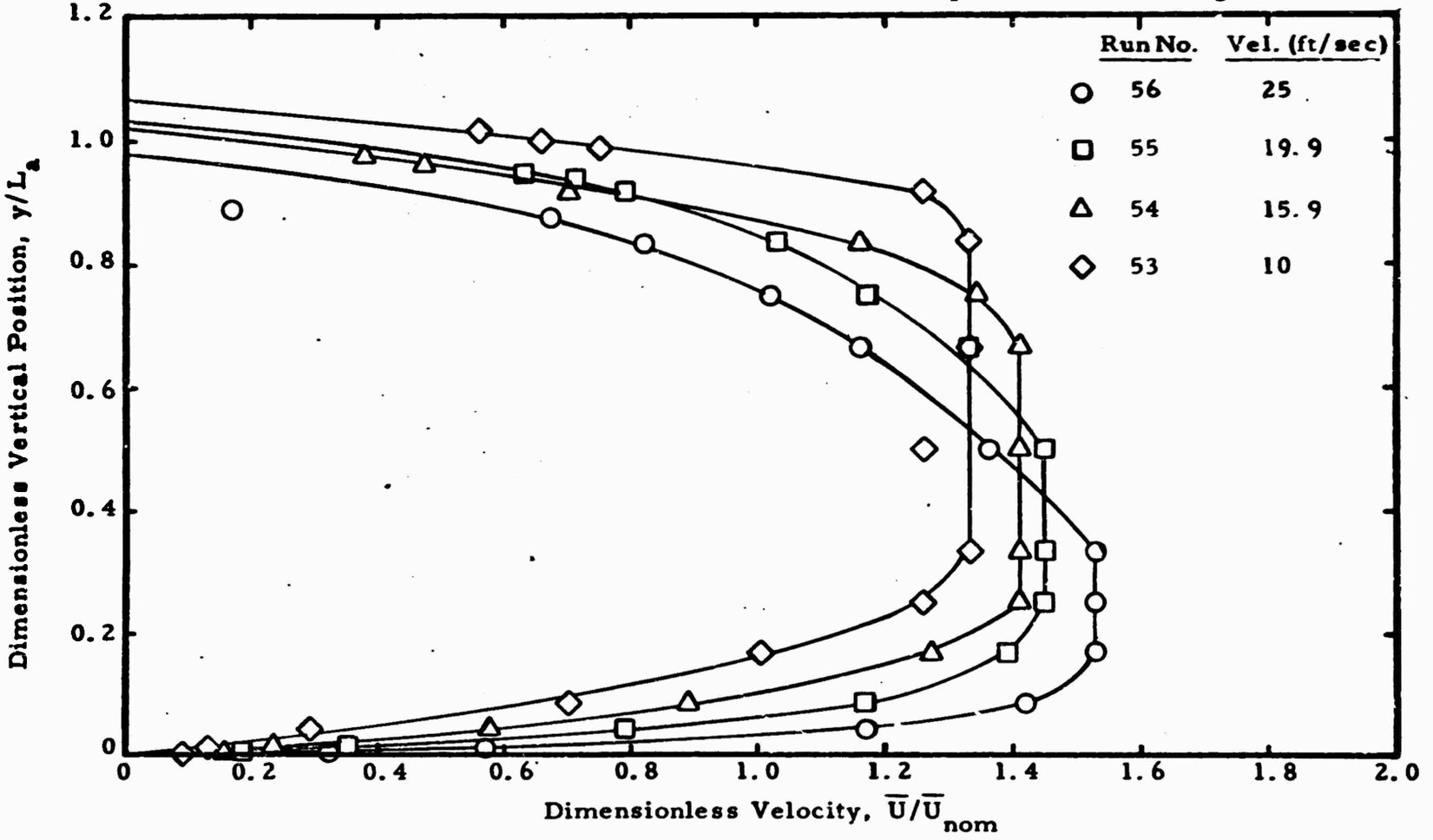

Figure 25 Mean Velocity Variation in Air Gap
(Nominal External Airflow Velocity = 10 ft/sec, Air Gap = 0.6 in.)

At the smaller fabric spacings the boundary layers on the skin simulator and fabric surfaces merge, leaving no room for potential flow (see Figures 19 and 20). The strongest interactions between fabric and skin surface occur for this condition. For larger spacings the influence of fabric on the skin boundary layer is diminished, especially at the lower ventilating flow rates.

Proper interpretation of these data depends upon knowledge of static pressure distributions along both surfaces of the fabric. At this time these pressures can only be measured at the fabric leading and trailing edges. It is also essential that future probings must be made at various x/H positions, where H is the skin simulator length.

The repeatability of data is indicated by separate traverses for identical test conditions, as shown in Figures 26, 27 and 28. This factor is especially important as dependence is placed upon the constancy of the flow when simulator heat and mass loss is related to measured profiles of temperature, velocity and concentration.

The effect of varying the external flow while maintaining a constant ventilating flow is shown in Figure 29. For this particular spacing and high ventilating flow rate, the data indicate a second order effect.

Figure 30 data show a consistent increase in centerline velocity as the spacing is decreased, even though the nominal external and ventilating flows remain constant. For higher flow rates, Figure 31 indicates little change.

To create a true zero flow condition in the external flow channel, it becomes necessary to physically block the air passage. The effects of upstream and downstream blockage are shown in Figure 32. These data show that downstream blockage does not stop the outer flow, as it can flow through the fabric into the air gap.

Air gap, L_a = 0.6 in.
Prob. stat., x = 8.4 in.
Run no. 53, 64
8.8-oz cotton sateen

Amb. Air Cond.
D. B. T. = 75 °F
W. B. T. = 51.5 °F
B. P. = 29.1 in. Hga

Airflow Cond.
Nom. ext. flow vel. = 10 ft/sec
Ext. flow stat. press. = — in. Hga
Nom. vent. flow vel. = 10 ft/sec
Vent. flow stat. press. = — in. Hga

Skin Sim. Sur. Cond.
Temp. = 75 °F
Dry

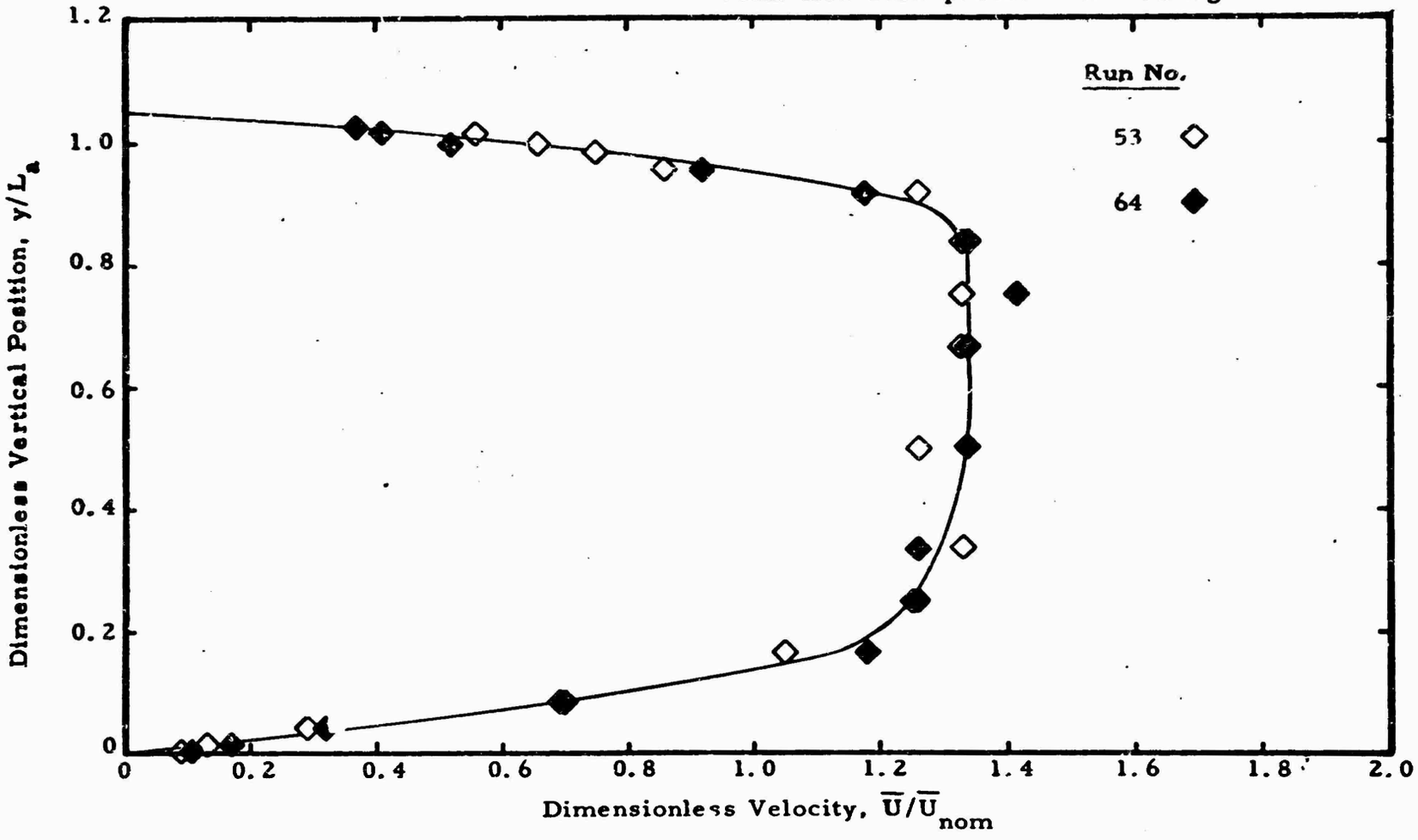

Figure 26. Mean Velocity Variation in Air Gap
(Nominal External Airflow Velocity = 10 ft/sec, Air Gap = 0.6 in.)

Air gap, L_a = 1.0 in.
Prob. stat., x = 8.4 in.
Run no. 16, 17
8.8-oz cotton sateen

Amb. Air Cond.
D. B. T. = 76 °F
W. B. T. = 53.5 °F
B. P. = 29.28 in. Hga

Airflow Cond.
Nom. ext. flow vel. = VAR. ft/sec
Ext. flow stat. press. = — in. Hga
Nom. vent. flow vel. = 16 ft/sec
Vent. flow stat. press. = — in. Hga

Skin Sim. Sur. Cond.
Temp. = 75 °F
Dry

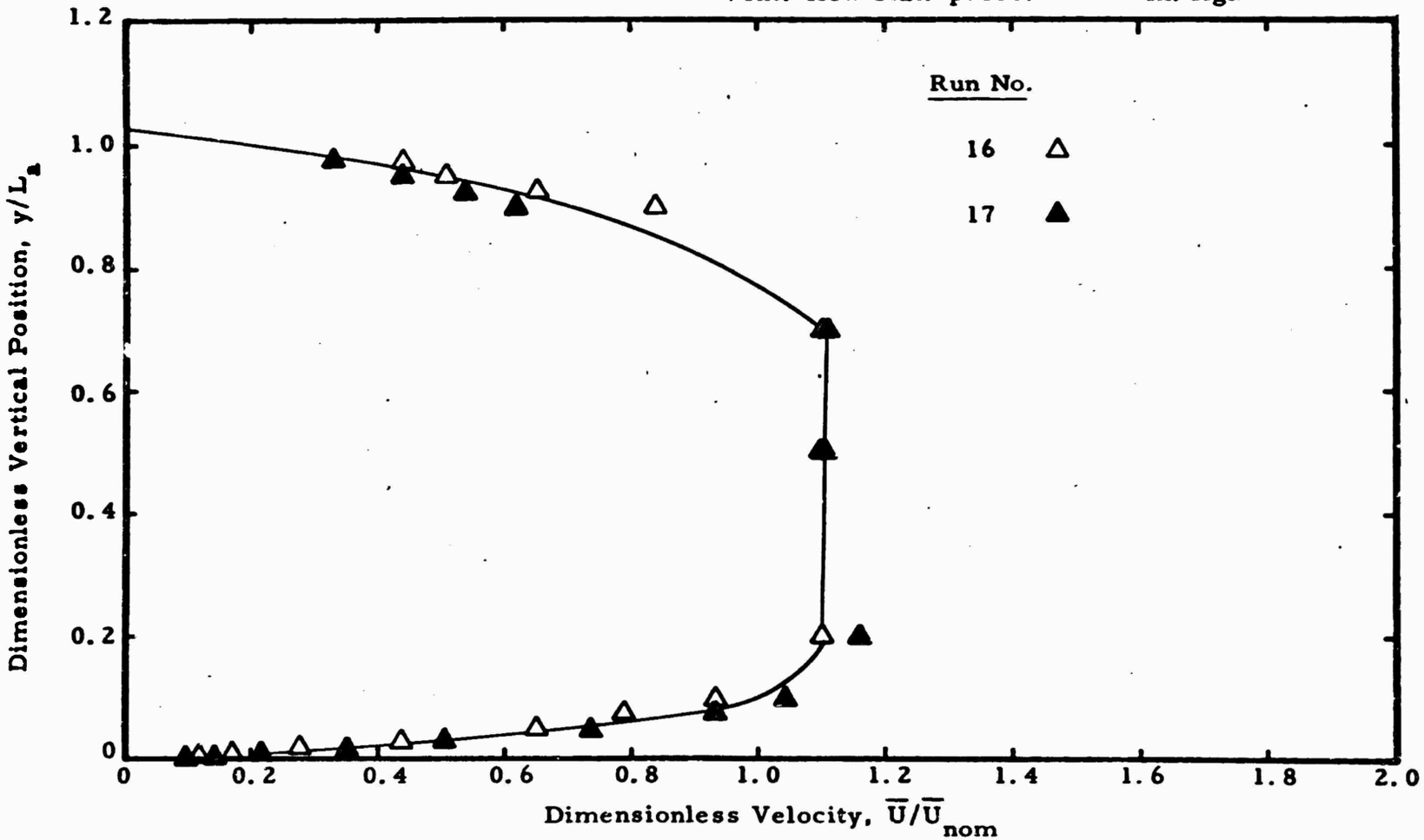

Figure 27. Mean Velocity Variation in Air Gap
(Nominal External Airflow Velocity = VAR ft/sec, Air Gap = 1.0 in.)

Air gap, L_a = .6 in.
Prob. stat., x = 0.4 in.
Run no. 57, 63
8.8-oz cotton sateen

Amb. Air Cond.
D. B. T. = 76 °F
W. B. T. = 52 °F
B. P. = 29.31 in. Hga

Airflow Cond.
Nom. ext. flow vel. = 15 ft/sec
Ext. flow stat. press. = — in. Hga
Nom. vent. flow vel. = 25 ft/sec
Vent. flow stat. press. = — in. Hga

Skin Sim. Sur. Cond.
Temp. = 76 °F
Dry

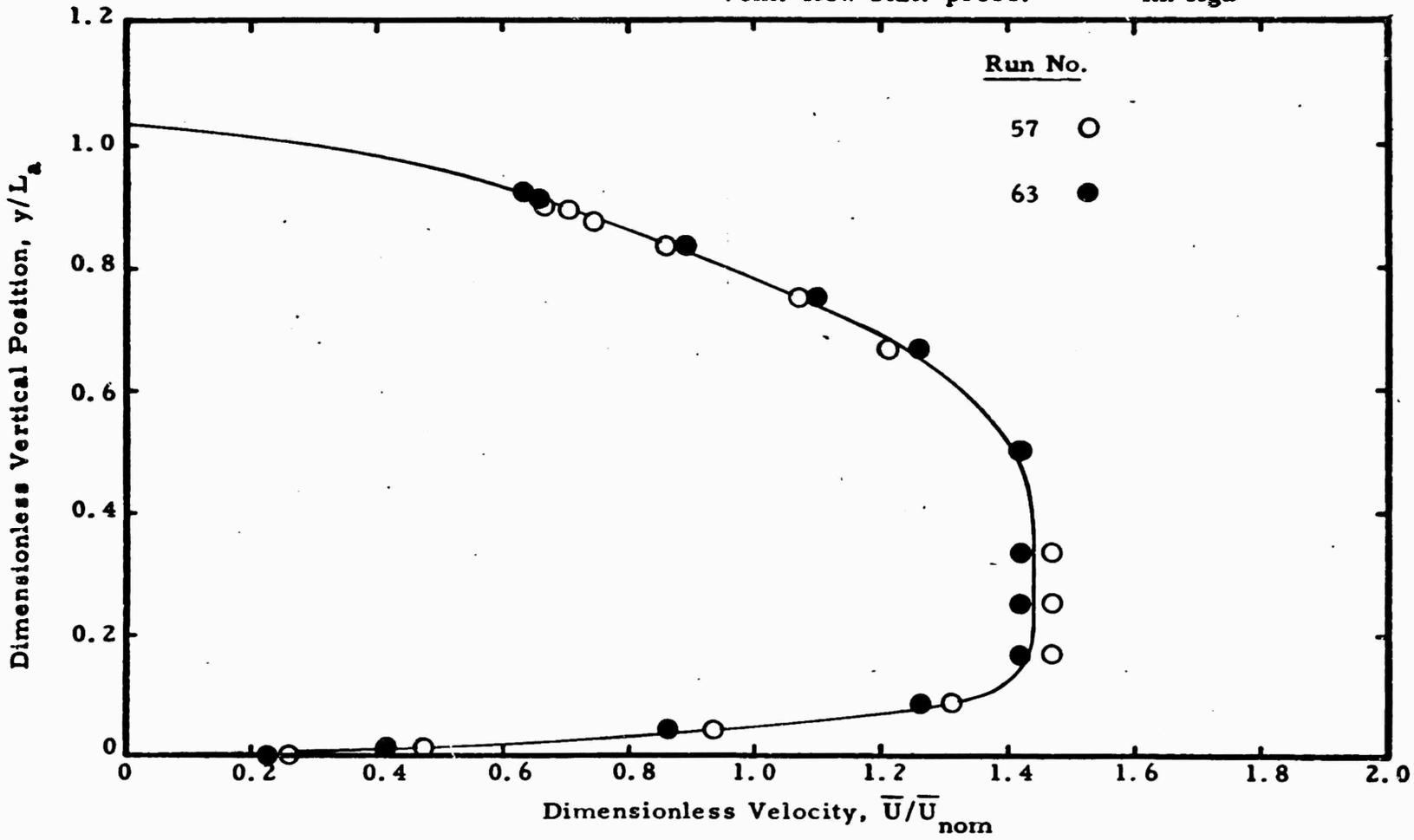

Figure 28 Mean Velocity Variation in Air Gap
(Nominal External Airflow Velocity = 15 ft/sec, Air Gap = 0.6 in.)

Air gap, L_a = 0.4 in.
Prob. stat.; x = 8.4 in.
Run no. 44, 45, 46, 47
8.8-oz cotton sateen

Amb. Air Cond.
D. B. T. = 76.1 °F
W. B. T. = 57.9 °F
B. P. = 29.00 in. Hga

Airflow Cond.
Nom. ext. flow vel. = VAR. ft/sec
Ext. flow stat. press. = — in. Hga
Nom. vent. flow vel. = 25 ft/sec
Vent. flow stat. press. = — in. Hga

Skin Sim. Sur. Cond.
Temp. = 76 °F
Dry

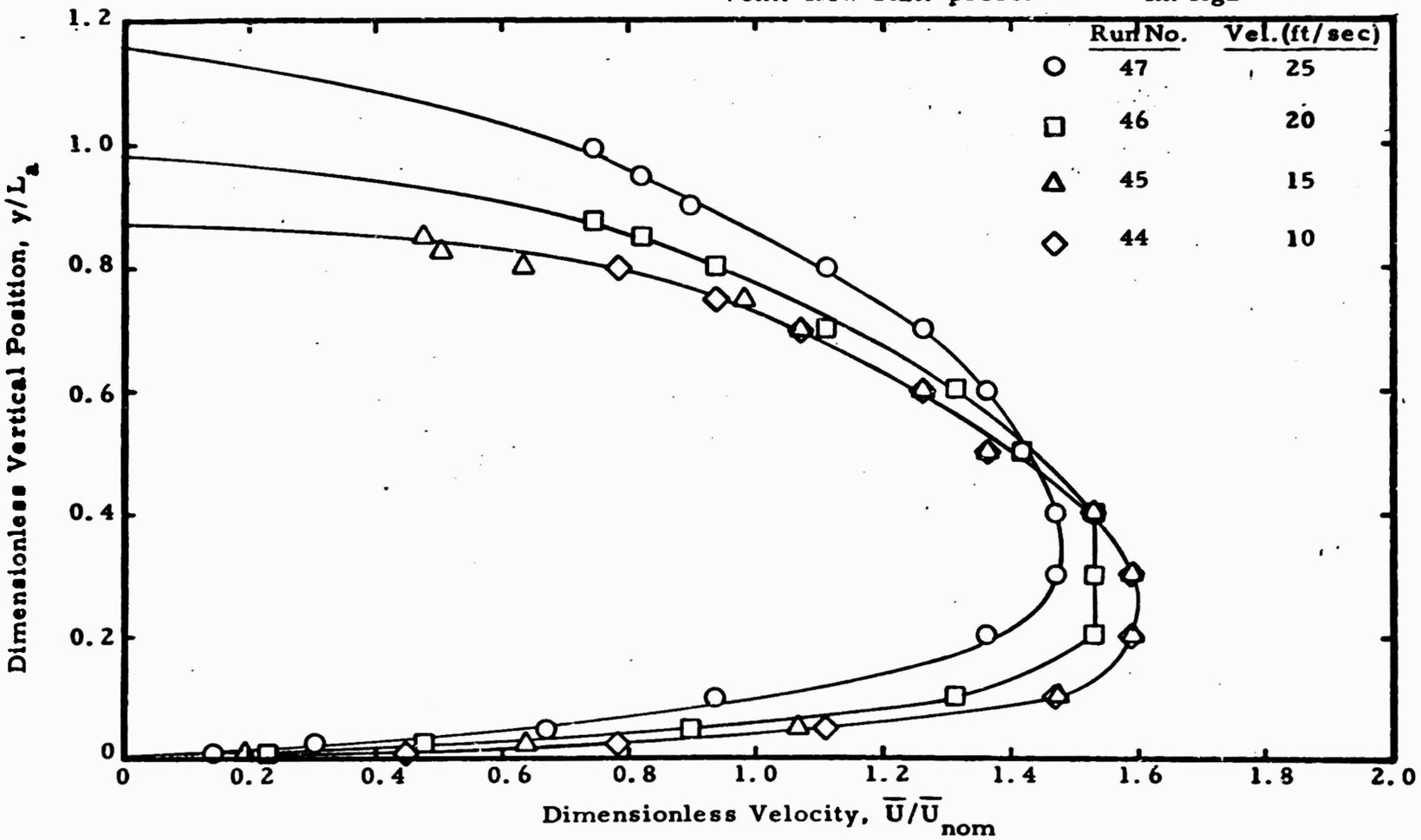

Figure 29. Mean Velocity Variation in Air Gap
(Nominal External Airflow Velocity = VAR. ft/sec, Air Gap = 0.4 in.)

Air gap, L_a = VAR in.
Prob. stat., x = 8.4 in.
Run no. 30, 36, 48, 59
8.8-oz cotton sateen

Amb. Air Cond.
D. B. T. = — °F
W. B. T. = — °F
B. P. = — in. Hga

Airflow Cond.
Nom. ext. flow vel. = 5 ft/sec
Ext. flow stat. press. = — in. Hga
Nom. vent. flow vel. = 5 ft/sec
Vent. flow stat. press. = — in. Hga

Skin Sim. Sur. Cond.
Temp. = 75 °F
Dry

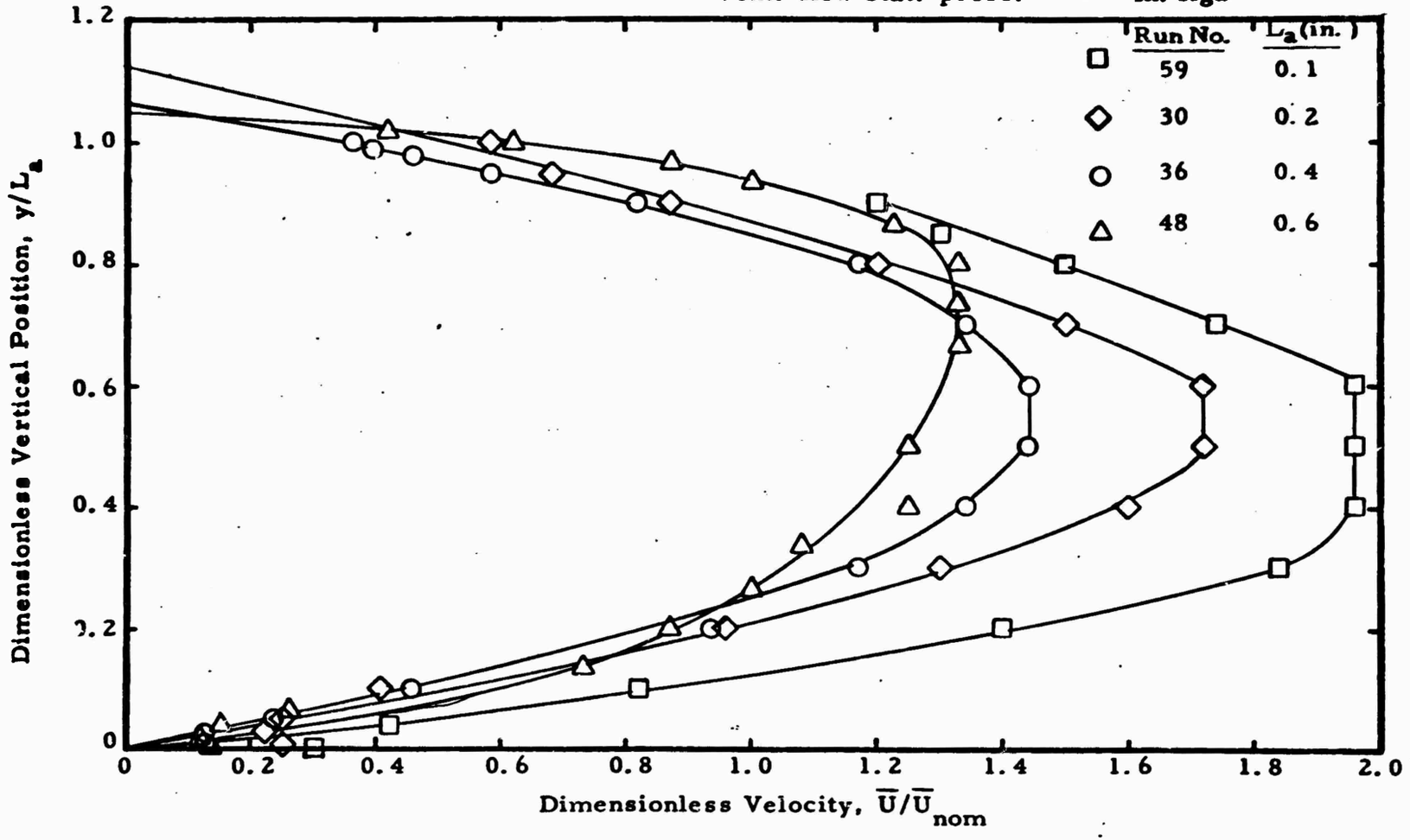

Figure 30. Mean Velocity Variation in Air Gap
(Nominal External Airflow Velocity = 5 ft/sec, Air Gap = VAR in.)

Air gap, L_a = VAR in.
Prob. stat., x = 8.4 in.
Run no. 44, 56
8.8-oz cotton sateen

Amb. Air Cond.
D. B. T. = 75 °F
W. B. T. = 57.5 °F
B. P. = 29.0 in. Hga

Airflow Cond.
Nom. ext. flow vel. = 10 ft/sec
Ext. flow stat. press. = — in. Hga
Nom. vent. flow vel. = 25 ft/sec
Vent. flow stat. press. = — in. Hga

Skin Sim. Sur. Cond.
Temp. = 75 °F
Dry

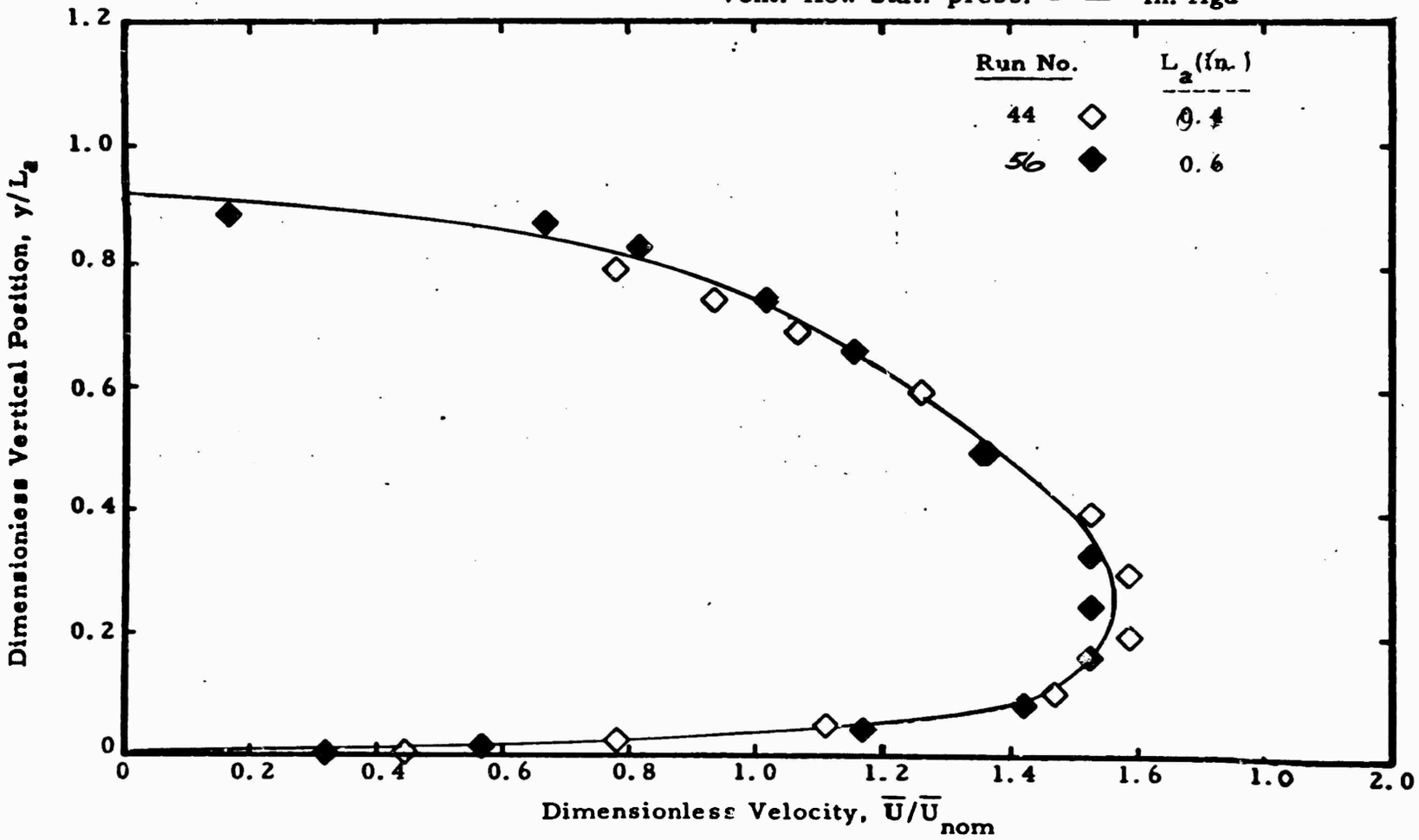

Figure 31. Mean Velocity Variation in Air Gap
(Nominal External Airflow Velocity = 10 ft/sec, Air Gap = VAR in.)

Air gap, L_a = 0.2 in.
Prob. stat., x = 8.4 in.
Run no. 27, 28
8.8-oz cotton sateen

Amb. Air Cond.
D. B. T. = 76.5 °F
W. B. T. = 52 °F
B. P. = 29.38 in. Hga

Airflow Cond.
Nom. ext. flow vel. = Neg ft/sec
Ext. flow stat. press. = — in. Hga
Nom. vent. flow vel. = ~5 ft/sec
Vent. flow stat. press. = — in. Hga

Skin Sim. Sur. Cond.
Temp. = 75 °F
Dry

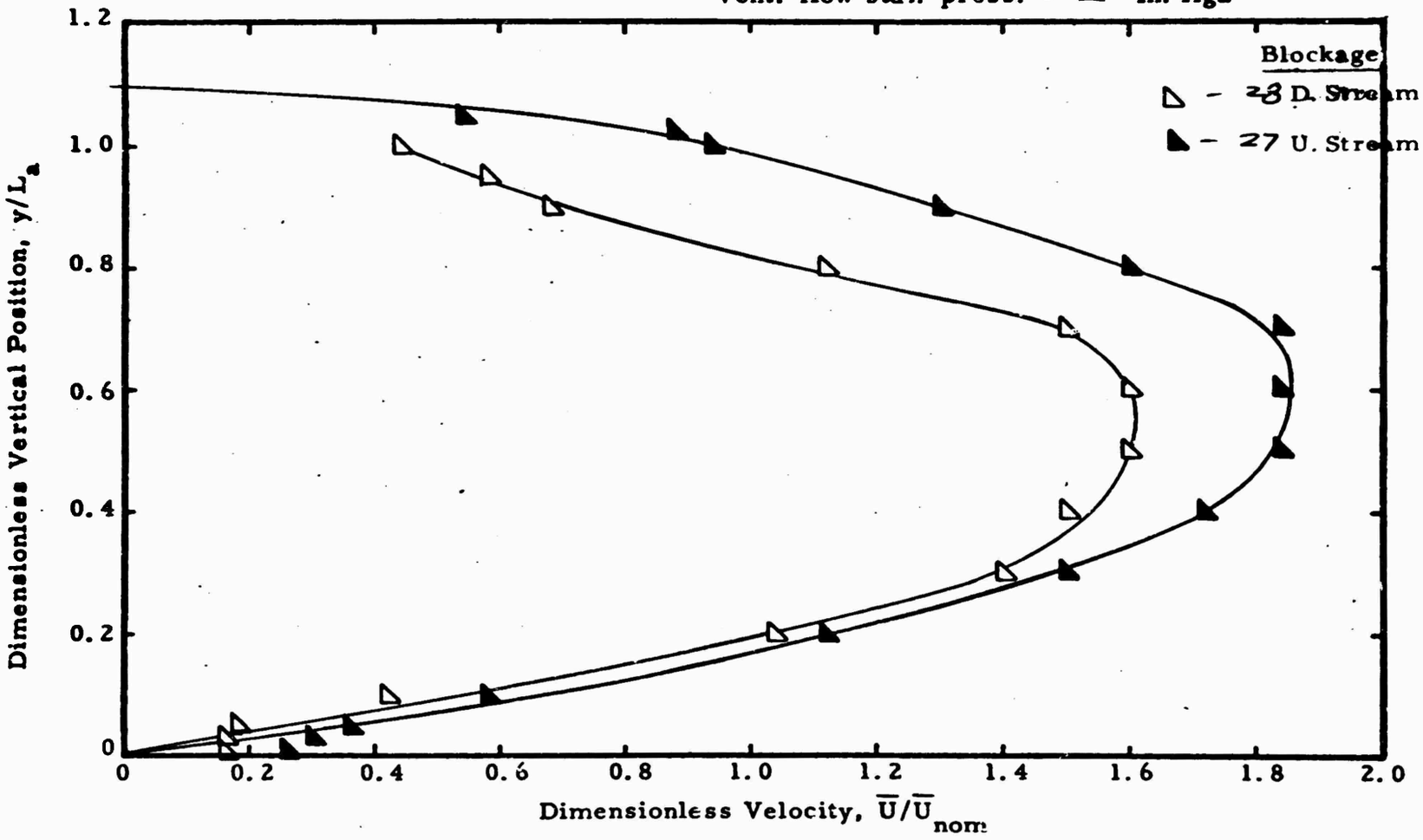

Figure 32. Mean Velocity Variation in Air Gap
(Nominal External Airflow Velocity = Neg ft/sec, Air Gap = 0.2 in.)

(2) Fluctuating Velocity Data.- Oscilloscope traces of the hot-wire bridge fluctuating voltage, which is related to flow velocity fluctuations, are shown in Figures 33 and 34. Figure 33 presents traces for a nominal fabric spacing, L_a of 0.4 inch for various combinations of external and ventilating flows. In general, the highest turbulence intensities, $u'/\bar{U}$ occur near the fabric, although an unusually high level at 44.9 percent is reached at the skin simulator surface for run no. 43. At the present time this high value cannot be explained.

Figure 34 shows data for two vertical positions of 0.005 and 0.20 inch at various nominal ventilating flow velocities $\bar{U}_{a_{nom}}$. The transition from laminar flow at lower velocities to turbulent flow at higher velocities, as evidenced by higher turbulence intensities ($\approx$20 percent), is clearly shown.

Figures 35 through 38 show turbulence intensity profiles for various ventilating flows at constant external velocities. Most of the data show high turbulence intensities in the boundary layers with lower values in the middle of the air gap. The high turbulence intensities near the fabric are probably caused by the fact that the instantaneous velocity vector U is not zero due to the cross flow across the fabric. It may be recalled that the hot-wire probe is relatively insensitive to the turbulent y velocity component v' for normal boundary layer flow conditions at low turbulence intensities. This can be seen by performing a vector addition of the fluctuating u' and v' components to the mean velocity $\bar{U}$. Because of cross flow, both the mean and fluctuating velocity components in the y direction are not zero and, in fact, are probably larger than the x components. This indicates a very complicated flow condition near the fabric. It is also possible that some of the low frequency contribution to the total turbulence intensity is provided by vibration of the fabric. The phenomena involved is being studied further.

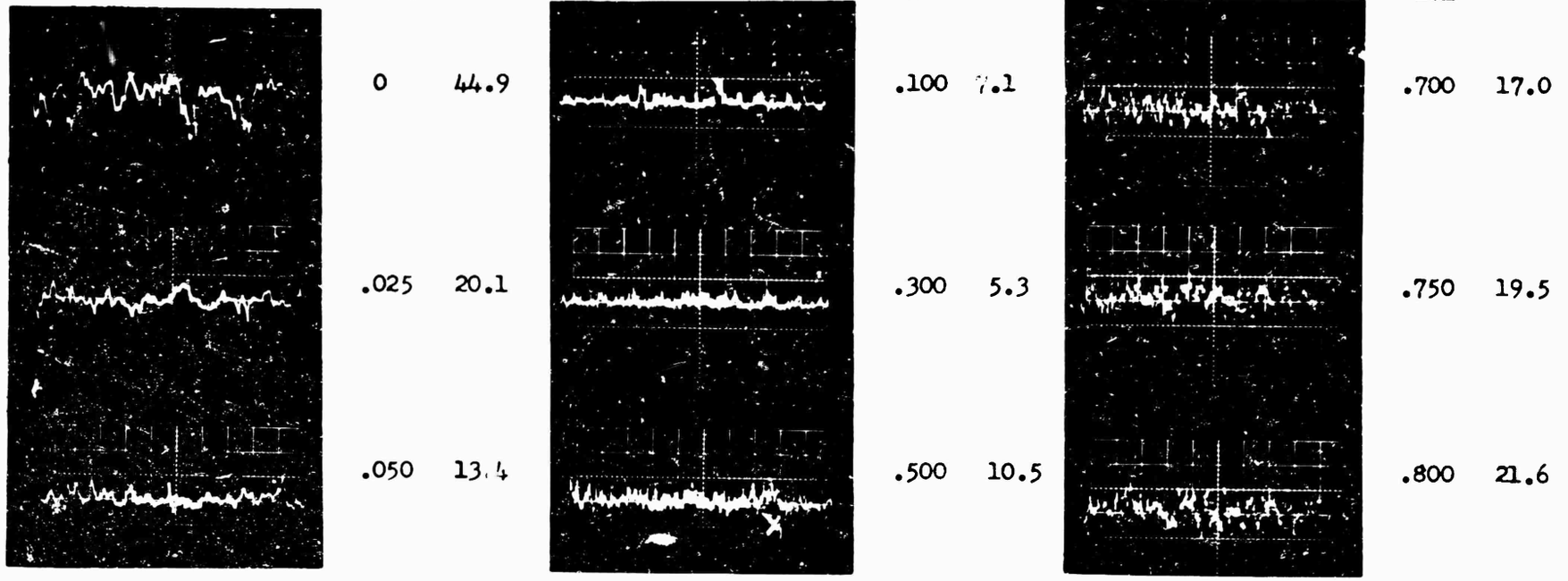

C.R.O. Vert. Sen. = 0.50 V/cm
C.R.O. Sweep Speed = 10 ms/cm

Run No. 43
$L_{a_{nom}}$ = 0.40 in.

Nom. Ext. Flow Vel. = 6.4 ft/sec
Nom. Vent. Flow Vel. = 25 ft/sec

Figure 33. Oscilloscope Traces of Fluctuating Velocity Component (Vertical Traverse)

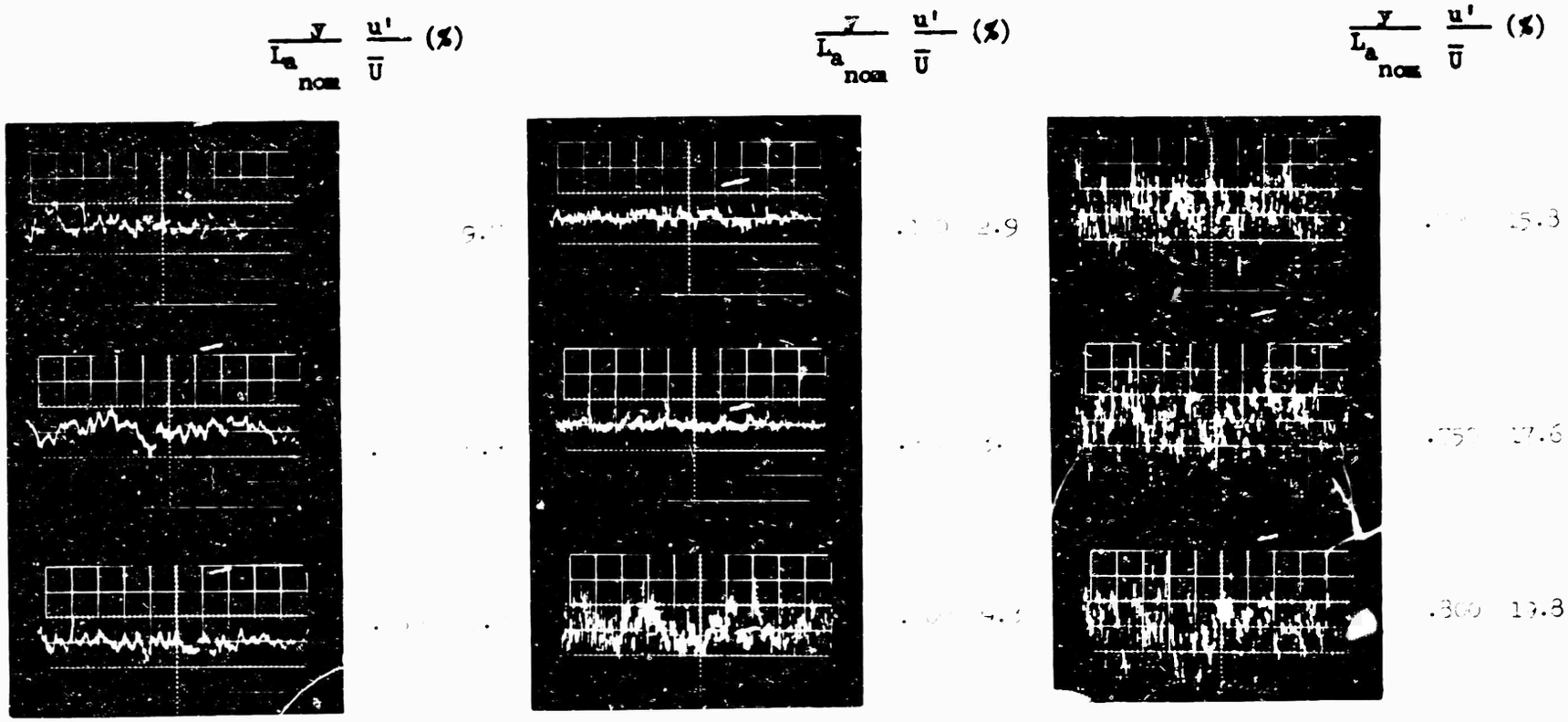

C.R.O. Vert. Sen. = 0.2 V/cm

C.R.O. Sweep Speed = 10 ms/cm

Run No. 65

$L_{a_{nom}}$ = 0.40 in.

Nom. Ext. Flow Vel. = 15 ft/sec

Nom. Vent. Flow Vel. = 25 ft/sec

Figure 33 (continued)

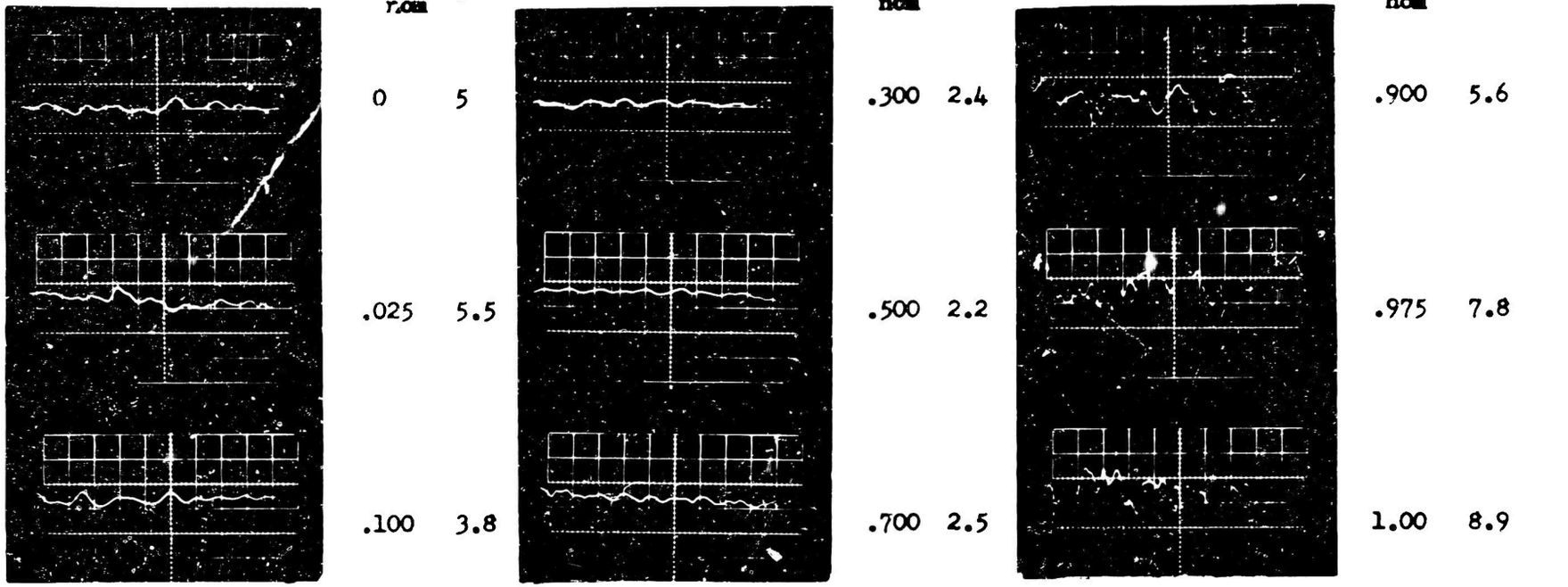

$\frac{y}{L_{a_{nom}}}$	$\frac{u'}{\bar{U}}$ (%)	$\frac{y}{L_{a_{nom}}}$	$\frac{u'}{\bar{U}}$ (%)	$\frac{y}{L_{a_{nom}}}$	$\frac{u'}{\bar{U}}$ (%)
0	5	.300	2.4	.900	5.6
.025	5.5	.500	2.2	.975	7.8
.100	3.8	.700	2.5	1.00	8.9

C.R.O. Vert. Sen. = 0.10 V/cm
C.R.O. Sweep Speed = 10 ms/cm

Run No. 37
$L_{a_{nom}}$ = 0.40 in.

Nom. Ext. Flow Vel. = 16.1 ft/sec
Nom. Vent. Flow Vel. = 16.7 ft/sec

Figure 33 (continued)

y = 0.005 in.
$L_{a_{nom}}$ = 0.4 in.
C.R.O. Sweep Speed = 10 ms/cm

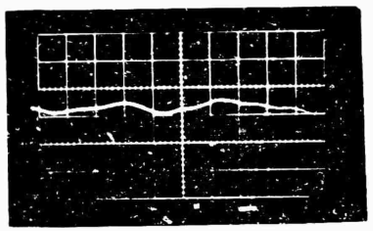

$\bar{U}_{a_{nom}}$ = 0 ft/sec

$\frac{u'}{\bar{U}}$ (%) = 3.8

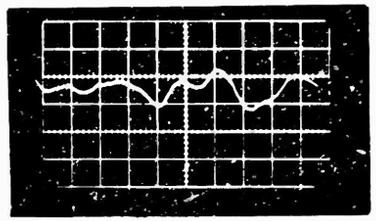

$\bar{U}_{a_{nom}}$ = 10 ft/sec

$\frac{u'}{\bar{U}}$ (%) = 4.7

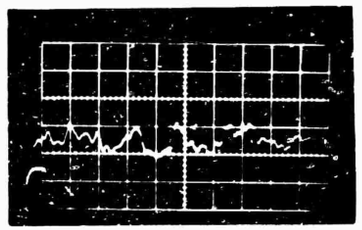

$\bar{U}_{a_{nom}}$ = 20 ft/sec

$\frac{u'}{\bar{U}}$ (%) = 10.8

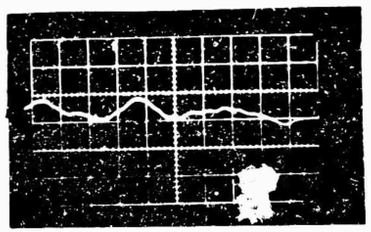

$\bar{U}_{a_{nom}}$ = 5 ft/sec

$\frac{u'}{\bar{U}}$ (%) = 4.5

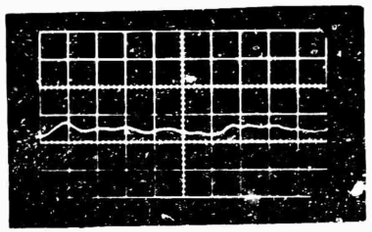

$\bar{U}_{a_{nom}}$ = 15 ft/sec

$\frac{u'}{\bar{U}}$ (%) = 5.1

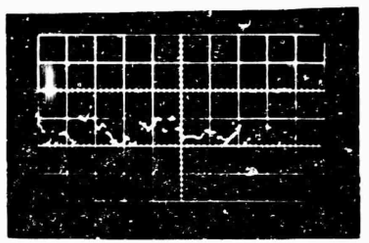

$\bar{U}_{a_{nom}}$ = 25 ft/sec

$\frac{u'}{\bar{U}}$ (%) = 24.4

Figure 34. Oscilloscope Traces of Fluctuating Velocity Component (Variation of Ventilating Flow Velocity)

y = 0.20 in.
L_x = 0.4 in.
nom
C.R.O. Sweep Speed = 10 ms/cm

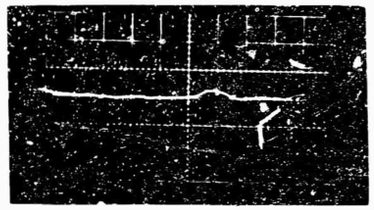

$\bar{U}_{a_{nom}}$ = 0 ft/sec

$\frac{u'}{\bar{U}}$ (%) = 3.1

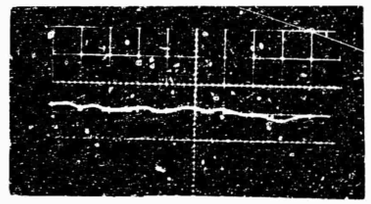

$\bar{U}_{a_{nom}}$ = 10 ft/sec

$\frac{u'}{\bar{U}}$ (%) = 1.6

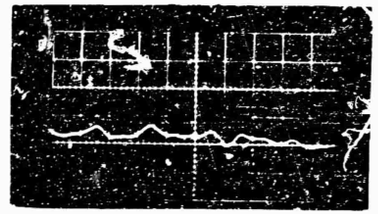

$\bar{U}_{a_{nom}}$ = 20 ft/sec

$\frac{u'}{\bar{U}}$ (%) = 7.0

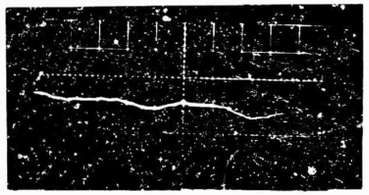

$\bar{U}_{a_{nom}}$ = 5 ft/sec

$\frac{u'}{\bar{U}}$ (%) = 2.0

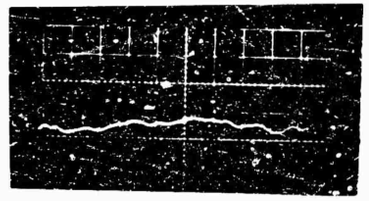

$\bar{U}_{a_{nom}}$ = 15 ft/sec

$\frac{u'}{\bar{U}}$ (%) = 1.0

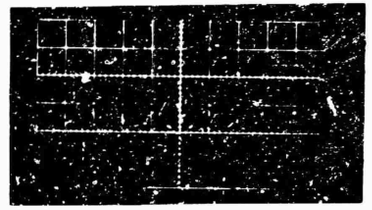

$\bar{U}_{a_{nom}}$ = 25 ft/sec

$\frac{u'}{\bar{U}}$ (%) = 10.4

Figure 34 (continued)

Air gap, L_a = 0.2 in.
Prob. stat., x = 8.4 in.
Run no. 25, 26, 27
8.8-oz cotton sateen

Amb. Air Cond.
D. B. T. = 73.5 °F
W. B. T. = 52 °F
B. P. = 29.39 in. Hga

Airflow Cond.
Nom. ext. flow vel. = MG ft/sec
Ext. flow stat. press. = — in. Hga
Nom. vent. flow vel. = MR ft/sec
Vent. flow stat. press. = — in. Hga

Skin Sim. Sur. Cond.
Temp. = 75 °F
Dry

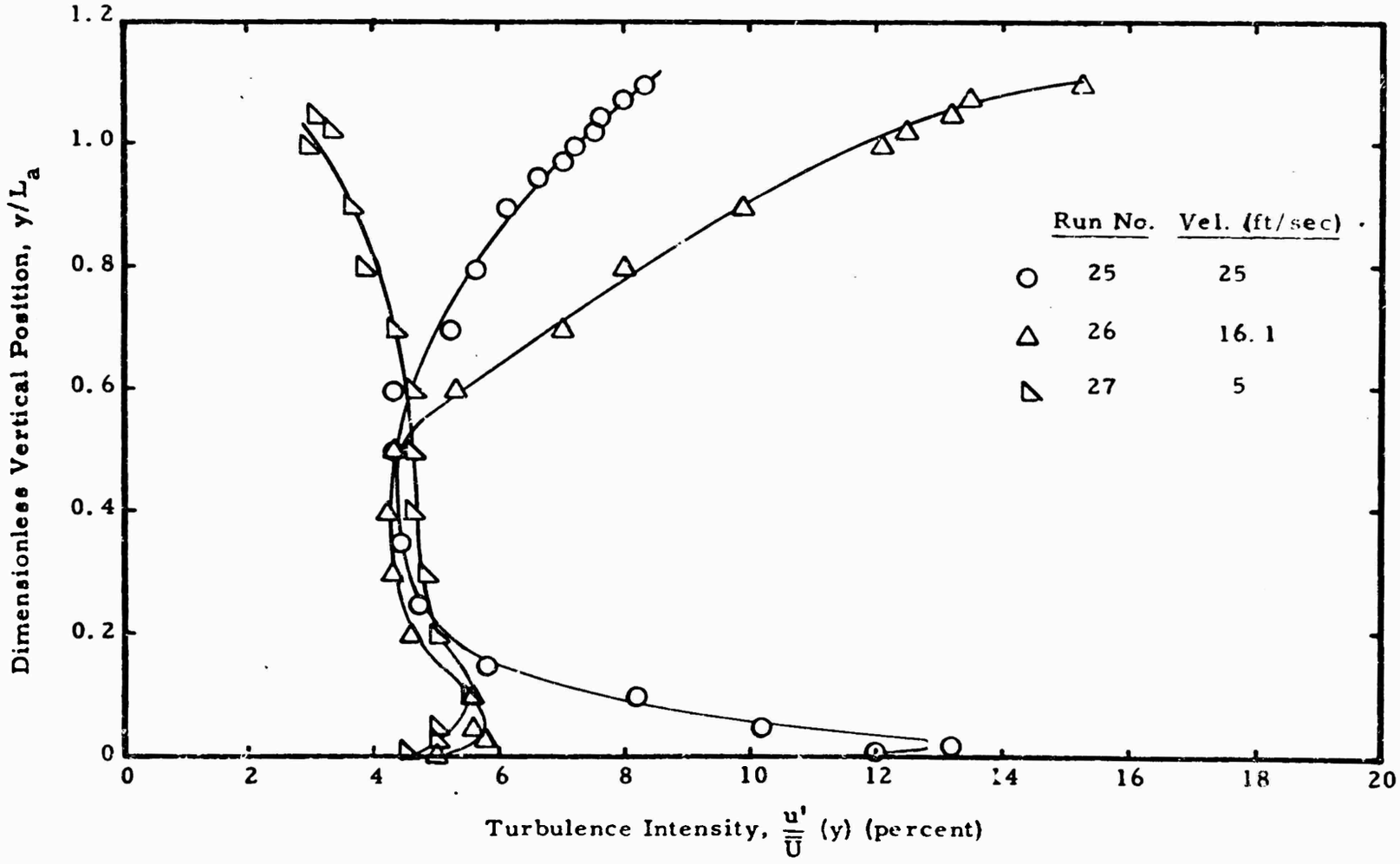

Figure 35. Turbulence Intensity Variation in Air Gap
(Nominal External Airflow Velocity = MG ft/sec, Air Gap = 0.2 in.)

Air gap, L_a = 0.4 in.
Prob. stat., x = 8.4 in.
Run no. 39, 40, 41, 42
8.8-oz cotton sateen

Amb. Air Cond.
D.B.T. = 76.1 °F
W.B.T. = 57.9 °F
B.P. = 28.94 in. Hga

Airflow Cond.
Nom. ext. flow vel. = NEG. ft/sec
Exi. flow stat. press. = — in. Hga
Nom. vent. flow vel. = VAR ft/sec
Vent. flow stat. press. = — in. Hga

Skin Sim. Sur. Cond.
Temp. = 76 °F
Dry

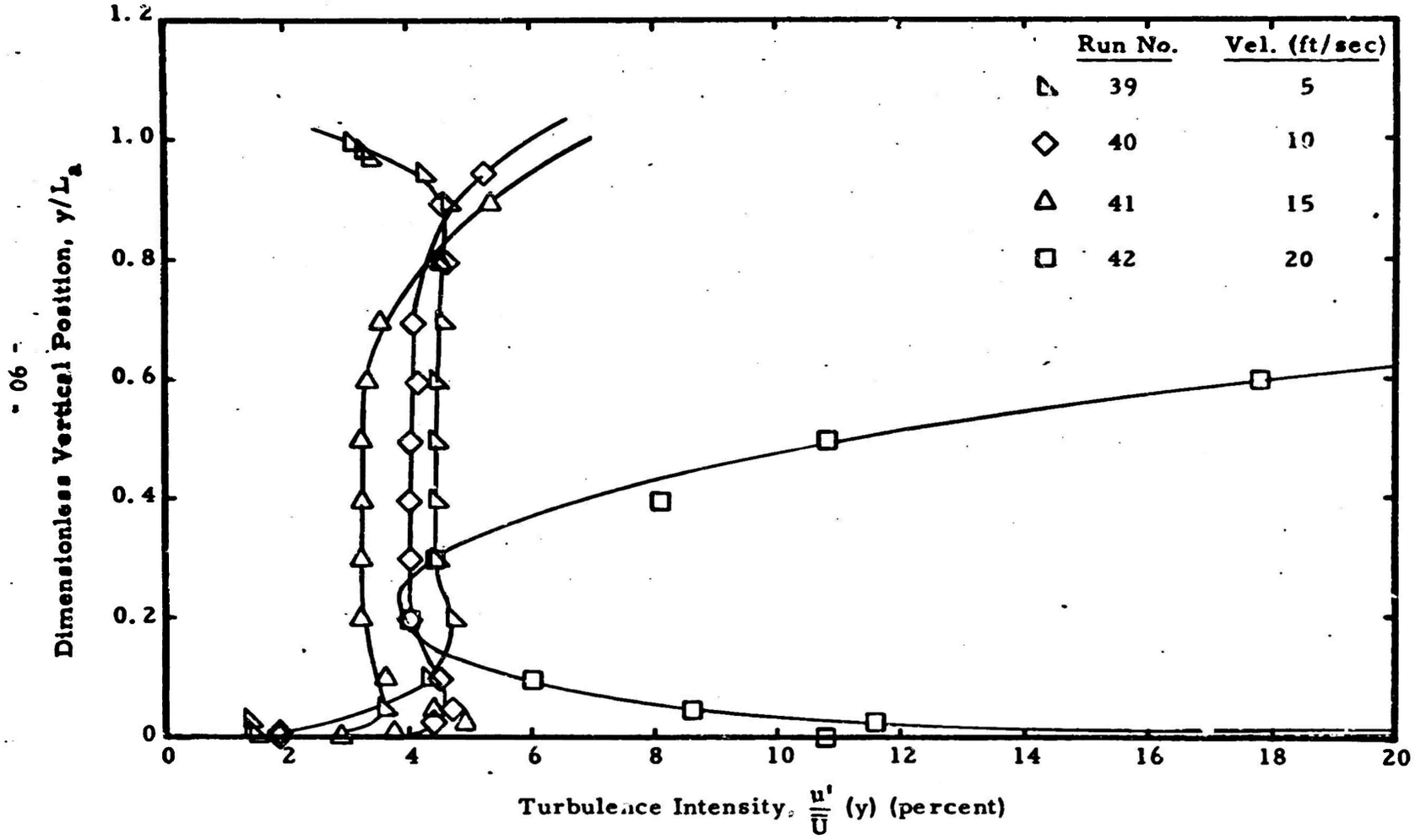

Figure 36. Turbulence Intensity Variation in Air Gap
(Nominal External Airflow Velocity = NEG. ft/sec, Air Gap = 0.4 in.)

Air gap, L_a = 0.6 in.
Prob. stat., x = 8.4 in.
Run no. 48, 49, 50, 51, 52
8.8-oz cotton sateen

Amb. Air Cond.
D. B. T. = 76 °F
W. B. T. = 52 °F
B. P. = 29.1 in. Hga

Airflow Cond.
Nom. ext. flow vel. = 5 ft/sec
Ext. flow stat. press. = — in. Hga
Nom. vent. flow vel. = VAR ft/sec
Vent. flow stat. press. = — in. Hga

Skin Sim. Sur. Cond.
Temp. = 76 °F
Dry

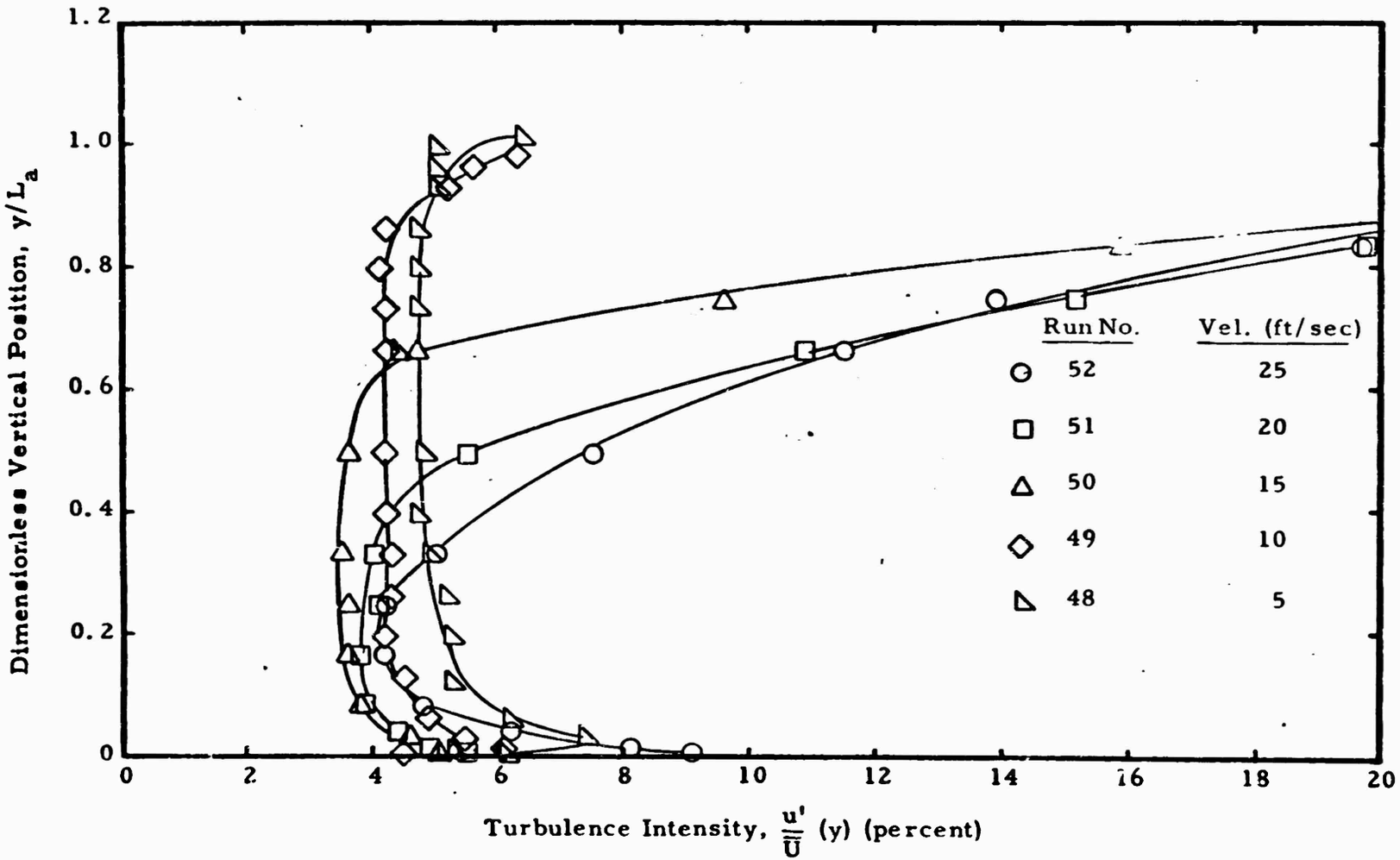

Figure 37. Turbulence Intensity Variation in Air Gap
(Nominal External Airflow Velocity = 5 ft/sec, Air Gap = 0.6in.)

Air gap, L_a = 0.6 in.
Prob. stat., x = 8.4 in.
Run no. 56, 55, 54, 53
8.8-oz cotton sateen

Amb. Air Cond.
D.B.T. = 76. °F
W.B.T. = 52. °F
B.P. = 29.10 in. Hga

Airflow Cond.
Nom. ext. flow vel. = 10 ft/sec
Ext. flow stat. press. = — in. Hga
Nom. vent. flow vel. = MR ft/sec
Vent. flow stat. press. = — in. Hga

Skin Sim. Sur. Cond.
Temp. = 74 °F
Dry

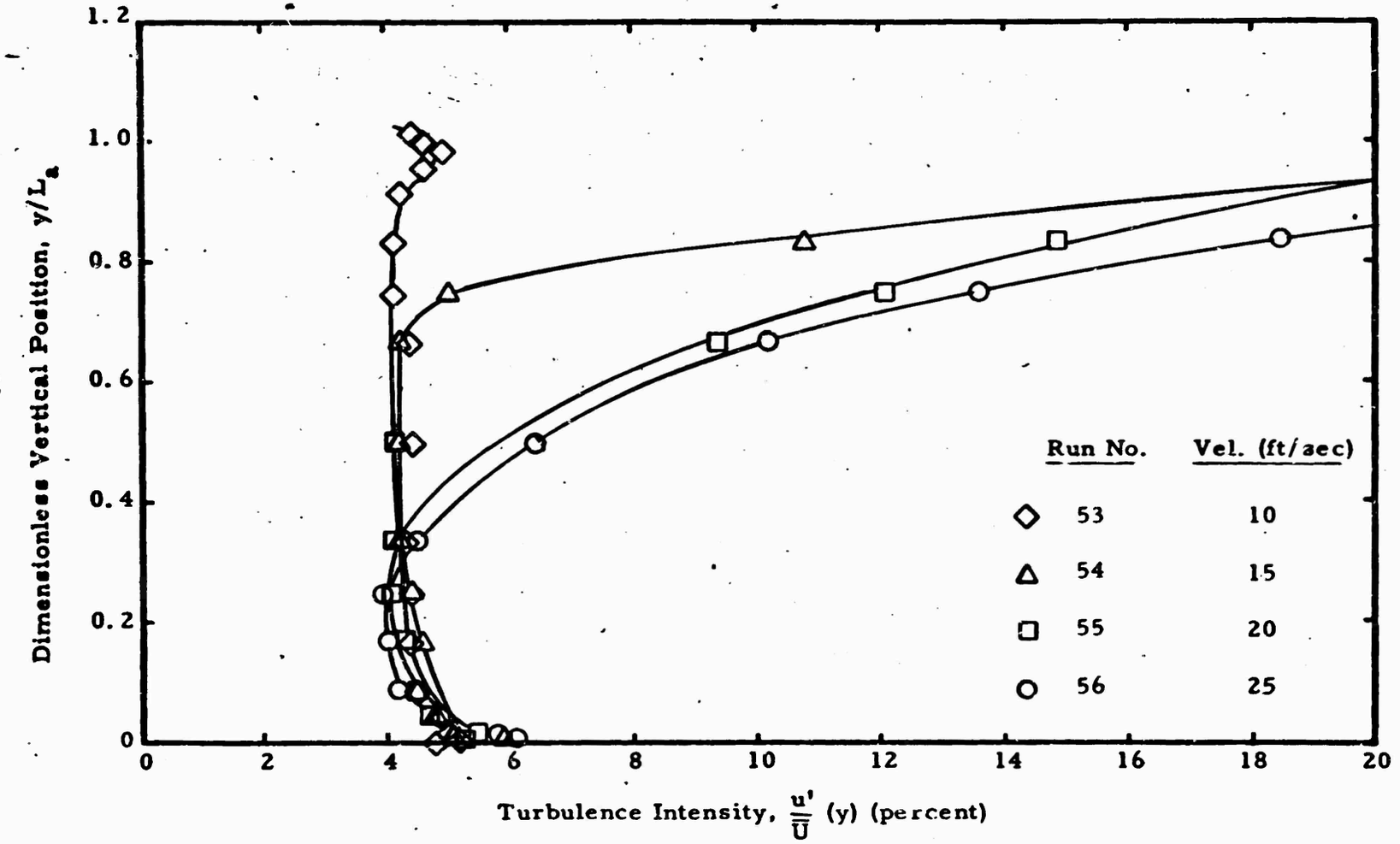

Figure 38. Turbulence Intensity Variation in Air Gap
(Nominal External Airflow Velocity = 10 ft/sec, Air Gap = 0.6 in.)

Shown in Figure 39 are traverses for a constant ventilating flow rate and variable external velocities. Except for the highest external velocity of 25 ft/sec, the influence on turbulence intensity is quite small.

Figure 40 shows data for various air gap spacings. For these particular flow conditions the effect of spacing is small, indicating essentially laminar flow conditions.

b. Variation of Test Section Configuration

It was decided to establish some of the gross characteristics of various possible experimental arrangements before proceeding with the bulk of the tests. Four different configurations were studied at ventilating flow velocities of 5, 15, and 25 ft/sec. The first two configurations were selected to establish the characteristics of a system in which no flow passes through the fabric. In these, as well as in the subsequent two arrangements, the inlet and exit planes for the external flow channel were blocked off and sealed. In addition, for the first two configurations studied, the cover plate at the top of the external flow channel was left in place and sealed tightly to prevent any inflow or outflow of air into this channel. For this condition, any flow of air within the external channel must come through the fabric from the air gap. Smoke tests at all air gap ventilating flow rates studied indicated that no flow existed in the external channel. This showed that the pressure difference across the cloth in these two experimental arrangements could be considered as negligible.

The variation of the power consumption of the skin simulator model for these two cases is presented in Figure 41. In the induction case, room air was drawn through the air gap channel by attaching the downstream end of the channel to the low pressure side of the pump. In the blowing case, the high pressure side of the pump was attached to the upstream section of tunnel by

Air gap, L_a = 0.4 in.	Amb. Air Cond.	Airflow Cond.	Skin Sim. Sur. Cond.
Prob. stat., x = 8.4 in.	D.B.T. = — °F	Nom. ext. flow vel. = VAR ft/sec	Temp. = 75 °F
Run no. 44, 45, 46, 47	W.B.T. = — °F	Ext. flow stat. press. = — in. Hga	Dry
8.8-oz cotton sateen	B.P. = 29.00 in. Hga	Nom. vent. flow vel. = 25 ft/sec	
		Vent. flow stat. press. = — in. Hga	

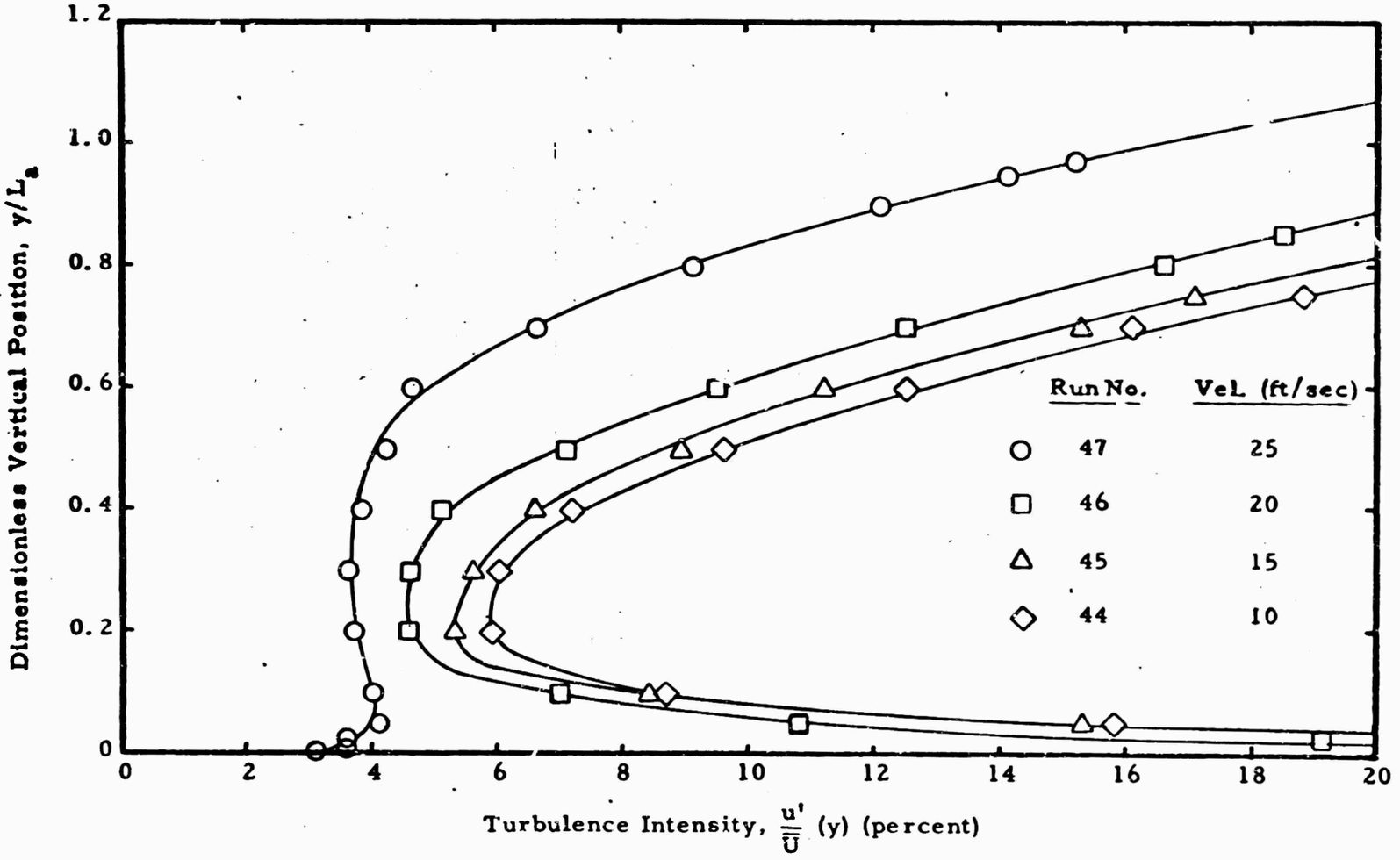

Figure 39. Turbulence Intensity Variation in Air Gap
(Nominal External Airflow Velocity = VAR ft/sec, Air Gap = 0.4 in.)

Air gap, L_a = VAR in.
Prob. stat., x = 8.4 in.
Run no. 30, 36, 48, 59
8.8-oz cotton sateen

Amb. Air Cond.
D. B. T. = — °F
W. B. T. = — °F
B. P. = — in. Hga

Airflow Cond.
Nom. ext. flow vel. = 5 ft/sec
Ext. flow stat. press. = — in. Hga
Nom. vent. flow vel. = 5 ft/sec
Vent. flow stat. press. = — in. Hga

Skin Sim. Sur. Cond
Temp. = 75 °F
Dry

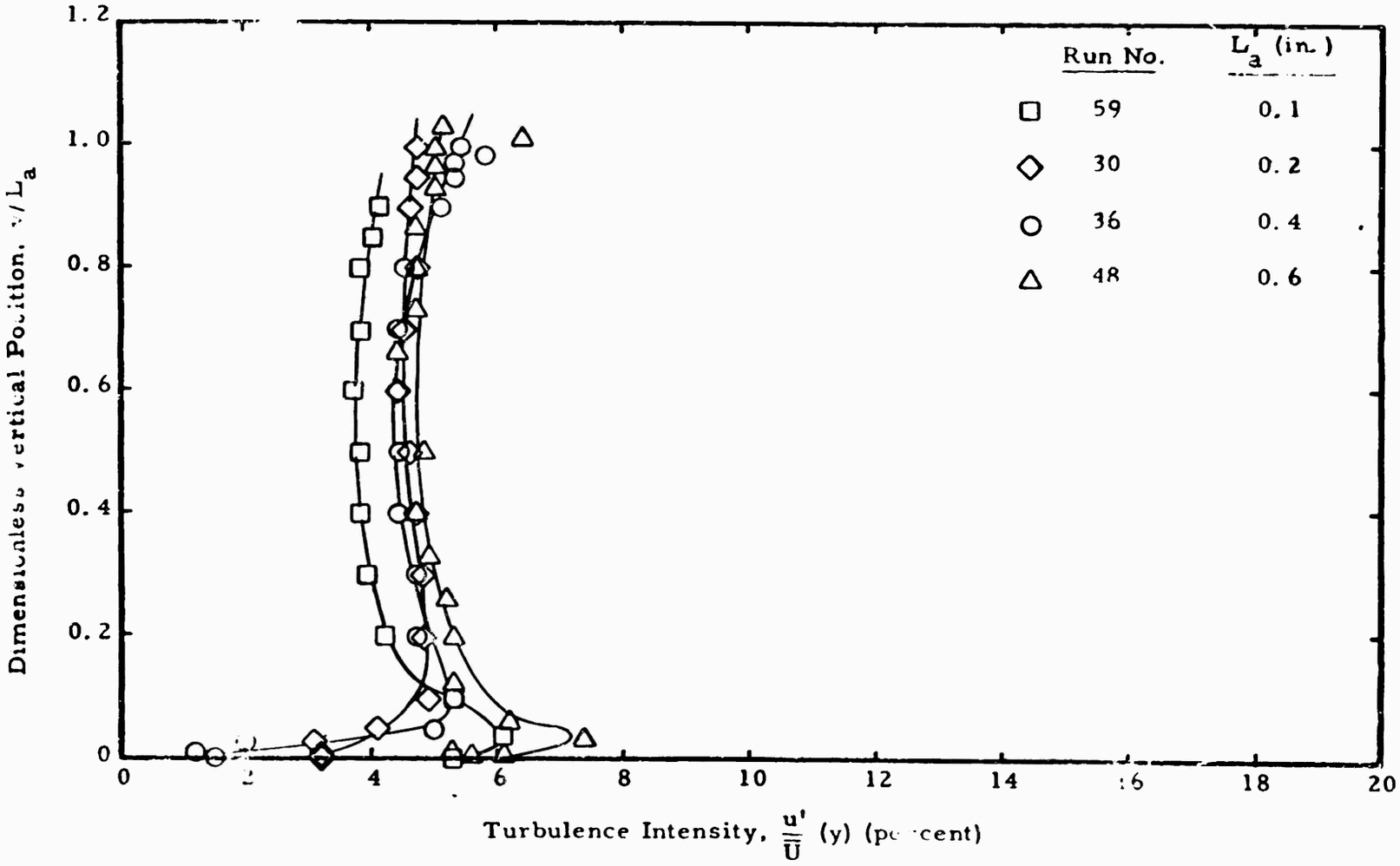

Figure 40. Turbulence Intensity Variation in Air Gap
(Nominal External Airflow Velocity = 5 ft/sec, Air Gap = VAR in.)

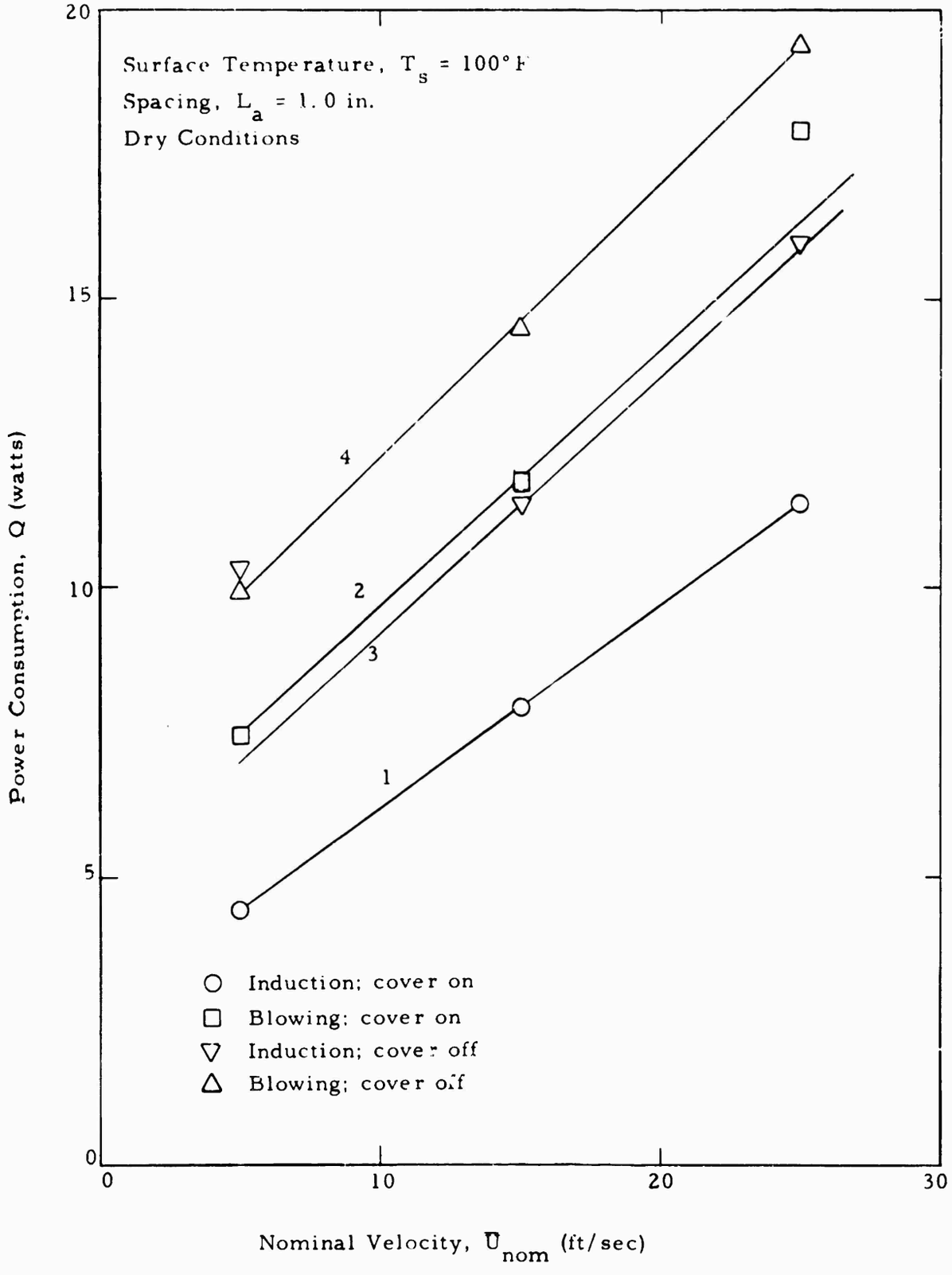

Figure 41. Power Consumption for Various Configurations

the flexible tubing and the downstream end of the channel exhausted into the atmosphere. The induction system provides a relatively smooth laminar flow through the test section while the blowing system was observed to provide turbulent flow within the air gap. Comparing curves 1 and 2 in Figure 41, it is noted that the blowing configuration (highly turbulent) produces a larger power consumption than that produced by the induction configuration (low turbulence level). This result is by no means surprising since a high turbulence level is observed to increase the rate of various transfer processes.

The same trend is noted when one compares curves 3 and 4, namely, the blowing case provides a larger heat loss than the induction case. In these last two cases, the cover plate was removed so that the external ambient pressure would always be equal to the atmospheric pressure. These configurations allow the flow of air either into or out of the air gap through the fabric surface. In the induction case (curve 3) the pressure within the air gap was less than the atmospheric pressure above the fabric surface. Therefore, there was a net inflow of air through the fabric. In the blowing case (curve 4) the internal pressure was greater than the ambient external pressure and a net outflow of air through the fabric surface was observed.

Since one would expect flow conditions to be turbulent in actual field conditions within the air gap, it was decided that a blowing configuration which produces these turbulence conditions should be utilized. It is also evident that in field conditions one may observe a pressure differential across the fabric. To simulate such a pressure difference, it is necessary to run the various experiments with the cover plate off. It is felt that with the cover off, blowing configuration provides the best laboratory simulation of expected field conditions.

2. Final Measurements

a. Dry Surface Conditions

No water was used in the skin simulant in these studies so that non-sweating conditions could be simulated. These tests were performed with the top channel blocked off and cover open. Temperature and velocity distributions through the air gap were recorded for air gap thicknesses of 0.2, 0.4, 0.6 and 1.0 inches at air gap velocities of 0, 5, 15 and 25 ft/sec.

The non-dimensional temperature distribution through the air gap for the various configurations are presented in Figures 42 through 45. The skin surface temperature is utilized in all of these figures as a reference temperature. The dimensionless temperature is determined by finding the difference between the local temperature in the air gap and the skin temperature, and dividing this difference by the maximum difference between the skin temperature and air gap temperature. The thickness of the thermal boundary layer is determined by the value of y/L_a at which the dimensionless temperature becomes unity.

Figures 42 through 45 indicate that the thermal boundary layer thickness at the probing station decreases as the velocity of flow in the air gap increases. One also notes that the temperature gradient at the surface ($y/L_a = 0$) increases with increasing ventilating flow rates. Since the heat transfer from the plate is proportional to the gradient of temperature at the plate surface, it follows that the heat transfer increases with an increasing ventilating flow rate. In all experimental studies conducted, the thermocouple probe utilized to measure the temperature distribution through the air gap never quite reached the temperature indicated by the thermocouple buried within the skin simulant near the surface.

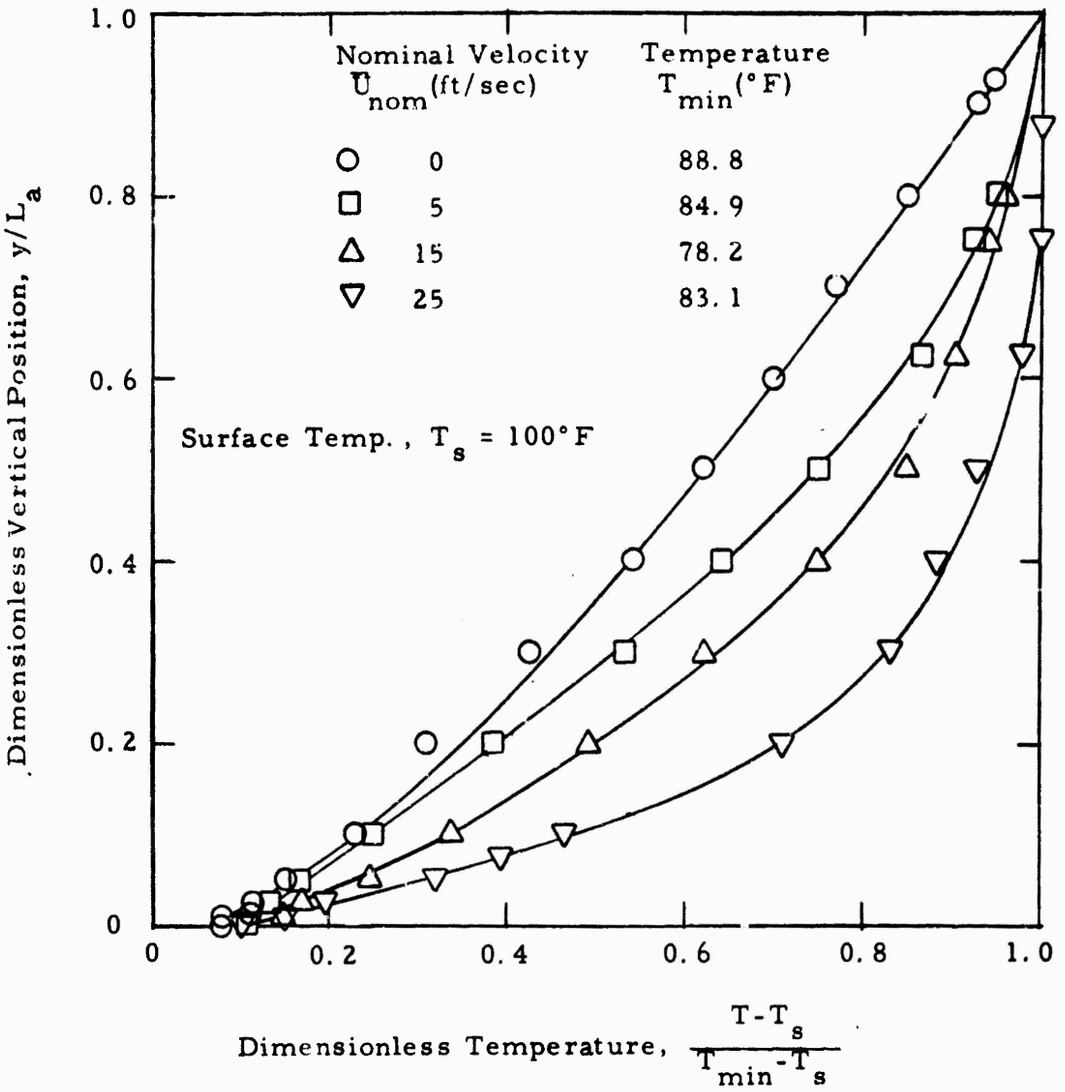

Figure 42. Dimensionless Temperature versus y/L_a for Various Ventilating Flow Rates (L_a = 0.2 in., Dry Surface)

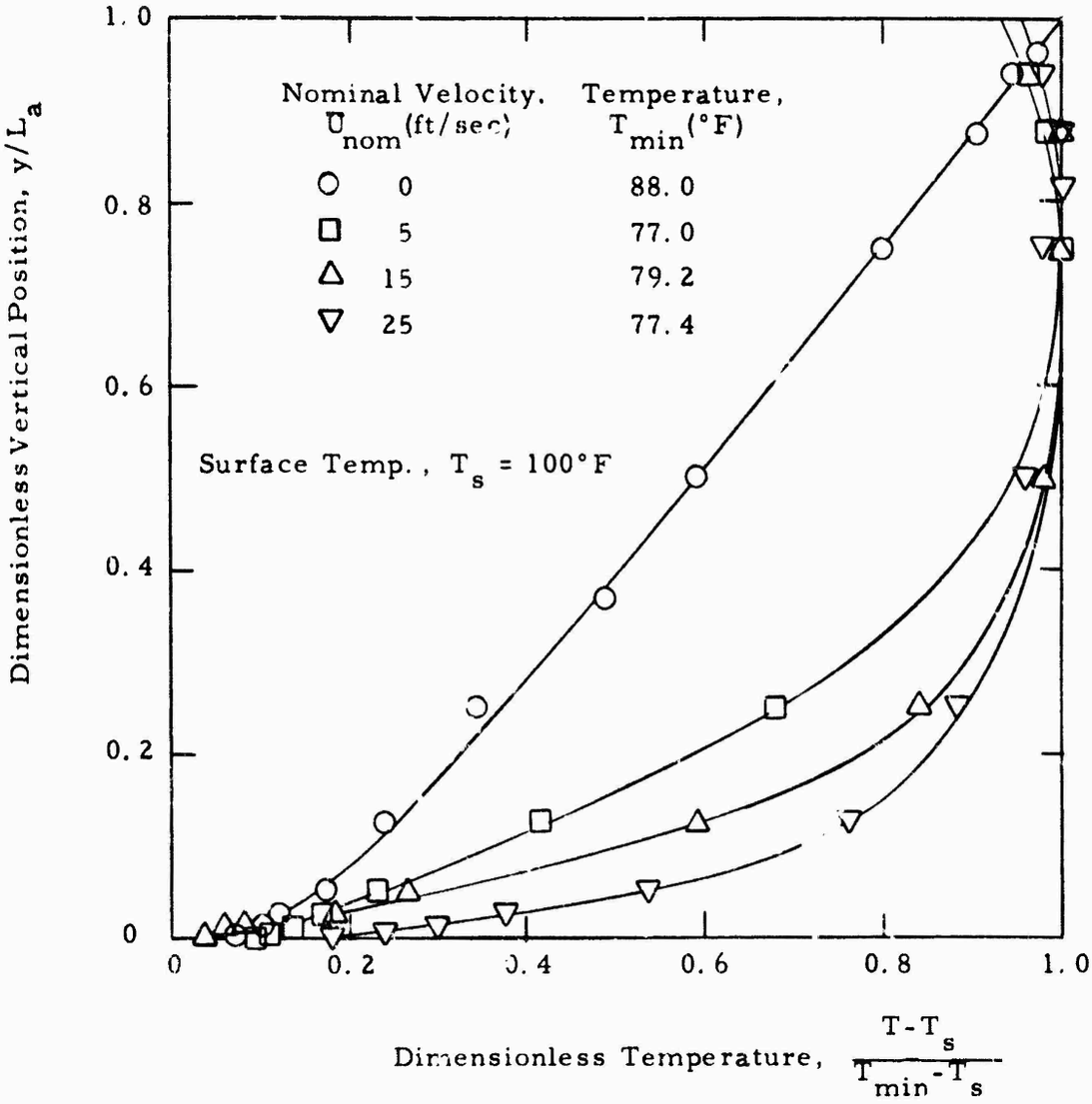

Figure 43. Dimensionless Temperature versus y/L_a for Various Ventilating Flow Rates (L_a = 0.4 in., Dry Surface)

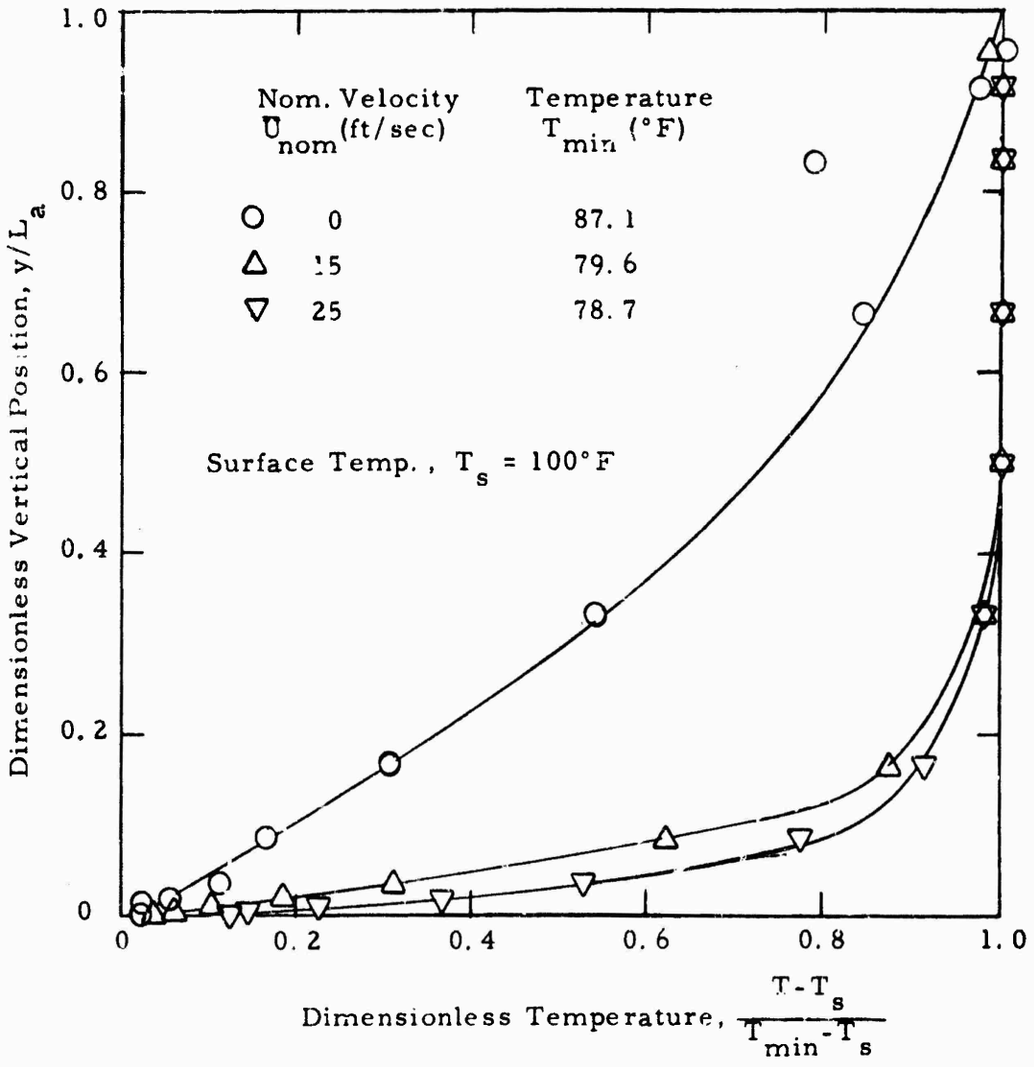

Figure 44. Dimensionless Temperature versus y/L_a for Various Ventilating Flow Rates (L_a = 0.6 in., Dry Surface)

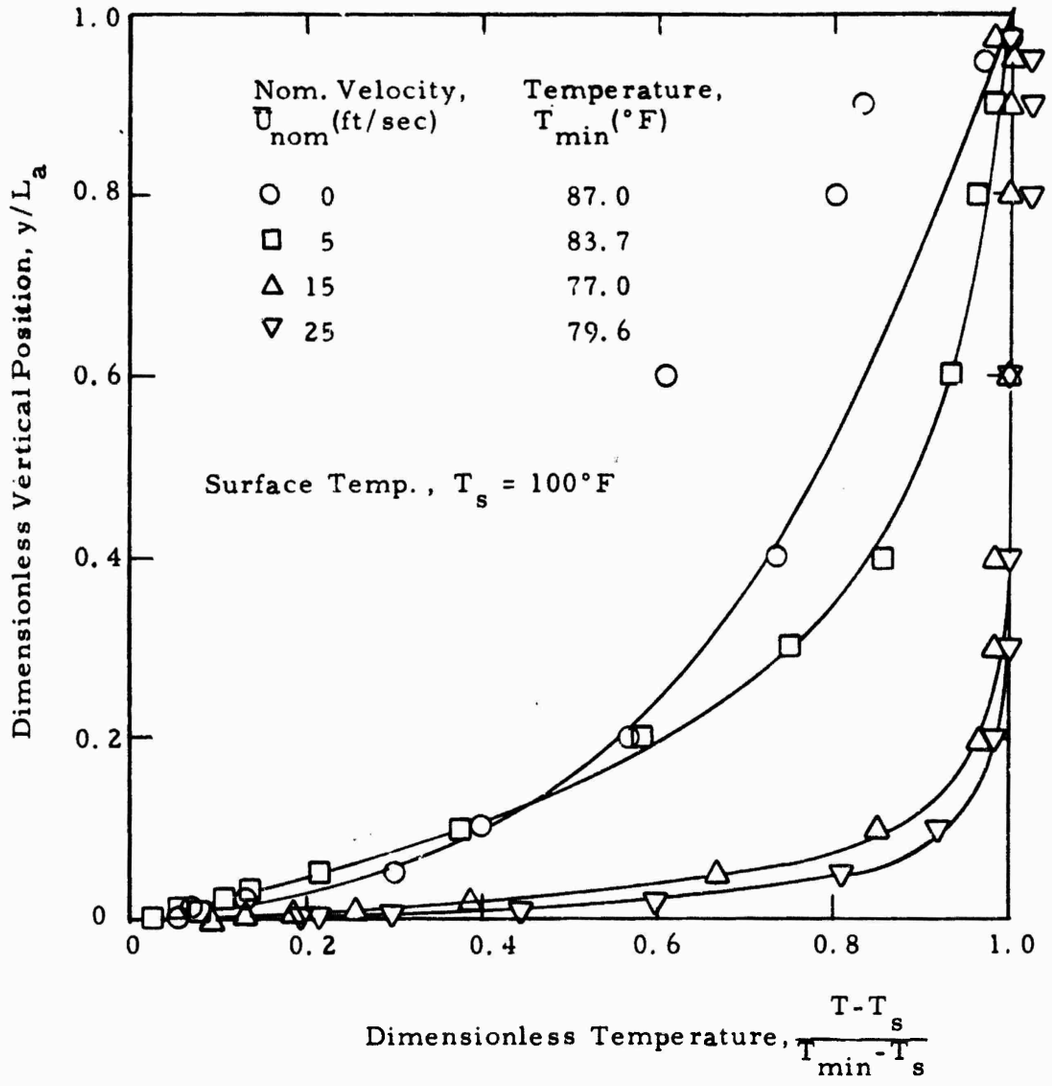

Figure 45. Dimensionless Temperature versus y/L_a for Various Ventilating Flow Rates (L_a = 1.0 in., Dry Surface)

This phenomenon has been repeatedly observed in similar experimental arrangement and can be attributed to various interactions when the probe reaches the proximity of the wall. Since the thermocouple within the skin simulant should indicate the skin simulant surface temperature more accurately than the probe, this indicated temperature was utilized as the reference value for these curves. It is because of these differences in probe and surface thermocouple temperature indications that the experimental points do not pass through the origin in the figures. Considerable scatter is evident in the zero velocity data at the larger spacings. This is probably due to combined conduction and free convection effects.

A dimensionless velocity, obtained by dividing the local by the maximum velocity, is presented in Figures 46 through 49 for the various spacings. It can be noted from these figures that the velocity profiles become more fully developed as the velocity increases. Figure 49 in particular shows the potential core characteristics of the flow when the air gap spacing is fairly large. One notes from this figure that an effective boundary layer has developed along the skin simulant and fabric surfaces and also that this boundary layer thickness decreases as the velocity of the flow increases.

A summary of all of the data for these initial dry surface experimental runs is presented in Table 2. The first column of this table indicates the run number assigned to each experiment. Columns 1 and 2 indicate the air gap thickness and ventilating flow velocity, respectively. Columns 3, 4 and 5 present the skin surface temperature, minimum temperature through the air gap, and temperature gradient at the skin simulant surface. The total heat generated by the skin simulant (Q) is presented in Column 6. The overall heat transfer coefficient for the skin simulant model may be conventionally defined by the expression:

$$U_s = \frac{Q}{A(T_s - T_{min})} \tag{97}$$

where U_s is the overall heat transfer coefficient.

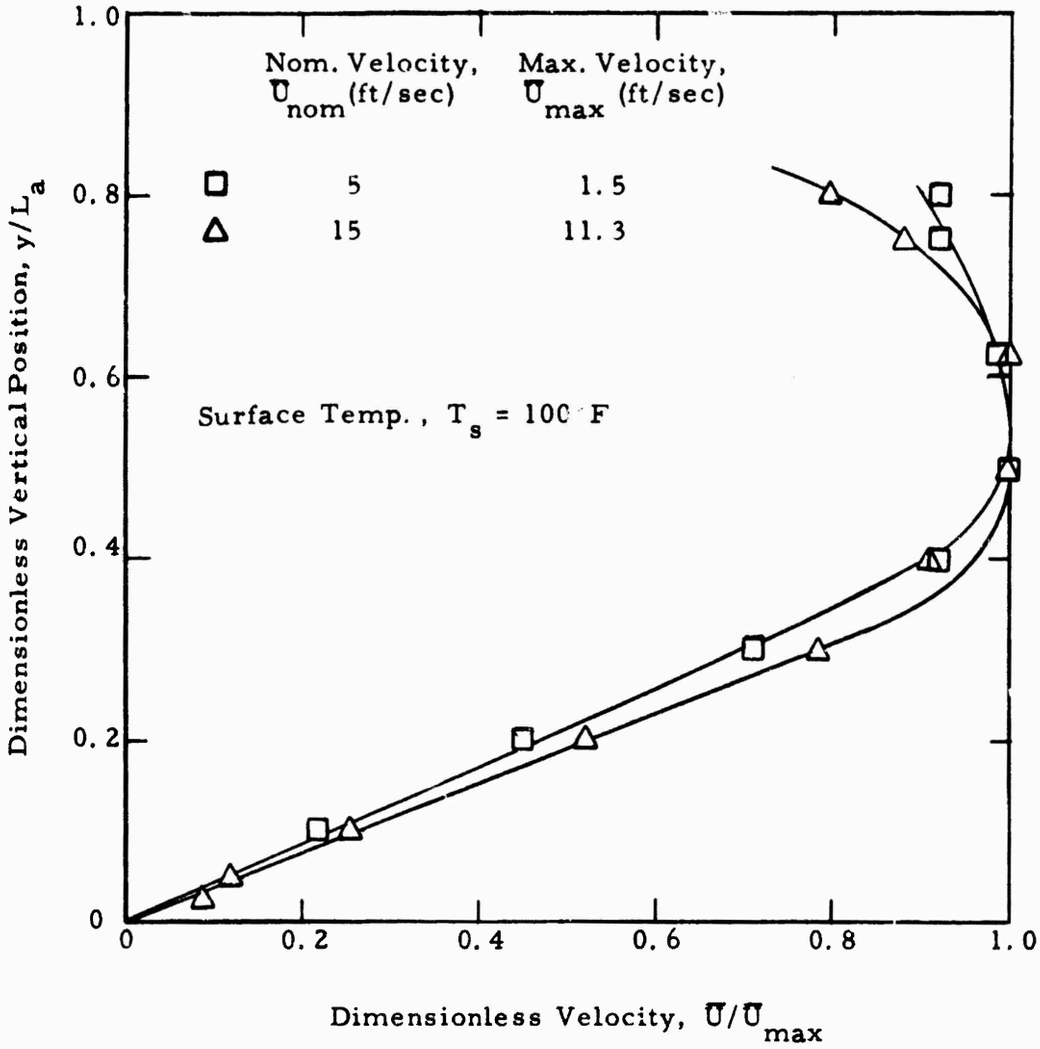

Figure 46. Dimensionless Velocity versus y/L_a for Various Ventilating Flow Rates (L_a=0.2 in., Dry Surface)

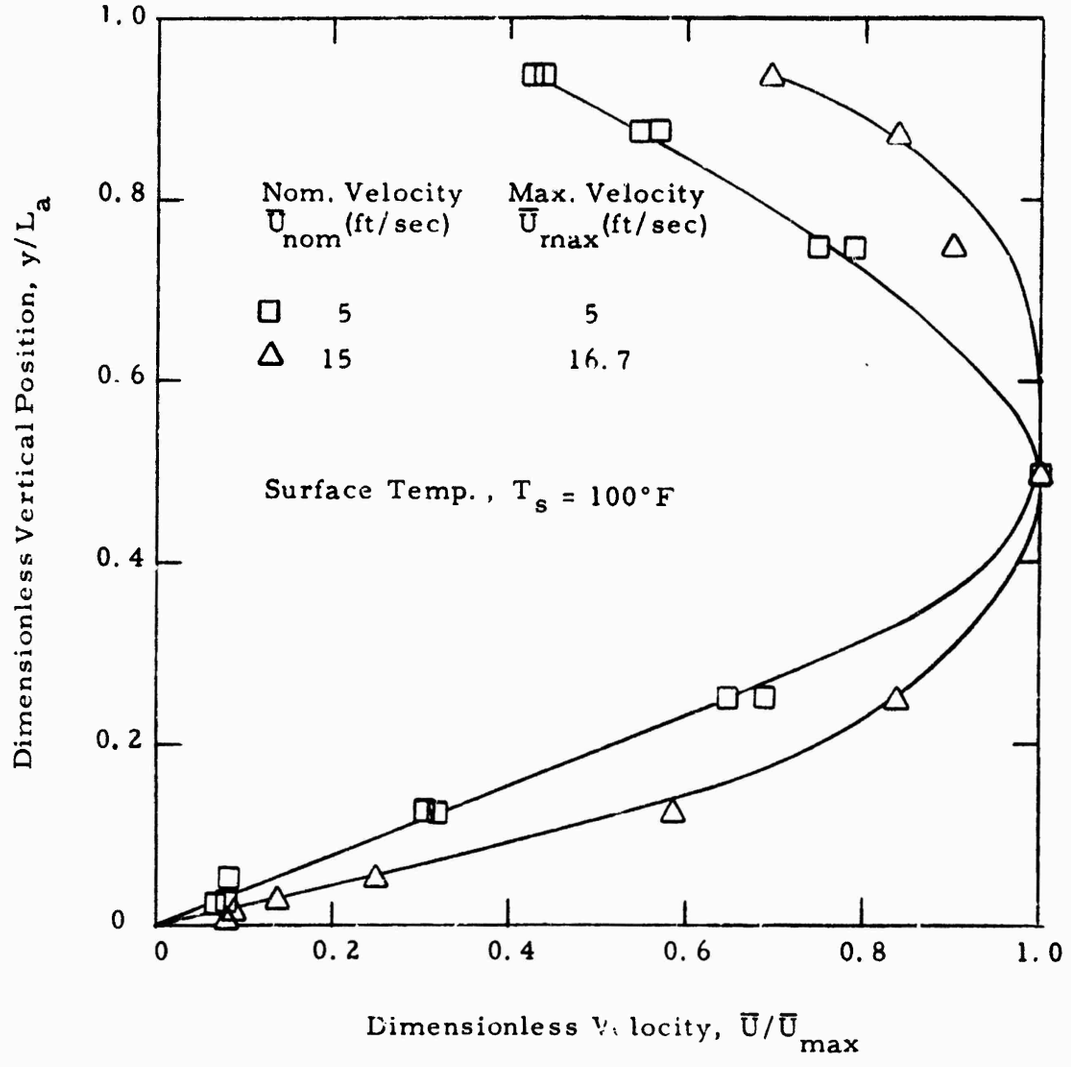

Figure 47. Dimensionless Velocity versus y/L_a for Various Ventilating Flow Rates (L_a = 0.4 in., Dry Surface)

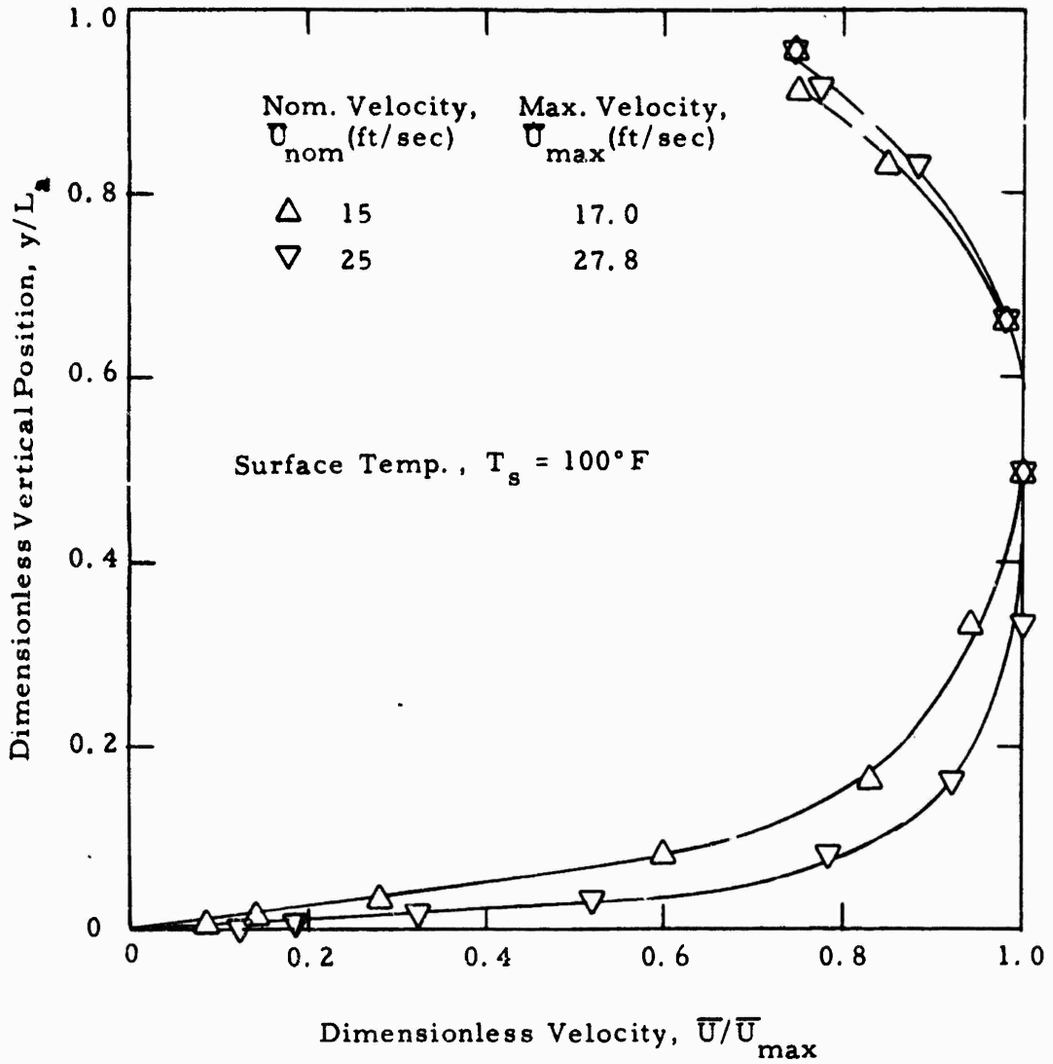

Figure 48. Dimensionless Velocity versus y/L_a for Various Ventilating Flow Rates (L_a = 0.6 in., Dry Surface)

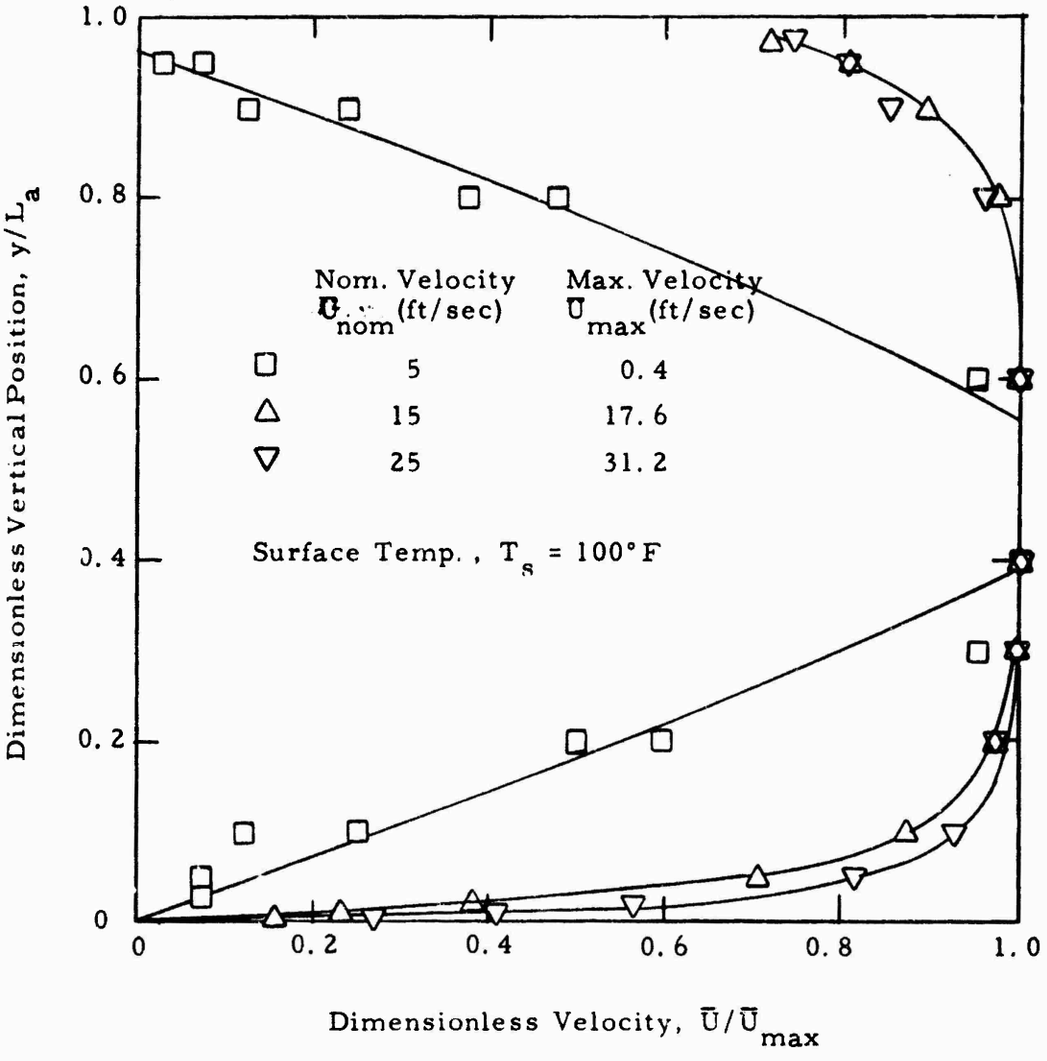

Figure 49. Dimensionless Velocity versus y/L_a for Various Ventilating Flow Rates (L_a = 1.0 in., Dry Surface)

Table 2. Dry Surface Experimental Results

	1	2	3	4	5	6	7	8	9	10	11	12
Run No.	L_a (in)	$\bar{U}$ (ft/sec)	T_s (^oF)	T_{min} (^oF)	$\left(\frac{dt}{dy}\right)_{y=0}$ (^oF)	Q (watts)	U_s $\frac{Btu}{ft^2\ hr\ ^oF}$	$\frac{U_s L_a/2}{k}\left[(RePr)^{-1}\ \frac{x}{L_a/2}\right]$		u_s $\frac{Btu}{ft^2\ hr\ ^oF}$	$\frac{u_s L_a/2}{k}\left[(RePr)^{-1}\ \frac{x}{L_a/2}\right]$	
T-1	1.0	5	76.5	76.5	0	0	--	--	--	--	--	--
T-2	1.0	5	100.1	83.7	-65	6.72	2.799	7.452	.0296	0.744	1.982	.0222
T-3	0.4	5	76.0	76.0	0	0	--	--	--	--	--	--
T-4	0.4	5	100.1	77.0	-160	9.00	2.661	2.834	.1850	1.301	1.385	.1386
T-5	0.2	5	100.5	84.9	-115	8.21	3.595	1.914	.7398	1.384	0.737	.5549
T-6	0.2	15	101.4	78.2	-270	12.55	3.696	1.968	.2466	2.186	1.164	.1850
T-7	0.4	15	100.5	79.2	-286	14.09	4.517	3.810	.0617	2.522	2.685	.0463
T-8	0.6	15	100.5	79.6	-318	13.34	4.358	6.962	.0274	2.857	4.565	.0206
T-9	1.0	15	100.5	77.0	-412	14.50	4.213	11.217	.0099	3.293	8.766	.0074
T-10	1.0	25	100.1	79.6	-880	19.40	6.465	17.212	.0059	8.062	21.463	.0044
T-11	0.6	25	100.1	78.7	-604	19.76	6.308	10.077	.0164	5.301	8.467	.0123
T-12	0.6	0	103.2	87.1	-46	6.34	2.690	4.297	--	0.537	0.857	--
T-13	1.0	0	100.1	87.0	-45	4.40	2.292	6.102	--	0.645	1.718	--
T-14	0.4	0	100.5	88.0	-35	4.87	2.662	2.835	--	0.526	0.560	--
T-15	0.2	0	100.1	88.8	-84	5.46	3.300	1.757	--	1.396	0.743	--
T-16	0.2	25	101.0	83.1	-386	17.93	6.842	3.643	.1480	4.050	2.156	.1110
T-17	0.4	25	99.2	77.4	-536	21.20	6.641	7.072	.0370	4.618	4.917	.0278

The values of the overall heat transfer coefficient as determined by Equation (1) are presented in Column 7 of Table 2. The more conventional way of presenting heat transfer coefficient data is in terms of the dimensionless Nusselt number. Consequently Column 8 presents the values of the Nusselt number based on the average heat transfer coefficient presented in Column 7. The theoretical analysis presented in Appendix D indicates that the dimensionless Nusselt number should depend upon the dimensionless parameter

$$Nu = Nu\left[(Re\ Pr)^{-1}\ \frac{x}{L_a/2}\right] \tag{98}$$

where Re represents the Reynolds number of the flow based on the channel half height. The values of this dimensionless grouping are presented in Column 9 of Table 2.

Similar to the definition of the overall heat transfer coefficient given by Equation (97) one may define a local coefficient by the relation:

$$u_s = \frac{-k\left(\frac{dT}{dy}\right)_{y=0}}{T_s - T_{min}} \tag{99}$$

where K is the conductivity of the air-water vapor mixture of the skin surface, and $(dT/dy)_{y=0}$ represents the skin surface temperature gradient.

Utilizing the probe data for the distribution of temperature through the air gap, the gradient of temperature at the skin surface was graphically determined and is presented in Column 5 of Table 2. The local transfer coefficient was then calculated utilizing Equation (99) together with the data of Columns 3, 4 and 5. This local transfer coefficient is presented in Column 10. The local Nusselt number defined in the manner

similar to the average Nusselt number but with the local transfer coefficient replacing the overall transfer coefficient, is presented in Column 11. The dimensionless parameter given by Equation (98) and evaluated for the local station under consideration (i.e., at x = 0.75 ft) is presented in Column 12 of Table 2.

The graphical representation of the variation of the average and local Nusselt number with the dimensionless parameter $(Re\ Pr)^{-1}\ \frac{x}{L_a/2}$ is presented in Figures 50 and 51, respectively. The solid experimental points shown in these figures are for the experimental cases where a wet surface was maintained on the skin simulant, and these will be discussed in part 2.b of this section. The curve in Figure 50 labeled "empirical" was obtained by passing a straight line through the experimental data for a dry surface. The curve labeled "theoretical", was obtained from Appendix D and the reader is referred to this appendix for the derivation thereof. It is of special interest to note that these two curves possess very similar and almost identical slopes with a major difference being in the multiplying constant. It is perhaps surprising to find such close agreement between theory and experiment, considering especially the many simplifying assumptions utilized in the development of the mathematical model which leads to the dashed curve in Figure 50. As shown in Appendix D, the local and average Nusselt numbers can be related by the expression:

$$\frac{U_s\ L_a/2}{k} = \frac{1}{x}\int_0^x \frac{u_s\ L_a/2}{k}\,dx$$

or (109)

$$\frac{u_s\ L_a/2}{k} = \frac{d}{dx}\left[x\ \frac{U_s\ L_a/2}{k}\right]$$

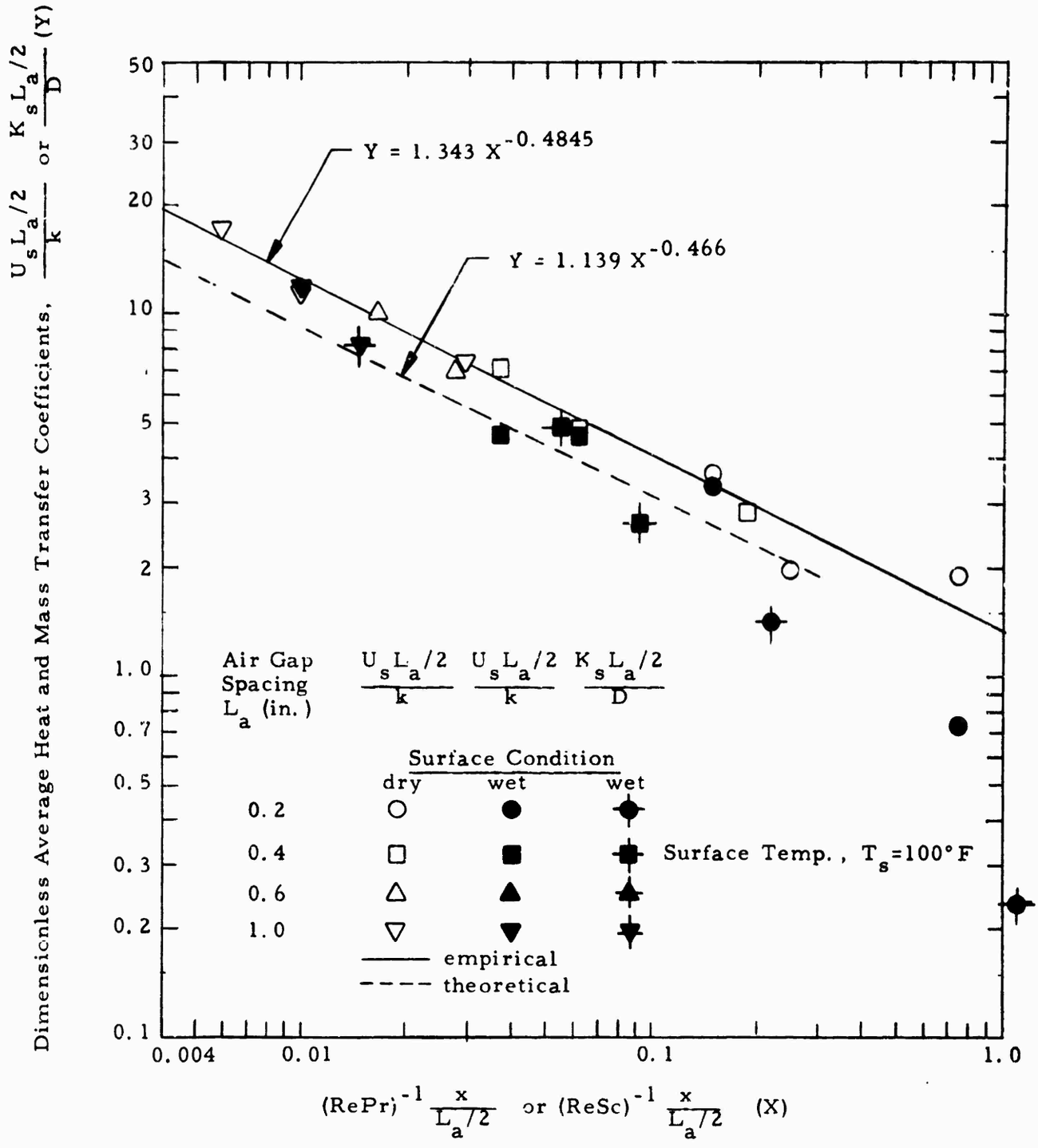

Figure 50. Dimensionless Average Heat and Mass Transfer Coefficients

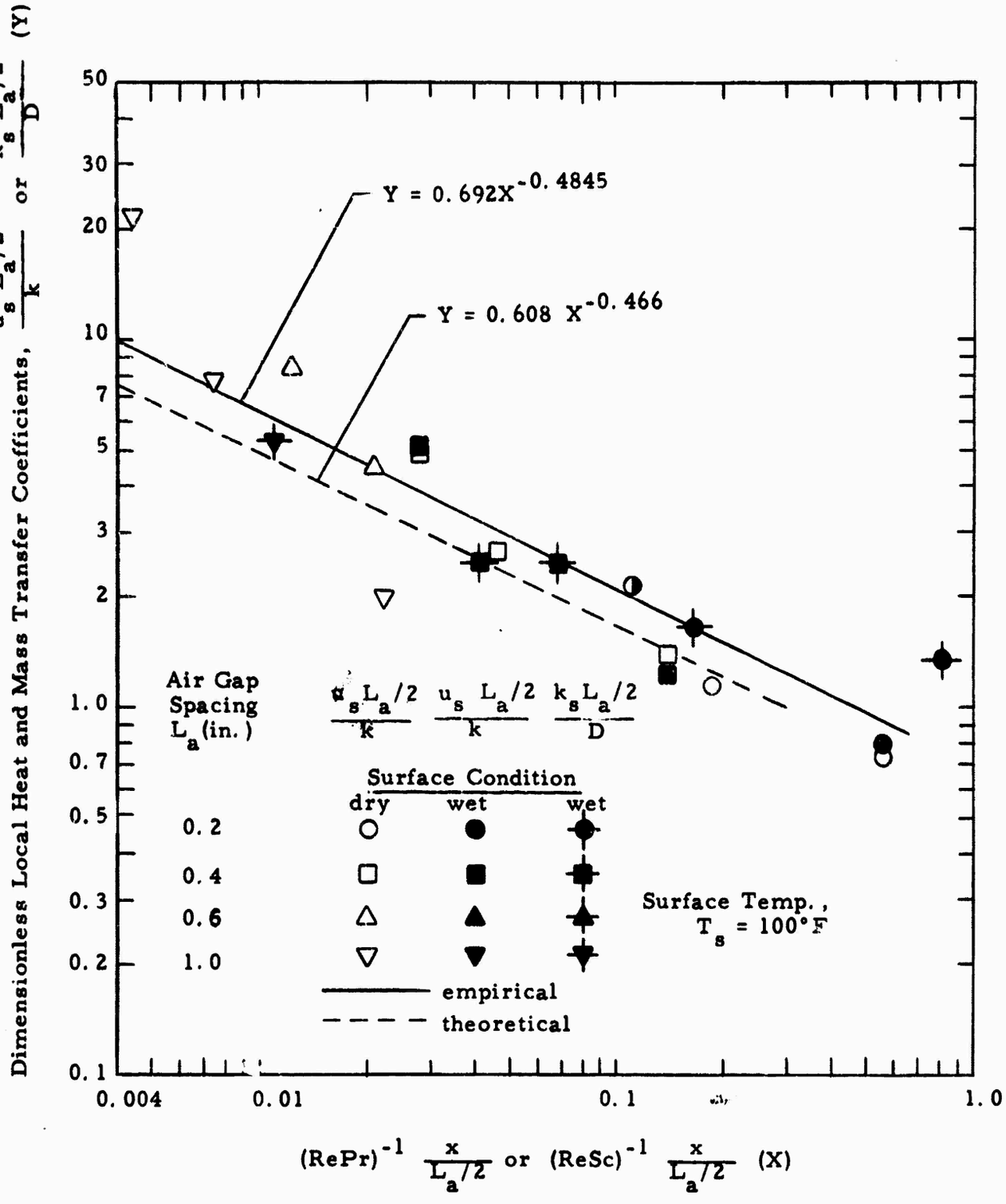

Figure 51. Dimensionless Local Heat and Mass Transfer Coefficients

Utilizing this relation together with the empirical equation from Figure 50, the variation of the local Nusselt number with the dimensionless parameter is shown in Figure 51 as a solid curve. One notes that this empirical curve correlates quite well with the local heat transfer data also. Since the average Nusselt numbers were obtained through temperature gradient surface data, the correlation observed through the empirical relation tends to indicate that the experimental data can be assumed to be fairly accurate.

b. Wet Surface Conditions

The dry surface experiments have provided a base with which one may compare the heat transfer characteristics of a wet simulant surface. The attainment of thermal as well as mass vapor transfer equilibrium with a wet simulant requires considerably more time than with a dry simulant surface. It was, therefore, not possible to obtain as many experimental runs with the wet simulant as with the dry simulant condition. The experiments completed, however, indicate a very strong similarity between the mass (vapor concentration) profiles and temperature profiles achieved in the dry simulant experiments. Figures 52 through 57 present the dimensionless dry and wet temperature distributions, together with the dimensionless vapor concentration profiles for various spacing and velocity configurations. At the higher velocities (Figures 52, 53, 56 and 57) one notes that the dimensionless temperature for the wet surface condition is slightly larger than the dimensionless temperature for the dry surface condition at the same value of y/L_a. One also notes that the dimensionless water vapor concentration values are less than the dimensionless temperature value for both wet and dry conditions at the same y/L_a. The reverse situation is noted to occur in Figure 54 for the low velocity 5 ft/sec case. That is, over the majority of the range of y/L_a from zero to one, the vapor concentration profile shows a larger value than the temperature profile for both wet and dry

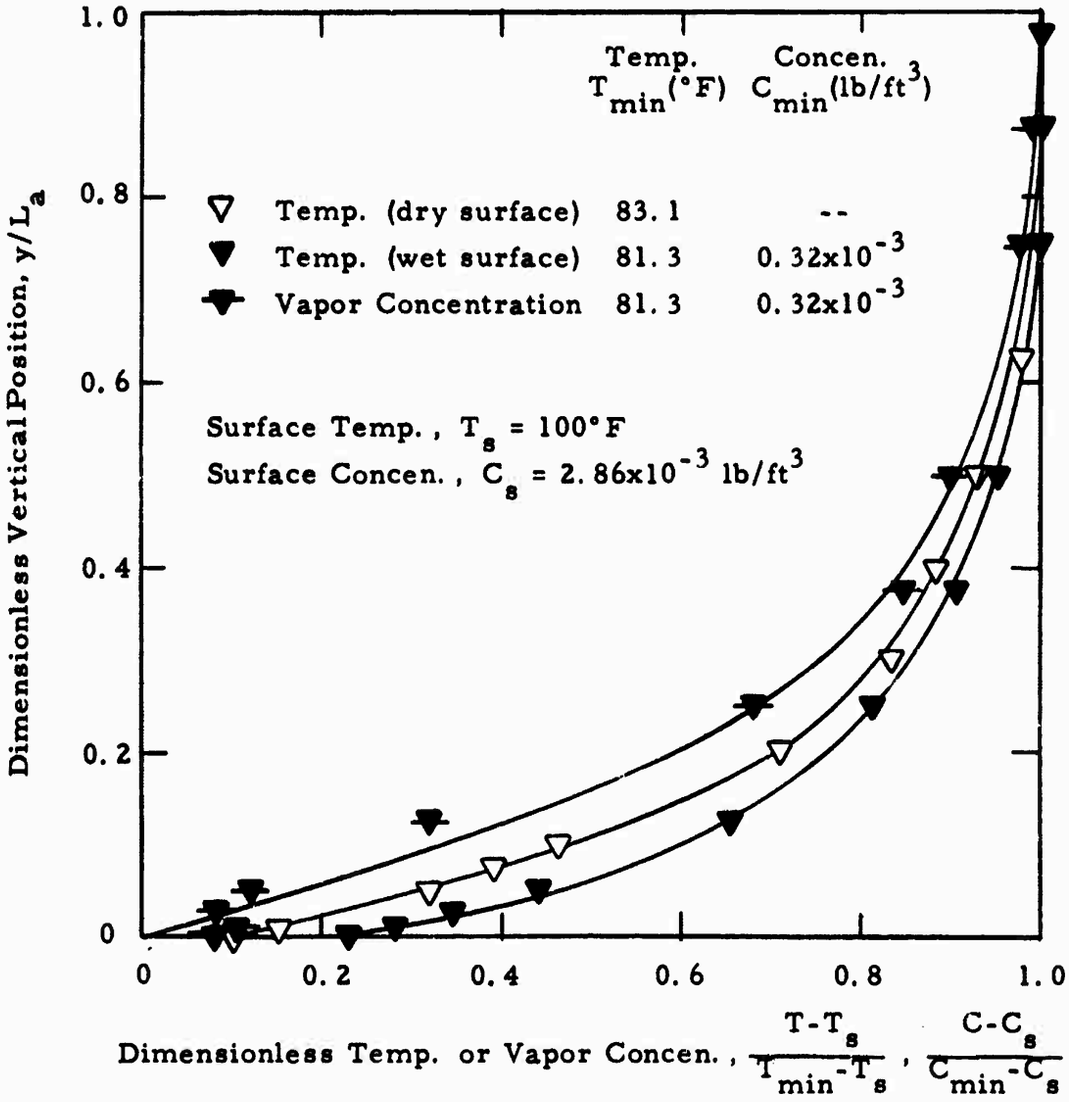

Figure 52. Dimensionless Temperature and Vapor Concentration versus y/L_a (L_a = 0.2 in. and $\bar{U}_{nom}$ = 25 ft/sec)

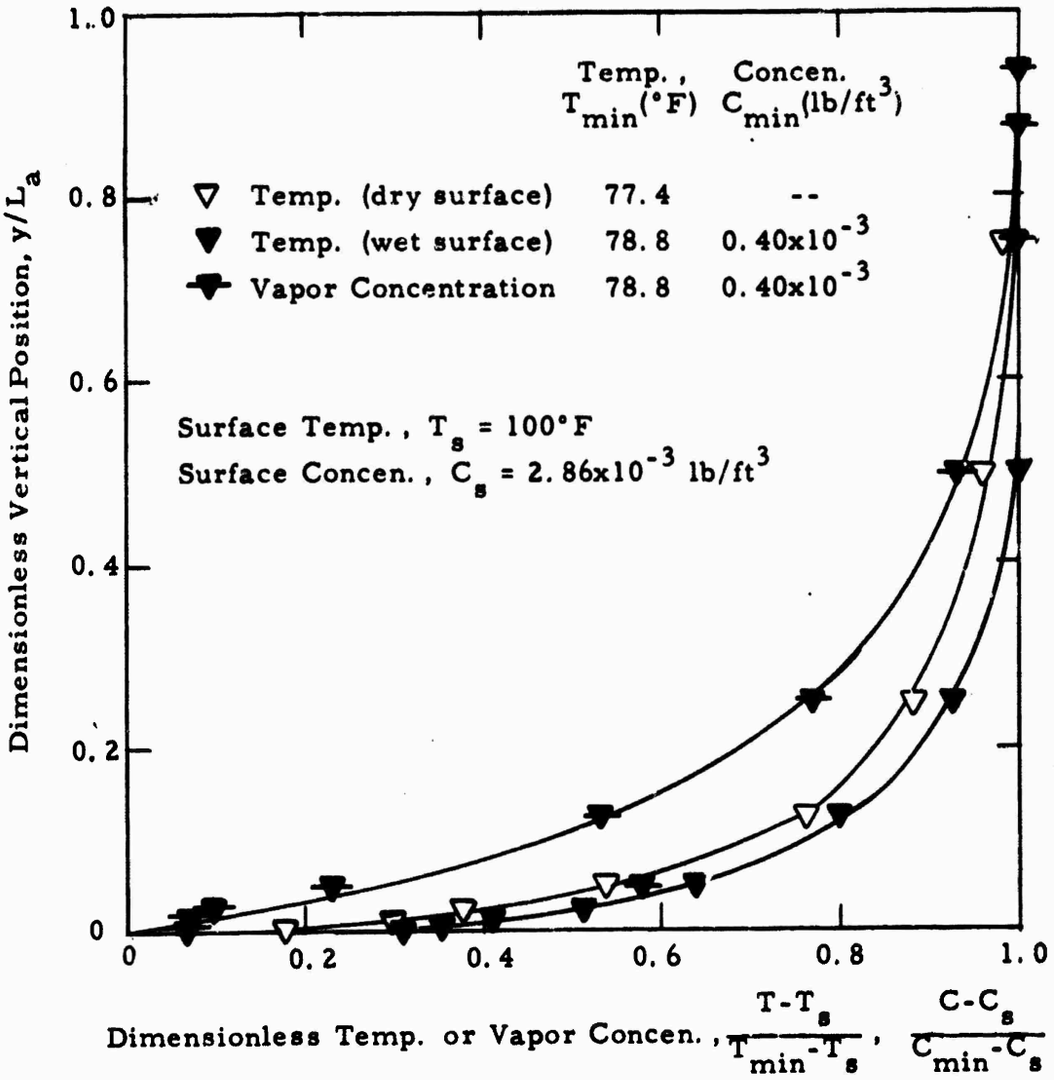

Figure 53. Dimensionless Temperature and Vapor Concentration versus y/L_a (L_a = 0.4 in. and $\bar{U}_{nom}$ = 25 ft/sec)

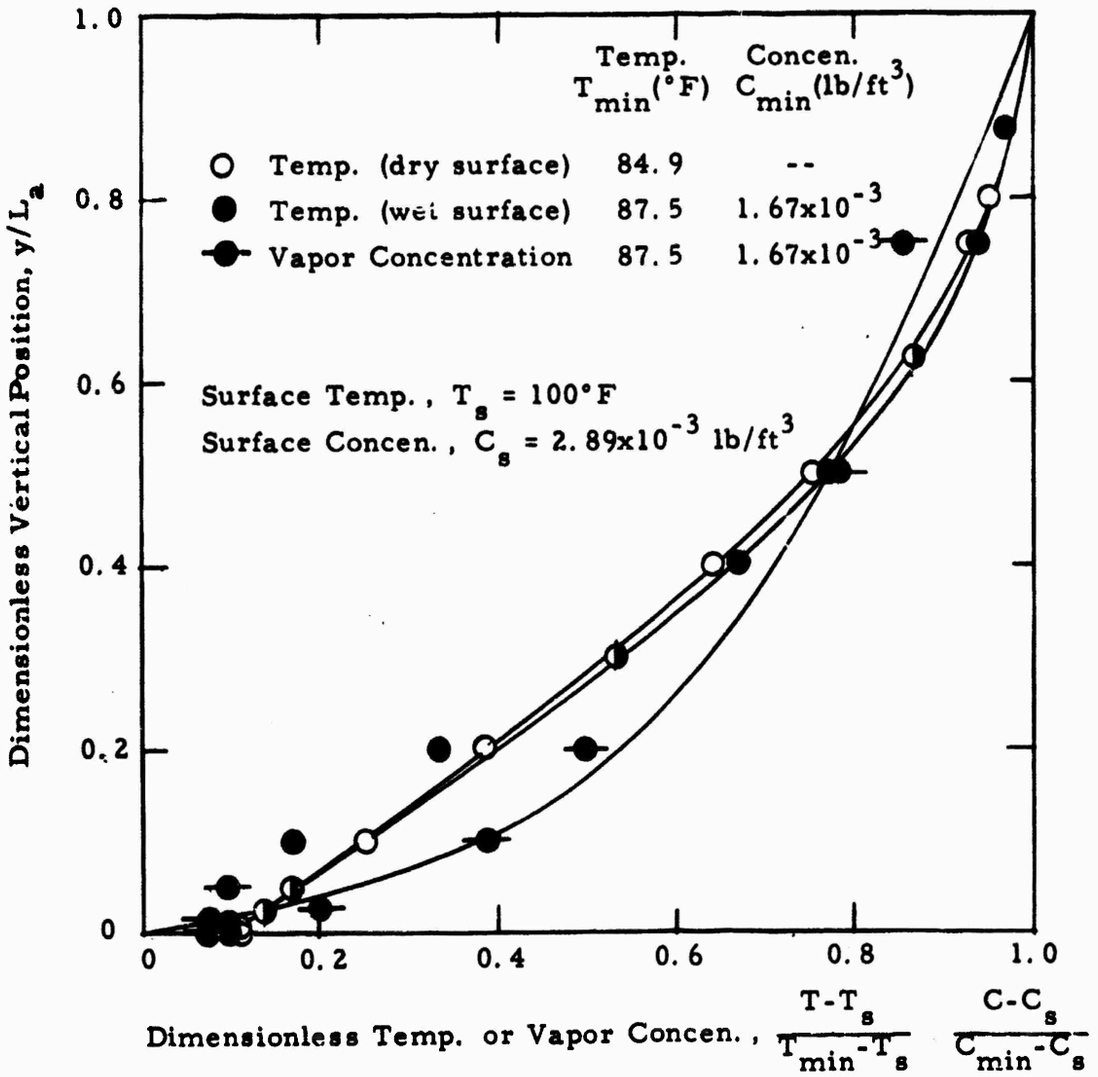

Figure 54. Dimensionless Temperature and Vapor Concentration versus y/L_a (L_a = 0.2 in. and $\bar{U}_{nom}$ = 5 ft/sec)

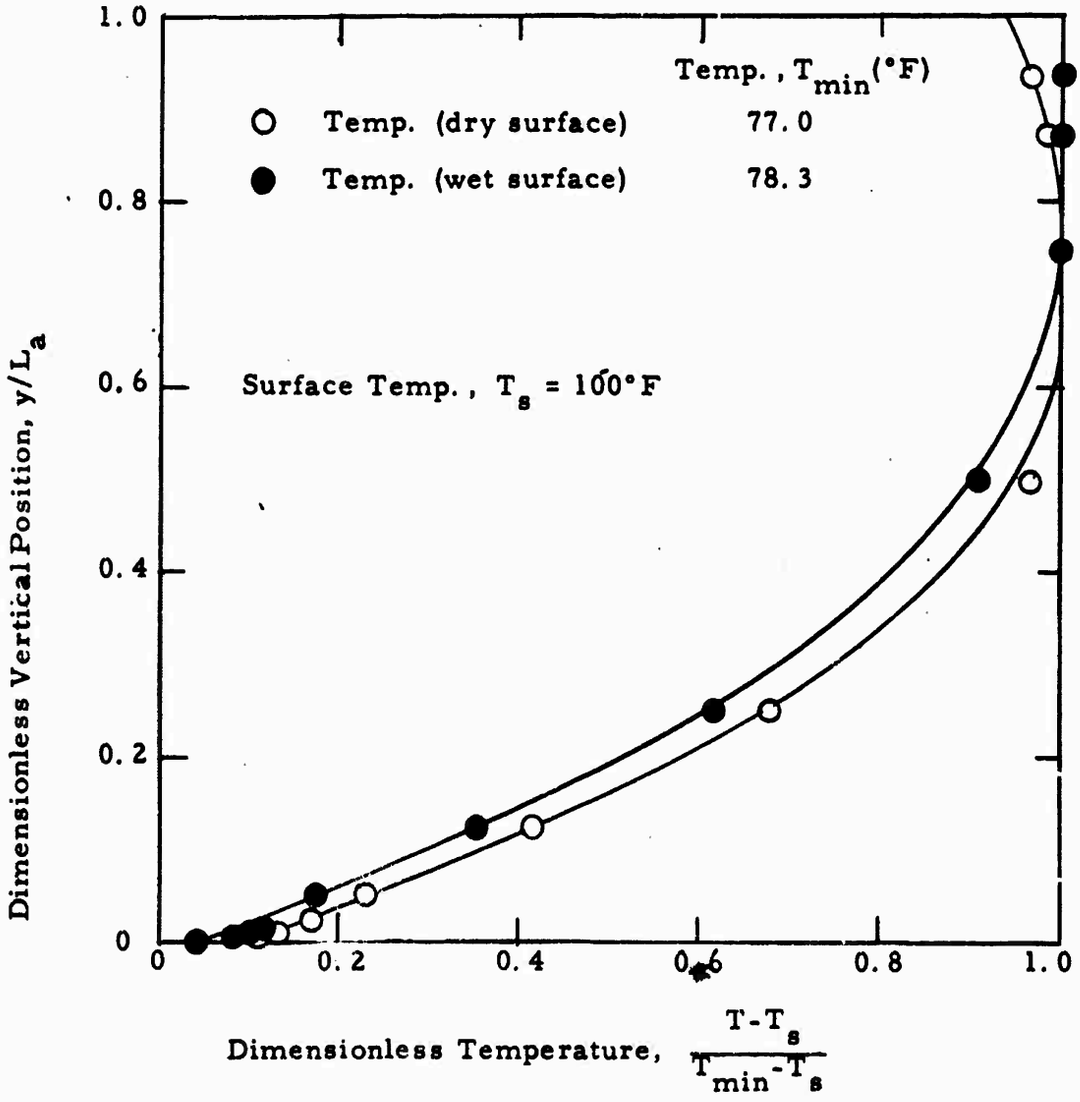

Figure 55. Dimensionless Temperature versus y/L_a (L_a = 0.4 in. and $\bar{U}_{nom}$ = 5 ft/sec.)

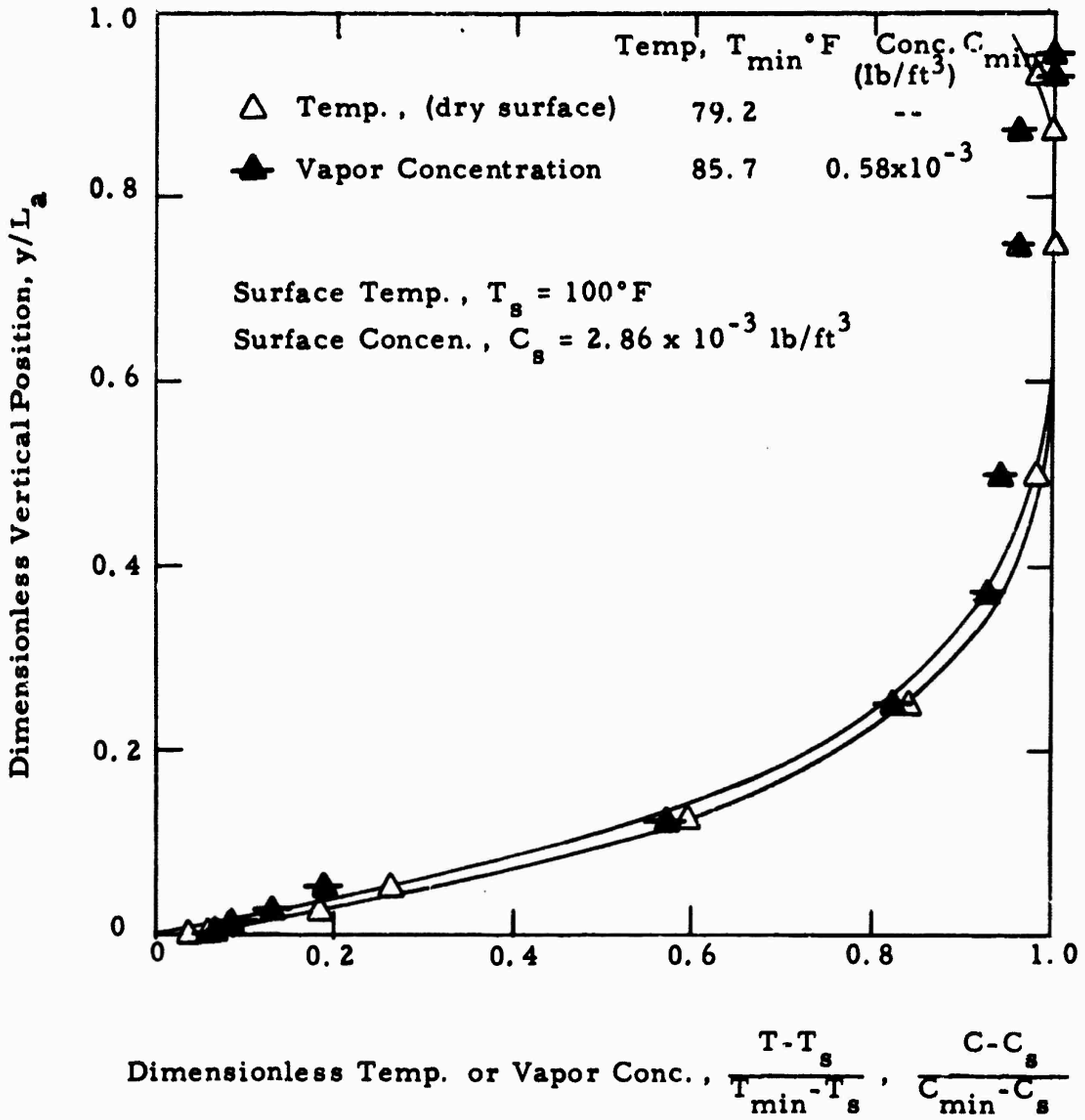

Figure 56. Dimensionless Temperature and Vapor Concentration versus y/L_a (L_a = 0.4 in. and $\bar{U}_{nom}$ = 15 ft/sec)

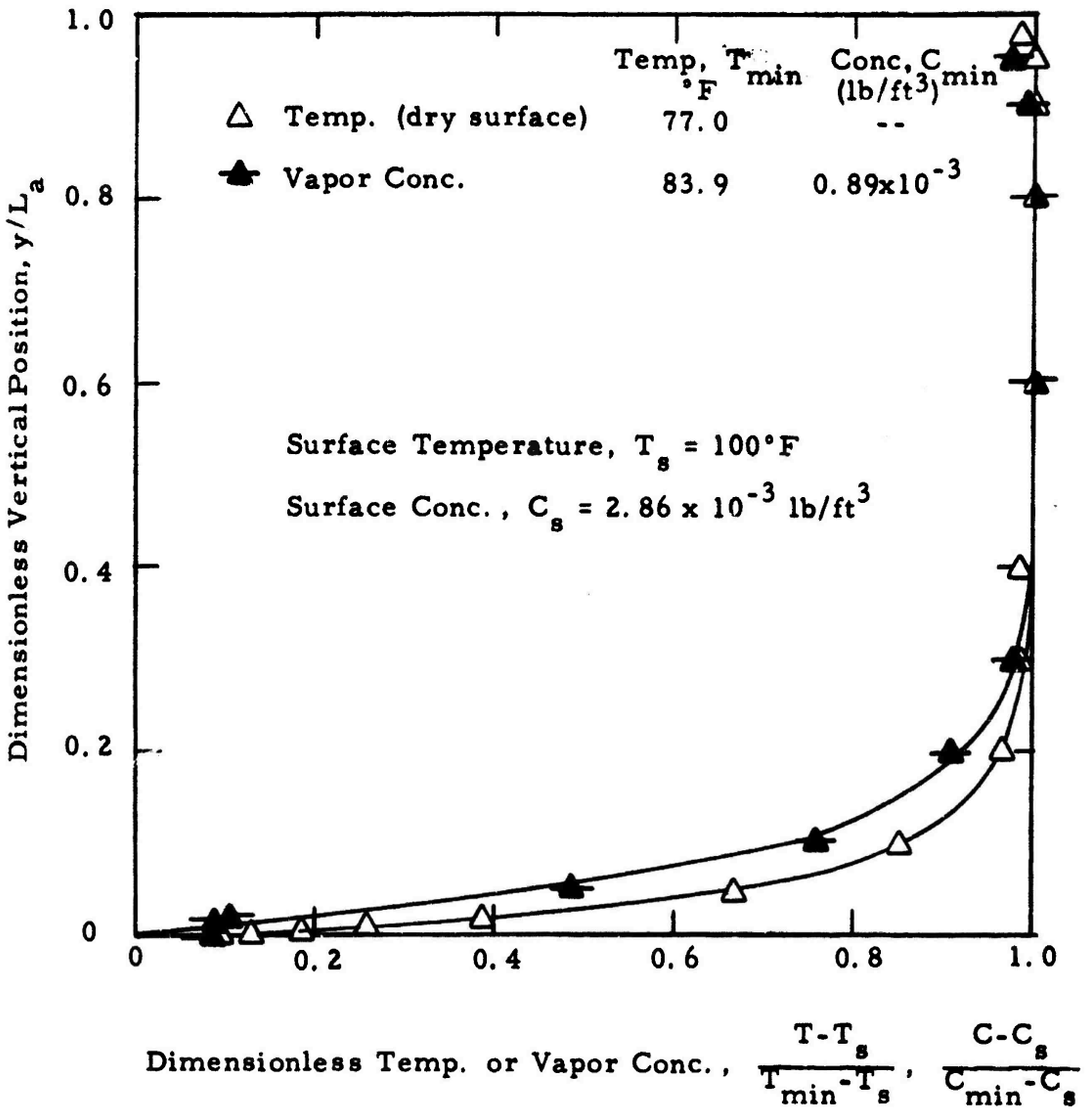

Figure 57. Dimensionless Temperature and Vapor Concentration versus y/La (L_a = 1.0 in. and $\bar{U}_{nom}$ = 15 ft/sec)

skin simulant surfaces. This can be attributed mainly to the fact that for low velocity measurements the overall variations in temperature or water vapor are considerably smaller than for the high velocity cases and, therefore, with the same value of absolute error, the percentage error will probably be considerably larger for low velocities. This then implies that the accuracy of the low velocity data can probably be considered to be less than that for the high velocity, and therefore, more confidence can be placed in the curves presented in Figures 52, 53, 56 and 57 than in the low velocity cases.

The experimental data recorded from the wet simulant surface test runs are presented in Table 3. Columns 1 through 4 show the value of the air gap spacing, ventilating flow rate, skin surface temperature, and minimum temperature within the air gap, respectively. Column 5 presents the temperature gradient at the skin simulant surface as measured from the temperature profiles. Utilizing Equation (99), Column 6 has been determined to give the local heat transfer coefficient. Similarly, the local Nusselt number and dimensionless downstream location parameter are presented in Columns 7 and 8 for each test considered. The total power output of the skin simulator model is presented in Column 10 with the total water vapor loss per unit time presented in Column 10. The heat required to evaporate the amount of water listed in Column 10 may be expressed by the relation:

$$Q_{evap} = \lambda \dot{M}_{evap} \tag{101}$$

where λ represents the heat of vaporization of water. Subtracting the evaporative heat loss (Column 11) from the total heat loss (Column 9), one obtains the convective heat loss as presented in Column 12. Utilizing Equation (97) the overall heat transfer coefficient can be calculated and the result is shown in Column 13. Similar to before, the overall Nusselt number and downstream dimensionless distance are presented in Columns 14 and 15, respectively.

Table 3. Wet Surface Experimental Results

Run No.	1 L_a (in)	2 $\bar{U}$ (ft/sec)	3 T_s (°F)	4 T_{min} (°F)	5 $\left(\frac{dt}{dy}\right)_{y=0}$ (°F/in)	6 u_s Btu/ft² hr °F	7 $\frac{u_s L_a/2}{k}$	8 $\left[(RePr)^{-1} \frac{x}{L_a/2}\right]$	9 Q (watts)	10 $\dot{M}_{evap}$ (lb/hr)	11 Q_{evap} (Btu/hr)	12 Q_{conv} (Btu/hr)	13 u_s Btu/ft² hr °F
TW-2	0.4	25	100.1	78.8	-547.5	4.827	5.141	.0278	152.5	.4579	474.2	46.6	4.376
TW-3	0.2	25	100.1	81.3	-405	4.046	2.154	.1110	100.0	.2728	282.5	59.0	6.277
TW-4	0.2	5	100.5	87.5	-104	1.502	0.800	.5549	9.3	.0221	22.8	8.9	1.374
TW-5	0.4	5	100.1	78.3	-134	1.154	1.229	.1386	12.15	--	--	--	--
TW-6	0.4	15	100.1	85.7	N.R.	--	--	--	78.10	.2271	235.1	31.6	4.392
TW-7	1.0	15	100.1	83.9	N.R.	--	--	--	85.35	.2469	255.64	35.64	4.426

Run No.	14 $\frac{U_s L_a/2}{k}$	15 $\left[(RePr)^{-1} \frac{x}{L_a/2}\right]$	16 $\left(\frac{dC}{dy}\right)_{y=0}$ lb/ft³ in	17 $C_s \times 10^3$ (lb/ft³)	18 $C_{min} \times 10^3$ (lb/ft³)	19 k_s (ft/hr)	20 $\frac{k_s L_a/2}{D}$	21 $\left[(ReSc)^{-1} \frac{x}{L_a/2}\right]$	22 K_s (ft/hr)	23 $\frac{K_s L_a/2}{D}$	24 $\left[(ReSc)^{-1} \frac{x}{L_a/2}\right]$
TW-2	4.660	.0370	-.0370	2.862	0.398	190.0	2.482	.0411	371.7	4.874	.0547
TW-3	3.342	.1480	-.0420	2.862	0.320	252.0	1.652	.1640	214.6	1.407	.2187
TW-4	0.732	.7398	-.0165	2.894	1.670	205.6	1.348	.8199	36.0	0.236	1.0930
TW-5	--	--	--	--	--	--	--	--	--	--	--
TW-6	4.677	.0617	-.0284	2.862	0.585	190.2	2.495	.0684	199.5	2.616	.0912
TW-7	11.784	.0099	-.0208	2.862	0.895	161.3	5.287	.0109	251.04	8.230	.0146

The vapor concentration gradient at the skin simulant model surface has been measured graphically from the plot of vapor concentration as a function of distance above the skin simulant model and is presented in Column 16. The surface and minimum values of the vapor concentration, as measured in each experimental case, are presented in Columns 17 and 18, respectively. The local mass transfer coefficient may be defined by the expression:

$$k_s = \frac{-D\left(\frac{dC}{dy}\right)_{y=0}}{C_s - C_{min}} \tag{102}$$

where D is the diffusion coefficient. Similar to the definition of the local heat transfer Nusselt number, one may define a local mass transfer Nusselt number by the expression:

$$Nu(x) = \frac{k_s L_a/2}{D} \tag{103}$$

A dimensionless downstream location as derived in Appendix D for mass transfer processes may also be defined in a manner analogous to the heat transfer case. The only difference between the dimensionless downstream location for the heat and mass transfer cases is seen to occur in the replacing of the Prandtl by the Schmidt number which is defined by:

$$Sc = \frac{\nu}{D} \tag{104}$$

This dimensionless downstream location is presented in Column 21. An overall mass transfer coefficient may, in an analogous manner to the heat transfer average coefficient, be defined by the expression:

$$K_s = \frac{\dot{M}_{evap}}{A(C_s - C_{min})} \tag{105}$$

Using the evaporative mass loss from Column 10, the skin simulant area of 1/2 ft^2, and the surface and minimum concentration values from Columns 17 and 18, one may find the average mass transfer coefficient as presented in Column 22. Defining the average mass transfer Nusselt number by the expression:

$$\overline{Nu} = \frac{K_s L_a/2}{D} \tag{106}$$

and the dimensionless downstream location by the expression:

$$x = (Re\ Sc)^{-1} \frac{x}{L_a/2} \tag{107}$$

Columns 23 and 24 are obtained.

The local and average heat and mass transfer Nusselt numbers are presented in Figures 50 and 51 for the various experiments completed under this project (by the solid symbols). Once again, one notes that a fairly good agreement between the theoretical and experimental values is obtained. Since the basic mechanisms which govern heat and mass water vapor loss are very similar in nature, one would expect the similarity indicated by Figures 50 and 51 to be found. Further, even though the number of experimental points included in these figures is small, it is felt that some of the discrepancies may be readily attributed to certain errors inherent in the experimental method; namely, the difficulty in measuring accurate profiles at low ventilating flow rates. It is important to note that larger values of the dimensionless downstream location correspond to small values of the ventilating flow velocity and that the largest discrepancies occur at large values of the dimensionless downstream location.

IV. STATEMENT OF MAN-HOURS EXPENDED

In carrying out the present research investigation, the following man-hours (by category) were expended:

Category 01 - Senior Technical Specialist	16.00 hours
Category 03 - Technical Specialist I	223.50
Category 05 - Senior Scientist	1884.50
Category 06 - Associate Scientist	16.00
Category 07 - Junior Scientist	214.00
Category 09 - Technical Editor	16.00
Category 10 - Senior E&R Technican	16.50
Category 11 - E&R Technician	763.00
Category 13 - Model Shop	24.25
Category 15 - Art and Photography	37.50
Category 16 - Binding and Collating	14.00
Total	3225.25 hours

V. SUMMARY AND CONCLUSIONS

The general objective of the present research study is to establish definitive relationships to those variables that control heat and mass (water vapor and/or liquid) flow through composite clothing systems under static and dynamic conditions. These data will ultimately be applied in the design and engineering of clothing systems for troops.

To accomplish the above objective a combined theoretical and experimental research program was initiated. The results of the first year of the investigation were reported in Reference 1. During these early studies a simplified mathematical model describing the temperature response of a skin-airspace-fabric system for various environmental and physical stresses was developed. Experimental studies included measurements of velocity, temperature, and humidity p. ofiles at the surface of a skin simulator model with air flow.

During the present phase of the program the mathematical model was improved and additional experiments were carried out. The following specific tasks were accomplished.

A. Analytical

1) The one-dimensional mathematical model, developed during the first year, was critically reviewed and several improvements were made, based upon analytical considerations and experimental data.

2) Existing physiological data were utilized to establish empirical relations describing the skin thermal conductivity, body heat generation rates, and sweat generation rates.

3) An analytical description of the absorption characteristics of cotton fibers was established with the use of existing experimental data.

4) A mathematical model describing the variations in fabric thermal conductivity was developed. A single parameter must be determined by experiment to completely specify the thermal properties of a fabric.

5) The differential equations were converted into an explicit finite difference form and programmed for solution on a Honeywell-1800 digital computer. Fabric and skin thermal properties have been allowed to vary with the spatial coordinate and time in the computer program by using the empirical relations discussed above.

6) The stability criteria for explicit numerical methods were established, indicating a strong dependence of time increment upon fabric porosity, temperature, and relative humidity. A real time increment of the order of 0.02 to 0.10 second is typical from stability considerations.

7) The computer program was checked for errors with a limited number of calculations and appears satisfactory and usable.

8) An integral, boundary layer-type of analysis was performed to predict the variation of the heat and mass transfer coefficients.

B. Experimental

1) An improved skin simulator model with better control of temperature and water distribution was designed and utilized in the experimental program.

2) A probe actuation mechanism that allows simultaneous positioning of mass flux, total temperature, and hot-wire probes was designed, fabricated, and utilized to reduce the time required for obtaining a complete set of profiles in the airspace. Miniature probes having face heights of the order of 0.001 to 0.005 inch were utilized for these measurements.

3) A fabric holding and positioning mechanism was developed that allowed rapid and accurate changes in the airspace height.

4) With the skin simulator surface temperature at equilibrium value, profiles of mean and fluctuating velocities were measured for fabric spacings of 0.1 to 1.0 inch and airflow velocities from 0 to 25 ft/sec.

5) With the skin simulator surface temperature maintained at 100°F, profiles of temperature, water vapor concentration, and velocity were measured in the airspace for fabric spacings of 0.1 to 1.0 inch and airflow velocities from 0 to 25 ft/sec. Total energy and water loss rates from the skin simulator surface were measured for each configuration.

6) Heat and mass transfer coefficients were calculated from the probing data and the heat and water loss measurements.

The analytical and experimental studies have yielded the following conclusions:

1) It is felt that the mathematical model developed in this project represents a reasonable balance between a purely theoretical and purely experimental approach to the determination of heat and mass transfer processes through clothing systems. The theoretical analysis has isolated several parameters which affect the transfer processes, including a) the body energy production rate, b) the magnitude of the heat and mass transfer coefficients at the fabric and skin surfaces, c) the airspace thickness, d) the ventilating flow rates, temperature, and humidity, e) the fabric porosity, thermal conductivity, and structure, and f) the ambient temperature, humidity, and wind conditions.

2) In view of the complex nature of the governing equations, numerical methods of solution must be employed and computer parameter studies conducted to establish the importance and significance of the many parameters listed above. Explicit finite difference techniques provide the simplest method of numerical analysis and were therefore utilized for this program. The extremely small real time increment (0.02 to 0.10 sec), combined with 15 seconds of computer time for each time increment, indicate that only short duration real time studies are economically feasible with the explicit program.

3) A computer parameter study should be conducted, as is evident from the complexity of the governing equations for the mathematical model. The study of long duration (of the order of one hour) real time problems cannot be economically performed with the explicit program. Preliminary studies have indicated that an implicit program can be prepared which may produce a substantial decrease in required computer time for any given real time span.

4) The simplified integral boundary layer-type of analysis developed in this study pertaining to the heat and mass transfer processes in the airspace provides predictions which agree with the experimental results within the accuracy of the experiments.

5) Reynolds' analogy between heat and mass transfer processes appears to be valid for the airspace. That is, plots of the dimensionless heat and mass transfer Nusselt numbers (Figures 50 and 51) are identical, within the limits of experimental error. Thus, measurements of either the heat loss or mass loss allows calculation of the other. The dimensionless heat and mass transfer coefficients increased by a factor of 10 as the dimensionless streamwise distance increased by a factor of 100.

6) More detailed physiological data on sweat production rates, thermal conductivity variations, and heat generation rates are desirable to improve the mathematical model of the body.

7) The water absorption characteristics of various materials, other than cotton (for example, wool), should be established and described by empirical relations.

8) The empirical constant "a", appearing in the fabric conductivity relation, should be established experimentally for various materials and its dependence upon type of weave, type of material, and possibly other parameters should be established.

9) Mean velocity profiles in the airspace of the skin simulator surface changed from laminar to turbulent as the ventilating flow velocity was increased from 5 ft/sec to 25 ft/sec. Velocity profiles near the fabric surface tended to be turbulent for all velocities.

10) Turbulent intensities in the airspace were about 5 percent over a wide range of test conditions. Values as large as 20 percent were measured at the fabric surface.

11) Variation of fabric spacing from 0.1 to 0.6 inch had little effect upon the turbulence intensities. A 60 percent increase in the centerline mean velocity resulted when the spacing was changed from 0.6 to 0.1 inch.

12) At moderate fabric spacings, with a ventilating velocity of 25 ft/sec, variations of the external flow velocity over the complete range had little effect on the airspace mean velocity profiles. A large change in the turbulence intensity near the fabric surface was noted, whereas little change was observed near the simulator surface.

13) Care should be exercised in interpreting experimental heat and mass loss results for different conditions of boundary layer growth and free stream turbulence levels caused by induction and forced-flow ventilating methods. At a ventilating flow velocity of 5 ft/sec, power consumption increased from 4 to 10 watts as the test configuration was changed from induction and cover on operation to blowing and cover off operation. The same percentage increase was noted over the entire velocity range (5 to 25 ft/sec).

14) At zero ventilating flow velocity, the temperature profile in the airspace was close to the linear shape expected for pure molecular conduction. At a fabric spacing of 0.2 inch, the temperature gradient near the simulator surface increased by a factor of 4, as the ventilating flow velocity was increased to 25 ft/sec. The percentage increase became larger as the fabric spacing was increased. This is a direct indication of the increase in heat and mass transfer as the ventilating flow velocity is increased.

15) The non-dimensional temperature and water vapor concentration profiles were similar in shape over a wide range of test conditions. Little effect on temperature profile was noted as the simulator surface condition was changed from dry to wet.

VI. REFERENCES

1) Larson, R. E., N. Konopliv, and R. A. Kuehnl. Heat and mass transfer through composite clothing systems. Litton Systems, Inc., Applied Science Division, Report No. 2635, Contract DA-19-129-AMC-183(N) (Oct. 6, 1964).

2) Crosbie, R. J., J. D. Hardy, and E. Fessenden. Electrical analog simulation of temperature regulation in man. In American Institute of Physics, Temperature, Its Measurement and Control Vol. 3, Part 3, New York, 1963.

3) Hardy, J. D. and E. F. DuBois. The significance of the average temperature of the skin. Temperature, Its Measurement and Control, Vol. 1, New York. 1941.

4) King, G. and A. B. D. Cassie. Propagation of temperature changes through textiles in humid atmospheres. Transactions of the Faraday Society 36: 445-65 (1940).

5) Gregory, J. The transfer of moisture through fabrics. Journal of Textile Institute. Vol. XXI (21) 1930 pp. T66-T84.

6) Keenan, J. H. and F. G. Keyes. Thermodynamic properties of steam. First Edition, John Wiley and Sons, Inc., New York, 1956.

7) Nissan, A. H., D. Hansen, and J. L. Walker. Heat transfer in porous media containing a volatile liquid. Chemical Engineering Progress Symposium Series. Vol. 59, No. 41, 1963.

8) Speakman, J. B., and N. H. Chamberlain. The thermal conductivity of textile materials and fabrics. Journal of the Textile Institute. Vol. XXI (21), 1930.

9) Eckert, E. R. G. and R. M. Drake, Jr. Heat and mass transfer. McGraw-Hill Book Co., Inc., New York, 1959.

10) Urquart, A. R. and A. M. Williams. The effect of temperature on the absorption of water by soda-boiled cotton. Journal of Textile Institute Transaction, 15: 559-72 (1924).

11) Chen, N. Y. Transient heat and moisture transfer to skin through thermally-irradiated cloth. Ph. D. Thesis, Massachusetts Institute of Technology, Feb. 1959.

12) Larson, R. E., L. W. Rust, and G. A. Gauvin. First progress report on investigations of heat and mass (water vapor and liquid) movement through clothing systems. Litton Systems, Inc., Applied Science Division, Report No. 2894, Contract No. DA-19-129-AMC-683(N) (3 November 1965).

VII. ACKNOWLEDGMENTS

The authors wish to thank Mr. Leo A. Spano, Project Monitor for the U. S. Army Natick Laboratories, for his assistance and cooperation during the past year. They also wish to thank Litton ASD personnel for consultation and contributions to this study, especially, Mr. E. A. Scales, who prepared the computer program for the finite difference calculations.

APPENDIX A

THE EVALUATION OF SKIN-RELATED CONSTANTS

NOMENCLATURE

Symbol	Definition and Dimensions
C	vapor concentration (lb/ft^3)
c	specific heat (Btu/lb °F)
c_p	specific heat at constant pressure (Btu/lb °F)
E	energy flux (Btu/ft^2 hr); energy production rate (Btu/ft^3 hr)
K	mass transfer coefficient (ft/hr)
k	thermal conductivity (Btu/ft hr °F)
k_{s_o}	reference skin conductivity (Btu/ft hr °F)
L_1	skin layer thickness of the skin-body system (ft)
L_2	muscle layer thickness of the skin-body system (ft)
L_3	deep body core thickness of the skin-body system (ft)
M_o	basal metabolism rate (symbol used in Crosbie, et al.) (Btu/ft^2 hr)
ΔM	increase in metabolism due to shivering (symbol used in Crosbie, et al.) (Btu/ft^2 hr)
$\dot{m}$	mass flux (lb/ft^2 hr)
Q	basal metabolism (Btu/ft^3 hr)
$\Delta Q_{shi.}$	increase in metabolism due to shivering (Btu/ft^3 hr)
q	heat flux (Btu/ft^2 hr)
r	relative humidity (dimensionless)
S	sweat generation rate (lb/ft^2 hr)
S_o	reference sweat generation rate (lb/ft^2 hr)

Symbol	Definition and Dimensions
T	temperature (°F)
ΔT_B	deviation of the instantaneous average body temperature from its reference value
t	time (hr)
U	heat transfer coefficient (Btu/ft^2 hr °F)
V	vaporization rate (Btu/ft^2 hr)
x	coordinate (ft)
α_1, α_2	physiological conductivity constants (1/°F)
$\alpha_{m_1}, \alpha_{m_2}, \alpha_{m_3}$	control coefficients for shivering (Btu/ft^3 hr °F; Btu/ft^3 hr °F^2; Btu/ft^3 hr °F)
α_s	first power proportional control coefficient for sweating (lb/ft^2 hr °F)
γ	physiological conductivity constant (hr/°F)
λ	heat of vaporization (Btu/lb)
λ_s	fourth power control coefficient for sweating (lb/ft^2 hr °F^4)
ρ	density (lb/ft^3)

Subscripts

a	ambient
B	average body value
max	maximum
ref	reference
R	rectal
sat	saturation

Subscripts	Definition and Dimensions
s	skin-body system; sweat
s_o	outer skin surface
v	vapor

THE EVALUATION OF SKIN-RELATED CONSTANTS

It has been noted in the main portion of the text that the numerical constants reported in Reference A-1 were based upon the finite difference solution for a 3-slice model. Since our analysis will utilize a 7-slice model, it was felt that a reevaluation of these constants was necessary. It has been found possible to obtain a closed form solution for the steady-state temperature distribution within the skin layers. This steady-state exact solution, to be presented in this appendix, can then be utilized to evaluate the pertinent physiological constants without any reliance whatsoever upon a discreet solution of finite difference equations.

1. Solutions for the Steady-State Temperature Distribution

Reference to Figure A-1 shows the major regions within the skin structure. Since there is no internal heat generation within the outer skin layer, the steady-state governing equation for this region may be written as:*

$$\frac{d^2T}{dx^2} = 0 \qquad \text{(A-1)}$$

The internal heat production in Region II may arise from either shivering or exercise. Assuming, as in the body of the text, that the internal heat production due to shivering depends only on the internal average body temperature and also that the skin conductivity depends only on the average internal body temperature, the governing equation for this region can be expressed as:

* The subscript "s" shall not always be used in this appendix since the entire Appendix A deals only with the skin.

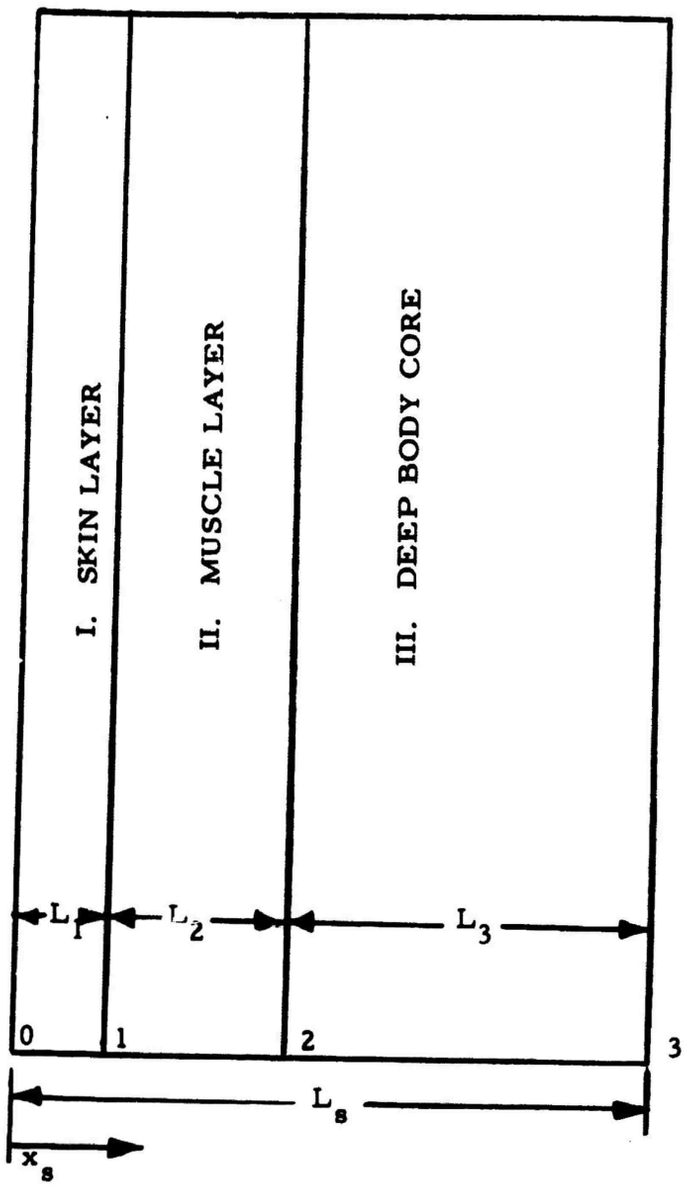

Figure A-1. Idealized Skin Structure

$$\frac{d^2T}{dx^2} + \frac{E + \Delta Q_{shi}}{k} = 0 \qquad \text{(A-2)}$$

The internal heat production within the deep body core region is designated as the basal metabolism and is assumed to remain constant for all conditions of internal body temperature distribution. With the skin conductivity once again assumed to depend only on average body temperature, the steady-state governing equation in this region may be expressed as:

$$\frac{d^2T}{dx^2} + \frac{Q}{k} = 0 \qquad \text{(A-3)}$$

where Q = basal metabolism.

Equation (A-1) may be integrated to yield the temperature distribution within the outer skin layer:

$$T - T_0 = \left(\frac{dT}{dx}\right)_0 x \qquad \text{(A-4)}$$

where $\left(\frac{dT}{dx}\right)_0$ represents the temperature gradient at the skin outer surface.

Integration at Equation (A-2) yields:

$$\frac{dT}{dx} - \left(\frac{dT}{dx}\right)_1 + \frac{E + \Delta Q_{shi}}{k} (x - L_1) = 0 \qquad \text{(A-5)}$$

The heat flowing through the interface between Regions I and II must be identical when computed from the temperature distributions in Regions I or II at the interface. From Equation (A 4) the gradient at $x = L_1$ may be expressed as:

$$\left(\frac{dT}{dx}\right)_1 = \left(\frac{dT}{dx}\right)_0$$

which when substituted into Equation (A-5) gives:

$$\left(\frac{dT}{dx}\right) = \left(\frac{dT}{dx}\right)_0 - \frac{E + \Delta Q_{shi}}{k} (x - L_1) \qquad \text{(A-6)}$$

Integrating once again, one obtains:

$$T - T_1 = \left(\frac{dT}{dx}\right)_0 (x - L_1) - \frac{E + \Delta Q_{shi}}{2k} (x - L_1)^2$$

Evaluating T_1 by using Equation (A-4) and substituting into the above expression yields the steady-state temperature distribution in the muscle layer of the body:

$$T = T_0 + \left(\frac{dT}{dx}\right)_0 x - \frac{E + \Delta Q_{shi}}{2k} (x - L_1)^2 \qquad \text{(A-7)}$$

Integration of Equation (A-3) yields the following expression for the temperature gradient within this region:

$$\frac{dT}{dx} - \left(\frac{dT}{dx}\right)_2 + \frac{Q}{k} (x - L_1 - L_2) = 0 \qquad \text{(A-8)}$$

The temperature gradient at interface 2 is evaluated by using Equation (A-6) with $x - L_1 = L_2$. This process yields the following expression:

$$\left(\frac{dT}{dx}\right)_2 = \left(\frac{dT}{dx}\right)_0 - \frac{E + \Delta Q_{shi}}{k} L_2$$

which when substituted into the previous expression gives:

$$\frac{dT}{dx} = \left(\frac{dT}{dx}\right)_0 - \frac{E + \Delta Q_{shi}}{k} L_2 - \frac{Q}{k} (x - L_1 - L_2) \qquad \text{(A-9)}$$

Integrating once again one obtains:

$$T - T_2 = \left[\left(\frac{dT}{dx}\right)_0 - L_2 \frac{E + \Delta Q_{shi}}{k}\right] (x - L_1 - L_2) - \frac{Q}{2k} (x - L_1 - L_2)^2 \qquad \text{(A-10)}$$

But, from Equation (A-7), one finds:

$$T_2 = T_0 + \left(\frac{dT}{dx}\right)_0 (L_1 + L_2) - \frac{E + \Delta Q_{shi}}{2k} L_2^2$$

and thus Equation (A-10) may be rewritten as:

$$T = T_0 + \left(\frac{dT}{dx}\right)_0 x - \frac{E + \Delta Q_{shi}}{2k} L_2^2 - \frac{E + \Delta Q_{shi}}{k} L_2 (x - L_1 - L_2)$$

$$- \frac{Q}{2k} (x - L_1 - L_2)^2 \qquad \text{(A-11)}$$

The boundary condition at 3 (no heat flows through interface 3) requires that the temperature gradient evaluated at $x = L_s$ be zero. Utilizing this boundary condition in Equation (A-11), one may determine the temperature gradient at the skin outer surface to be:

$$\left(\frac{dT}{dx}\right)_0 = \frac{1}{k} \left[L_2 (E + \Delta Q_{shi}) + L_3 Q\right] \qquad \text{(A-12)}$$

Thus, Equations (A-4), (A-7) and (A-11) may now be rewritten in terms of internal generation of heat as well as the thermal conductivity as follows:

Region I:

$$T = T_0 + \frac{1}{k}\left[L_2 (E + \Delta Q_{shi}) + L_3 Q\right] x \qquad \text{(A-13)}$$

Region II:

$$T = T_0 + \frac{1}{k}\left[L_2(E + \Delta Q_{shi}) + L_3 Q\right] x - \frac{E + \Delta Q_{shi}}{2k} (x - L_1)^2 \qquad \text{(A-14)}$$

Region III:

$$T = T_0 + \frac{1}{k}\left[L_2(E + \Delta Q_{shi}) + L_3 Q\right] x - \frac{E + \Delta Q_{shi}}{2k} L_2\left[L_2 + 2(x - L_1 - L_2)\right]$$

$$- \frac{Q}{2k} (x - L_1 - L_2)^2 \qquad \text{(A-15)}$$

By setting $x - L_1 - L_2 = L_3$ one may also evaluate the rectal temperature. This process yields:

$$T_R = T_0 + \frac{1}{k}\left[L_2(E + \Delta Q_{shi}) + L_3 Q\right] L_s - \frac{E + \Delta Q_{shi}}{2k} L_2(L_2 + 2L_3) - \frac{Q}{2k} L_3^2 \qquad \text{(A-16)}$$

The average body temperature is found through an integration of the local body temperature throughout the three layers within the skin structure. The integration process is straightforward and one may evaluate the average body temperature to give:

$$T_B = T_0 + \frac{1}{2}\left[\frac{E + \Delta Q_{shi}}{k}\right]\left[1 - \frac{1}{3}\left(\frac{L_2}{L_s}\right)^2 - \left(\frac{L_2}{L_s}\right)\left(\frac{L_3}{L_s}\right) - \left(\frac{L_3}{L_s}\right)^2\right] L_2 L_s$$

$$+ \frac{Q}{2k}\left[1 - \frac{1}{3}\left(\frac{L_3}{L_s}\right)^2\right] L_3 L_s \qquad \text{(A-17)}$$

This expression may be rearranged to give the skin surface temperature as a function of the average body temperature, skin conductivity, internal heat generation, as well as the various layer thicknesses. Thus, one finds: (replacing the symbol T_0 by T_{s_0} for the skin surface temperature)

$$T_{s_0} = T_B - \frac{L_2 L_s}{2}\left(\frac{E + \Delta Q_{shi}}{k}\right)\left[1 - \frac{1}{3}\left(\frac{L_2}{L_s}\right)^2 - \left(\frac{L_2}{L_s}\right)\left(\frac{L_3}{L_s}\right) - \left(\frac{L_3}{L_s}\right)^2\right]$$

$$- \frac{L_3 L_s}{2}\,\frac{Q}{k}\left[1 - \frac{1}{3}\left(\frac{L_3}{L_s}\right)^2\right] \qquad \text{(A-18)}$$

Similarly, the rectal temperature may also be evaluated in terms of the abovementioned variables and parameters. This process yields the following relation:

$$T_R = T_B + \frac{L_2 L_s}{2}\left(\frac{E + \Delta Q_{shi}}{k}\right)\left[1 - \left(\frac{L_2}{L_s}\right) - 2\left(\frac{L_3}{L_s}\right) + \frac{1}{3}\left(\frac{L_2}{L_3}\right)^2 + \left(\frac{L_2}{L_s}\right)\left(\frac{L_3}{L_s}\right)\right.$$

$$\left. + \left(\frac{L_3}{L_s}\right)^2\right] + \frac{L_3 L_s}{2}\,\frac{Q}{k}\left[1 - \frac{L_3}{L_s} + \frac{1}{3}\left(\frac{L_3}{L_s}\right)^2\right] \qquad \text{(A-19)}$$

Under steady-state conditions the total amount of heat entering the skin outer surface from within the skin (q_0) must equal the total internal heat production (due to shivering, exercise, and basal metabolism). Utilizing relation (A-12) one may now write:

$$q_0 = k\left(\frac{dT}{dx}\right)_0 = L_2\,(E + \Delta Q_{shi}) + L_3\,Q$$
$$= L_s\left[\left(\frac{L_2}{L_s}\right)\,(E + \Delta Q_{shi}) + \left(\frac{L_3}{L_s}\right)\,Q\right] \qquad \text{(A-20)}$$

Introduction of the following dimensionless variables:

$$\bar{L}_1 = L_1/L_s,\ \bar{L}_2 = L_2/L_s,\ \bar{L}_3 = L_3/L_s, \qquad \text{(A-21)}$$

yields the following expressions for the skin surface temperature, the rectal temperature, and the heat loss at the skin surface in terms of the average body temperature and internal heat generations:

$$T_{s_0} = T_B - \bar{L}_2\left[1 - \tfrac{1}{3}\,\bar{L}_2^{\,2} - \bar{L}_2\bar{L}_3 - \bar{L}_3^{\,2}\right]\frac{L_s^{\,2}}{2}\left(\frac{E + \Delta Q_{shi}}{k}\right) - \bar{L}_3\left[1 - \tfrac{1}{3}\bar{L}_3^{\,2}\right]\frac{L_s}{2}\,\frac{Q}{k} \qquad \text{(A-22)}$$

$$T_R = T_B + \bar{L}_2\left[1 - \bar{L}_2 - 2\bar{L}_3 + \tfrac{1}{3}\,\bar{L}_2^{\,2} + \bar{L}_2\bar{L}_3 + \bar{L}_3^{\,2}\right]\frac{L_s^{\,2}}{2}\left(\frac{E + \Delta Q_{shi}}{k}\right)$$
$$+ \bar{L}_3\left[1 - \bar{L}_3 + \tfrac{1}{3}\,\bar{L}_3^{\,2}\right]\frac{L_s^{\,2}}{2}\,\frac{Q}{k} \qquad \text{(A-23)}$$

$$q_0 = L_s\left[\bar{L}_2\,(E + \Delta Q_{shi}) + \bar{L}_3\,Q\right] \qquad \text{(A-24)}$$

2. Evaluation of the Physiological Constants

The equations presented in the preceding section may now be utilized to evaluate the various physiological constants which are required in the main body of the text. To facilitate this evaluation, the experimental values indicated in Figure 3 of Reference A-1 shall now be utilized. The basal metabolism (per unit volume) is obtained by dividing the value presented in Reference A-1 (designated by M_0) by the thickness of the deep body core. Thus one finds:

$$Q = \frac{M_0}{0.032} = \frac{37}{0.032} = 130 \text{ Btu/ft}^3\text{hr} \qquad \text{(A-25)}$$

The internal heat generation due to shivering is found by dividng the increase in metabolism presented in Reference A-1 (designated by ΔM) by the thickness of the muscle layer, which yields:

$$\Delta Q_{shi} = \frac{\Delta M}{0.142} \text{ Btu/ft}^3\text{hr} \qquad \text{(A-26)}$$

Subtracting Equation (A-22) from (A-23), setting the exercise energy production (E) equal to zero, and inserting the following thickness values:

$$L_s = 0.056 \text{ m}; \quad \Gamma_1 = \frac{1}{7}; \quad \Gamma_2 = \frac{2}{7}; \quad \Gamma_3 = \frac{4}{7}$$

One may evaluate the thermal conductivity from the following equation:

$$k_s = \frac{1.72 \times 10^{-4} \Delta Q_{shi} + 1.0}{T_R - T_{s_0}} \frac{(\text{Btu})}{\text{ft hr}^0\text{F}} \qquad \text{(A-27)}$$

With the thermal conductivity now evaluated, the average body temperature can be evaluated from Equation (A-22). The rectal temperature similarly may be evaluated from Equation (A-23). Equating the energy loss to the air at the skin surface to the energy entering the skin surface from within the skin structure itself, one may write the following expression:

$$V + U_s (T_{s_0} - T_a) = M_0 + \Delta M$$

where

V = vaporization heat loss.

Solving this expression for the vaporization loss one finds:

$$V = M_0 + \Delta M - U_s (T_{s_0} - T_a) \qquad \text{(A-28)}$$

The heat transfer coefficient for the skin surface as reported in Reference A-1 is 1.09 Btu/ft^{2}hr°F. Using this value with the above equation as well as the experimental data of Figure 3 in Reference A-1 one may evaluate the vaporization rate at the skin surface.

The experimental values from Reference A-1 together with the values determined by the expressions developed in this section are presented in Table A-1. The values of the thermal conductivity as presented in Table A-1 are plotted in Figure A-2. It is noted from this figure that the thermal conductivity as a function of the average body temperature may be satisfactorily approximated by four linear segments. One notes from this figure that the reference body temperature (where the slope of the conductivity vs. body temperature curve changes abruptly) may be selected to be equal to 92.7°F. . The expressions which are found to describe the experimental points of Figure A-2 are listed below.

$$k_s = k_{s_0} \left[1 + \alpha_1 \Delta T_B\right] \leq 1.511\, k_{s_0} \quad \text{for } T_B > 0$$

$$k_s = k_{s_0} \left[1 + \alpha_2 \Delta T_B\right] \geq 0.675\, k_{s_0} \quad \text{for } T_B \leq 0$$

where

$$\alpha_1 = 0.405 \ (1/°F)$$

$$\alpha_2 = 0.181 \ (1/°F)$$

$$k_{s_0} = 0.29 \ (\text{Btu/ft hr°F})$$

$$\Delta T_B = T_B - 100 \ (°F)$$

Table A-1. Experimental Data

T_a (exp) (°C)	T_{s_0} (exp) (°C)	T_R (exp) (°C)	$T_R - T_{s_0}$ (exp) (°C)	ΔM (exp) (kcal/m^2 hr)	ΔQ_{shi} (Eq. A-26) (kcal/m^3 hr)	k_s (Eq. A-27) (kcal/m hr °C)	T_B (Eq. A-22) (°C)	V (Eq. A-28) (kcal/m^2 hr)
23	30.94	36.62	5.68	11.74	733.88	0.294	34.62	6.66
24	31.46	36.73	5.27	8.13	508.06	0.305	34.86	5.59
25	32.05	36.78	4.73	5.87	366.94	0.333	35.06	5.50
26	32.60	36.83	4.23	3.16	197.56	0.362	35.27	5.18
27	33.10	36.92	3.82	1.36	84.69	0.393	35.50	6.03
28	33.60	37.01	3.41	0	0	0.434	35.73	7.32
30	34.44	37.15	2.71	0	0	0.547	36.13	13.47
32	34.78	37.24	2.46	0	0	0.603	36.31	22.27
34	34.96	37.32	2.36	0	0	0.626	36.43	31.91
36	35.01	37.28	2.27	0	0	0.651	36.43	42.25
38	35.15	37.47	2.32	0	0	0.638	36.60	52.11

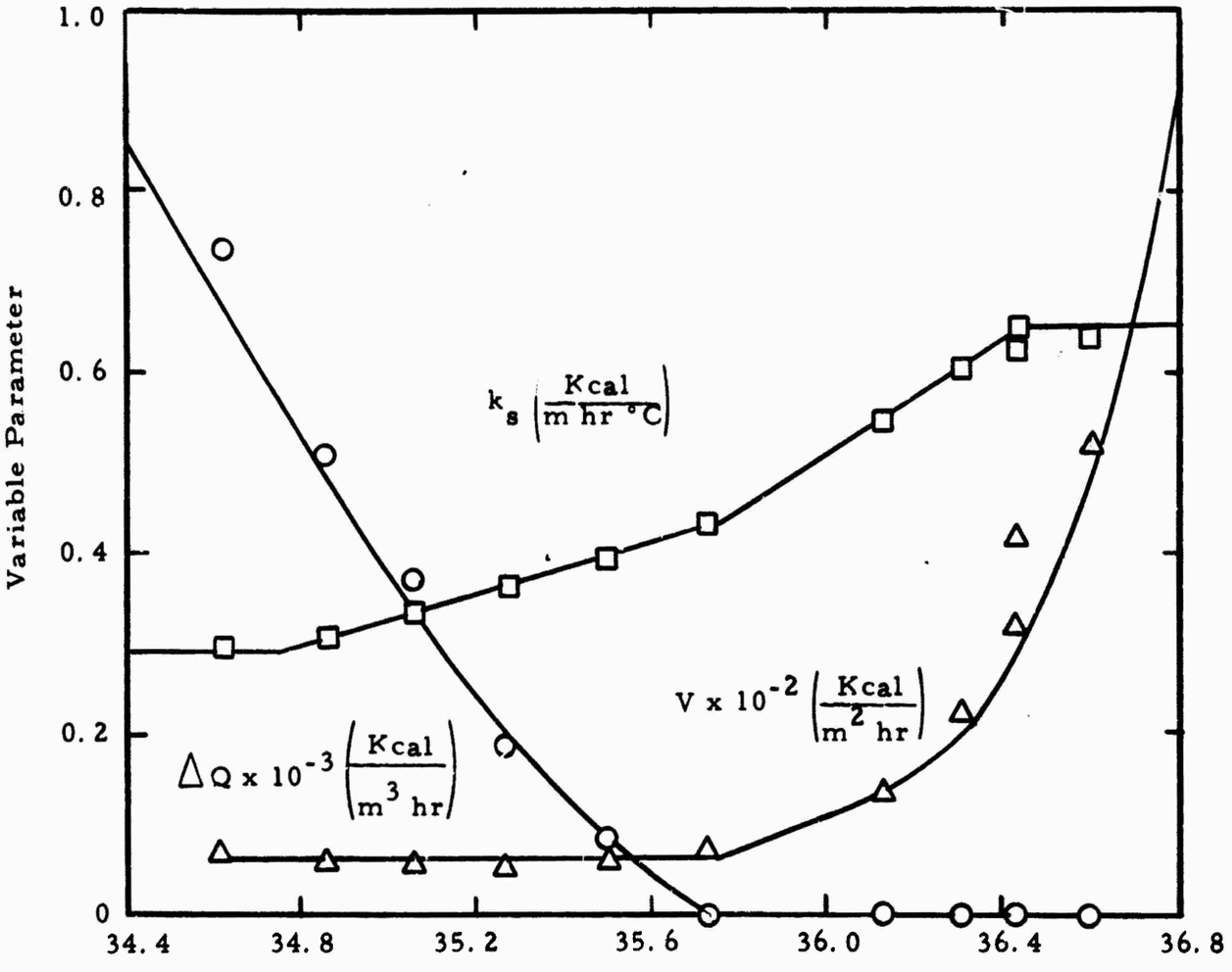

Figure A-2. Experimental and Empirical Variations with T_B

Experimental studies discussed in Reference A-1 indicate that the skin conductivity also depends upor the time rate of change of the average body temperature for transient situations. We shall, therefore, include an additional rate control term in the above equations as suggested by Crosbie, et al.[A-1] Therefore, the skin conductivity for transient, as well as steady-state, situations will be expressed as:

$$k_s = k_{s_0}\left[1 + \alpha_1\ \Delta T_B + \gamma \frac{dT_B}{dt}\right] \leq 1.511\ k_{s_0} \quad \text{for } T_B > 0$$

$$= k_{s_0}\left[1 + \alpha_2\ \Delta T_B + \gamma \frac{dT_B}{dt}\right] \geq 0.675\ k_{s_0} \quad \text{for } T_B \leq 0 \qquad \text{(A-29)}$$

where

γ represents the rate control coefficient (hr/°F) (see Section 4).

It was found that the increase in metabolism due to shivering may be satisfactorily approximated by a parabolic function of $-30.2^{\circ}F \leq \Delta T_B \leq 0$: That is:

$$\Delta Q_{shi} = -\alpha_{m_1}\ \Delta T_B + \alpha_{m_2}\ \Delta T_B^{\,2} \quad \text{for } -30.2^{\circ}F \leq \Delta T_B \leq 0$$

$$\alpha_{m_1} = 19.4\ \text{Btu/ft}^3\ \text{hr}^{\circ}\text{F} \qquad \text{(A-30)}$$

$$\alpha_{m_2} = 16.2\ \text{Btu/ft}^3\ \text{hr}^{\circ}\text{F}$$

And for $\Delta T_B < -30.2^{\circ}F$ the increase in metabolism due to shivering may be adequately expressed as:

$$\Delta Q_{shi} = 570 - \alpha_{m_3}\ (1 + \Delta T_B) \qquad \text{(A-31)}$$

$$\alpha_{m_3} = 51.9\ \text{Btu/ft}^3\ \text{hr}^{\circ}\text{F}$$

For $\Delta T_B > 0$ the increase in metabolism due to shivering is 0.

As in Reference A-1 the vaporization loss as a function of ΔT_B may be approximated by a fourth order polynomial(for $\Delta T_B > 0$). Thus, one finds:

$$V = V_0 + \alpha_v \Delta T_B + \lambda_v \Delta T_B^4 \quad \text{for } \Delta T_B > 0$$

$$V = V_0 \quad \text{for } \Delta T_B \leq 0$$

$$V_0 = 2.21 \text{ Btu/ft}^2\text{hr} \qquad (A\text{-}32)$$
$$\alpha_v = 3.07 \text{ Btu/ft}^2\text{hr}^\circ\text{F}$$
$$\lambda_v = 2.02 \text{ Btu/ft}^2\text{hr}^\circ\text{F}^4$$

One sees from Figure A-2 that the various empirical fits for conductivity, metabolism increase due to shivering, and vaporization provide very good approximations to the experimental points. Thus, these data (empirical curves) shall be used in the main portion of the text.

3. Evaluation of dT_B/dt

An expression which provides the time rate of change of the average body temperature is required in the skin governing equations for thermal conductivity (Eq. 8). . Also, as will be seen in the following section, such an expression is required to evaluate the value of Υ appearing in Equation (8). .

If one integrates Eq. (25) with respect to the skin coordinate from the outer to the inner surface (holding time constant) such an expression can be obtained. Thus, one obtains from Eq. (25).

$$\int_0^{L_s} (c\rho)_s \frac{\partial T_s}{\partial t} \, dx_s = \int_0^{L_s} k_s \frac{\partial^2 T_s}{\partial x_s^2} \, dx_s + \int_0^{L_s} Q' \, dx_s \qquad (A\text{-}33)$$

The heat capacity ($c\rho$) of the skin has been assumed constant elsewhere and the skin conductivity depends only on the average body temperature (a function of time). Therefore, one may remove $(c\rho)_s$ and k_s from the spacial integrals in Equation (A-33). Using the expressions for Q' (Eq. 45) and the abovementioned facts, Equation (A-33) may be rewritten as:

$$(c\rho)_s \int_0^{L_s} \frac{\partial T_s}{\partial x_s}\, dx_s = k_s \int_0^{L_s} \frac{\partial}{\partial x_s}\left[\frac{\partial T_s}{\partial x_s}\right] dx_s + \int_{L_1}^{L_1+L_2} (E + \Delta Q_{shi})dx_s + \int_{L_1+L_2}^{L_s} Q\, dx_s \qquad \text{(A-34)}$$

Since the integration in (A-34) is with respect to x_s, the time derivative in the left-hand term may be removed from the integral. Integration then yields:

$$(c\rho)_s \frac{d}{dt}\left[\int_0^{L_s} T_s dx_s\right] = k_s \left[\left(\frac{\partial T_s}{\partial x_s}\right)_{x_s=L_s} - \left(\frac{\partial T_s}{\partial x_s}\right)_{x_s=0}\right] + (E + \Delta Q_{shi})\, L_2 + Q L_3 \qquad \text{(A-35)}$$

However, by definition:

$$\frac{1}{L_s}\int_0^{L_s} T_s\, dx_s = T_B \qquad \text{(A-36)}$$

Also, since no heat flows through the surface at $x_s = L_s$:

$$\left(\frac{\partial T_s}{\partial x_s}\right)_{x_s = L_s} = 0 \qquad \text{(A-37)}$$

Utilization of the boundary condition at the skin outer surface (Eq. A-30) and the previous two expressions in relation (A-35) leads to:

$$(c\rho)_s L_s \frac{dT_B}{dt} = (E + \Delta Q_{shi}) L_2 + Q L_3 - \dot{m}_s \left[c_{p_v} (T_{s_0} - T_{ref}) + \lambda\right] - U_s (T_{s_0} - T_a) \qquad \text{(A-38)}$$

which may be rewritten as:

$$\frac{dT_B}{dt} = \frac{E + \Delta Q_{shi}}{(c\rho L)_s} L_2 + \frac{Q}{(c\rho L)_s} L_3 - \frac{\dot{m}_s}{(c\rho L)_s} \left[c_{p_v} (T_{s_0} - T_{ref}) + \lambda\right] - \frac{U_s}{(c\rho L)_s} (T_{s_0} - T_a) \qquad \text{(A-39)}$$

This is the expression which was sought and will be utilized in the following section.

4. Evaluation of Υ

The computer solution indicated in Figure 4 of Reference A-1 will now be utilized to evaluate Υ. This figure shows the transient response of a nude subject moved suddenly from a warm room (89.6°F) to a cold room (6.8°F). The assumed initial condition was that of thermal equilibrium. If one rewrites Equation (A-39) in the notation of Crosbie, A-1 there results:

$$\frac{d T_B}{dt} = \frac{E L_2 + \Delta M + M_0 - V - U_s (T_{s_0} - T_a)}{(c\rho)_s L_s} \qquad \text{(A-40)}$$

For the case under consideration, the exercise energy production was zero (E=0). Indicating the conditions immediately prior to and after entering the cold room with a superscript (-) and (+), respectively, one may write two equations:

$$\left(\frac{d T_B}{dt}\right)^{(-)} = \frac{\Delta M^{(-)} + M_0 - V^{(-)} - U_s \left[T_{s_0}^{(-)} - T_a^{(-)}\right]}{(c\rho)_s L_s} \qquad \text{(A-41)}$$

$$\left(\frac{d T_B}{dt}\right)^{(+)} = \frac{\Delta M^{(+)} + M_0 - V^{(+)} - U_s \left[T_{s_0}^{(+)} - T_a^{(+)}\right]}{(c\rho)_s L_s} \qquad \text{(A-42)}$$

Since the subject was in equilibrium before entering the cold room, $\left(\frac{d T_B}{dt}\right)^{(-)} = 0$. Also, since the skin temperature distribution cannot change abruptly when the subject enters the room, one may safely assume:

$$T_{s_0}^{(+)} = T_{s_0}^{(-)}$$
$$T_B^{(+)} = T_B^{(-)} \qquad \text{(A-43)}$$

Also, since the metabolism (ΔM) and vaporization rate (V) are assumed to depend only on T_B, one may write:

$$\Delta M^{(+)} = \Delta M^{(-)}$$
$$V^{(+)} = V^{(-)} \qquad \text{(A-44)}$$

Subtracting Equation (A-41) from (A-42) and using the abovementioned equalities, one finds:

$$\left(\frac{d T_B}{dt}\right)^{(+)} = \frac{U_s\left[T_a^{(+)} - T_a^{(-)}\right]}{(c\rho)_s L_s} \qquad \text{(A-45)}$$

The difference in skin conductivity immediately before and after entering the cold room utilizing Eq. (26) and relation (A-43) may be expressed as:

$$k_s^{(+)} - k_s^{(-)} = k_{s_0} \gamma \left(\frac{d T_B}{dt}\right)^{(+)} \qquad \text{(A-46)}$$

Solving for γ and introducing (A-45) for $\left(\frac{d T_B}{dt}\right)^{(+)}$, one obtains:

$$\gamma = \frac{(c\rho)_s L_s\left[k_s^{(+)} - k_s^{(-)}\right]}{k_{s_0} U_s\left[T_a^{(+)} - T_a^{(-)}\right]} \qquad \text{(A-47)}$$

From Figure 4 of Reference A-1, one finds $k_s^{(+)} - k_s^{(-)} = -0.0000374$ Btu/ m hr °C. Also, from the given conditions of the problem and physiological constants derived elsewhere in this report, it may be written:

$$(c\rho)_s = 11.5 \text{ Btu/ft}^2\,^\circ\text{F}$$

$$k_{s_0} = 0.0000804 \text{ Btu/ft sec }^\circ\text{F}$$

$$U_s = 0.000302 \text{ Btu/ft}^2 \text{ sec }^\circ\text{F}$$

$$T_a^{(+)} - T_a^{(-)} = -3.2^\circ\text{F}$$

Substitution of these values into Equation (A-47) yields:

$$\Upsilon = 0.30715 \text{ hr/°C}$$

$$= 614.28 \text{ sec/°F}$$

Rounding off these values, we shall assume Υ to be:

$$\Upsilon = 615 \text{ sec/°F} \qquad \text{(A-48)}$$

5. Determination of the Sweat Rate

An expression describing the sweat rate per unit skin area is required for the skin governing equations presented in Section II. It is important to note that the vaporization rate is not necessarily identical to the sweat rate since the vaporization rate is governed by ambient and skin surface conditions. (Refer to the discussion in Section II-B.) Thus, an effort has been made to determine if the data for vaporization, presented in Section 2, reflect the actual sweat rate or if they reflect, in fact, the limitations imposed by mass transfer considerations.

The maximum mass transfer rate at the skin surface is given by Eq. (20) in the text as:

$$\dot{m}_s = K_s (C_{s_0} - C_a) \qquad \text{(A-49)}$$

Corresponding to this rate, the maximum vaporization possible can be written as:

$$V_{max} = \lambda K_s (C_{s_0} - C_a) \qquad \text{(A-50)}$$

where λ represents the heat of vaporization of water. The vapor concentration at the skin surface equals the saturation concentration which exists at the skin outer surface temperature. Thus, C_{s_0} may be expressed mathematically as:

$$C_{s_0} = C_{sat} (T_{s_0})$$

where $C_{sat}(T)$ = saturation concentration at a temperature T (lb/ft^3).

Defining the relative humidity as $r = \frac{C}{C_{sat}}$, the ambient vapor concentration may be expressed as:

$$C_a = r_a C_{sat} (T_a)$$

where r_a = ambient relative humidity. Substitution of these expressions into Equation (A-50) gives:

$$V_{max} = \lambda K_s \left[C_{sat} (T_{s_0}) - r_a C_{sat} (T_a) \right] \qquad \text{(A-51)}$$

Data for free evaporation of water from a paper by Gregory[A-2] have been utilized to determine a proper value for the mass transfer coefficient (K_s). The results of experimental studies of free evaporation yield the following information.[A-2]

$$\dot{m}_s = 1.44 \times 10^{-5} \text{ gm/cm}^2 \text{ sec} = 2.949 \times 10^{-5} \text{ lb/ft}^2 \text{ sec}$$

$$T_{s_0} = 37.5°C = 99.5°F$$

$$T_a = 20.5°C = 68.9°F$$

$$r_a = 0.63$$

The saturation concentrations corresponding to T_{s_0} and T_a from Reference A-3 are 2.8133×10^{-3} lb/ft^3 and 1.1120×10^{-3}, respectively. Equation (A-49) applies for free evaporation and, using this experimental data, one may determine K_s as:

$$K_s = \frac{2.949 \times 10^{-5}}{2.8133 \times 10^{-3} - 0.63\,(1.1120 \times 10^{-3})}$$

$$= 1.396 \times 10^{-2} \text{ ft/sec}$$

Figures A-3 and A-4 will now be used to establish the sweat rate. Shown in Figure A-3 are the variations of the rectal and skin temperatures, the vaporization loss and the metabolic rate as a function of the ambient temperature as computed using the relations presented in this appendix. The circled points represent the experimental data of Hardy and DuBois.[A-4] It can be seen that the agreement between theory and experiment is excellent, confirming the empirical formulations.

The vaporization curve is reproduced in Figure A-4 along with curves giving the maximum possible vaporization (Equation A-51) at various ambient relative humidities. Two possibilities exist with regard to the vaporization (V).

1) The curve V represents the entire sweat rate.

2) The curve V represents a portion of the sweat rate with the remaining sweat "running off" the body and providing no cooling effect.

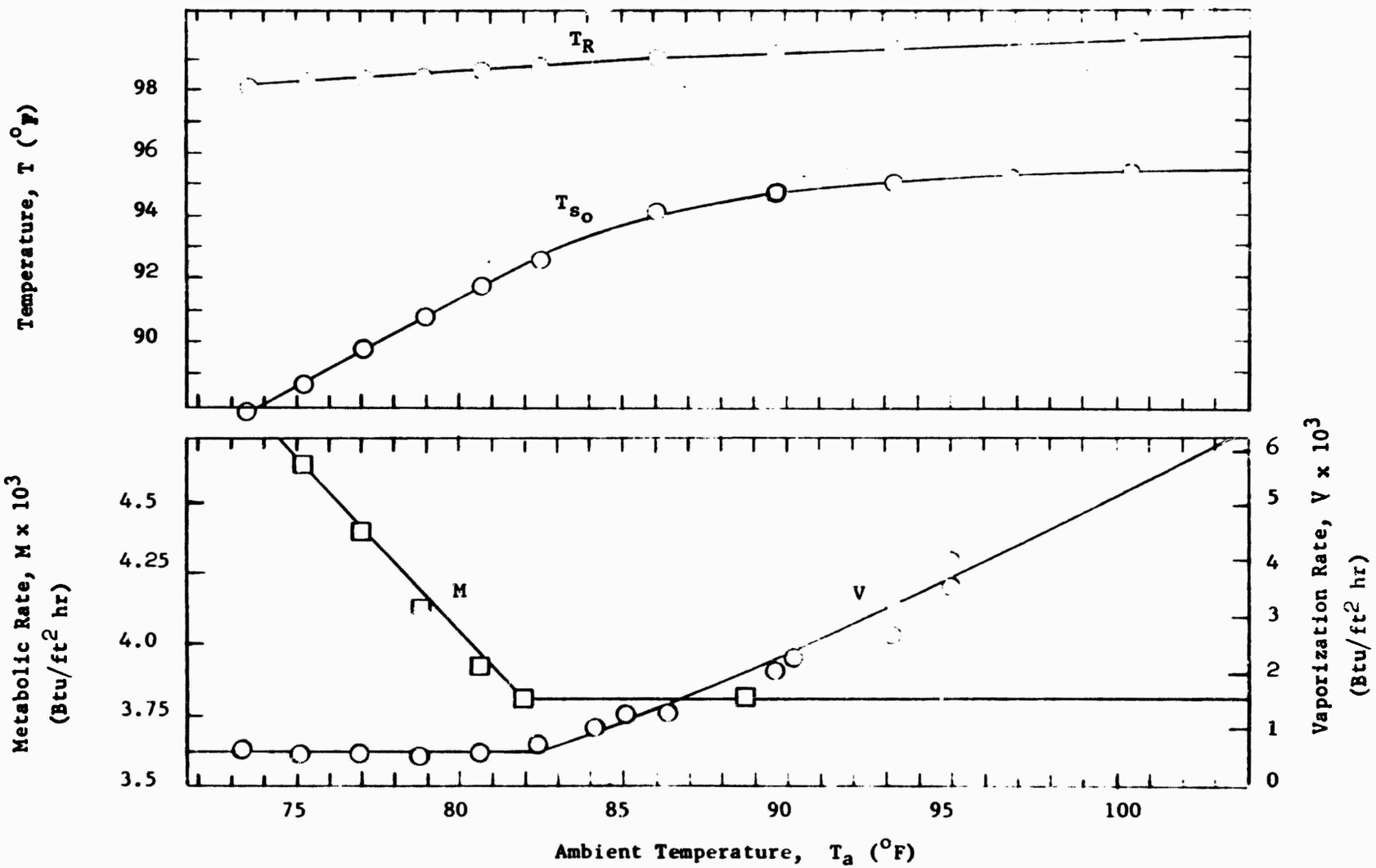

Figure A-3. Comparison Between Experimental and Analytical Steady-State Results

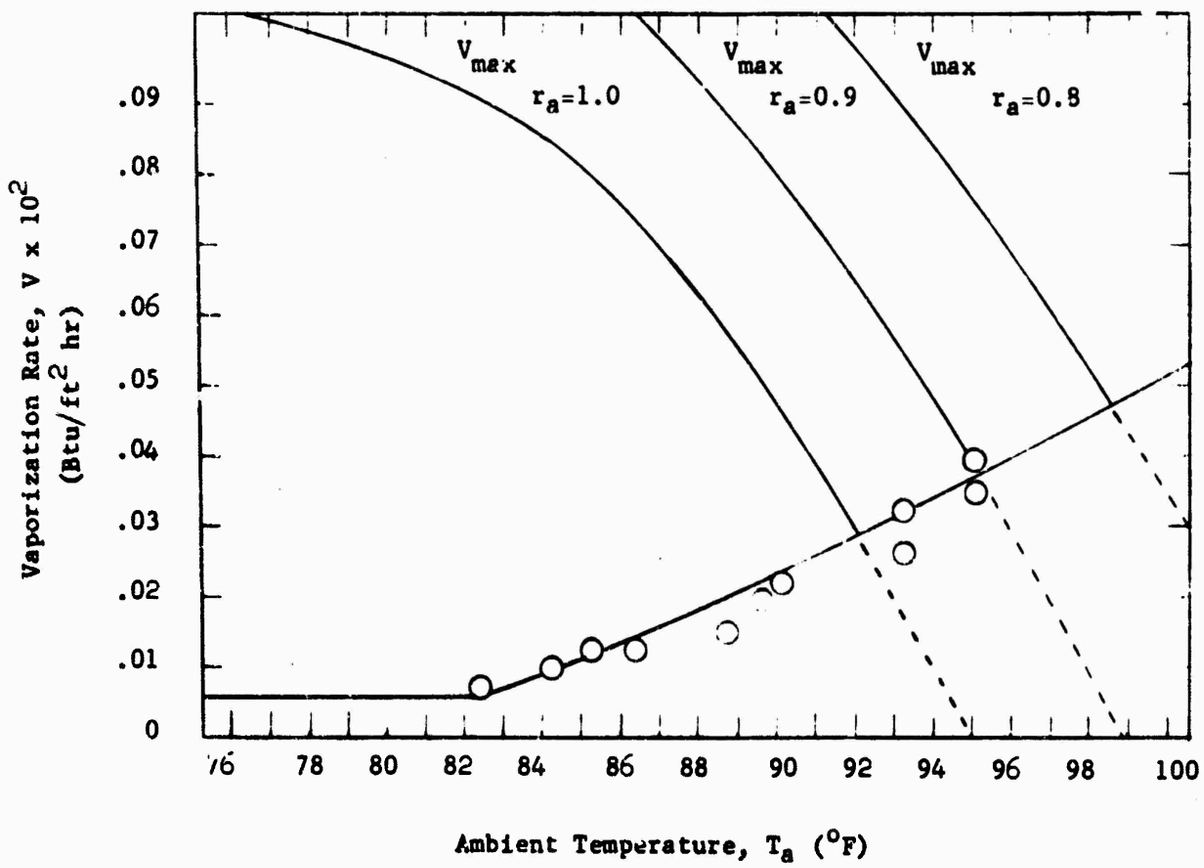

Figure A-4. Vaporization Rate Variation with Ambient Temperature

The consequences of possibility 2 will now be examined. If 2 is a true description of the physical situation, there is an excess of sweat which cannot be evaporated. This implies that the moisture being evaporated (V) represents the maximum possible amount under the existing ambient conditions. However, even in the worst possible situation (100% relative humidity) the curve labeled $r_a = 1.0$ indicates that, up to approximately $T_a = 92°F$, the ambient and skin surface conditions are of a magnitude which would allow more moisture to evaporate than was experimentally observed. Thus, condition "2" above is definitely impossible up to $T_a = 92°F$. Actually it is most probable that the humidity conditions employed in the experimental studies of Reference A-4 (the conditions are not stated in the paper) were no higher than 50 to 70 percent. It can, therefore, be assumed that the ambient relative humidity employed in these experiments was low enough (at least $r_a = 90\%$) such that all of the moisture available was evaporated. As a consequence of this, the vaporization curve in Figure A-4 as well as the vaporization Equation (A-32) represents the entire sweat production rate (in terms of evaporative equivalent).

As a result of the preceding analysis, the sweat generation rate may be expressed by the relation:

$$S = \frac{V}{\lambda} \qquad \text{(A-52)}$$

Since the mathematical model of the skin assumes the sweat rate to depend only on the average body temperature (and not the state of activity), Equation (A-32) can be utilized in (A-52) for V, and the resulting expression for S written as:

$$S = S_0 + \alpha_s \Delta T_B + \lambda_s \Delta T_B^4 \quad \text{for } \Delta T_B > 0$$

$$= S_0 \quad \text{for } \Delta T_B \leq 0$$

where:

$$S_0 = 10.0688 \text{ gm/hr m}^2 = 5.7285 \times 10^{-7} \text{ lb/ft}^2 \text{ sec}$$

$$\alpha_s = 25.138 \text{ gm/m}^2 \text{ hr } ^\circ\text{C} = 7.9457 \times 10^{-7} \text{ lb/ft}^2 \text{ sec } ^\circ\text{F}$$

$$\lambda_s = 96.895 \text{ gm/m}^2 \text{ hr } ^\circ\text{C}^4 = 5.2514 \times 10^{-7} \text{ lb/ft}^2 \text{ sec } ^\circ\text{F}^4$$

REFERENCES

A-1. Crosbie, R. J., J. D. Hardy and E. Fessenden. Electrical analog simulation of temperature regulation in man. In American Institute of Physics, Temperature, Its Measurement and Control. Vol. 3, Part 3, New York, 1963.

A-2. Gregory, J. The transfer of moisture through fabrics. Journal of the Textile Institute. Vol. XXI (21) 1930, pp. T66-T84.

A-3. Keenan, J. H. and F. G. Keyes. Thermodynamic properties of steam. First edition, John Wiley and Sons, Inc., New York, 1956.

A-4. Hardy, J. D. and E. F. DuBois. The significance of the average temperature of the skin. Temperature, Its Measurement and Control. Vol. 1, New York, 1941.

APPENDIX B

EVALUATION OF FABRIC-RELATED CONSTANTS

NOMENCLATURE

Symbol	Definition and Dimension
a	percentage of fabric which is in a parallel arrangement
C	concentration (lb/ft^3)
F_1, F_2, F_3	functions
k	thermal conductivity (Btu/ft hr °F)
m	mass (lb)
M	dimensionless mass of absorbed water vapor
$M_{1.0}$	maximum dimensionless mass of absorbed water vapor
r	relative humidity (dimensionless)
T	temperature (°F)
V	volume (ft^3)
α	geometric (volumetric) porosity of the fabric (dimensionless)
ρ	density (lb/ft^3)
σ	$(\partial M/\partial C)_T$ (ft^3/lb)
ω	$(\partial M/\partial T)_C$ (1/°F)

Subscripts

f	fabric
fi	fiber
l	liquid
sat	saturation

EVALUATION OF FABRIC-RELATED CONSTANTS

1. Determination of the Fabric Conductivity (k_f)

It was pointed out in Section III-B that an expression describing the average fabric conductivity at any point x_f is required for use in the governing equations. Since the thermal conductivity of water is one order of magnitude larger than that of cotton fibers, it is conceivable that the absorption processes within the fabric could materially alter the overall conductivity. Hence, this appendix presents a method whereby one may determine the variation of k_f with the amount of absorbed water.

For the following derivation, it shall be assumed that the fabric is composed of three materials, namely, fibers, water, and air. Two extremes in configuration are imaginable.

1) The three materials are arranged in a parallel fashion

2) The three materials are arranged in a series fashion.

For such arrangements, it can be shown that the thermal conductivity is given by:

$$k = \frac{V_{fi}}{V} k_{fi} + \frac{V_{air}}{V} k_{air} + \frac{V_\ell}{V} k_\ell \qquad \text{(parallel arrangement)}$$

$$\frac{1}{\kappa} = \frac{V_{fi}}{V} \frac{1}{k_{fi}} + \frac{V_{air}}{V} \frac{1}{k_{air}} + \frac{V_\ell}{V} \frac{1}{k_\ell} \qquad \text{(series arrangement)}$$

where:

V_{fi}/V = volume of fibers per unit volume of fabric

V_{air}/V = volume of air per unit volume of fabric

V_ℓ/V = volume of liquid per unit volume of fabric.

The volumetric ratio of fibers is expressed in terms of the volumetric porosity by the relation

$$\frac{V_{fi}}{V} = 1 - \alpha \qquad \text{(B-1)}$$

The remaining fabric volume is occupied by the liquid and air and, since $V_{fi} + V_{air} + V_\ell = V$, one may write,

$$\frac{V_\ell + V_{air}}{V} = \alpha \qquad \text{(B-2)}$$

However, the volume occupied by the liquid can be expressed as $V_\ell = m_\ell/\rho_\ell$ and that of the fiber by $V_{fi} = m_{fi}/\rho_{fi}$, dividing the relations gives:

$$\frac{V_\ell}{V_{fi}} = \frac{m_\ell}{m_{fi}} \frac{\rho_{fi}}{\rho_\ell}$$

Noting that $m_\ell/m_{fi} = M$ and using Equation (B-1) one can write

$$\frac{V_\ell}{V} = M \frac{\rho_{fi}}{\rho_\ell} \frac{V_{fi}}{V} = (1-\alpha)\frac{\rho_{fi}}{\rho_\ell} M \qquad \text{(B-3)}$$

Using this relation in (B-2) gives:

$$\frac{V_{air}}{V} = \alpha - (1 - \alpha)\frac{\rho_{fi}}{\rho_{\ell}} M \qquad \text{(B-4)}$$

It shall now be assumed, as in Reference B-1, for a general situation, that in an incremental thickness (δx), a length of $a\delta x$ is composed of series elements and $(1-a)\delta x$ of parallel elements (refer to Figure B-1).

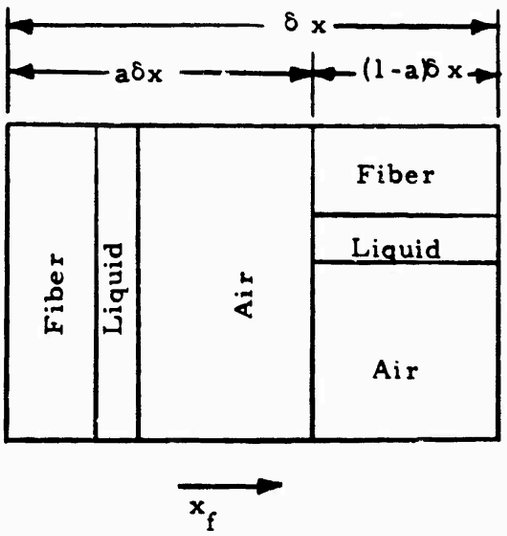

Figure B-1. Schematic of the Composite Slab

Designating the conductivity of the series and parallel sections by k_a and k_{1-a}, respectively, the conductivity of the composite slab can be written as:

$$\frac{1}{k_f} = \frac{a}{k_a} + \frac{1-a}{k_{1-a}} \qquad \text{(B-5)}$$

where

$$\frac{1}{k_a} = (1 - \alpha)\frac{1}{k_{fi}} + (1 - \alpha)\frac{\rho_{fi}}{\rho_\ell} M \frac{1}{k_\ell} + \left[\alpha - (1 - \gamma)\frac{\rho_{fi}}{\rho_\ell} M\right] \frac{1}{k_{air}}$$

$$k_{l-a} = (1 - \alpha) k_{fi} + (1 - \alpha) \frac{\rho_{fi}}{\rho_\ell} M k_\ell + \left[\alpha - (1 - \alpha)\frac{\rho_{fi}}{\rho_\ell} M\right] k_{air}$$

All parameters appearing in this equation are known, with the exception of "a" which shall be determined for cotton fabric in the following section.

2. Evaluation of Cotton Fabric Parameters

The results of experimental studies performed by Speakman and Chamberlain[B-1] shall be utilized to determine an appropriate value for "a" (appearing in Equation B-5). These experiments were conducted with loose cotton fibers with no preferential orientation and also with various woven cotton fabrics. Ambient conditions were kept identical in all tests and were:

$$T_a = 25°C\ (77°F);\quad r = 65\%$$

Corresponding to this condition, the air and water conductivity amounts to[B-2]

$$k_{air} = 6.2585 \times 10^{-5}\ \text{cal/cm sec}^{\circ}\text{C} = 0.01508\ \text{Btu/ft hr}\ ^{\circ}\text{F}$$

$$k_\ell = 1.4505 \times 10^{-3}\ \text{cal/cm sec}^{\circ}\text{C} = 0.3495\ \text{Btu/ft hr}\ ^{\circ}\text{F}$$

The amount of water absorbed under these conditions is[B-3] M = 0.068.

The value of the fiber conductivity is determined with the aid of the experimental data[B-1] for unwoven, loosely packed cotton. Such samples possess no "preferential direction" characteristics and it appears reasonable that such a sample is composed of half parallel and half series elements. In terms of the parameter "a", this means that it can probably safely assume a = 1/2 for unwoven fiber packages. The ratio of fiber-to-liquid density is 1.565.[B-4] Referring to Equation (B-5) it is noted that all constants are known, with the exception of k_{fi}. By assuming various values for the fiber conductivity and comparing Equation (B-5) with the experimental data for each assumed value, it is possible to determine a value which gives a "best fit" to the experimental points. Figure B-2 shows the predicted variation of k_f with α (as determined from Equation B-5) when a value $k_{fi} = 2.02 \times 10^{-5}$ Btu/ft sec °F is selected. Also shown are the experimental data for loose, unwoven cotton from Reference B-1. The agreement is noted to be quite good, especially in the middle range of α. It shall, therefore, be assumed that the fiber conductivity is:

$$k_{fi} = 2.02 \times 10^{-5} \text{ Btu/ft sec } ^\circ\text{F}$$

Utilizing this value, along with previously quoted values for the other constants, curves can be drawn which show the variation of k_f with α for various values of the parameter "a". These curves are presented in Figure B-3, along with the experimentally determined values of k_f for various woven fabrics.[B-1]

The differences between the various fabrics tested will not be delved into. It is important to note, however, that the experimental points to the lower left of an envelope of curves were mainly from fabrics which were heavily finished. Since the mathematical model (Equation B-5) does not include these effects, it is not reasonable to expect agreement. One notes, though, that almost all experimental points fall within the envelope ($0 \leq a \leq 1$) and can, therefore, be described by

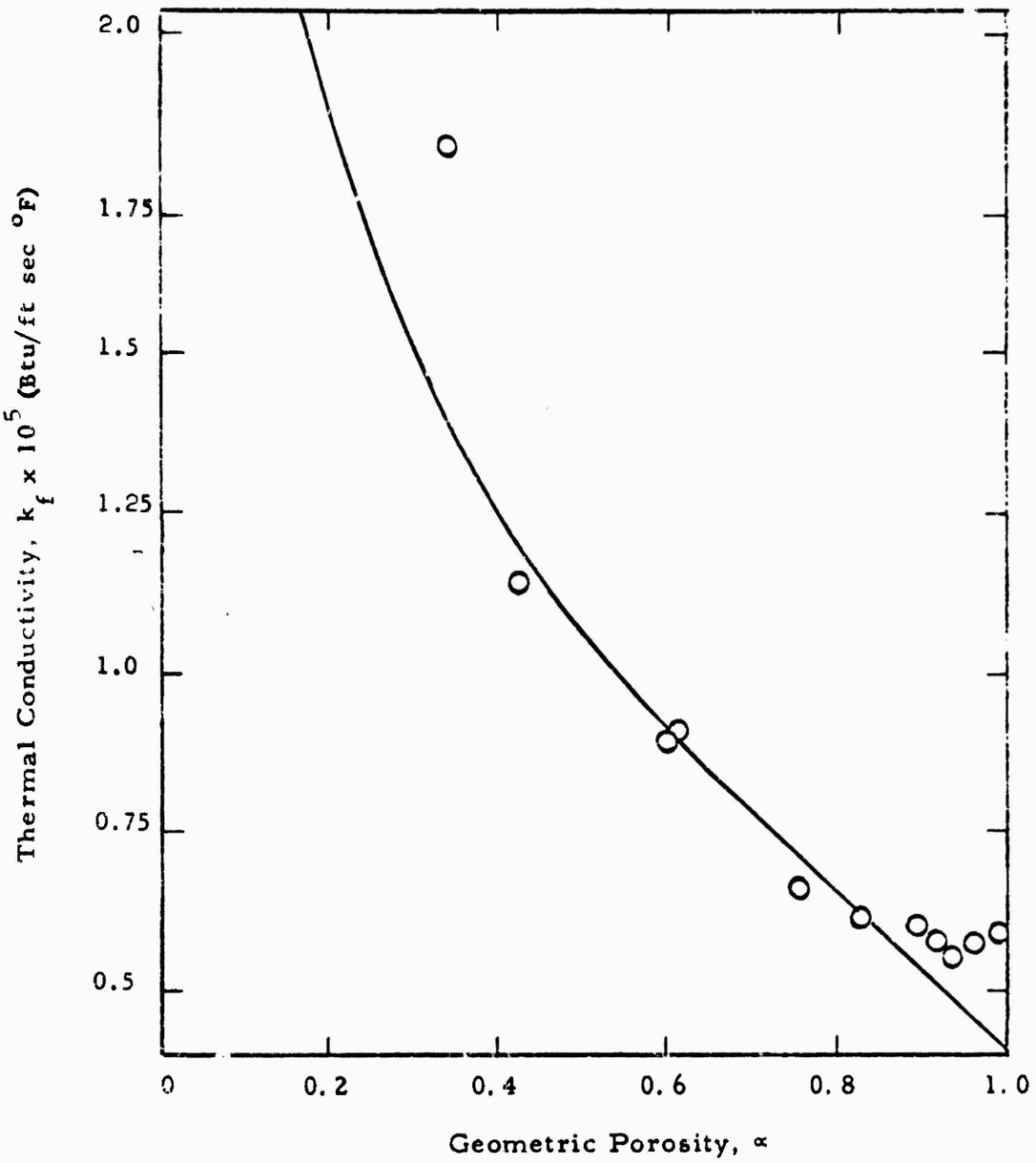

Figure B-2. Variation of Thermal Conductivity of Loose Cotton Fibres with Geometric Porosity

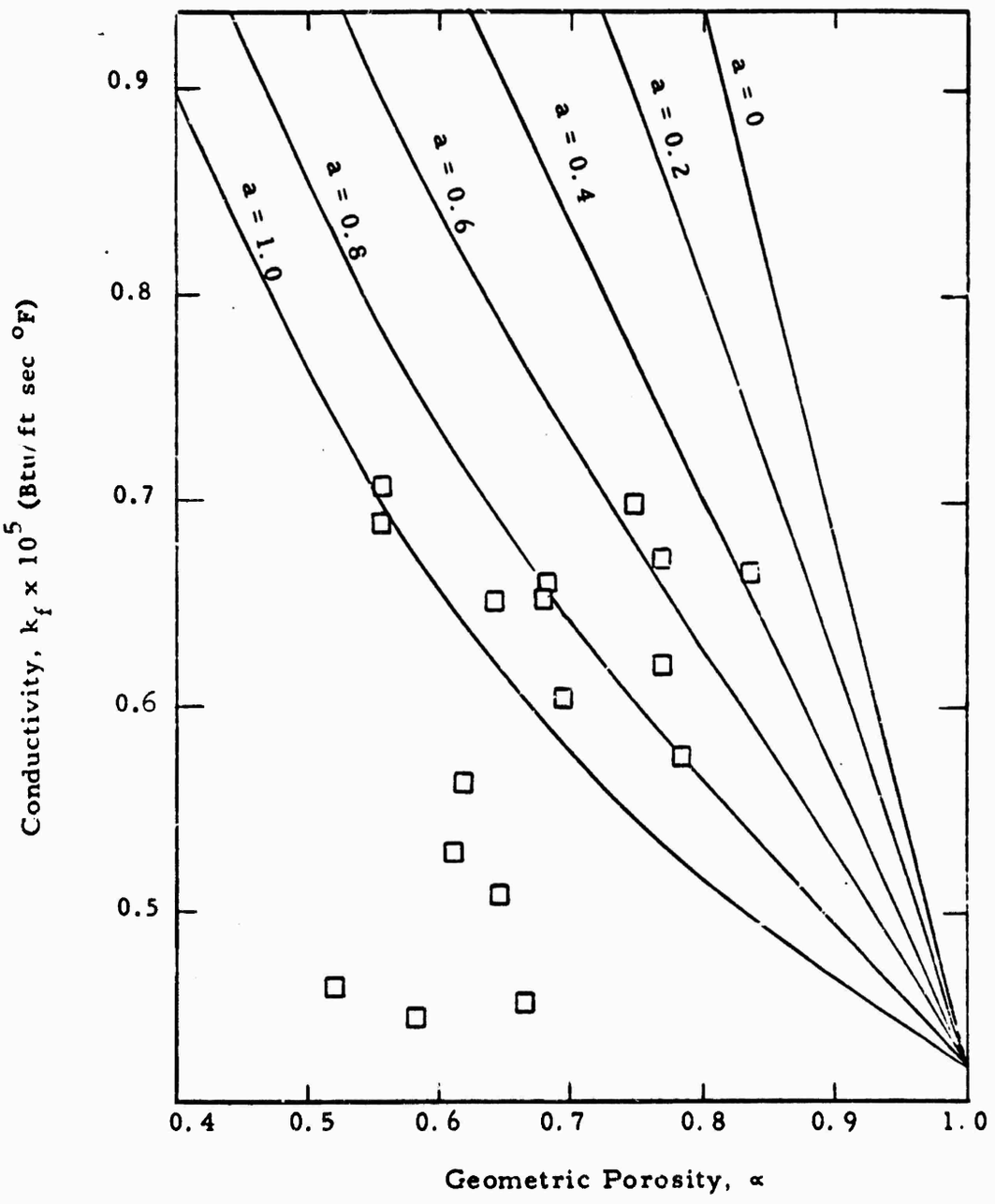

Figure B-3. Variation of Fabric Conductivity with Geometric Porosity for Cotton Fabrics

Equation (B-5), once the dependence of "a" upon type of weave and thickness (and possibly other parameters) is established. Such relationships are beyond the scope of the present program and it is necessary, at this point, to choose a reasonable value for "a" from Figure B-3. The most dense grouping of points is found in the range $0.7 \leq a \leq 1$. Thus, a representative value of "a" would most likely be $a = 0.8$. There is, however, a considerable simplification in the equation for k_f if $a = 1$ is selected and it may be desirable for a first order approximate analysis, to use this value of unity.

It is interesting to note that the abovementioned range for "a" implies that woven fabrics can be considered to be composed of approximately 80 to 100 percent series elements.

3. Evaluation of M, ω and σ for Cotton Fabrics

The solution of the fabric governing equation requires a knowledge of the variation of M, ω and σ with the local temperature and vapor concentration. Experiments were conducted by Urquhart and Williams[B-3] to determine the dependence of M on temperature and relative humidity. By utilizing the results of these experiments, it has been possible to establish an empirical set of equations describing this variation.

If one defines the maximum absorbed moisture (which occurs at a relative humidity of 1.0) for any temperature (T) as $M_{1.0}(T)$, and forms the ratio $M/M_{1.0}$, a universal curve for restricted temperature and all relative humidity ranges can be established as presented in Figure B-4. The variation of $M_{1.0}$ with temperature is presented in Figure B-5. The circled points appearing in Figure B-4 indicate the maximum and minimum experimental values from Reference B-3 for each value of r and for the temperature range $68^{\circ}F \leq T \leq 122^{\circ}F$. An indication of the dispersion in the data is presented in Table B-1 in which the percentage dispersion at each relative humidity r, is defined by

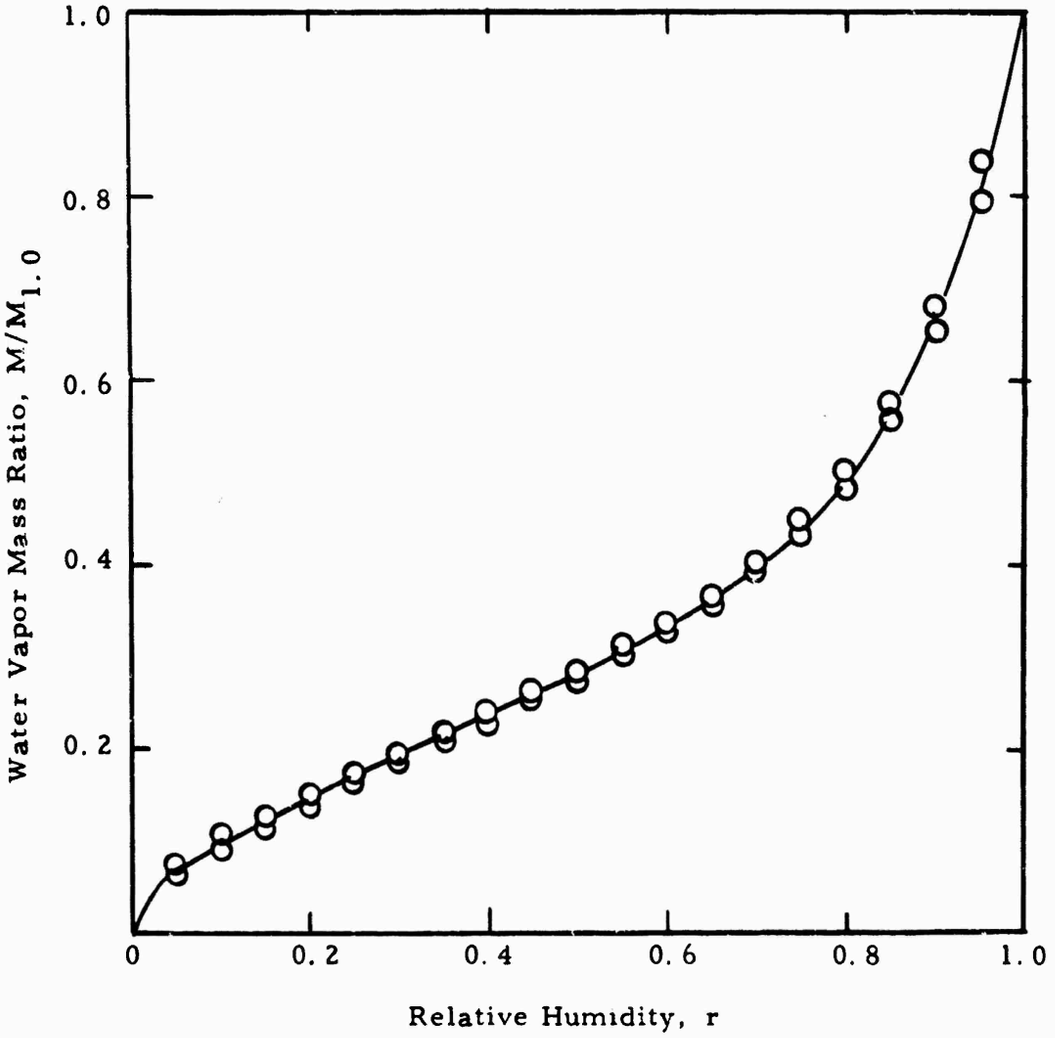

Figure B-4. Variation of Absorbed Water Vapor Mass with Relative Humidity for Cotton Fibers

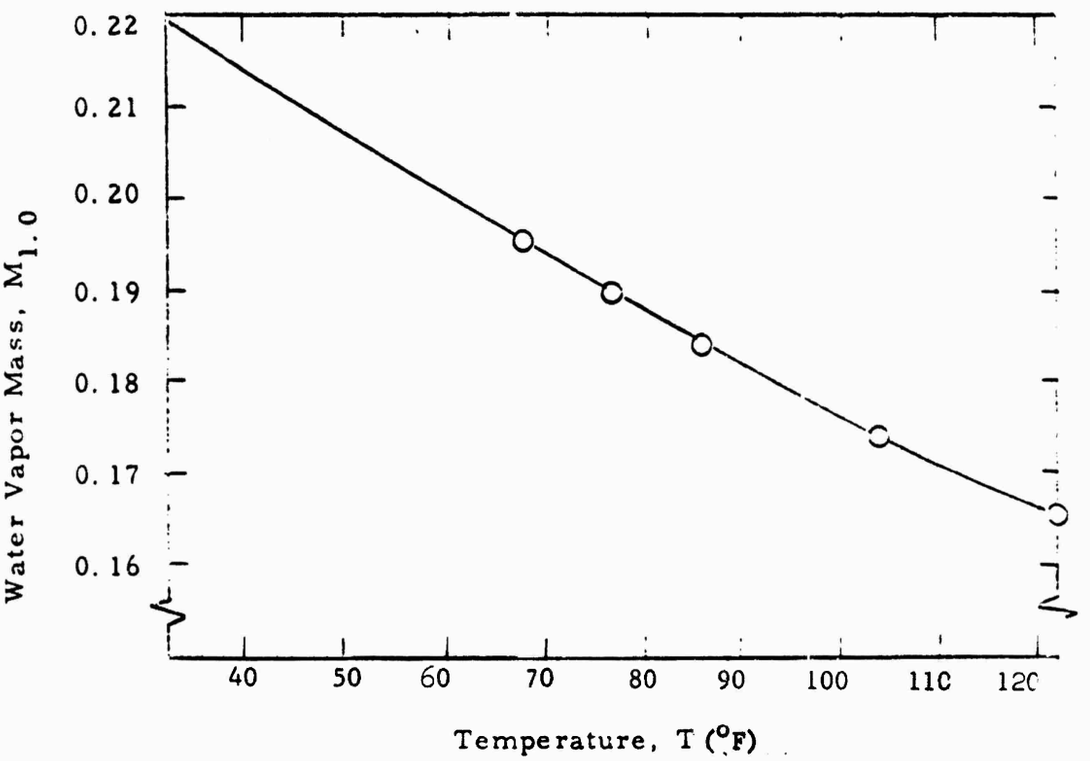

Figure B-5. Variation of the Maximum Absorbed Water Vapor Mass with Temperature for Cotton Fibers

$$\Delta(r) = \frac{\left(\frac{M}{M_{1.0}}\right)_{max} - \left(\frac{M}{M_{1.0}}\right)_{min}}{\left(\frac{M}{M_{1.0}}\right)_{average}} \times 100 \quad (\%)$$

Table B-1

DISPERSION OF MASS ABSORPTION DATA

r	Δ	r	Δ	r	Δ	r	Δ
0.05	19.5	0.30	4.1	0.55	3.2	0.80	4.2
0.10	17.1	0.35	4.1	0.60	2.0	0.85	3.8
0.15	10.9	0.40	4.6	0.65	2.8	0.90	4.3
0.20	10.1	0.45	2.0	0.70	2.6	0.95	5.3
0.25	6.6	0.50	1.2	0.75	4.0		

The average dispersion in data over the entire range of relative humidity was determined to be 5.9 percent, and this is reduced to about 4 percent if the points below r = 0.25 are excluded.

The curve shown in Figure B-4 is described by the following set of equations:

for $0 \leq r \leq 0.05$

$$\frac{M}{M_{1.0}} = 2.8765\, r - 46.19\, r^2 + 325.2\, r^3$$

for $0.05 \leq r \leq 0.15$

$$\frac{M}{M_{1.0}} = 0.0690 + 0.6965\,(r - 0.05) - 2.6928\,(r - 0.05)^2 + 10.718\,(r - 0.05)^3$$

for $0.15 \leq r \leq 0.50$

$$\frac{M}{M_{1.0}} = 0.1219 + 0.46328\,(r - 0.15)$$

for $0.50 \leq r \leq 0.70$

$$\frac{M}{M_{1.0}} = 0.2840 + 0.46328\,(r - 0.5) - 0.0908\,(r - 0.5)^2 + 3.147\,(r - 0.5)^3$$

for $0.70 \leq r \leq 0.90$

$$\frac{M}{M_{1.0}} = 0.3982 + 0.8046\,(r - 0.7) - 0.6475\,(r - 0.7)^2 + 16.5975\,(r - 0.7)^3$$

for $0.90 \leq r \leq 1.00$

$$\frac{M}{M_{1.0}} = 0.6660 + 2.5373\,(r - 0.9) + 6.4810\,(r - 0.9)^2 + 15.46\,(r - 0.9)^3$$

and the variation of $M_{1.0}$ with T is described by (for $32°F \leq T \leq 120°F$):

$$M_{1.0} = 0.2193 - 6.61481 \times 10^{-4}\,(T - 32) - 7.20165 \times 10^{-7}\,(T - 32)^2 + 1.60037 \times 10^{-8}\,(T - 32)^3$$

To evaluate σ and ω, one writes M as

$$M = M_{1.0}(T)\ \frac{M}{M_{1.0}}\ (r)$$

or, with the following definitions:

$$\frac{M}{M_{1.0}} = F_1(r)$$

$$M_{1.0} = F_2(T)$$

the above expression becomes

$$M = F_1(r)\, F_2(T) \tag{B-6}$$

From the main body of this report σ and ω are defined by

$$\sigma = \frac{\partial M}{\partial C} \tag{B-7}$$

$$\omega = -\frac{\partial M}{\partial T} \tag{B-8}$$

Utilization of Equation (B-6) gives:

$$\sigma = \frac{\partial}{\partial C}\left[F_1(r)\, F_2(T)\right]$$

$$\omega = -\frac{\partial}{\partial T}\left[F_1(r)\, F_2(T)\right]$$

or, expanding:

$$\begin{aligned} \sigma &= F_1(r)\frac{\partial}{\partial C}\, F_2(T) + F_2(T)\, \frac{\partial}{\partial C}\, F_1(r) \\ \omega &= -F_1(r)\, \frac{\partial}{\partial T}\, F_2(T) - F_2(T)\, \frac{\partial}{\partial T}\, F_1(r) \end{aligned} \tag{B-9}$$

With the chain rule for differentiation, one may write:

$$\frac{F_2(T)}{\partial C} = 0$$

$$\frac{\partial}{\partial C}\, F_1(r) = \frac{d F_1(r)}{dr}\, \frac{\partial r}{\partial C}$$

$$\frac{\partial F_2(T)}{\partial T} = \frac{d F_2(T)}{dT}$$

$$\frac{\partial F_1(r)}{\partial T} = \frac{d F_1(r)}{dr} \frac{\partial r}{\partial T}$$

Since the relative humidity is defined by:

$$r = \frac{C}{C_{sat}(T)}$$

and if we define the function

$$C_{sat}(T) = F_3(T) \qquad \text{(B-10)}$$

one may obtain the following:

$$\frac{\partial r}{\partial C} = \frac{\partial}{\partial C} \left[\frac{C}{F_3(T)}\right] = \frac{1}{F_3(T)}$$

$$\frac{\partial r}{\partial T} = \frac{\partial}{\partial T} \left[\frac{C}{F_3(T)}\right] = - \frac{C}{F_3^{\,2}(T)} \frac{d}{dt} F_3(T)$$

$$= - r \frac{d}{dt} \left[F_3(T)\right] / F_3(T)$$

Substituting these relations into (B-9), the following equations for σ and ω are obtained:

$$\sigma = \frac{F_2(T)}{F_3(T)} F_1'(r)$$

$$\omega = \frac{F_2(T)}{F_3(T)} F_3'(T)\, r\, F_1'(r) - F_2'(T)\, F_1(r) \qquad \text{(B-11)}$$

where the primes indicate differentiation with respect to the argument of the function, i.e., $F_1'(r) = \frac{d}{dt} F_1(r)$.

The functions $F_1(r)$ and $F_2(T)$ were presented previously and $F_3(T)$ (C_{sat}) can be determined from tables (Ref. 6). Therefore, σ and ω can be evaluated for different values of relative humidity (r) and temperature (T). These variations are presented in Figure B-6 for various values of r and T.

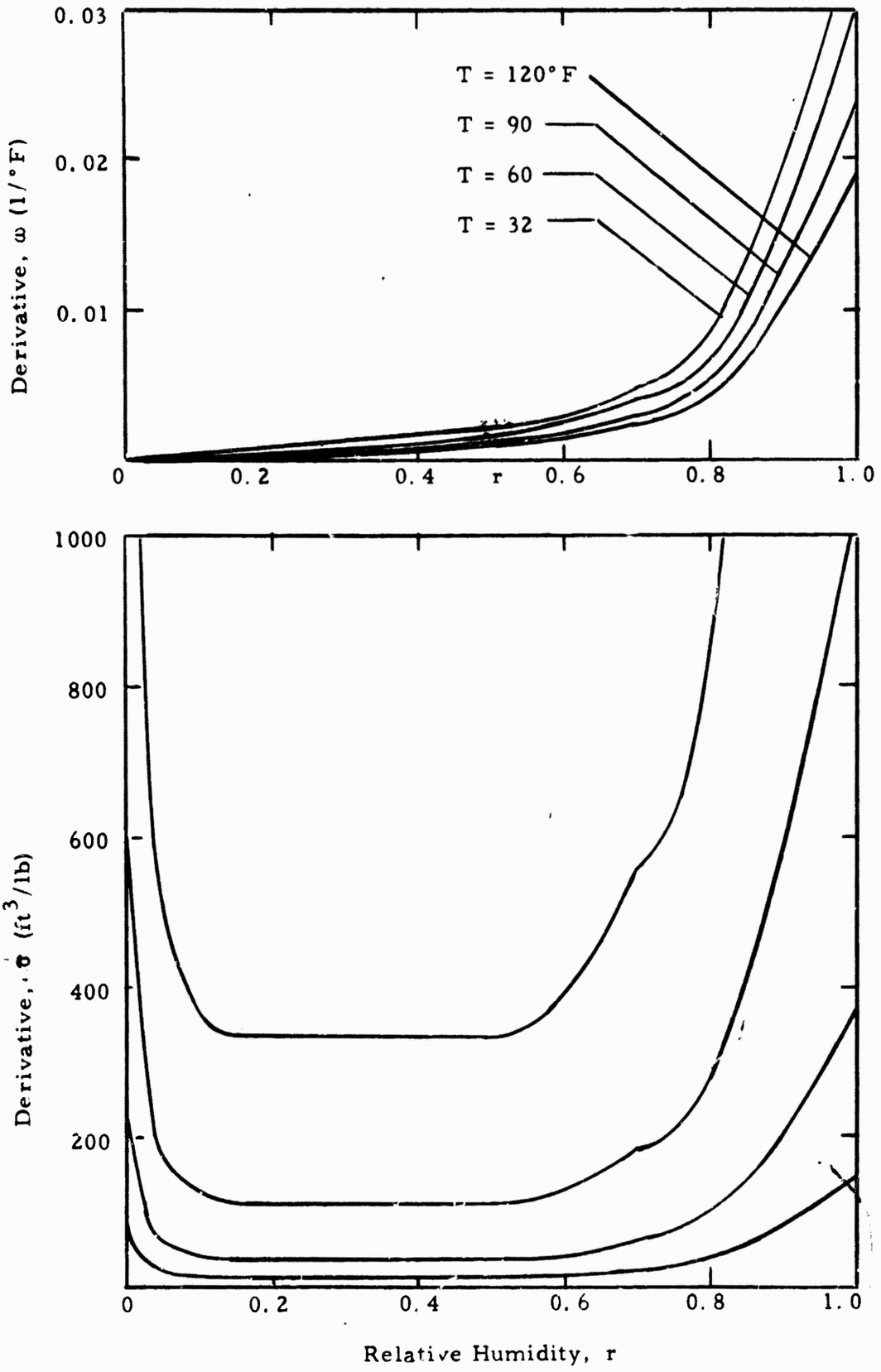

Figure B-6. Variation of σ' and ω with Temperature and Relative Humidity for Cotton Fibers

REFERENCES

B-1. Speakman, J. B. and N. H. Chamberlain. The thermal conductivity of textile materials and fabrics. Journal of the Textile Institute. Vol. XXI (21)-1930.

B-2. Eckert, E. R. G. and R. M. Drake, Jr. Heat and mass transfer. McGraw-Hill Book Co., Inc., New York, 1959.

B-3. Urquhart, A. R. and A. M. Williams. The effect of temperature on the absorption of water by soda-boiled cotton. Journal of the Textile Institute, 15: 559-72 (1924).

B-4. Chen, N. Y. Transient heat and moisture transfer to skin through thermally-irradiated cloth. Ph.D. Thesis, Massachusetts Institute of Technology, Feb. 1959.

APPENDIX C

SOLUTION OF EQUATIONS

NOMENCLATURE

Symbol	Definition and Dimensions
A_s	total skin surface area (ft^2)
A, B	constants in the polynomial approximation
C	vapor concentration (lb/ft^3)
c	specific heat (Btu/lb °F)
c_p	specific heat at constant pressure (Btu/lb °F)
D	vapor diffusion coefficient (ft^2/hr)
E	energy production rate due to exercising ($Btu/ft^3 hr$)
$g_1 - g_8$	functions
K	mass transfer coefficient (ft/hr)
$K_o; K_1; K_s$	mass transfer coefficient at fabric outer surface; fabric inner surface; and skin outer surface, respectively (ft/hr)
k	thermal conductivity (Btu/ft hr °F)
k_{s_o}	reference skin conductivity (Btu/ft hr °F)
L	thickness of fabric, air space, or skin-body system (ft)
L_1	skin layer thickness of the skin-body system (ft)
L_2	muscle layer thickness of the skin-body system (ft)
L_3	deep body core thickness of the skin-body system (ft)
M	dimensionless mass of absorbed water vapor
$\dot{m}$	mass flux ($lb/ft^2 hr$)
m_{avai}	mass of liquid available for evaporation at the skin surface (lb/ft^2)

Symbol	Definition and Dimensions
$N + 1$	number of nodes
Q	basal metabolism ($Btu/ft^3 hr$)
ΔQ_{shi}	increase in metabolism due to shivering ($Btu/ft^3 hr$)
r	relative humidity (dimensionless)
S	sweat generation rate ($lb/ft^2 hr$)
S_o	reference sweat generation rate ($lb/ft^2 hr$)
T	temperature (°F)
ΔT_B	deviation of the instantaneous average body temperature from its reference value (°F)
t	time (hr)
Δt	time increment (hr)
$\Delta t_{c_{i,j}}; \Delta t_{T_{i,j}}$	maximum allowable time increment for time t_i at fabric node j for the concentration and temperature equations, respectively (hr)
$\Delta t_{c_{a_i}}; \Delta t_{T_{a_i}}$	maximum allowable time increment for time t_i in the air gap for the concentration and temperature equations, respectively (hr)
u	arbitrary variable
U	heat transfer coefficient ($Btu/ft^2 hr\,°F$)
$U_o; U_1; U_s$	heat transfer coefficient at fabric outer surface; fabric inner surface; and skin outer surface, respectively ($Btu/ft^2 hr\,°F$)
$\dot{V}_1, \dot{V}_2$	total volumetric flow rate through the fabric and airspace, respectively (ft^3/hr)
x	coordinate (ft)
α	geometric (volumetric) porosity of the fabric (dimensionless)

Symbol	Definition and Dimensions
α_1, α_2	physiological conductivity constants (1/°F)
$\alpha_{m_1}, \alpha_{m_2}, \alpha_{m_3}$	control coefficients for shivering (Btu/ft^3 hr °F; Btu/ft^3 hr °F^2; Btu/ft^3 hr °F)
α_s	first power proportional control coefficient for sweating (lb/ft^2 hr °F)
γ	physiological conductivity constant (hr/°F)
δ	increment in spacial coordinate (see Figure C-1) (ft)
λ	heat of vaporization (Btu/lb)
λ_s	fourth power control coefficient for sweating (lb/ft^2 hr °F^4)
ρ	density (lb/ft^3)
σ	$(\partial M/\partial C)_T$ (ft^3/lb)
ω	$(\partial M/\partial T)_C$ (1/°F)

Subscripts

a	airspace
B	average body value
c	compressor
f	fabric
fi	fiber
i	time increment number
j	node number
ℓ	liquid
min	minimum

Subscripts	Definition and Dimensions
sat	saturation
s	skin-body system; sweat
v	vapor
∞	free stream

SOLUTION OF EQUATIONS

1. Explicit Finite Difference Equations

The nonlinear nature of the various governing equations developed previously precludes the possibility of obtaining analytical, closed form solutions for the temperature and vapor concentration distributions in the fabric-air gap-skin system. Consequently, numerical methods of solution must be resorted to as discussed in Reference C-1. Utilizing finite difference approximations for the various partial derivatives appearing in the governing equations, a series of algebraic relations may be developed which relate the value of any variable (say, u) at a time $t + \delta t$ to the value of the variable at time t.

The subscripts f and s shall not be employed at this time. It is to be understood that whenever a subscript is not indicated, the equation applies to either the fabric or skin portions. In general, if one divides a slab into N slices of equal thickness, the geometric representation shown in Figure C-1 arises. The first and second partial derivatives of a variable u with respect to x at any interior nodal point j (j = 1, 2, ... N) is approximated by passing a second order polynomial through the values of u at nodes j-1, j, and j+1. It should be noted that nodes 0 and 2 are not equidistant from node 1 and, therefore, it is to be expected that the finite difference representation for node 1 will differ somewhat from that determined for an interior node. A similar statement can be made for node N by symmetry considerations. Therefore, an interior node (j = 2, 3, ..., N-2, N-1) will first be considered. A second order polynomial can be expressed as:

$$u = u_j + Ax + Bx^2 \qquad (C\text{-}1)$$

where x represents the distance measured from node j (positive to the right). u_j represents the value of u at the j^{th} node (x = 0). A and B can

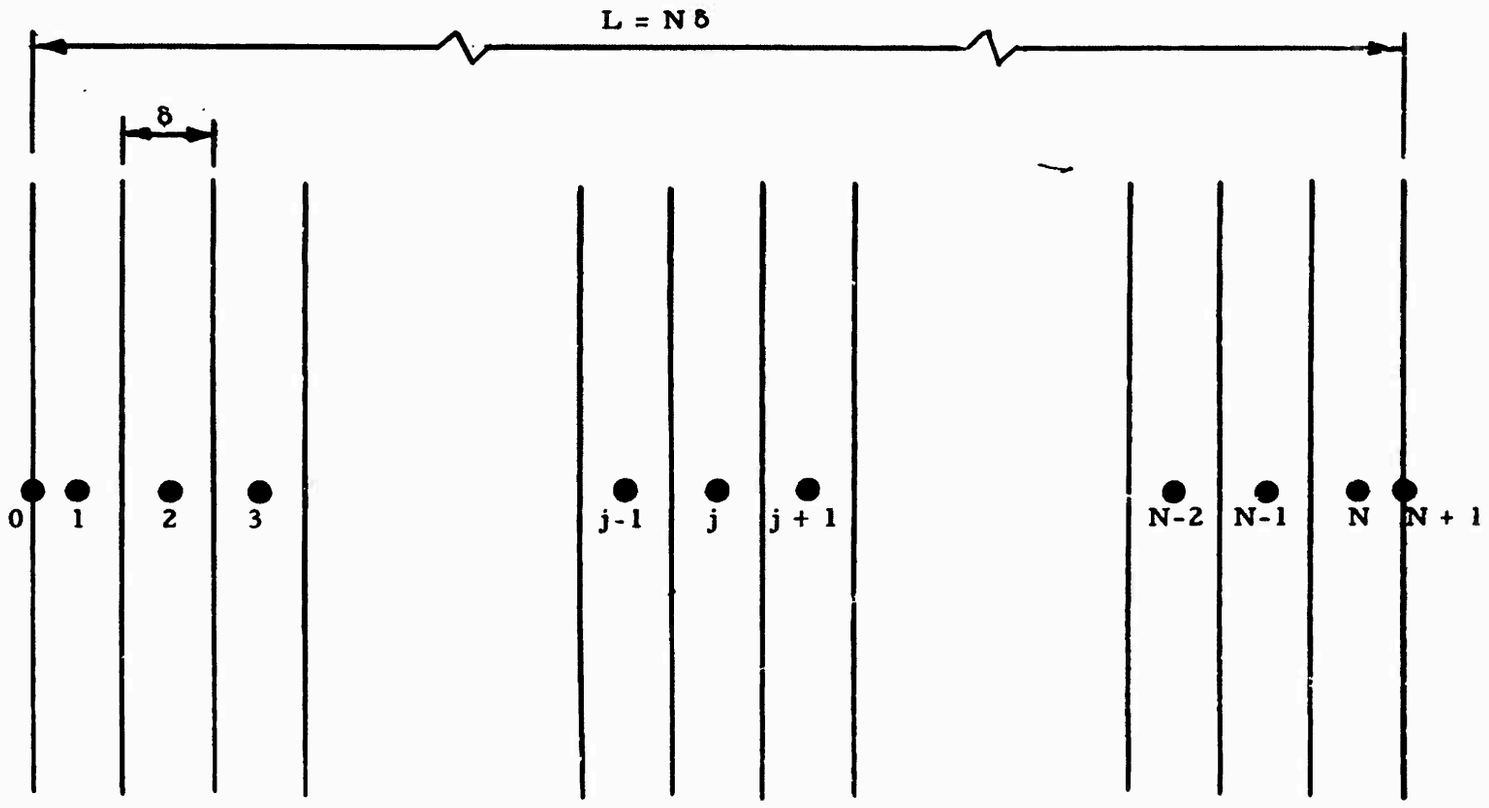

Figure C-1. Geometry and Nomenclature for an N-Slice Slab

be evaluated by noting that $u = u_{j+1}$ at $x = \delta$ and $u = u_{j-1}$ at $x = -\delta$. Utilizing these conditions, one may evaluate A and B to obtain:

$$A = \frac{u_{j+1} - u_{j-1}}{2\delta} \qquad B = \frac{u_{j+1} - 2u_j + u_{j-1}}{2\delta^2} \qquad \text{(C-2)}$$

The finite difference approximation for the first and second derivatives at node j can be expressed as:

$$\left(\frac{\partial u}{\partial x}\right)_j = \left(\frac{\partial u}{\partial x}\right)_{x=0} = A \qquad \text{(C-3)}$$

$$\left(\frac{\partial^2 u}{\partial x^2}\right)_j = \left(\frac{\partial^2 u}{\partial x^2}\right)_{x=0} = 2B$$

and therefore,

$$\left(\frac{\partial u}{\partial x}\right)_j = \frac{u_{j+1} - u_{j-1}}{2\delta}$$

$$\left(\frac{\partial^2 u}{\partial x^2}\right)_j = \frac{u_{j+1} - 2u_j + u_{j-1}}{\delta^2} \qquad \text{for } j = 2, 3, \ldots\ldots N-2, N-1. \qquad \text{(C-4)}$$

Using the same type of analysis, one can evaluate

$$\left(\frac{\partial u}{\partial x}\right)_1, \left(\frac{\partial^2 u}{\partial x^2}\right)_1, \text{ and } \left(\frac{\partial u}{\partial x}\right)_o \text{ to be:}$$

$$\left(\frac{\partial u}{\partial x}\right)_1 = \frac{u_2 - 4u_o + 3u_1}{3\delta}$$

$$\left(\frac{\partial^2 u}{\partial x^2}\right)_1 = \frac{u_2 - 3u_1 + 2u_o}{\frac{3}{4}\delta^2} \qquad \text{(C-5)}$$

$$\left(\frac{\partial u}{\partial x}\right)_o = \frac{9u_1 - 8u_o - u_2}{3\delta}$$

Similar methods yield, for the N^{th} node:

$$\left(\frac{\partial u}{\partial x}\right)_N = \frac{4u_{N+1} - 3u_N - u_{N-1}}{3\delta}$$

$$\left(\frac{\partial^2 u}{\partial x^2}\right)_N = \frac{2u_{N+1} - 3u_N + u_{N-1}}{\frac{3}{4}\delta^2} \qquad \text{(C-6)}$$

$$\left(\frac{\partial u}{\partial x}\right)_{N+1} = \frac{8u_{N+1} - 9u_N + u_{N-1}}{3\delta}$$

The finite difference representation for the N^{th} node in the skin structure can be simplified by introducing the boundary condition $\left(\frac{\partial u}{\partial x}\right)_{N+1} = 0$. With this relation, one obtains for the N^{th} node:

$$\left(\frac{\partial u}{\partial x}\right)_N = \frac{u_N - u_{N-1}}{2\delta}$$

$$\left(\frac{\partial^2 u}{\partial x^2}\right)_N = -\frac{u_N - u_{N-1}}{\delta^2}$$

and $u_{N+1} = u_N + \frac{1}{\delta}(u_N - u_{N-1})$.

All the preceding relations can now be utilized in the appropriate differential equations and boundary conditions. In the following finite difference equations, the subscript i refers to the number of the time increment and the subscript j refers to the number of the nodal point. To develop these equations, we have evaluated all spacial derivatives and functions (i.e., ω, σ, M) at a time t_i, that is, at the beginning of the time increment.

For the fabric, one obtains:

Node 1

$$\left[1 + \frac{1-\alpha}{\alpha}\rho_{fi}\sigma_{i,j}\right]\left[\frac{C_{f_{i+1,1}} - C_{f_{i,1}}}{\Delta t_i}\right] - \left(\frac{1-\alpha}{\alpha}\right)\rho_{fi}\omega_{i,j}\left[\frac{T_{f_{i+1,1}} - T_{f_{i,1}}}{\Delta t_i}\right]$$

$$= \frac{4D}{3\delta_f^2}\left[C_{f_{i,2}} - 3C_{f_{i,1}} + 2C_{f_{i,o}}\right] + \frac{\dot{V}_1}{3\alpha A_s \delta_f}\left[C_{f_{i,2}} - 4C_{f_{i,o}} + 3C_{f_{i,1}}\right] \quad (C\text{-}8)$$

and

$$\left(\frac{1-\alpha}{\alpha}\right)\rho_{fi}\left[c_{fi} + c_\ell M_{i,1} + \lambda\omega_{i,1}\right]\left[\frac{T_{f_{i+1,1}} - T_{f_{i,1}}}{\Delta t_i}\right] - \left(\frac{1-\alpha}{\alpha}\right)\rho_{fi}\lambda\sigma_{i,1} \cdot \left[\frac{C_{f_{i+1,1}} - C_{f_{i,1}}}{\Delta t_i}\right]$$

$$= \frac{\dot{V}_1}{3\alpha A_s \delta_f}\left[c_{p_v} C_{f_{i,1}} + c_{p_{air}}\rho_{air}\right]\left[T_{f_{i,2}} - 4T_{f_{i,o}} + 3T_{f_{i,1}}\right] \quad (C\text{-}9)$$

$$+ \frac{4}{3\alpha\delta_f^2} k_{f_{i,1}}\left[T_{f_{i,2}} - 3T_{f_{i,1}} + 2T_{f_{i,o}}\right]$$

$$+ \frac{1}{9\alpha\delta_f^2}\left[\frac{dk_f}{dM}\right]_{i,1}\left[T_{f_{i,2}} - 4T_{f_{i,o}} + 3T_{f_{i,1}}\right]\left\{\sigma_{i,1}\left[C_{f_{i,2}} - 4C_{f_{i,o}} + 3C_{f_{i,1}}\right] - \omega_{i,1}\left[T_{f_{i,2}} - 4T_{f_{i,o}} + 3T_{f_{i,1}}\right]\right\}$$

Interior Nodes ($j = 2, 3, \ldots\ldots N_f - 2, N_f - 1$)

$$\left[1 + \left(\frac{1-\alpha}{\alpha}\right)\rho_{fi,i,j}\sigma_{i,j}\right]\left[\frac{C_{f_{i+1,j}} - C_{f_{i,j}}}{\Delta t_i}\right] - \left(\frac{1-\alpha}{\alpha}\right)\rho_{fi}\omega_{i,j}\left[\frac{T_{f_{i+1,j}} - T_{f_{i,j}}}{\Delta t_i}\right]$$

$$= \frac{D}{\varepsilon_f^2}\left[C_{f_{i,j-1}} - 2C_{f_{i,j}} + C_{f_{i,j+1}}\right] + \frac{\dot{V}_1}{2\alpha A_s \delta_f}\left[C_{f_{i,j+1}} - C_{f_{i,j-1}}\right] \qquad \text{(C-10)}$$

and

$$\left(\frac{1-\alpha}{\alpha}\right)\rho_{fi,i}\left[c_{fi,} + c_\ell M_{i,j} + \lambda\omega_{i,j}\right]\left[\frac{T_{f_{i+1,j}} - T_{f_{i,j}}}{\Delta t_i}\right] - \left(\frac{1-\alpha}{\alpha}\right)\rho_{fi}\lambda\sigma_{i,j}$$

$$\cdot\left[\frac{C_{f_{i+1,j}} - C_{f_{i,j}}}{\Delta t_i}\right]$$

$$= \frac{\dot{V}_1}{2\alpha A_s \delta_f}\left[c_{p_v} C_{f_{i,j}} + c_{p_{air}}\rho_{air}\right]\left[T_{f_{i,j+1}} - T_{f_{i,j-1}}\right] \qquad \text{(C-11)}$$

$$+ \frac{1}{\alpha\delta_f^2} k_{f_{i,j}}\left[T_{f_{i,j+1}} - 2T_{f_{i,j}} + T_{f_{i,j-1}}\right]$$

$$+ \frac{1}{4\alpha\delta_f^2}\left[\frac{dk_f}{dM}\right]_{i,j}\left[T_{f_{i,j+1}} - T_{f_{i,j-1}}\right]\left\{\sigma_{i,j}\left[C_{f_{i,j+1}} - C_{f_{i,j-1}}\right]\right.$$

$$\left. - \omega_{i,j}\left[T_{fi,j+1} - T_{fi,j-1}\right]\right\}$$

Node N_f

$$\left[1 + \left(\frac{1-\alpha}{\alpha}\right) \rho_{fi}\, \sigma_{i,N_f}\right]\left[\frac{C_{f_{i+1,N_f}} - C_{f_{i,N_f}}}{\Delta t_i}\right] - \left(\frac{1-\alpha}{\alpha}\right)\rho_{fi}\omega_{i,N_f}\left[\frac{T_{f_{i+1,N_f}} - T_{f_{i,N_f}}}{\Delta t_i}\right]$$

$$= \frac{4D}{3\delta_f^2}\left[2C_{f_{i,N_f+1}} - 3C_{f_{i,N_f}} + C_{f_{i,N_f-1}}\right] + \frac{\dot{V}_1}{3\alpha A_s \delta_f}\left[4C_{f_{i,N_f+1}} - 3C_{f_{i,N_f}} - C_{f_{i,N_f-1}}\right] \quad \text{(C-12)}$$

and:

$$\left(\frac{1-\alpha}{\alpha}\right)\rho_{fi}\left[c_{fi} + c_\ell M_{i,N_f} + \lambda\omega_{i,N_f}\right]\left[\frac{T_{f_{i+1,N_f}} - T_{f_{i,N_f}}}{\Delta t_i}\right] - \left(\frac{1-\alpha}{\alpha}\right)\rho_{fi}\lambda\sigma_{i,N_f}$$

$$\cdot\left[\frac{C_{f_{i+1,N_f}} - C_{f_{i,N_f}}}{\Delta t_i}\right]$$

$$= \frac{\dot{V}_1}{3\alpha A_s \delta_f}\left[c_{p_v} C_{f_{i,N_f}} + c_{p_{air}}\rho_{air}\right]\left[4T_{f_{i,N_f+1}} - 3T_{f_{i,N_f}} - T_{f_{i,N_f-1}}\right] \quad \text{(C-13)}$$

$$+ \frac{4k_{f_{i,N_f}}}{3\alpha\delta_f^2}\left[2T_{f_{i,N_f+1}} - 3T_{f_{i,N_f}} + T_{f_{i,N_f-1}}\right]$$

$$+ \frac{1}{9\alpha\delta_f^2}\left[\frac{dk_f}{dM}\right]_{i,N_f}\left[4T_{f_{i,N_f+1}} - 3T_{f_{i,N_f}} - T_{f_{i,N_f-1}}\right]\left\{\sigma_{i,N_f}\left[4C_{f_{i,N_f+1}}\right.\right.$$

$$\left.\left. - 3C_{f_{i,N_f}} - C_{f_{i,N_f-1}}\right] - \omega_{i,N_f}\left[4T_{f_{i,N_f+1}} - 3T_{f_{i,N_f}} - T_{f_{i,N_f-1}}\right]\right\}$$

For the air gap, one obtains:

$$\frac{C_{a_{i+1}} - C_{a_i}}{\Delta t_i} = \frac{1}{L_a}\left[\dot{m}_{s_i} + K_1 (C_{f_{i,N_f+1}} - C_{a_i}) + \frac{\dot{V}_1}{A_s}(C_c - C_{f_{i,N_f+1}}\right.$$

$$\left. + \frac{\dot{V}_2}{A_s}(C_c - C_{a_i})\right] \qquad \text{(C-14)}$$

and:

$$\frac{T_{a_{i+1}} - T_{a_i}}{\Delta t_i} = \frac{1}{L_a (C_{a_i} c_{p_v} + \rho_{air} c_{p_{air}})}\left\{U_s (T_{s_{i,o}} - T_{a_i}) + U_1 (T_{f_{i,N_f+1}} - T_{a_i})\right.$$

$$+ \frac{\dot{V}_1 c_{p_v}}{A_s}\left[C_c (T_c - T_{a_i}) - C_{f_{i,N_f+1}} (T_{f_{i,N_f+1}} - T_{a_i})\right]$$

$$+ \frac{\dot{V}_2 c_{p_v}}{A_s} C_c (T_c - T_{a_i}) \qquad \text{(C-15)}$$

$$\left. + \rho_{air} c_{p_{air}}\left[\frac{\dot{V}_1}{A_s}(T_c - T_{f_{i,N_f+1}}) + \frac{\dot{V}_2}{A_s}(T_c - T_{a_i})\right]\right\}$$

As in Reference C-1, $N_s = 7$ (seven internal nodes) will, at this point be chosen. Thus, the finite difference equations for the skin can be summarized as:

Node 1

$$(c\rho)_s \left[\frac{T_{s_{i+1,1}} - T_{s_{i,1}}}{\Delta t_i} \right] = k_{s_i} \frac{4}{3\delta_s^2} \left[T_{s_{i,2}} - 3T_{s_{i,1}} + 2T_{s_{i,o}} \right] \quad \text{(C-16)}$$

Nodes 2 and 3 (j = 2, 3)

$$(c\rho)_s \left[\frac{T_{s_{i+1,j}} - T_{s_{i,j}}}{\Delta t_i} \right] = \frac{k_{s_i}}{\delta_s^2} \left[T_{s_{i,j+1}} - 2T_{s_{i,j}} + T_{s_{i,j-1}} \right] + Q' \quad \text{(C-17)}$$

where $Q' = E$ for $\Delta T_{B_i} > 0$

$$= E - \alpha_{m_1} \Delta T_{B_i} + \alpha_{m_2} \Delta T_{B_i}^2 \text{ for } -1.8°F \leq \Delta T_{B_i} \leq 0$$

$$= E + 1.77214 \times 10^{-2} - \alpha_{m_3} (1.8 + \Delta T_{B_i}) \text{ for } \Delta T_{B_i} < -1.8°F.$$

Nodes 4, 5, and 6 (j = 4, 5, 6)

$$(c\rho)_s \left[\frac{T_{s_{i+1,j}} - T_{s_{i,j}}}{\Delta t_i} \right] = \frac{k_{s_i}}{\delta_s^2} \left[T_{s_{i,j+1}} - 2T_{s_{i,j}} + T_{s_{i,j-1}} \right] + Q. \quad \text{(C-18)}$$

Node 7

$$(c\rho)_s \left[\frac{T_{s_{i+1,7}} - T_{s_{i,7}}}{\Delta t_i} \right] = \frac{k_{s_i}}{\delta_s^2} \left[T_{s_{i,6}} - T_{s_{i,7}} \right] + Q. \quad \text{(C-19)}$$

Node 8

$$T_{s_{i+1,8}} = T_{s_{i+1,7}} + \frac{1}{8}\,(T_{s_{i+1,7}} - T_{s_{i+1,6}}). \qquad \text{(C-20)}$$

Several of the auxiliary functions appearing in the preceding equations are listed below.

As shown in Appendix B, the functions σ, μ, M, k_f, and $\frac{dk_f}{dM}$ are functions of the local relative humidity (r) and temperature (T). With $T_{f_{i,j}}$ known, one may determine $C_{sat_{i,j}}$ and thus evaluate $r_{i,j} = C_{fi,j}/C_{sat_{i,j}}$. The five functions listed above can then be evaluated for each fabric node and inserted in the appropriate places in the finite difference equations.

The moisture available for evaporation can be expressed as:

$$m_{avai_i} = m_{avai_{i-1}} + (S_{i-1} - \dot{m}_{s_{i-1}})\,\Delta t_{i-1} \qquad \text{(C-21)}$$

Since all quantities appearing in this relation were computed in the last time interval, one can calculate m_{avai_i} and then determine $\dot{m}_{s_i}$ from:

$$\dot{m}_{s_i} = K_s\,(C_{s_i} - C_{a_i}) \text{ when } m_{avai_i} > 0 \qquad \text{(C-22)}$$

$$= \min\left[S_i, K_s\,(C_{s_i} - C_{a_i})\right] \text{ when } m_{avai_i} \leq 0.$$

Using a trapezoidal integral approximation, the average body temperature is given by:

$$T_{B_i} = \frac{\delta_s}{L_s}\left[\frac{1}{4}\,T_{s_{i,o}} + \frac{3}{4}\,T_{s_{i,1}} + T_{s_{i,2}} + T_{s_{i,3}} + T_{s_{i,4}} + T_{s_{i,5}} + T_{s_{i,6}} + \frac{3}{4}\,T_{s_{i,7}} + \frac{1}{4}\,T_{s_{i,8}}\right] \qquad \text{(C-23)}$$

and ΔT_{B_i} by:

$$\Delta T_{B_i} = T_{B_i} - 96.35\ (°F). \tag{C-24}$$

Thus, S_i is given by:

$$S_i = \min \left[S_o + \alpha_s \Delta T_{B_i} + \lambda_s \Delta T_{B_i}^{\ 4};\ 60\ S_o \right] \text{for } \Delta T_{B_i} > 0 \tag{C-25}$$

$$= S_o \text{ for } \Delta T_{B_i} \leq 0.$$

The time rate of change of body temperature may be evaluated from:

$$\left[\frac{dT_B}{dt}\right]_i = \frac{L_2 (E + \Delta Q_{shi_i}) + L_3 Q - U_s (T_{s_{i,o}} - T_{a_i}) - \lambda \dot{m}_{s_i}}{(c\rho)_s L_s} \tag{C-26}$$

where $\Delta Q_{shi_i} = 0$ for $\Delta T_{B_i} > 0$ (C-27)

$$= -\alpha_{m_1} \Delta T_{B_i} + \alpha_{m_2} \Delta T_{B_i}^{\ 2} \text{ for } -1.8°F \leq T_{B_i} \leq 0$$

$$= 1.77214 \times 10^{-2} - \alpha_{m_3} (1.8 + \Delta T_{B_i}) \text{ for } \Delta T_{B_i} < -1.8°F.$$

With $\left(\frac{dT_B}{dt}\right)_i$ known, one can determine k_{s_i} from:

$$k_{s_i} = k_{s_o} \left[1 + \alpha_1 \Delta T_{B_i} + \gamma \left(\frac{dT_B}{dt}\right)_i \right] \text{for } \Delta T_{B_i} > 0$$

$$= k_{s_o} \left[1 + \alpha_2 \Delta T_{B_i} + \gamma \left(\frac{dT_B}{dt}\right)_i \right] \text{for } \Delta T_{B_i} \leq 0 \tag{C-28}$$

subject to the condition:

$$0.55\, k_{s_o} \leq k_{s_i} \leq 1.7\, k_{s_o}. \qquad \text{(C-2..}$$

Thus, one sees that the value of the local temperature and vapor concentration at the interior fabric nodes and air gap, as well as the temperature distribution at the interior skin nodes, at a time t_i, can be determined if the temperature and concentration distribution are known at the preceding time increment. The new temperature and concentration values at the surface nodes can then be determined by using the surface boundary conditions.

The boundary condition at the fabric outer surface (Node 0) can be expressed in finite difference form as:

$$C_{f_{i+1,0}} = \frac{\frac{\alpha D}{3\delta_f}\left[9\,C_{f_{i+1,1}} - C_{f_{i+1,2}}\right] + K_o C_\infty}{K_o + \frac{8\alpha D}{3\delta_f}} \qquad \text{(C-30)}$$

and:

$$T_{f_{i+1,o}} = \frac{\left[\frac{9T_{f_{i+1,1}} - T_{f_{i+1,2}}}{3\delta_f}\right] + \frac{U_o T_\infty}{k_{f_{i+1,o}}}}{\frac{8}{3\delta_f} + \frac{U_o}{k_{f_{i+1,o}}}}. \qquad \text{(C-31)}$$

All quantities appearing on the right side of the first equation have been evaluated and therefore, $C_{f_{i+1,o}}$ is known. The solution of the second equation for $T_{f_{i+1,o}}$ is not as easy since $k_{f_{i+1,o}}$ depends upon $T_{f_{i+1,o}}$. Thus, an iteration process is required and has been incorporated within the computer program.

Similarly, the boundary condition at the fabric inner surface (Node $N_f + 1$) provides the following relations:

$$C_{f_{i+1,N_f+1}} = \frac{\frac{\alpha D}{3\delta_f}\left[9C_{f_{i+1,N_f}} - C_{f_{i+1,N_f-1}}\right] + K_1 C_{a_{i+1}}}{\frac{8\alpha D}{3_f} + K_1} \qquad \text{(C-32)}$$

and:

$$T_{f_{i+1,N_f+1}} = \frac{\left[\frac{9\,T_{f_{i+1,N_f}} - T_{f_{i+1,N_f-1}}}{3\delta_f}\right] + \frac{U_1 T_{a_{i+1}}}{k_{f_{i+1,N_f+1}}}}{\frac{8}{3\delta_f} + \frac{U_1}{k_{f_{i+1,N_f+1}}}} \qquad \text{(C-33)}$$

and a similar iteration process is required to determine $T_{f_{i+1,N_f+1}}$

The boundary condition at the skin outer surface can be expressed as:

$$T_{s_{i+1,o}} = \frac{\frac{T_{s_{i+1,2}} + 3\,T_{s_{i+1,1}}}{3\delta_s} k_{s_{i+1}} + U_s T_{a_{i+1}} - \lambda \dot{m}_{s_{i+1}}}{U_s + \frac{4k_{s_{i+1}}}{3\delta_s}}. \qquad \text{(C-34)}$$

Since $k_{s_{i+1}}$ depends upon $T_{s_{i+1,o}}$ (as well as the known values of $T_{s_{i+1,j}}$; j = 1 - 8) and $\dot{m}_{s_{i+1}}$ depends upon $T_{s_{i+1,o}}$ (through the dependence of C_{sat} upon T), we see once again that an iteration process is required to evaluate $T_{s_{i+1,o}}$.

2. Stability Criteria

The finite difference equations for problems which possess constant property values lead to a well-known stability criteria which restricts the magnitude of the time and spacial increments through the relation:

$$\overline{M} = \frac{c\rho}{k} \frac{\delta^2}{\Delta t} \geq 2$$

at interior node points. The factor "2" changes for Nodes 1 and N_f but is constant for all time.

In our problem, the various coefficients vary with time and this leads to a stability criteria in which the limiting value of the stabilisty modulus ($\overline{M}$) varies both with time and spatial coordinate. A brief discussion on the applicable criteria will now be given.

Two equations for each fabric node have been developed in the preceding section which may be expressed symbolically as:

$$A_1\left[\frac{C_{f_{i+1,j}} - C_{f_{i,j}}}{\Delta t_i}\right] - A_2\left[\frac{T_{f_{i+1,j}} - T_{f_{i,j}}}{\Delta t_i}\right] = A_3\left[\frac{\partial C_f}{\partial x}\right]_{i,j} + A_4\left[\frac{\partial^2 C_f}{\partial x^2}\right]_{i,j} \quad \text{(C-35)}$$

and:

$$B_1\left[\frac{T_{f_{i+1,j}} - T_{f_{i,j}}}{\Delta t_i}\right] - B_2\left[\frac{C_{f_{i+1,j}} - C_{f_{i,j}}}{\Delta t_i}\right] \quad \text{(C-36)}$$

$$= B_3\left[\frac{\partial T_f}{\partial x}\right]_{i,j} + B_4\left[\frac{\partial^2 T_f}{\partial x^2}\right]_{i,j} + B_5\left[\frac{\partial T_f}{\partial x_f}\right]_{i,j}\left[\frac{\partial C_f}{\partial x_f}\right]_{i,j} - B_6\left[\frac{\partial T_f}{\partial x_f}\right]^2_{i,j}.$$

The coefficients A_1 - A_4 and B_1 - B_6 depend upon the various values of T_{f_j} and C_{f_j} at the preceding time increment. One may solve these two equations to obtain:

$$(A_1B_1 - A_2B_2)\left[\frac{C_{f_{i+1,j}} - C_{f_{i,j}}}{\Delta t_i}\right] = A_3B_1\left[\frac{\partial C_f}{\partial x}\right]_{i,j} + A_4B_1\left[\frac{\partial^2 C_f}{\partial x^2}\right]_{i,j}$$

$$+ A_2B_3\left[\frac{\partial T_f}{\partial x}\right]_{i,j} + A_2B_4\left[\frac{\partial^2 T_f}{\partial x^2}\right]_{i,j} \qquad (A)$$

$$+ A_2B_5\left[\frac{\partial T_f}{\partial x}\right]_{i,j}\left[\frac{\partial C_f}{\partial x}\right]_{i,j} - A_2B_6\left[\frac{\partial T_f}{\partial x}\right]^2_{i,j}$$

and:

$$(A_1B_1 - A_2B_2)\left[\frac{T_{f_{i+1,j}} - T_{f_{i,j}}}{\Delta t_i}\right] = A_1B_3\left[\frac{\partial T_f}{\partial x}\right]_{i,j} + A_1B_4\left[\frac{\partial^2 T_f}{\partial x^2}\right]_{i,j}$$

$$+ A_1B_5\left[\frac{\partial T_f}{\partial x}\right]_{i,j}\left[\frac{\partial C_f}{\partial x}\right]_{i,j} - A_1B_6\left[\frac{\partial T_f}{\partial x}\right]^2_{i,j} \qquad (B)$$

$$+ A_3B_2\left[\frac{\partial C_f}{\partial x}\right]_{i,j} + A_4B_2\left[\frac{\partial^2 C_f}{\partial x^2}\right]_{i,j} .$$

We shall only consider the first equation here since the same process is used for the second relation. If one introduces the finite difference forms into the right side of the equation and regroups terms, the following expression is obtained:

$$(A_1B_1 - A_2B_3)\frac{C_{f_{i+1,j}}}{\Delta t_i} = \left[\frac{A_1B_1 - A_2B_2}{\Delta t_i} - \phi\right] C_{f_{i,j}} + \theta. \quad \text{(C-37)}$$

ϕ represents all coefficients of $C_{f_{i,j}}$ which appeared on the right side of Equation (A) while θ represents the balance of the terms (not containing a factor $C_{f_{i,j}}$). The stability criteria for Equation (A) is found by requiring the coefficient of $C_{f_{i,j}}$ to be positive.[C-1] Thus, one finds

$$\frac{A_1B_1 - A_2B_2}{\Delta t_i} - \phi > 0$$

or:

$$\Delta t_i < \frac{\phi}{A_1B_1 - A_2B_2} . \quad \text{(C-38)}$$

We define the maximum allowable time increment for the j^{th} node concentration equation as:

$$\Delta t_{c_{i,j}} = \frac{\phi_{i,j}}{(A_1B_1 - A_2B_2)_{i,j}} \quad \text{(C-39)}$$

where the subscript c indicates the concentration equation evaluated at t_i and at the j^{th} node. One may then write:

$$\Delta t_i < \Delta t_{c_{i,j}} . \quad \text{(C-40)}$$

Similarly, from Equation (B), one may calculate a $\Delta t_{T_{i,j}}$ with the condition:

$$\Delta t_i < \Delta t_{T_{i,j}} . \qquad \text{(C-41)}$$

Repeating this process for each interior fabric node, various values for $\Delta t_{c_{i,j}}$ and $\Delta t_{T_{i,j}}$ (T refers to the temperature equation) may be determined.

Using the same approach, one may also determine values of $\Delta t_{c_{a_i}}$ and $\Delta t_{T_{a_i}}$ from the air gap equations for concentration (C) and temperature (T), respectively. Analysis of the interior skin node equations for stability indicates that, for all reasonable systems, the minimum allowable time increment in the skin is at least a hundred times larger than that determined for the fabric and air gap.

Since Δt_i must be chosen such that it is less than each of the two computed Δt's at each node, the stability criteria for the entire fabric-air gap-skin system can be satisfied by choosing Δt_i such that:

$$\Delta t_i < \underset{j=1-N_f}{\text{minimum}} \left[\text{all positive } (\Delta t_{c_{i,j}}, \Delta t_{T_{i,j}}, \Delta t_{c_{a_i}}, \Delta t_{T_{a_i}}) \right] . \qquad \text{(C-42)}$$

The various critical values of the Δt's are tabulated below:

for $j = 1$

$$\Delta t_{c_{i,1}} = \frac{g_1(i,1)}{\frac{4}{\delta_f^2} g_2(i,1) - \frac{1}{\delta_f} g_3(i,1) - \frac{(T_{f_{i,2}} - 4T_{f_{i,o}} + 3T_{f_{i,1}})}{3\delta_f^2} g_4(i,1)} \qquad \text{(C-43)}$$

$$\Delta t_{T_{i,1}} = \frac{g_1(i,1)}{\frac{4}{\delta_f^2} g_5(i,1) - \frac{1}{\delta_f} g_6(i,1) - \frac{(C_{f_{i,2}} - 4C_{f_{i,o}} + 3C_{f_{i,1}})}{3\delta_f^2} g_7(i,1) + \frac{(3T_{f_{i,1}} + 2T_{f_{i,2}} - 8T_{f_{i,o}})}{3\delta_f^2} g_8(i,1)} \qquad \text{(C-44)}$$

for $j = 2, 3, \ldots\ldots N_f - 1$

$$\Delta t_{c_{i,j}} = \frac{\delta_f^2}{2} \frac{g_1(i,j)}{g_2(i,j)} \qquad \text{(C-45)}$$

$$\Delta t_{T_{i,j}} = \frac{\delta_f^2}{2} \frac{g_1(i,j)}{g_5(i,j)} \qquad \text{(C-46)}$$

for $j = N_f$

$$\Delta t_{c_{i,N_f}} = \frac{g_1(i,N_f)}{\frac{4}{\delta_f^2} g_2(i,N_f) + \frac{1}{\delta_f} g_3(i,N_f) + \frac{(4T_{f_{i,N_f+1}} - 3T_{f_{i,N_f}} - T_{f_{i,N_f-1}})}{3\delta_f^2} g_4(i,N_f)} \qquad \text{(C-47)}$$

$$\Delta t_{T_{i,N_f}} = \frac{g_1(i,N_f)}{\frac{4}{\delta_f^2} g_5(i,N_f) + \frac{1}{\delta_f} g_6(i,N_f) + \frac{(4C_{f_{i,N_f+1}} - 3C_{f_{i,N_f}} - C_{f_{i,N_f-1}})}{3\delta_f^2} g_7(i,N_f) + \frac{(3T_{f_{i,N_f}} - 2T_{f_{i,N_f-1}} - 8T_{f_{i,N_f+1}})}{3\delta_f^2} g_8(i,N_f)} \qquad \text{(C-48)}$$

and for the air gap:

$$\Delta t_{c_{a_i}} = \frac{L_a}{K_1 + K_s + \frac{\dot{V}_2}{A_s}} \quad \text{when } \dot{m}_{s_i} \text{ is given by } K_s(C_{s_i} - C_{a_i}) \qquad \text{(C-49)}$$

$$= \frac{L_a}{K_1 + \frac{\dot{V}_2}{A_s}} \quad \text{when } \dot{m}_{s_i} \text{ is given by } S_i$$

$$\Delta t_{T_{a_i}} = \frac{(c_{p_v} C_{a_i} + c_{p_{air}} \rho_{air}) L_a}{U_l + U_s + \frac{\dot{V}_1 + \dot{V}_2}{A_s} c_{p_v} C_c + \frac{\dot{V}_2}{A_s} c_{p_{air}} \rho_{air} - \frac{\dot{V}_1}{A_s} c_{p_v} C_{f_{i,N_f+1}}} \quad \text{(C-50)}$$

The various functions (g's) are given by:

$$g_1(i,j) = \left[1 + \left(\frac{1-\alpha}{\alpha}\right) \rho_{fi} \sigma_{i,j}\right]\left(\frac{1-\alpha}{\alpha}\right) \rho_{fi} (c_{fi} + c_\ell M_{i,j}) + \left(\frac{1-\alpha}{\alpha}\right) \rho_{fi} \lambda \omega_{i,j} \quad \text{(C-51)}$$

$$g_2(i,j) = D\left(\frac{1-\alpha}{\alpha}\right) \rho_{fi} \left[c_{fi} + c_\ell M_{i,j} + \lambda \omega_{i,j}\right] \quad \text{(C-52)}$$

$$g_3(i,j) = \frac{\dot{V}_1}{\alpha A_s} \left(\frac{1-\alpha}{\alpha}\right) \rho_{fi} \left[c_{fi} + c_\ell M_{i,j} + \lambda \omega_{i,j}\right] \quad \text{(C-53)}$$

$$g_4(i,j) = \left(\frac{1-\alpha}{\alpha}\right) \rho_{fi} \omega_{i,j} \sigma_{i,j} \frac{1}{\alpha} \left[\frac{dk_f}{dM}\right]_{i,j} \quad \text{(C-54)}$$

$$g_5(i,j) = \frac{k_{f_{i,j}}}{\alpha} \left[1 + \left(\frac{1-\alpha}{\alpha}\right) \rho_{fi} \sigma_{i,j}\right] \quad \text{(C-55)}$$

$$g_6(i,j) = \frac{\dot{V}_1}{\alpha A_s} \left[1 + \left(\frac{1-\alpha}{\alpha}\right) \rho_{fi} \sigma_{i,j}\right] \left[c_{p_v} C_{f_{i,j}} + c_{p_{air}} \rho_{air}\right] \quad \text{(C-56)}$$

$$g_7(i,j) = \frac{\sigma_{i,j}}{\alpha} \left[1 + \left(\frac{1-\alpha}{\alpha}\right) \rho_{fi} \sigma_{i,j}\right] \left[\frac{dk_f}{dM}\right]_{i,j} \quad \text{(C-57)}$$

$$g_8(i,j) = \frac{\omega_{i,j}}{\alpha} \left[1 + \left(\frac{1-\alpha}{\alpha}\right) \rho_{fi} \sigma_{i,j}\right] \left[\frac{dk_f}{dM}\right]_{i,j} \quad \text{(C-58)}$$

3. Estimation of Δt_i

By examining the various relations for the Δt's for the fabric, it is found, through an order of magnitude analysis, that the dominating term in the denominator for $\Delta t_{c_{i,1}}$ and $\Delta t_{c_{i,N_f}}$ is the term containing g_2. Similarly, it is found, for $\Delta t_{T_{i,1}}$ and $\Delta t_{T_{i,N_f}}$, the dominating term to be g_5. Thus, the following approximation may be made:

$$\left.\begin{aligned} \Delta t_{c_{i,j}} &\approx \frac{\delta_f^2}{4}\,\frac{g_1(i,j)}{g_2(i,j)} \\ \Delta t_{T_{i,j}} &\approx \frac{\delta_f^2}{4}\,\frac{g_1(i,j)}{g_5(i,j)} \end{aligned}\right\} \quad \text{and} \quad \begin{matrix} j = 1 \\ j = N_f \end{matrix} \qquad \text{(C-59)}$$

$$\left.\begin{aligned} \Delta t_{c_{i,j}} &= \frac{\delta_f^2}{2}\,\frac{g_1(i,j)}{g_2(i,j)} \\ \Delta t_{T_{i,j}} &= \frac{\delta_f^2}{2}\,\frac{g_1(i,j)}{g_5(i,j)} \end{aligned}\right\} \quad j = 2, 3, \ldots\ldots N_f - 1 \qquad \text{(C-60)}$$

Comparing the first two equations with the last two, it can be seen that the minimum allowable time increment (for most practical fabric systems) is determined by fabric nodes 1 or N_f. Using the cotton fabric parameters listed in Appendix B, Figure C-2 has been prepared. This figure shows the variation of $\frac{1}{4}\ g_1/g_2$ and $\frac{1}{4}\ g_1/g_5$ with r, considering the fabric porosity and temperature as parameters. The ratio g_1/g_5 was found to vary only slightly with temperature and, therefore, only a single curve is shown for each α which approximates the function for both T = 60 and T = 100°F.

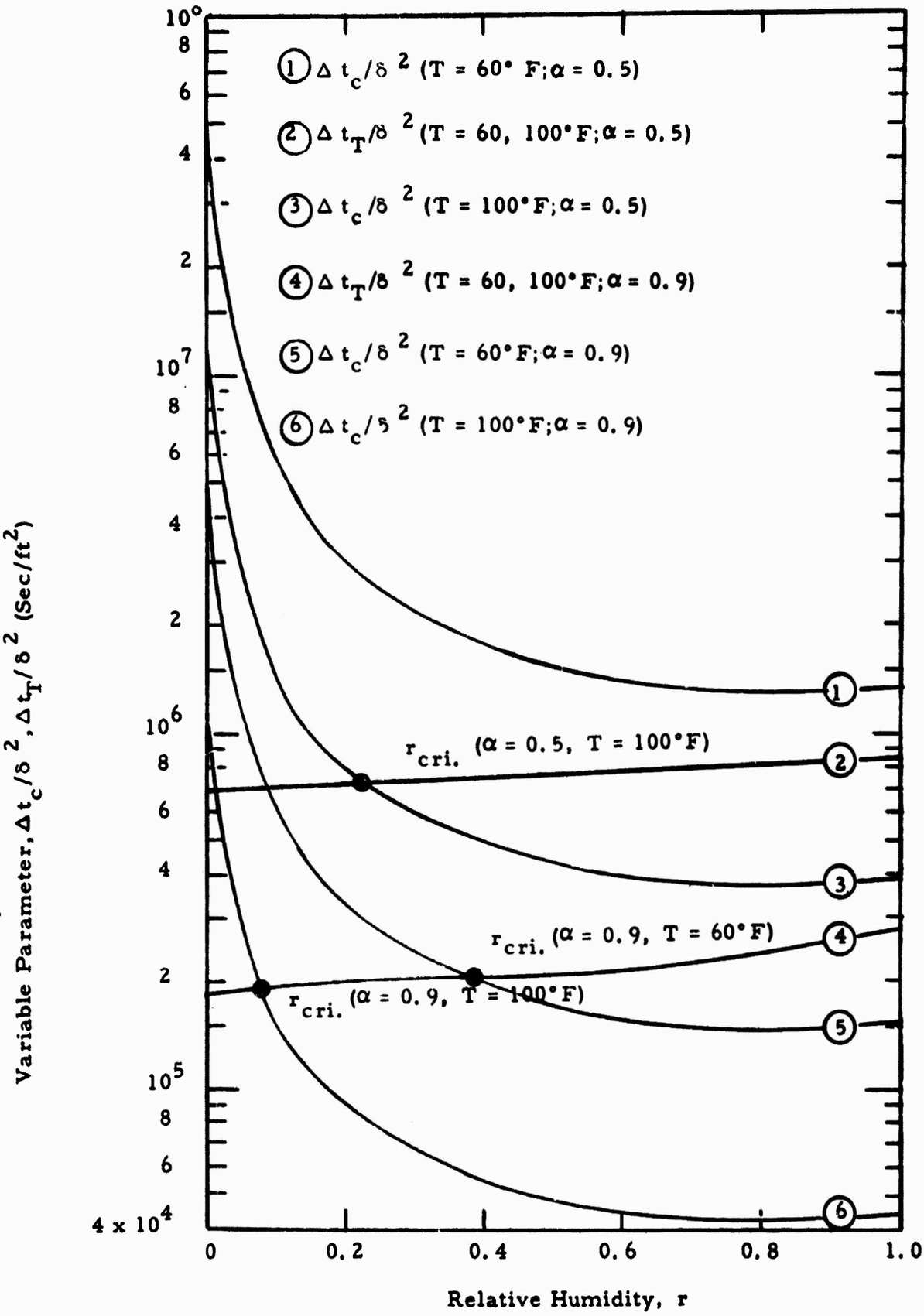

Figure C-2. Variation of Stability Parameters with Relative Humidity

It is noted that, in some cases, the curves for $\Delta t_{c_{i,j}}$ and $\Delta t_{T_{i,j}}$ intersect one another. The value of r at which this occurs will be denoted with the symbol r_{cri}. Comparing curves 1 and 2 (geometric porosity = 0.5, temperature = 60°F), it is noted that an intersection does not occur. Since a value of Δt_i which lies below each of these curves must be selected, it is obvious that selecting Δt_i less than $\Delta t_{T_{i,j}}$ (curve 2) satisfies this condition. This indicates that for low temperatures and high fabric densities (low porosity), the temperature stability condition is the dominating one. Keeping α at 0.5 and increasing the temperature shifts the concentration stability curve downward (to curve 3) but produces little change in the temperature stability curve (curve 2). For this increased temperature level (100°F), it can be seen that the two curves intersect at approximately $r_{cri} = 0.22$. Δt_i must be chosen such that $\Delta t_i <$ in $\left[\Delta t_{c_{i,j}} ; \Delta t_{T_{i,j}}\right]$. This condition is satisfied by selecting the following set of relations:

$$\Delta t_i < \Delta t_T \quad \text{for } r < 0.22$$

$$\Delta t_i < \Delta t_c \quad \text{for } r > 0.22.$$

Thus, for $\alpha = 0.5$ at T = 100°F, it is noted that the temperature stability criteria is the limiting factor for $r < 0.22$ while the concentration stability criteria is the limiting factor for $r > 0.22$.

A similar reasoning process for $\alpha = 0.9$ (curves 4, 5, and 6) can be utilized. The following behavior may be inferred from Figure C-2:

1) The critical value of r decreases as the temperature level increases.

2) For $r < r_{cri}$, the temperature stability criteria is the limiting factor for the selection of Δt_i.

3) For $r > r_{cri}$, the concentration stability criteria is the limiting factor for the selection of Δt_i.

4. Computer Program

A computer program has been prepared for solution of the finite difference equations presented previously. Program HANDM (Heat and Mass Transfer) was written in AUTOMATH 1800 language for the Honeywell H-1800 computer system. AUTOMATH 1800 language is almost identical to the standard FORTRAN. With a few minor changes in certain library functions, the program can be made compatible with other computer systems, i.e., Control Data computers, models 1604 and above. At the present time, it is estimated that each time increment requires approximately 12 seconds of computer time on the H-1800 or CDC 1604 computers.

A flow diagram for the present program HANDM is shown in Figure C-3.

5. Sample Calculation

A sample calculation has been made, using the Honeywell 1800 computer, to test the computer program presented in the preceding section. The fabric was divided into four sections and an initial linear temperature distribution was assumed (T_{f_0} = 85°F, T_{f_5} = 86°F). The initial vapor concentration is assumed constant at 0.6759×10^{-3} lb/ft^3. The ambient air temperature amounts to 75°F.

The temperature distribution within the skin was assumed to be basal and steady state with $\Delta T_B = 0$ initially. At t = 0, the subject starts exercising at a rate E = 0.7038 Btu/ft^3 sec. Other parameters which were selected are tabulated below.

K_s = 0.22917 ft/sec

U_s = 0.0040417 Btu/ft^2 sec °F

$\dot{V}_1 = \dot{V}_2 = 0$

L_a = 0.0104 ft

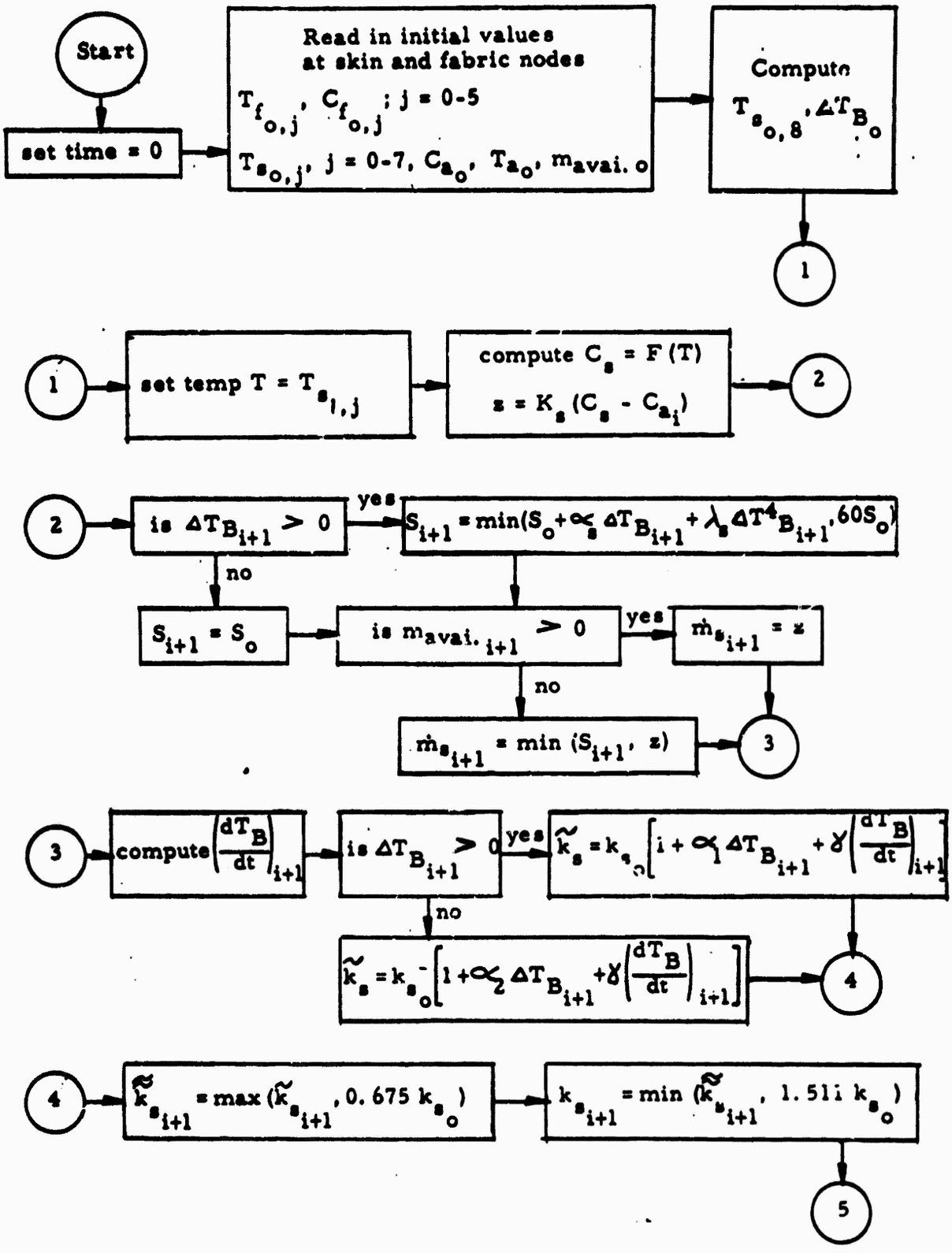

Figure C-3. Computer Flow Diagram for Program HANDM

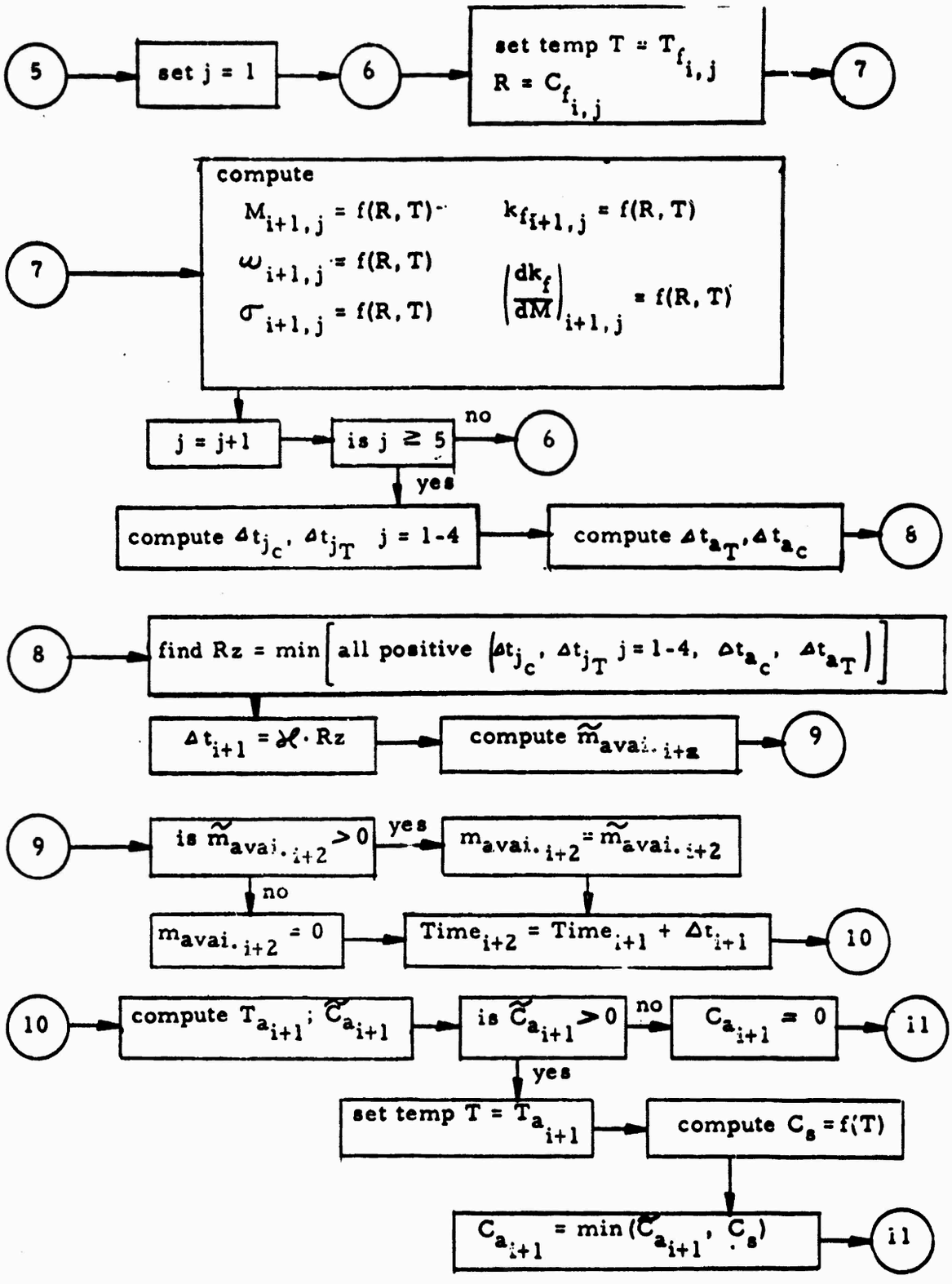

Figure C-3(continued)

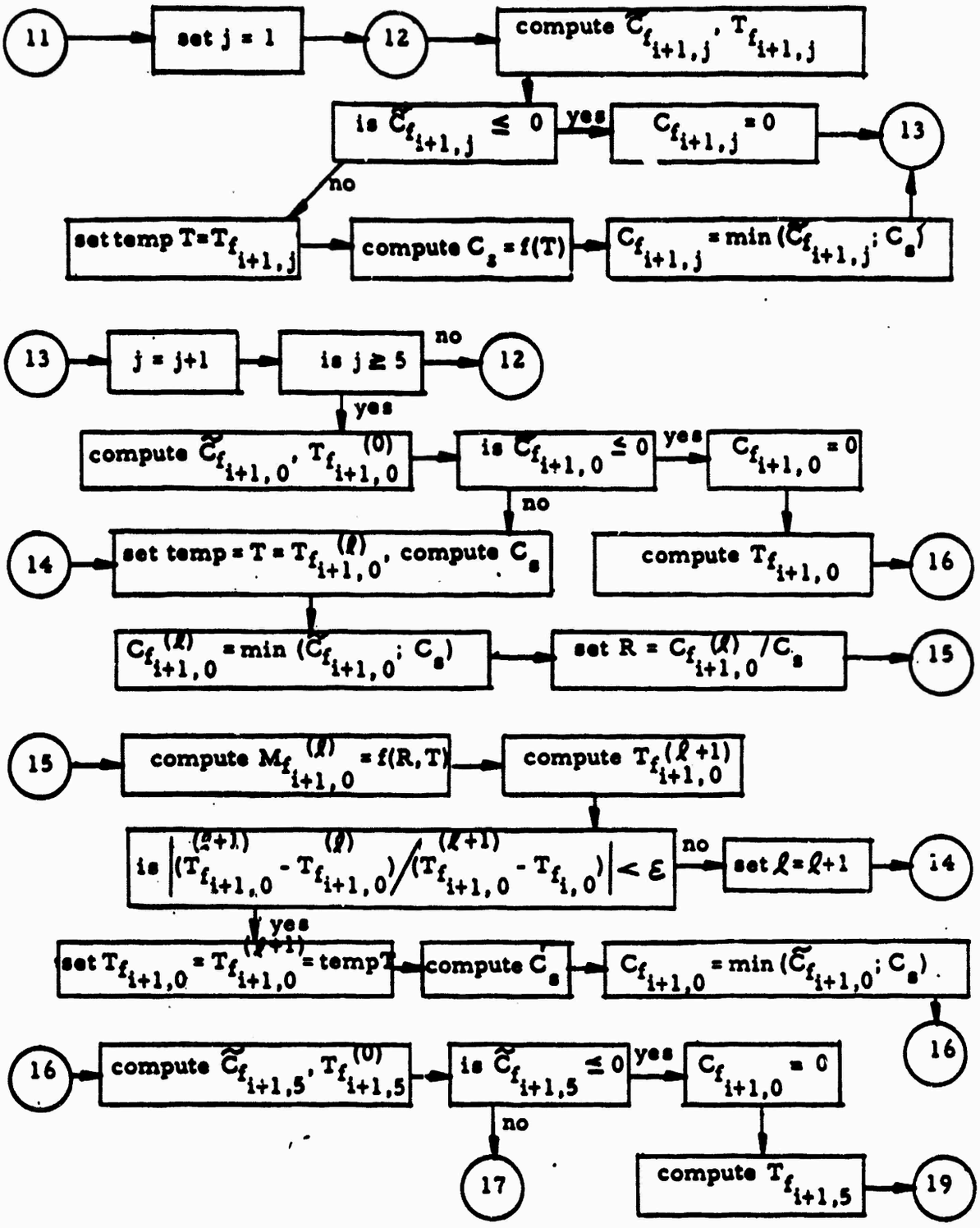

Figure C-3(continued)

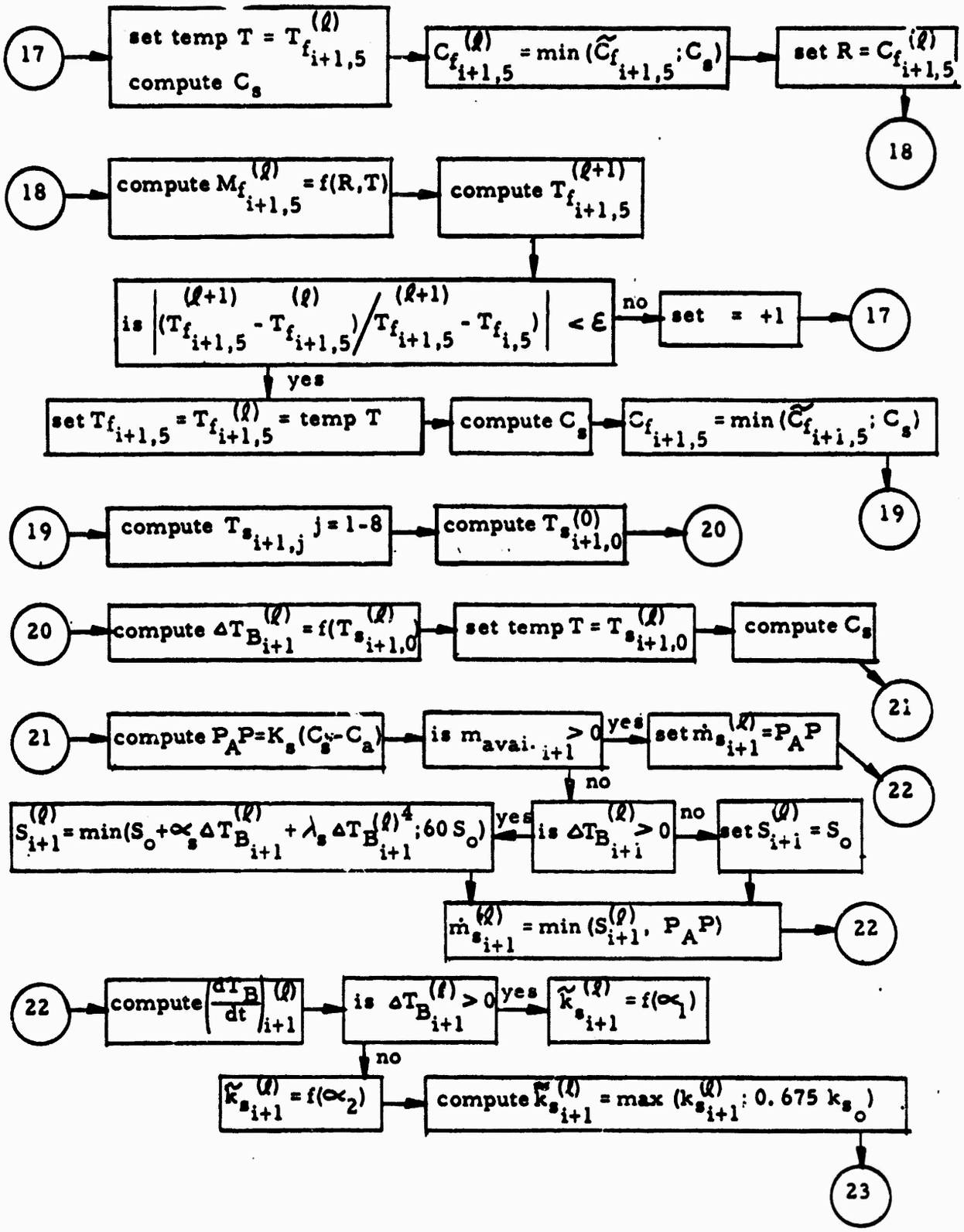

Figure C-3(continued)

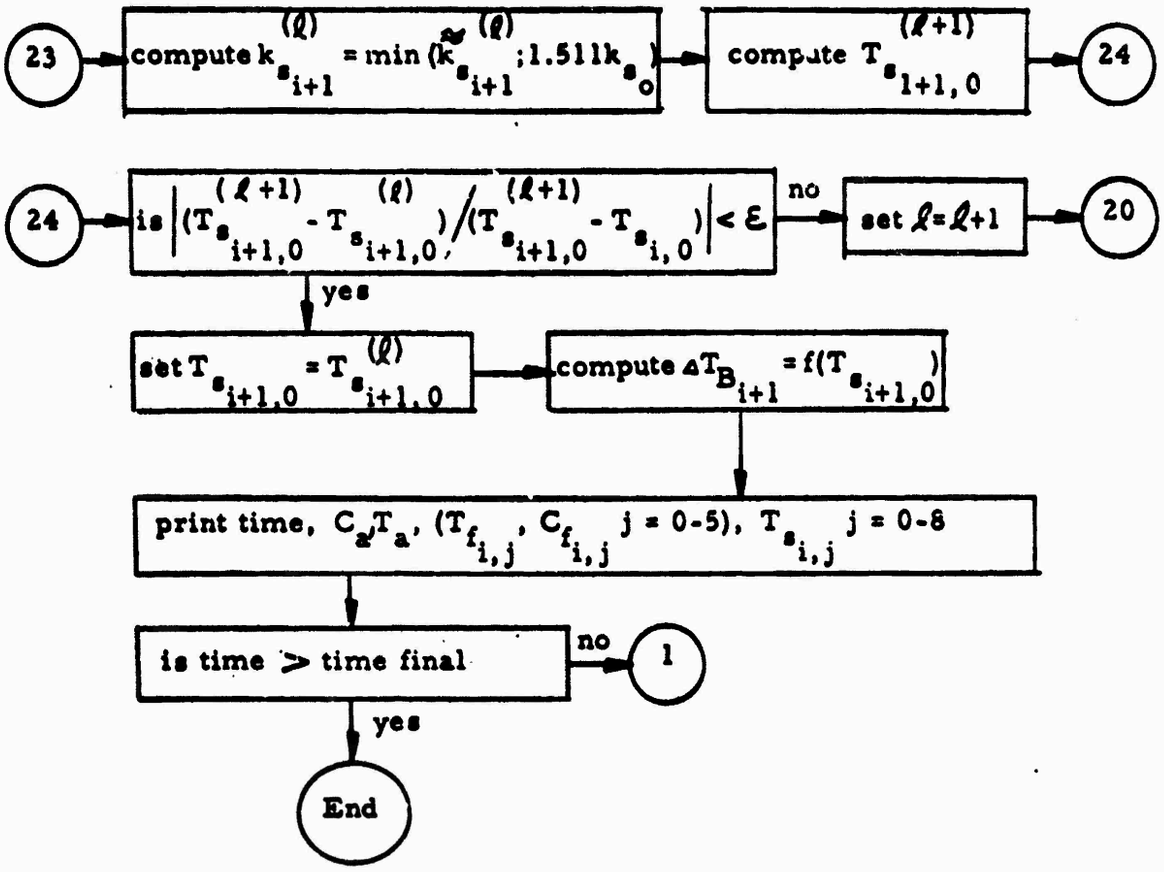

Figure C-3(continued)

$$D = 0.0002222 \text{ ft}^2/\text{sec}$$

$$K_o = 0.0561 \text{ ft/sec}$$

$$K_1 = 0.22917 \text{ ft/sec}$$

$$U_o = 9.8889 \times 10^{-4} \text{ Btu/ft}^2 \text{ sec } ^\circ\text{F}$$

$$U_1 = 4.0417 \times 10^{-3} \text{ Btu/ft}^2 \text{ sec } ^\circ\text{F}$$

$$L_f = 0.00141 \text{ ft}$$

$$\alpha = 0.875.$$

The variation of temperature with time at each fabric node is presented in Figure C-4 and that of the air gap and surface skin node in Figure C-5. The temperature at the remaining skin nodes did not change during this limited computer run because of the extremely large values of δ_s compared with δ_f.

It is noted from these figures that the large values of the transfer coefficients (reflecting the effects of air movement caused by exercising) causes an initial rapid loss of heat at the fabric and skin outer surfaces as well as a gain of heat at the fabric inner surface. The manner in which these temperature changes propagate into the fabric interior as time progresses is also noted.

It appears at present, from this very limited study, that the computer program is satisfactory and can now be utilized in a systematic parameter study, the parametric values being supplied by the experimental phase of this project.

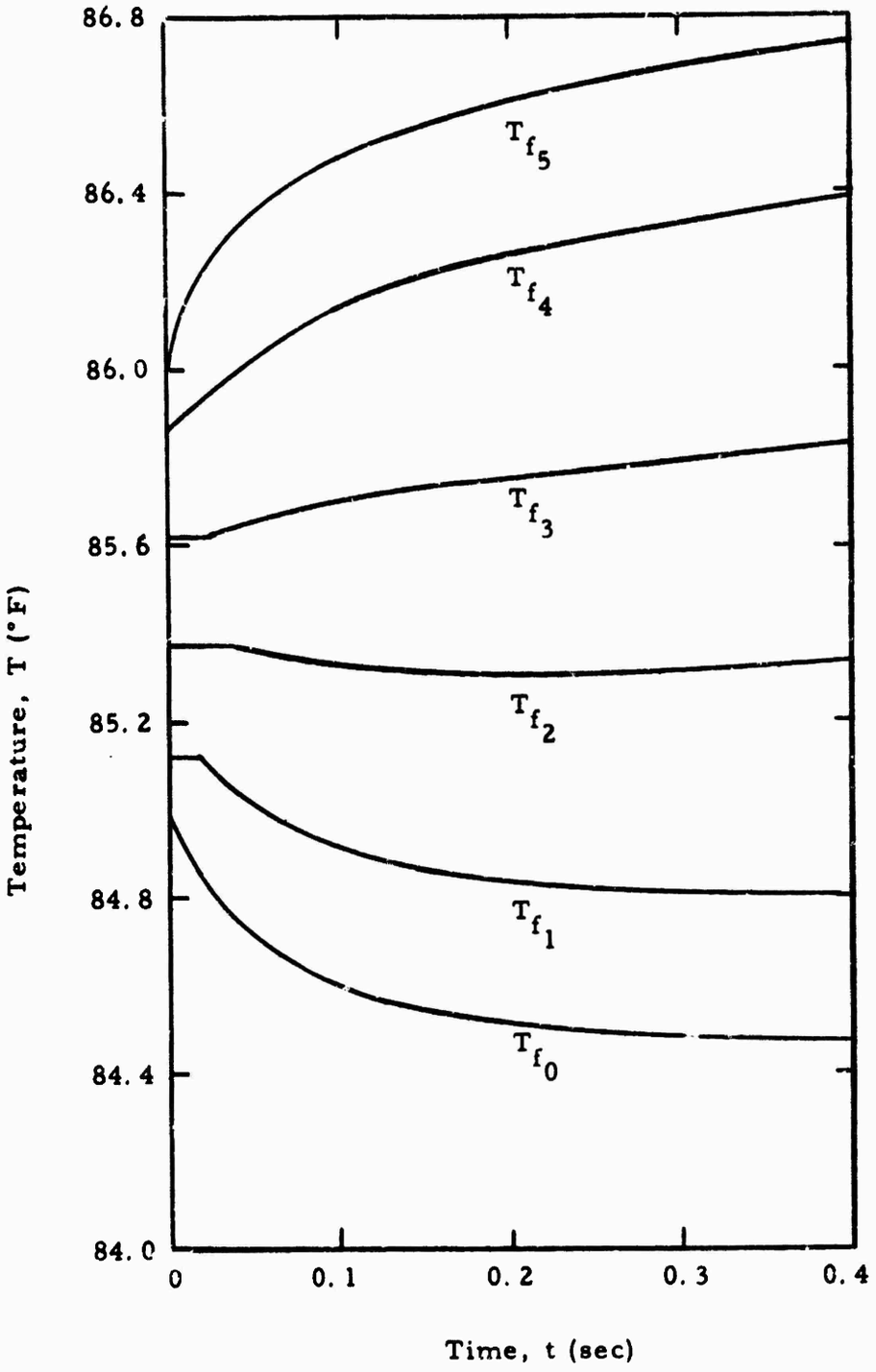

Figure C-4. Variation of Fabric Temperature with Time

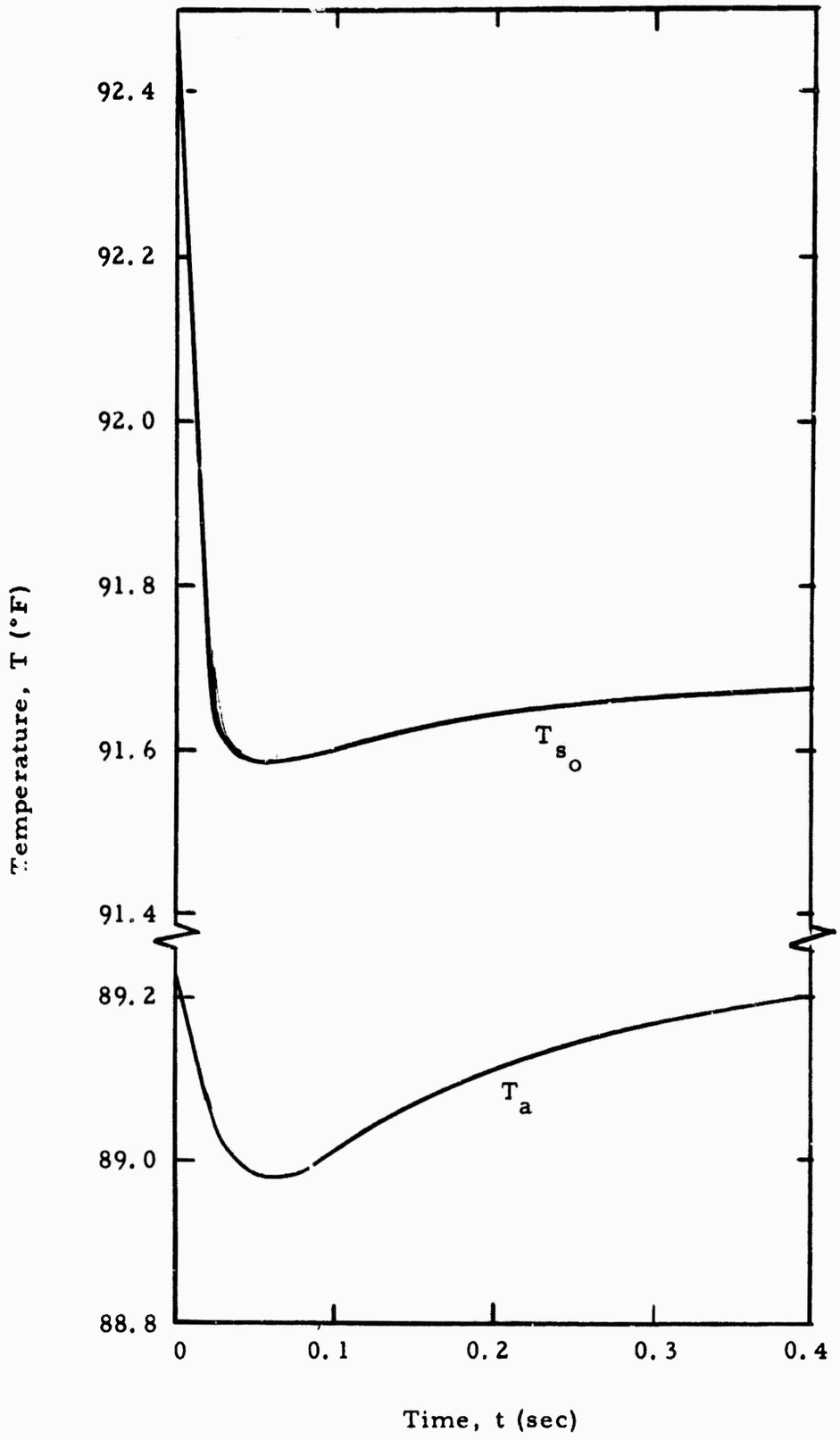

Figure C-5. Variation of the Air Gap and Skin Surface Temperatures with Time

REFERENCES

C-1. Larson, R. E., N. Konopliv, and R. A Kuehnl. Heat and mass transfer through composite clothing systems. Litton Systems, Inc., Applied Science Division, Report No. 2635, Contract DA-19-129-AMC-183(N). (October 6, 1964).

APPENDIX D

INTEGRAL ANALYSIS OF THE THERMAL AND WATER VAPOR BOUNDARY LAYER GROWTH

NOMENCLATURE

Symbol	Definition and Dimension
A	area (ft^2)
C	vapor concentration (lb/ft^3)
c_p	specific heat at constant pressure (Btu/lb °F)
D	diffusion coefficient (ft^2/hr)
f, g	functions
I	integral
k	thermal conductivity (Btu/ft hr °F)
k_s	local mass transfer coefficient $= \frac{D\left(\frac{dC}{dy}\right)_{y=0}}{C_a - C_s}$ (ft/hr)
K_s	average mass transfer coefficient $= \frac{\dot{M}_s}{(C_s - C_a)\,A}$ (ft/hr)
L_a	channel height (or air gap spacing) (ft)
$\dot{M}_s$	total rate of water loss from the surface of a plate of area A (lb/hr)
Pr	Prandtl number $= \frac{\mu c_p}{k}$
q	heat flux (Btu/ft^2 hr)
Q	total heat loss per unit time from the surface of a plate of area A (Btu/hr)
Re	Reynolds number $= \frac{\rho V L_a/2}{\mu}$

Symbol	Definition and Dimension
Sc	Schmidt number = ν/D
T	temperature (°F)
u_s	local heat transfer coefficient $= \frac{k\left(\frac{dT}{dy}\right)_{y=0}}{T_a - T_s}$ (Btu/ft^2 hr °F)
U_s	average heat transfer coefficient $= \frac{Q}{(T_s - T_a)\,A}$ (Btu/ft^2 hr °F)
v	local velocity (ft/hr)
V	maximum velocity (ft/hr)
x	downstream coordinate (ft)
$\bar{x}$	dimensionless downstream coordinate = $\frac{x}{L_a/2}$
y	vertical coordinate (ft)
α	thermal diffusivity = $\frac{k}{c_p \rho}$ (ft^2/hr)
β	dimensionless boundary layer thickness = $\frac{\delta}{L_a/2}$
δ	boundary layer thickness (ft)
η	dimensionless vertical coordinate = $\frac{y}{L_a/2}$
μ	viscosity (lb/hr ft)
ν	kinematic viscosity (ft^2/hr)

Symbol	Definition and Dimension
ζ	dimensionless vertical coordinate = y/δ
ρ	density (lb/ft^3)

Subscripts

a	air gap
s	simulant surface
t	thermal
v	vapor

INTEGRAL ANALYSIS OF THE THERMAL AND WATER VAPOR BOUNDARY LAYER GROWTH

The integral thermal boundary layer equation, as presented in Reference D-1 (p. 169, Equation 7-2), can be expressed as:

$$\frac{d}{dx}\int_0^{\delta_T} (T_a - T)\, v\, dy = \alpha \left(\frac{dT}{dy}\right)_{y=0} \qquad \text{(D-1)}$$

In a manner analogous to the one utilized to develop Equation (D-1), it may be shown that the vapor boundary layer equation can be written as:

$$\frac{d}{dx}\int_0^{\delta_v} (C_a - C)\, v\, dy = D \left(\frac{dC}{dy}\right)_{y=0} \qquad \text{(D-2)}$$

where:

C_a = ambient (free stream) vapor density (or concentration)

C = local vapor density

D = diffusion coefficient.

Comparing Equations (D-1) and (D-2), it is noted that they are identical in form to one another. Therefore, only Equation (D-1) will be analysed with the understanding that the results of the analysis may be extended to Equation (D-2) easily.

As in other integral boundary layer approximations, [D-1, D-2] it will be assumed that the temperature distribution is universal and can be expressed as:

$$\frac{T_a - T}{T_a - T_s} = 1 - g_t(\zeta_t) \qquad \text{(D-3)}$$

where:

T_s = skin surface temperature

$$\zeta_t = \frac{y}{\delta_t} \qquad \text{(D-4)}$$

and the function $g_t(\zeta_t)$ satisfies the conditions that:

$$g_t(0) = 0; \quad g_t(1) = 1 \qquad \text{(D-5)}$$

These conditions imply that:

$$\text{at } \zeta_t = 0 \ (y=0), \ T = T_s$$

$$\text{at } \zeta_t = 1 \ (y=\delta_t), \ T = T_a$$

Differentiation of (D-3) yields:

$$\left(\frac{dT}{dy}\right)_{y=0} = (T_a - T_s)\left[\frac{d\zeta_t}{dy}\ \frac{dg_t(\zeta_t)}{d\zeta_t}\right]_{y=0} = \frac{(T_a - T_s)}{\delta_t}\ g_t'(0) \qquad \text{(D-6)}$$

where $g_t'(0) = \left(\frac{dg_t}{d\zeta_t}\right)_{\zeta_t=0}$

Introducing (D-3), (D-4) and (D-6) into (D-1) and assuming the surface and free stream temperatures remain constant in the downstream direction, one obtains:

$$\frac{d}{dx}\int_0^1 \left[1 - g_t(\zeta_t)\right] v\, \delta_t d\zeta_t = \frac{\alpha}{\delta_t}\, g_t'(0) \qquad \text{(D-7)}$$

We next assume the velocity distribution is universal and can be expressed as:

$$\frac{v}{V} = f(\eta) \qquad \text{(D-8)}$$

where

$$\eta = \frac{y}{L_a/2}$$

L_a = channel height

The function $f(\eta)$ is assumed to satisfy the relations:

$$f(0) = 0; \quad f(1) = 1$$

The second relation implies that the maximum velocity occurs on the channel centerline and equals V.

From the definitions of ζ_t and η, one notes that:

$$\frac{\eta}{\zeta_t} = \frac{\delta_t}{L_a/2}$$

Defining $\beta_t = \frac{\delta_t}{L_a/2}$ (dimensionless thermal boundary layer thickness)

one may write

$$\eta = \beta_t \zeta_t \qquad \text{(D-9)}$$

Introducing relations (D-8) and (D-9) into (D-7), it is found:

$$\frac{d}{dx}\left[V\beta_t \int_0^1 \left[1 - g_t(\zeta_t)\right] f(\beta_t\zeta_t)\, d\zeta_t\right] = \frac{\alpha\, g_t'(0)}{(L_a/2)^2}\,\frac{1}{\beta_t} \qquad \text{(D-10)}$$

Assuming that the flow is not accelerated, (V = constant), it can be rewritten (D-10) in the form:

$$\frac{d}{d\bar{x}}\left[\beta_t I_t(\beta_t)\right] = \frac{\alpha g_t'(0)}{V L_a/2}\,\frac{1}{\beta_t} \qquad \text{(D-11)}$$

where

$$\bar{x} = \frac{x}{L_a/2}$$

$$I_t(\beta_t) = \int_0^1 \left[1 - g_t(\zeta_t)\right] f(\beta_t\zeta_t)\, d\zeta_t$$

The local heat transfer coefficient is defined by the relation:

$$q = -u_s (T_a - T_s) = -k \left(\frac{dT}{dy}\right)_{y=0}$$

or

$$u_s = \frac{k\left(\frac{dT}{dy}\right)_{y=0}}{T_a - T_s} \qquad \text{(D-12)}$$

Introducing relations (D-6) yields

$$u_s = \frac{k\, g_t'(0)}{\delta_t}$$

In dimensionless form, this becomes:

$$\frac{u_s L_a/2}{k} = \frac{g_t'(0)}{\beta_t} \qquad \text{(D-13)}$$

The dimensionless grouping on the left side of this relation is recognized to be the local Nusselt number based on the half channel height.

The average heat transfer coefficient over a length x of the plate can be expressed as:

$$U_s = \frac{1}{x}\int_0^x u_s\, dx$$

or

$$\frac{U_s L_a/2}{k} = \frac{1}{\bar{x}}\int_0^{\bar{x}} \frac{u_s L_a/2}{k}\, d\bar{x} \qquad \text{(D-14)}$$

Introducing (D-13) gives:

$$\frac{U_s L_a/2}{k} = \frac{g_t'(0)}{\bar{x}}\int_0^{\bar{x}} \frac{d\bar{x}}{\beta_t} \qquad \text{(D-15)}$$

Solving Equation (D-11) for $\frac{g_t'(0)}{\beta_t}$ and substituting into the above relation yields:

$$\frac{U_s L_a/2}{k} = \frac{V L_a/2}{\alpha \bar{x}} \int_{\bar{x}=0}^{\bar{x}} \frac{d}{d\bar{x}} \left[\beta_t I_t(\beta_t)\right] d\bar{x}$$

$$= \frac{V L_a/2}{\alpha \bar{x}} \beta_t I_t(\beta_t) \qquad \text{(D-16)}$$

Equation (D-11) may be rearranged and solved for $\bar{x}$ to obtain:

$$\frac{\alpha \bar{x}}{V L_a/2} = \frac{1}{g_t'(0)} \int_{\beta_t=0}^{\beta_t} \beta_t \frac{d}{d\beta_t} \left[\beta_t I_t(\beta_t)\right] d\beta_t \qquad \text{(D-17)}$$

which, when substituted into (D-16) gives:

$$\frac{U_s L_a/2}{k} = \frac{g_t'(0)\, \beta_t I_t(\beta_t)}{\int_0^{\beta_t} \beta_t \frac{d}{d\beta_t} \left[\beta_t I_t(\beta_t)\right] d\beta_t} \qquad \text{(D-18)}$$

The grouping $\frac{V L_a/2}{\alpha}$ appearing on the left side of (D-17) can be written as:

$$\frac{V L_a/2}{\alpha} = \frac{\rho V L_a/2}{\rho \alpha} = \frac{\rho V L_a/2}{\mu} \cdot \frac{\mu}{\rho \alpha} = \frac{\rho V L_a/2}{\mu} \cdot \frac{\mu}{\rho \frac{k}{c_p \rho}}$$

$$= \frac{\rho V L_a/2}{\mu} \cdot \frac{\mu c_p}{k}$$

Since:

$$\frac{\rho V L_a/2}{\mu} = Re = \text{Reynolds number based on the channel half height and centerline velocity}$$

$$\frac{\mu c_p}{k} = Pr = \text{Prandtl number.}$$

It may be written:

$$\frac{V L_a/2}{\alpha} = Re\,Pr \tag{D-19}$$

The relation between the dimensionless thermal boundary layer thickness (β_t) and dimensionless downstream location ($\bar{x}$) can now be written as:

$$\frac{\bar{x}}{Re\,Pr} = \frac{1}{g_t'(0)} \int_0^{\beta_t} \beta_t \frac{d}{d\beta_t} \left[\beta_t I_t(\beta_t)\right] d\beta_t \tag{D-20}$$

The local and average heat transfer coefficients are then given by:

$$\frac{u_s L_a/2}{k} = \frac{g_t'(0)}{\beta_t} \tag{D-21}$$

and

$$\frac{U_s L_a/2}{k} = \frac{g_t'(0)\,\beta_t I_t(\beta_t)}{\int_0^{\beta_t} \beta_t \frac{d}{d\beta_t} \left[\beta_t I_t(\beta_t)\right] d\beta_t} \tag{D-22}$$

A similar treatment for the vapor boundary layer leads to the following equations:

$$\frac{\bar{x}}{Re\,Sc} = \frac{1}{g_t'(0)} \int_0^{\beta_v} \beta_v \frac{d}{d\beta_v} \left[\beta_v I_v(\beta_v)\right] d\beta_v \qquad \text{(D-23)}$$

$$\frac{k_s L_a/2}{D} = \frac{g_t'(0)}{\beta_v} \qquad \text{(D-24)}$$

$$\frac{K_s L_a/2}{D} = \frac{g_v'(0)\, \beta_v I_v(\beta_v)}{\int_0^{\beta_v} \beta_v \frac{d}{d\beta_v}\left[\beta_v I_v(\beta_v)\right] d\beta_v} \qquad \text{(D-25)}$$

where

$$\beta_v = \frac{\delta_v}{L_a/2} = \text{dimensionless vapor boundary layer thickness}$$

$$g_v(\zeta_v) = 1 - \frac{C_a - C}{C_a - C_s}$$

$$\zeta_v = \frac{y}{\delta_v}$$

$$I_v(\zeta_v) = \int_0^1 \left[1 - g_v(\zeta_v)\right] f(\beta_v \zeta_v)\, d\zeta_v$$

$$k_s = \text{local mass transfer coefficient} = \frac{D\left[\frac{dC}{dy}\right]_{y=0}}{C_a - C_s}$$

$$K_s = \text{average mass transfer coefficient} = \frac{\dot{M}_s}{(C_s - C_a)A}$$

Comparing Equations (D-20) to (D-22) with (D-23) to (D-25), the similar form of the corresponding equations is noted.

To obtain numerical results, the following functions were chosen:

$$g(\zeta) = 2\zeta - \zeta^2$$

$$f(\beta) = \begin{cases} (\beta\zeta)^{1/7} & \text{for } \beta\zeta \leq 1 \\ (2 - \beta\zeta)^{1/7} & \text{for } 1 \leq \beta\zeta \leq 2 \end{cases}$$

The function selected for $f(\beta\zeta)$ corresponds to a turbulent velocity profile. This function has been chosen since experiments have indicated a fairly flat, turbulent type velocity profile exists.

The integration of the pertinent equations is fairly straightforward but quite lengthy. The results of this integration are presented below and tabulated in Table D-1.

for $\beta \leq 1$

$$\frac{1}{g'(0)} \int_0^{\beta} \beta \frac{d}{d\beta} \left[\beta I(\beta)\right] d\beta = 0.06929\beta^{15/7}$$

for $1 \leq \beta \leq 2$

$$\frac{1}{g'(0)} \int_0^{\beta} \beta \frac{d}{d\beta} \left[\beta I(\beta)\right] d\beta = 0.06929 + \frac{7}{4} \ln\beta$$

$$+ 7\left[\frac{1}{2} + \frac{1}{11} - \frac{4}{15}\right]\left[\frac{1}{\beta} - 1\right]$$

$$+ \frac{7}{2}\left[\frac{1}{2} + \frac{2}{11} - \frac{8}{15}\right]\left\{\frac{3}{8}\left[1 - (2-\beta)^{8/7}\right]\right.$$

$$- \frac{2}{15}\left[1 - (2-\beta)^{15/7}\right]$$

$$\left. + 2\left[1 - \frac{(2-\beta)}{\beta}^{8/7}\right]\right\}$$

$$- 11\left[\frac{1}{2} + \frac{2}{11} - \frac{8}{15}\right] \int_{2-\beta}^{1} \frac{\zeta^{1/7}}{2-\zeta} d\zeta$$

Table D-1.

RESULTS OF INTEGRATION

β_t or β_v	$(Re\,Pr)^{-1}\,\bar{x}$ or $(Re\,Sc)^{-1}\,\bar{x}$	$\frac{u_s L_a/2}{k}$ or $\frac{k_s L_a/2}{D}$	$\frac{U_s L_a/2}{k}$ or $\frac{K_s L_a/2}{D}$
0	0	∞	∞
0.1	0.00050	20.000	37.500
0.2	0.00220	10.000	18.750
0.3	0.00523	6.666	12.500
0.4	0.00970	5.000	9.375
0.5	0.01569	4.000	7.500
0.6	0.02318	3.333	6.250
0.7	0.03222	2.857	5.360
0.8	0.04295	2.500	4.690
0.9	0.05528	2.222	4.166
1.0	0.06929	2.000	3.750
1.1	0.08517	1.818	3.402
1.2	0.10248	1.666	3.123
1.3	0.12217	1.538	2.870
1.4	0.14213	1.429	2.683
1.5	0.16534	1.333	2.494
1.6	0.18939	1.250	2.341
1.7	0.21386	1.176	2.219
1.8	0.24253	1.111	2.085
1.9	0.27088	1.053	1.981
2.0	0.29875	1.000	1.899

REFERENCES

D-1. Eckert, E. R. G. and R. M. Drake, Jr. Heat and mass transfer. McGraw-Hill Book Co., Inc., New York, 1959.

D-2. Schlichting, Hermann. Boundary layer theory. McGraw-Hill Book Co., Inc., New York, 1960.

APPENDIX E

MEAN AND FLUCTUATING VELOCITY HOT-WIRE EQUATIONS

NOMENCLATURE

Symbol	Definition
A	surface area of hot-wire or hot-wire constant (ordinate intercept)
a	local sound speed, length/time
B	hot-wire constant (slope)
c_p	specific heat of air, heat/mass/temperature
D	diameter of hot-wire, length
E	voltage, volts
e	RMS voltage, volts
H	total rate of heat loss from hot-wire, heat/time
h	heat transfer coefficient, heat/length^2/time/temperature
I	current, amps
Kn	Knudsen number, $\frac{\lambda}{D_w}$
k	thermal conductivity of air, heat/length/time/temperature
ℓ	length of hot-wire
M	Mach number, $\frac{U}{a}$
Nu	Nusselt number, $\frac{h D_w}{k}$
Pr	Prandtl number, $\frac{C_p \mu}{k}$
R	resistance, ohms

Symbol	Definition
Re	Reynolds number, $\frac{U D_w \rho}{\mu}$
T	temperature, °F
U	stream velocity (mean), length/time
u	fluctuating velocity, length/time
α	linear temperature resistance coefficient of hot-wire
η	temperature recovery ratio, $\frac{T_e}{T_t}$
λ	mean free path, length
μ	viscosity of air, mass/length/time
ρ	density of air, mass/length^3
τ	temperature ratio, $\frac{T_w - T_t}{T_t}$

Subscripts

b	hot-wire bridge value
e	recovery temperature of unheated hot-wire
m	uncorrected value
o	reference temperature (32°F)
t	total temperature
w	hot-wire
1	restricted constant

Superscripts

n	hot-wire constant (Reynolds number exponent)
'	restricted constant

MEAN AND FLUCTUATING VELOCITY HOT-WIRE EQUATIONS

1. General

In recent years new interest has been shown in using hot-wire anemometry techniques to measure mean and fluctuating flow quantities. Wider application of this technique has resulted from the improvement of circuit designs and the development of film probes. The use of the hot-wire anemometer to measure boundary layer velocity profiles offers several advantages over the more common method of total head probings: its small size allows measurements to be made closer to the wall, with better spatial resolution; it retains high sensitivity at low velocities; and most importantly it enables one to measure velocity fluctuations over wide frequency bands. Good results can be reasonably expected when the hot-wire anemometer is used to measure mean and fluctuating velocities at constant and near-ambient stream densities--provided a proper calibration has been performed. Success is even more readily attainable if the random velocity fluctuations are small in comparison to the mean velocity. Under low-density conditions and at near-zero mean velocities, the ability of the constant-temperature hot-wire anemometer to respond reliably and accurately to rapidly fluctuating velocities decreases.

Changes in the variables characterizing the thermodynamic and kinematic state of a fluid flow can be sensed by a hot-wire anememeter. An understanding of the nature of the perturbation and an adequate knowledge of the heat-transfer processes involved are necessary for correct interpretation of the signals received.

In compressible flow, the convective heat transfer to a hot-wire is affected by changes in mass flow and stagnation temperature. Both these variables respond in turn to three distinctly different disturbance fields, as indicated by first-order perturbation theory for the flow of a compressible, viscous, heat-conducting gas. Each of these perturbation components obeys independent differential equations. Except for some special types of flow, these disturbance fields are composed of a vorticity mode, an entropy mode, and a sound-wave mode. For small-intensity disturbances, these modes are independent and separable; however, as the intensity increases, they interact with each other and must be treated as a composite disturbance. By analyzing the hot-wire fluctuation diagram, Kovasznay[E-1] was able to determine the presence of coexisting modes under certain restrictive conditions.

Morkovin and Phinney[E-2] showed that the hot-wire probe is much more sensitive to the vorticity and entropy modes than to the sound-wave mode. Shear layer measurements indicated that sound intensities as high as 120 decibels caused negligible variations in density, velocity, and total temperature compared to the variations associated with the vorticity and entropy modes.

When one is interested in analyzing the performance of a hot-wire probe from the standpoint of heat transfer, end-loss corrections to the Nusselt number values must be made. This necessity arises from the construction of hot-wire probes, which requires the attachment of a fine sensing wire to relatively massive end supports by soldering or welding techniques. In continuum flow it is usually assumed that the supports are at the wire recovery temperature. For a heated wire, this implies a continuously decreasing temperature from the center to the supports.[E-3]

The first theoretical treatment of end losses was apparently given by King,[E-4] who assumed that the heat loss depends linearly on the temperature difference and that the supports are not heated by conduction from the wire. A nonlinear theory has been more recently developed by Betchov,[E-5] and additional results have been reported by Winovich and Stine.[E-6] It seems to be the present consensus that the various uncertainties inherent in hot-wire measurements make it unnecessary to apply the more elaborate theory of Betchov. Most workers in the field follow the method of King as modified by Kovasznay[E-7] and Kovasznay and Tormark.[E-8]

It is important to appreciate that the uncertainties of these corrections are large enough to make individual probe calibration mandatory for accurate measurements.

2. Steady Flow

The foundation work in probe calibration was performed by King.[E-4] This work has been continued by ASD in the investigations reported in References E-9 and E-10 and by the authors cited in References E-11 through E-18. These findings affirm the general relation for heat loss:

$$Nu = Nu(M, Re, Pr, Kn, \tau, \ell/D_w), \qquad (E\text{-}1)$$

A useful explicit form of Equation (E-1) is

$$Nu = A + B \cdot Re^n, \qquad (E\text{-}2)$$

in which A and B are nominal constants and are functions to some extent of the other parameters in Equation (E-1). In practice, the values of A, B, and n are empirically determined by calibrating individual probes under proper flow conditions. Following King,[E-4] the value n = 1/2 is commonly used. Subsequent work has shown, however, that n is not

strictly constant. For example, Collis and Williams[E-19] found the following values of n:

	$0.02 < Re < 44$	$44 < Re < 140$
n	0.45	0.51
A	0.24	0.00
B	0.56	0.48

McAdams[E-11] has summarized heat transfer data on circular cylinders for the range, $0.1 < Re < 2.5 \times 10^5$. For the smaller range, $0.1 < Re < 10^3$, the data are well represented by

$$Nu = 0.32 + 0.43\, Re^{0.52}. \qquad \text{(E-3)}$$

These variations in n are not significant for most work using calibrated probes. Accordingly, the common practice is to write Equation (E-2) in the form,

$$Nu_m = A + B \cdot Re^{1/2}, \qquad \text{(E-4)}$$

where Nu_m is the Nusselt number based on uncorrected measured values of heat loss from the wire. By using the given definitions for the Nusselt number and the heat transfer coefficient and noting that $H = I^2 R_w$,

$$Nu_m = \frac{I^2 R_w}{\pi \ell k_t (T_w - T_e)}, \qquad \text{(E-5)}$$

where k_t is the thermal conductivity of air evaluated at the stagnation temperature.

By using only the linear temperature coefficient of resistance α,

$$R_w = R_o \left[1 + \alpha(T_w - T_o)\right] \qquad \text{(E-6a)}$$

$$R_e = R_o \left[1 + \alpha(T_e - T_o)\right]; \qquad \text{(E-6b)}$$

R_o is the wire resistance at the reference temperature T_o, which is commonly chosen to be 32°F. From the last two equations,

$$R_w - R_e = \alpha R_o (T_w - T_e)$$

or

$$T_w - T_e = \frac{R_w - R_e}{\alpha R_c}. \qquad \text{(E-7)}$$

By substituting Equation (E-7) into Equation (E-5),

$$Nu_m = \frac{\alpha R_o}{\pi \ell k_t} \left(\frac{I^2 R_w}{R_w - R_e} \right). \qquad \text{(E-8)}$$

By combining Equations (E-4) and (E-8),

$$I^2 R_w = \frac{\pi \ell k_t (R_w - R_e)}{\alpha R_o} (A + B \cdot Re^{1/2}) \qquad \text{(E-9)}$$

Under constant-temperature operation of the hot wire, R_w is also constant. If, in addition, the equilibrium and total temperatures are constant, Equation (E-9) gives

$$I^2 = A_1 + B_1 \cdot Re^{1/2}; . \qquad \text{(E-10)}$$

Since R_w = a constant, an alternative form is

$$E_w^2 = A_2 + B_2 \cdot Re^{1/2}, \qquad \text{(E-11)}$$

where E_w is the voltage across the hot-wire. In these equations the quantities A_1, B_1, A_2, B_2 are constants when the flow conditions are suitably restricted. The dependence of I^2 and E_w^2 upon the velocity U can be made explicit in regions of constant temperature and density, since $Re^{1/2}$ is proportional to $U^{1/2}$.

Then

$$I^2 = A_1 + B_1' U^{1/2} \qquad \text{(E-10a)}$$

and

$$E_w^2 = A_2 + B_2' U^{1/2} . \qquad \text{(E-11a)}$$

Again, through calibration over appropriately limited ranges of the flow variables, the quantities A_1, B_1', A_2, B_2' are constants; and Equations (E-10a) and (E-11a) relate measurable values of I and E_w to U.

It is sometimes convenient to write Equation (E-9) in the form,

$$\frac{I^2 R_w}{R_w - R_e} = A' + B' (\rho U)^{1/2}, \qquad \text{(E-12)}$$

which shows the dependence of the heat-loss parameter on mass flux (ρU).

3. Fluctuating Flow

It is now desirable to obtain an expression relating a measurable voltage to the fluctuating component of the velocity. Let us consider the flow variables as U, ρ, and T_t. Following Baldwin[E-15] and Boltz,[E-12] Equation (E-5) is solved to obtain

$$I^2 = \left(\frac{\pi \ell k_t}{R_w}\right) (T_w - \eta T_t)\, Nu_m, \qquad \text{(E-13)}$$

where the temperature recovery factor, $\eta \equiv T_e/T_t$ has been used. For brevity, $G \equiv k_t (T_w - \eta T_t)\, Nu_m$ will be defined and the differential wire current will be written:

$$dI = \frac{\pi \ell}{2 I R_w} \left(\frac{\partial G}{\partial U}\, dU + \frac{\partial G}{\partial \rho}\, d\rho + \frac{\partial G}{\partial T_t}\, d T_t\right). \qquad \text{(E-14)}$$

Constant-temperature operation implies that R_w is a constant. Then $d(I R_w) = R_w\, dI \equiv e$, the voltage increment associated with the current change dI. By expanding the deviations in Equation (E-14) and taking the increments $\delta U \approx dU$, $\delta\rho \approx d\rho$, and $\delta T_t \approx d T_t$,

$$e = \frac{\pi \ell}{2 I} \left\{ \left[- k_t\, Nu_m\, T_t \frac{\partial \eta}{\partial U} - k_t\, \eta\, Nu_m \frac{\partial T_t}{\partial U} + k_t (T_w - \eta T_t) \frac{\partial Nu_m}{\partial U} \right] \delta U + \right.$$

$$\left[k_t (T_w - \eta T_t) \frac{\partial Nu_m}{\partial \rho} \right] \delta\rho + \qquad \text{(E-15)}$$

$$\left. \left[(T_w - \eta T_t)\, Nu_m \frac{\partial k_t}{\partial T_t} - k_t\, \eta Nu_m + k_t (T_w - \eta T_t) \frac{\partial Nu_m}{\partial T_t} \right] \delta T_t \right\}$$

If we assume that ρ and T_t are constant, Equation (E-15) simplifies to

$$e = \frac{I R_w}{2} \left[- \left(1 + \frac{\gamma - 1}{2} M^2\right) \frac{M}{\tau} \frac{\partial \eta}{\partial M} + \frac{M}{Nu_m} \left(1 + \frac{\gamma - 1}{2} M^2\right) \frac{\partial Nu_m}{\partial M} \right] \frac{\delta U}{U}, \quad \text{(E-16)}$$

where we have used the chain-rule relation,

$$\frac{\partial}{\partial U} = \frac{\partial M}{\partial U} \frac{\partial}{\partial M} = \frac{1}{a} \left(1 + \frac{\gamma - 1}{2} M^2\right) \frac{\partial}{\partial M} . \quad \text{(E-17)}$$

In using the data of Baldwin[E-15] and Cybulski and Baldwin[E-16] on versus M over a parametric range of $0.1 \leq K \leq 4.7$, one finds that the two terms within the square brackets of Equation (E-16) are of such magnitudes that the first is only about two percent of the second. If we retain only the larger term, we can write

$$e = \frac{I R_w M}{2 Nu_m} \left(1 + \frac{\gamma - 1}{2} M^2\right) \frac{\partial Nu_m}{\partial M} \frac{\delta U}{U} . \quad \text{(E-18)}$$

It is of practical interest to put Equation (E-18) in a different form. To this end we substitute Nu_m from Equation (E-8) into Equation (E-18) by making use of Equation (E-17) and the relation,

$$\frac{\partial}{\partial U} = \frac{\partial (\rho U)^{1/2}}{\partial U} \frac{\partial}{\partial (\rho U)^{1/2}} ,$$

so that

$$e = (\rho U)^{1/2} \left(\frac{R_w - R_e}{4 I} \right) \frac{\partial}{\partial (\rho U)^{1/2}} \left(\frac{I^2 R_w}{R_w - R_e} \right) \frac{\delta U}{U} \quad \text{(E-19)}$$

In Equation (E-12) it is noted that B' is the slope of the straight line which represents $I^2 R_w/(R_w - R_e)$ as a function of $(U)^{1/2}$. That is,

$$B' = \frac{\partial}{\partial (\rho U)^{1/2}} \left(\frac{I^2 R_w}{R_w - R_e} \right) ,$$

which, when substituted into Equation (E-19), gives

$$e = (\rho U)^{1/2} \left(\frac{R_w - R_e}{4I} \right) B' \frac{\delta U}{U} .$$

It will be more convenient to let $u = \delta U$, where u is the fluctuating component of the total instantaneous velocity, $U = \overline{U} + u$. By taking root-mean-square values (denoted by a superscript prime),

$$e' = (\rho U)^{1/2} \left(\frac{R_w - R_e}{4I} \right) B' \frac{u'}{U} . \qquad \text{(E-20)}$$

It has been assumed that η is a constant, implying that Re is also a constant. Since u'/U (%) is a physical quantity of interest, Equation (E-20) gives

$$\frac{u'}{U} = \frac{400 I}{(\rho U)^{1/2} B' (R_w - R_e)} e' (\%). \qquad \text{(E-21)}$$

In the constant-temperature anemometer, the output signal E_b is taken from a bridge circuit; this circuit is kept in balance (i.e., R_w is held constant) by a feedback circuit which varies the bridge current I_b. A schematic of the bridge is shown in Figure E-1. The voltages E_b and E_w consist of constant time-average values and the smaller fluctuating components e_b and e, respectively. The relation between e_b and e can be obtained from the condition,

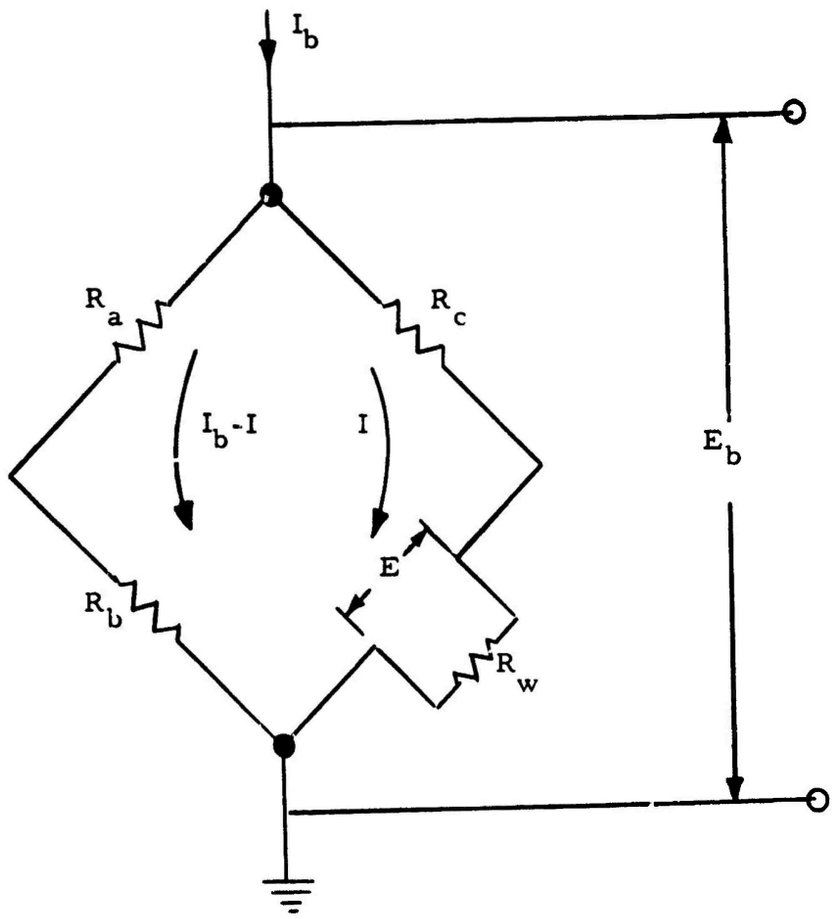

Figure E-1. Hot-Wire Bridge Circuit

$$I\,(R_c + R_w) = (I_b - I)\,(R_a + R_b) = E_b,$$

from which

$$I R_w \left(\frac{R_c + R_w}{R_w} \right) = E_b$$

or

$$E \left(\frac{R_c + R_w}{R_w} \right) = E_b.$$

For the fluctuating components only,

$$e \left(\frac{R_c - R_w}{R_w} \right) = e_b,$$

from which

$$e' = \left(\frac{R_w}{R_c + R_w} \right) e_b'; \qquad \text{(E-22)}$$

e_b' is measured with a true rms meter.

We will now make the assumption that the fluctuating values are much smaller than the mean values (e.g., $u'/\overline{U} << 1$) to the extent that

$$(\overline{U} + u')^{1/2} \approx (\overline{U})^{1/2} \left(1 + \frac{u'}{2\,\overline{U}}\right).$$

This means that $I \approx \overline{I}$, $U \approx \overline{U}$, and $E_b \approx \overline{E}_b$. The usual panel meter indicates mean values, making it more useful to have the equations in terms of mean quantities.

By substituting e' of Equation (E-22) i 'o Equation (E-21),

$$\frac{u'}{\overline{U}} = \frac{400\,\overline{I}}{(\rho\overline{U})^{1/2}\,B'\,(R_w - R_e)} \left(\frac{R_w}{R_c + R_w}\right) e_b' \,(\%). \qquad \text{(E-23)}$$

With the DISA anemometer the mean bridge voltage $\overline{E}_b$ can be read from a panel meter. The circuit is arranged so that the mean wire current $\overline{I}$ and bridge voltage are proportional, being related by the equation

$$(\overline{I})^2 = \frac{1.082\,(\overline{E}_b)^2}{(100 + R_w + R_\ell)^2} \qquad \text{(E-24)}$$

where R_ℓ is the total cable and lead resistance of the probe. When Equations (E-12) and (E-24) are combined, it can be written

$$(\overline{E}_b)^2 = A + B\,(\rho\overline{U})^{1/2} \qquad \text{(E-25)}$$

where

$$A = \frac{(R_w - R_e)\,(100 + R_w + R_\ell)^2}{1.082\,R_w}\,A'$$

$$B = \frac{(R_w - R_e)\,(100 + R_w + R_\ell)^2}{1.082\,R_w}\,B'.$$

The analysis leading to Equation (E-23) can be carried out starting with King's law in the form of Equation (E-25).

$$B' (\rho \overline{U})^{1/2} = (\overline{E}_b)^2 - (\overline{E}_{bo})^2 \qquad \text{(E-26)}$$

where

$$(\overline{E}_{bo})^2 = \lim_{\substack{x \to \infty \\ U = 0}} (\overline{E}_b)$$

The corresponding form of Equation (E-23) is

$$\frac{u'}{\overline{U}} = \frac{400\ \overline{E}_b}{(\overline{E}_b)^2 - (\overline{E}_{bo})^2}\ e_b \text{ (\%)}. \qquad \text{(E-27)}$$

REFERENCES

E-1. Kovasznay, L. S. G. Turbulence in supersonic flow. J. Aeronaut. Sci. 20: 657-74, 682 (1953).

E-2. Morkovin, M. V. and R. E. Phinney. Extended applications of hot-wire anemometry to high-speed turbulent boundary layers. Johns Hopkins University, Department of Aeronautics (June 1958).

E-3. Corrsin, S. Turbulence: experimental methods. In Handbuch der Physik, vol. 8, part 2. Berlin, Springer-Verlag, 1963. pp. 524-90.

E-4. King, L. V. On the convection of heat from small cylinders in a stream of fluid: determination of the convection constants of small platinum wires with application to hot-wire anemometry. Phil. Trans. Roy. Soc. London, Ser. A 214: 373-432 (1914).

E-5. Betchov, R. Nonlinear theory of a hot-wire anemometer. NACA TM 1346 (1952). Originally publ, in Verhandel. Koninkl. Ned. Akad. Wetenschap. 52: 195-207 (1949).

E-6. Winovich, W. and H. A. Stine. Measurements of the nonlinear variation with temperature of heat-transfer rate from hot wires in transonic and supersonic flow. NACA TN 3965 (1957).

E-7. Kovasznay, L. S. G. Turbulence measurements. In Physical Measurements in Gas Dynamics and Combustion. Princeton, N.J., Princeton University Press, 1954. pp. 219-76.

E-8. Kovasznay, L. S. G. and S. I. A. Tormark. Heat loss of hot-wires in supersonic flow. Johns Hopkins University, Department of Aeronautics, Bumblebee Report No. 127 (April 1950).

E-9. Hanson, A. R., R. E. Larson and F. R. Krause. Hot wire techniques in low density flows with high turbulence levels. In NASA Technical Memo. X-53295. Aero-Astrodynamics Research Review no. 2 (April 1, 1965) pp 77-91.

E-10. Larson, R. E., A. R. Hanson, F. R. Krause and W. K. Dahm. Heat transfer below reattaching turbulent flows. AIAA Paper No. 65-825, presented at AIAA Aerothermochemistry of Turbulent Flows Conference, San Diego, California, December 13-15, 1965.

E-11. McAdams, W. H. Heat transmission. 3rd. ed. N. Y., McGraw-Hill 1954.

E-12. Boltz, F. W. Hot-wire heat-loss characteristics and anemometry in subsonic continuum and slip flow. NASA TN D-773 (1961).

E-13. Spangenberg W. G. Heat-loss characteristics of hot-wire anemometers at various densities in transonic and supersonic flow. NACA TN 3381 (1955).

E-14. Lowell, H. H. Design and applications of hot-wire anemometers for steady-state measurements at transonic and supersonic airspeeds. NACA TN 2117 (1950).

E-15. Baldwin, L. V. Slip-flow heat transfer from cylinders in subsonic airstreams. NACA TN 4369 (1958).

E-16. Cybulski, R. J. and L. V. Baldwin. Heat transfer from cylinders in transition from slip flow to free-molecule flow. NASA Memo. 4-27-59E (1959).

E-17. Laurence. J. C. and V. A. Sandborn. Heat transfer from cylinders. In Symposium on Measurement in Unsteady Flow, American Society of Mechanical Engineers, Hydraulic Division Conference, May 21-23, 1962, Proceedings. N. Y., ASME, 1962. pp. 36-43.

E-18. Sandborn, V. A. and J. A. Laurence. Heat loss from yawed hot wires at subsonic Mach numbers. NACA TN 3563 (1955).

E-19. Collis, D. C. and M. J. Williams. Two-dimensional convection from heated wires at low Reynolds numbers. J. Fluid Mech. 6: 357-84 (1959).

Unclassified

Security Classification

DOCUMENT CONTROL DATA - R & D

(Security classification of title, body of abstract and indexing annotation must be entered when the overall report is classified)

1. ORIGINATING ACTIVITY (Corporate author) APPLIED SCIENCE DIVISION Litton Systems, Inc. 2003 East Hennepin, Minneapolis, Minnesota 55413	2a. REPORT SECURITY CLASSIFICATION Unclassified 2b. GROUP

3. REPORT TITLE

INVESTIGATIONS OF HEAT AND MASS (WATER VAPOR AND LIQUID) MOVEMENT THROUGH CLOTHING SYSTEMS

4. DESCRIPTIVE NOTES (Type of report and inclusive dates)

ANNUAL REPORT - for the period 25 June 1965 - 24 June 1966

5. AUTHOR(S) (First name, middle initial, last name)

R. E. Larson, L. W. Rust, A. R. Kydd, C. A. Gauvin

6. REPORT DATE	7a. TOTAL NO. OF PAGES	7b. NO. OF REFS
September 1968	251	12

8a. CONTRACT OR GRANT NO. DA 19-129-AMC-683(N) b. PROJECT NO. 1K012501A032 c. d.	9a. ORIGINATOR'S REPORT NUMBER(S) 9b. OTHER REPORT NO(S) (Any other numbers that may be assigned this report) 69-31-CM; C&OM-56

10. DISTRIBUTION STATEMENT

This document has been approved for public release and sale; its distribution is unlimited.

11. SUPPLEMENTARY NOTES	12. SPONSORING MILITARY ACTIVITY
	U. S. Army Natick Laboratories Natick, Massachusetts 01760

13. ABSTRACT

This report of research on the Investigations of Heat and Mass (Water Vapor and Liquid) Movement Through Clothing Systems summarizes the results of a theoretical and experimental research program.

Modifications and improvements were made on the mathematical model and governing equations previously described in the First Annual Progress Report. The equations were converted into an explicit finite difference term and programmed for solution on the Honeywell 1800 digital computer.

Experimental studies included measurements of profiles of mean and fluctuating velocity, temperature, and water vapor concentration for various fabric spacings and ventilating velocities. Transfer coefficient data obtained from these profiles were compared with total water and heat loss rates.

DD FORM 1 NOV 68 1473 REPLACES DD FORM 1473, 1 JAN 64, WHICH IS OBSOLETE FOR ARMY USE.

Unclassified

Security Classification

14. KEY WORDS	LINK A		LINK B		LINK C	
	ROLE	WT	ROLE	WT	ROLE	WT
Testing	8					
Mathematical models	8					
Moving	8,9					
Water vaper	9		8,9			
Liquids	9					
Heat	9					
Fabrics	5		5		9	
Measurement			8		8	
Velocity			8,9			
Fluctuating			0			
Mean			0			
Temperature			8,9			
Concentration			8,9			
Spacing					9	
Ventilation					4	
Flow measurement					4	
Clothing systems	4					